Evaluation of *Escherichia coli* biofilms in controlled hydrodynamic conditions using flow cells

A Dissertation presented to the
UNIVERSITY OF PORTO
for the degree of Doctor in
Chemical and Biological Engineering
by

Patrícia Maria Alves Borges

Supervisor: Prof. Filipe José Mergulhão

LEPABE – Laboratory for Process Engineering, Environment, Biotechnology and Energy
Department of Chemical Engineering
Faculty of Engineering, University of Porto

Porto, December 2020

This work was funded by Base Funding - UIDB/00511/2020 of the Laboratory for Process Engineering, Environment, Biotechnology and Energy – LEPABE - funded by national funds through the FCT/MCTES (PIDDAC). Patrícia Alves acknowledges the receipt of a Ph.D. Grant from the Portuguese Foundation from Science and Technology (FCT) (PD/BD/114317/2016). The support from the EU COST Actions iPROMEDAI (TD1305) and ENIUS (CA16217) is also acknowledged.

"Surely, in the light of history,
it is more intelligent to hope rather than to fear,
to try rather than not to try.
For one thing, we know beyond all doubt:
Nothing has ever been achieved by the person who says,
'It can´t be done'."
Eleanor Roosevelt

Ao Hélder
À minha mãe, ao meu pai
Aos meus avós
À minha irmã, afilhado e sobrinha

Acknowledgments

The process of obtaining a doctorate in Chemical and Biological Engineering was a long journey that will remain in my memory forever, as it shaped the course of my life. This adventure could not have been possible without all the people, to whom I am sincerely grateful:

First, I would like to express my deepest gratitude to my supervisor, Prof. Filipe Mergulhão, for all the support and opportunities given over these years. Specially for helping me shape this path allowing me to explore my ideas and never putting boundaries to my perseverance.

I am also grateful to Dr. João Miranda from the Centro de Estudos de Fenómenos de Transporte (CEFT) group for the help in the work developed in this thesis and for all the support.

I would like to acknowledge the PhD scholarship (PD/BD/114317/2016) from Fundação para a Ciência e Tecnologia (FCT), who funded this study.

I wish to thank the support from the EU COST Actions for improved Protection of Medical Devices Against Infection (iPROMEDAI) (TD1305) and the European Network of Bioadhesion Expertise (ENBA) for all the meetings, summer courses and short term scientific missions that allowed me to grow personally and professionally.

To all those in the Department of Chemical Engineering and LEPABE, I would like to express my sincere thanks for providing good working facilities.

To all my LabE007 and E008 colleagues, with special thanks to Joana, Inês, Alexandra, Maria João, Marta, Sara and Rita who were with me during all these years and for our friendship. I also would like to thank to Joana Moreira, Carla Ferreira and Luciana Gomes for being always ready to help me.

Of course, without the support of my family and childhood friends, none of this would be possible:
I would like to thank my parents José Maria and Antonieta, for the unconditional support.
To my sister Carmen, for give me the most important little persons in my life, Liam and Emma, my nephews.

My most special thanks to Hélder, who during this stage became my husband, but who has always been my greatest confidant, my strength, the one who always believed in me and in a bright future. Thank you for your true love! Grow old with me!

Last but not least, I would like to thank to all my friends, especially to Cláudia, Daniela, Luís, Frederico, Nuno, Ana Luísa, Inês, Ana Margarida, Virgínia, Fernando, Dina and Hugo, for the good times that we always had together, for all the support but most important for walking with me side by side.

Thank you!

Abstract

Infections related to bacterial colonization of medical devices are a growing concern given the socio-economic impacts in healthcare systems. Bacterial adhesion and subsequent biofilm growth can be affected by several factors as the surface properties, which prompted the development of novel materials to prevent or reduce adhesion. The studies addressing hydrodynamics and their effects on biomaterials are very scarce. An important step in the development of these materials is the availability of platforms where the surface performance can be assayed in defined hydrodynamic conditions as those found by bacteria in real contexts, which is a critical step in the translation of research into practical applications. The main goal of this thesis was the development and characterization of a standardized *in vitro* assay based on a parallel plate flow cell (PPFC) system to investigate how the initial bacterial adhesion process unfolds. Besides, the antifouling performance of modified surfaces was studied regarding their effectiveness under a broad range of hydrodynamic conditions that can be found in many biomedical applications. All the analysis was performed using *Escherichia coli*, given its relevance in biomedical settings.

When studying initial adhesion on a PPFC it is important to verify if hydrodynamic blocking is not occurring at the assay conditions so that cells can freely adhere to the surface under evaluation. In this study, a convenient image analysis method was proposed to assess if blocking is affecting the experiments. The monitorization of the adhesion process was performed in real-time using microscope imaging. The process consisted of using radial distribution functions analysing the probability of adhesion of one cell with respect to other cells in their vicinity and to establish if significant areas are blocked. Results shown that hydrodynamic blocking was not occurring under the experimental conditions tested. Additionally, a real-time mass balance for *E. coli* adhesion was established, showing that under the experimental conditions used, sedimentation was more important than desorption during initial bacterial adhesion.

The PPFC system was then used to evaluate the anti-adhesion properties of a peptide coating and two polymer brushes during a 30 min assay (corresponding to the initial adhesion phase). The effect of the medium composition (citrate buffer and enriched medium) was evaluated. Results showed that the peptide coating could reduce up to 70% of *E. coli* adhesion over a broad range of shear conditions. The importance of the chemical composition of the surrounding fluid was highlighted as it affected the performance of the surface. Regarding the polymer brushes, poly[oligo(ethylene glycol) methyl ether methacrylate] (poly(MeOEGMA)) and

the poly[N-(2-hydroxypropyl) methacrylamide] (poly(HPMA)), results demonstrate the ability to reduce initial adhesion. Importantly, the performance of these surfaces was not affected by shear stress. The brushes displayed a similar behavior despite the differences in their chemical composition and surface energy. Both surfaces have shown ultra-low adsorption of macromolecules from the medium when tested with relevant biological fluids (urine and serum).

After the initial screening of the surface's performance, biofilm formation assays were performed for the polymer brushes using synthetic urine medium and an assay time of 24 h. Both polymer bushes were evaluated *in vitro* in conditions that mimic a urinary catheter (shear strain rate of 15/s). The results obtained with the brush were compared to those obtained with two control surfaces, polydimethylsiloxane (PDMS; the most common material for catheters) and glass. The antifouling behavior of poly(HPMA) was maintained during biofilm maturation, even in a simulated post-bladder infection period when the reduction in total cell number reached 87%. Biofilms were shown to adapt their architecture during that period and viable but nonculturable (VBNC) cells, that are more resistant to antibiotic treatment, adsorbed weakly on the brushes and were completely washed away. Moreover, *E. coli* biofilms formed on the poly(MeOEGMA) brushes were subjected to ampicillin, a common antibiotic prescribed in urinary tract infections to evaluate their susceptibility. The antifouling effect was noticeable during the initial adhesion and subsequent biofilm maturation and enhanced regarding cell removal after ampicillin exposure (on average 88% of reduction in the total cell number). The biofilms formed adapt their architecture and cells presented an elongated morphology during that period. Results showed that the tested surfaces are promising in preventing *E. coli* adhesion and biofilm formation, particularly at the shear conditions prevailing in the urinary tract and can potentially be used to reduce biofilm formation on these devices.

Keywords: Bacterial adhesion; *Escherichia coli*; parallel plate flow cell; hydrodynamics; blocking; sedimentation; antifouling coatings; antibiotic susceptibility.

Resumo

As infeções relacionadas com a colonização de bactérias em dispositivos médicos são uma preocupação crescente, dado os impactos socioeconómicos nos sistemas de saúde. A adesão bacteriana e o subsequente desenvolvimento do biofilme podem ser afetados por vários fatores, como as propriedades da superfície, o que levou ao desenvolvimento de novos materiais para prevenir ou reduzir a adesão. Os estudos que abordam a hidrodinâmica e os seus efeitos nos biomateriais são muito escassos. Um passo importante no desenvolvimento desses materiais é a disponibilidade de plataformas onde o desempenho da superfície pode ser avaliado em condições hidrodinâmicas definidas, como as encontradas por bactérias em contextos reais, que é um passo crítico na passagem de um ambiente de investigação para aplicações práticas. O principal objetivo desta tese foi o desenvolvimento e a caracterização de um ensaio padronizado *in vitro* baseado num sistema de célula de fluxo de placas paralelas (do inglês *parallel plate flow cell*, PPFC) para investigar como o processo inicial de adesão bacteriana se desenvolve. Além disso, foi avaliada a performance anti-adesão de superfícies modificadas quanto à sua eficácia quando sujeitas a diferentes condições hidrodinâmicas que podem ser encontradas em aplicações biomédicas. Toda a análise foi realizada com *Escherichia coli*, dada a sua relevância em ambientes biomédicos.

Ao estudar a adesão inicial numa PPFC, é importante verificar se o processo de bloqueio hidrodinâmico (do inglês *hydrodynamic blocking*) não está a ocorrer nas condições do ensaio, para que as células possam aderir livremente à superfície de teste. Neste estudo, foi proposto um método de análise de imagem para avaliar se o bloqueio está a afetar as experiências. A monitorização do processo de adesão foi realizada em tempo real, utilizando imagens obtidas a partir do microscópio. O processo consistiu em usar funções de distribuição radial analisando a probabilidade de uma célula aderir em relação a outras células próximas e verificar se áreas significativas são bloqueadas por células já aderidas. Os resultados mostraram que o bloqueio hidrodinâmico não ocorreu nas condições experimentais testadas. Além disso, foi estabelecido um balanço de massa em tempo real para a adesão de *E. coli*, mostrando que nas condições experimentais utilizadas, a sedimentação é mais importante que a dessorção na adesão bacteriana inicial.

O sistema PPFC foi então usado para avaliar as propriedades anti-adesão de um revestimento peptídico e dois revestimentos poliméricos (*polymer brushes*) durante um ensaio de 30 min (correspondente à fase inicial de adesão). O efeito da composição do meio (tampão citrato e meio enriquecido) foi avaliado. Os resultados mostraram que o revestimento peptídico pode

reduzir até 70% da adesão de *E. coli* quando sujeito a diferentes tensões de corte. Verificou-se que a composição química do fluido circundante afeta o desempenho da superfície. Em relação aos polímeros, poly[oligo(ethylene glycol) methyl ether methacrylate] (poly(MeOEGMA)) e poly[N-(2-hydroxypropyl) methacrylamide] (poly(HPMA)), os resultados demonstram a capacidade de reduzir a adesão inicial. É importante referir que o desempenho dessas superfícies não foi afetado pelas tensões de corte. Ambos os revestimentos exibiram um comportamento semelhante, apesar das diferenças na sua composição química e energia de superfície. Ambas as superfícies mostraram uma muito baixa adsorção de macromoléculas do meio quando testadas com fluidos biológicos relevantes (urina e soro).

Após a análise inicial do desempenho das superfícies, foram realizados ensaios de formação de biofilme usando meio de urina sintético durante 24 h de ensaio. Ambas as superfícies foram avaliadas *in vitro* em condições hidrodinâmicas que mimetizam um cateter urinário (taxa de deformação, do inglês *shear rate*, de 15/s). Os resultados obtidos com os polímeros foram comparados aos obtidos com duas superfícies de controlo, polidimetilsiloxano (PDMS; o material mais comum em cateteres) e vidro. O comportamento anti-biofilme do poly(HPMA) foi mantido durante a fase de maturação, mesmo após um período de infeção simulado da bexiga quando a redução no número total de células atingiu os 87%. Os biofilmes demonstraram capacidade de adaptar a sua arquitetura durante esse período e as células viáveis, mas não cultiváveis (do inglês *viable but nonculturable,* VBNC), mais resistentes ao tratamento com antibióticos, apresentaram uma fraca adsorção ao polímero e foram completamente removidas. Além disso, os biofilmes de *E. coli* formados no poly(MeOEGMA) foram submetidos a ampicilina, um antibiótico comummente prescrito em infeções do trato urinário, de forma a avaliar a sua suscetibilidade. O efeito anti-biofilme foi observado durante a adesão inicial e subsequente maturação do biofilme e foi particularmente notório em relação à remoção de células após exposição à ampicilina (em média 88% de redução no número células totais). Os biofilmes formados adaptam a sua arquitetura e as células apresentaram uma morfologia alongada durante esse período. Os resultados mostraram que as superfícies testadas são promissoras na prevenção da adesão e formação de biofilmes de *E. coli*, particularmente à tensão de corte predominante no trato urinário e podem potencialmente ser usadas para reduzir a formação de biofilme nesses dispositivos.

Palavras-chave: Adesão bacteriana; *Escherichia coli*; célula de fluxo de placas paralelas; hidrodinâmica; bloqueio hidrodinâmico; sedimentação; revestimentos anti-biofilme; suscetibilidade a antibiótico.

Table of contents

List of figures

Chapter 2

Chapter 3

Chapter 4

Chapter 5

Chapter 6

Chapter 7

Chapter 8

List of tables

Chapter 2

Chapter 3

Chapter 5

Chapter 6

Chapter 7

Nomenclature

Abbreviations

2D	Two-dimensional
3D	Three-dimensional
AFM	Atomic force microscopy
ATR-FTIR	Attenuated total reflection (ATR)-Fourier-transform infrared (FITR) spectroscopy
ATR-IR	Infrared attenuated total reflection (ATR-IR) spectroscopy
BAI	Biomaterial-associated infection
CA	Cellulose acetate
CAUTI	Catheter-associated urinary tract infection
CB	Citrate buffer
CBD	Calgary biofilm device
CFD	Computational fluid dynamics
CFU	Colony formation units
CLSM	Confocal laser scanning microscopy
CV	Crystal violet
DAPI	4′-6-diamidino-2-phenylindole
DLVO theory	Derjaguin, Landau, Verwey, Overbeek theory
DOPA	3,4-dihydroxy-L-phenylalanine
EM	Enriched medium
EPS	Extracellular polymeric substances
ExPEC	Extraintestinal pathogenic *Escherichia coli*
GAATR-FTIR	Grazing angle attenuated total reflection Fourier-transform infrared
GFP	Green fluorescent protein
Gram -	Gram-negative
Gram +	Gram-positive
HCAI	Healthcare-associated infections
IAR	Initial adhesion rates
IMD	Indwelling medical devices
L/D	Live/Dead
MAPs	Mussel adhesive proteins
MBEC	Minimum biofilm eradication concentration
MIC	Minimum inhibitory concentration
NI	Nosocomial infection
OCT	Optical coherence tomography
OD	Optical density
PCA	Plate count agar
PDMS	Polydimethylsiloxane
poly(HPMA)	Poly[N-2-hydroxypropyl) methacrylamide]
poly(MeOEGMA)	Poly[oligo(ethyleneglycol) methyl ether methacrylate]
PPFC	Parallel plate flow cell

PS	Polystyrene
QCM	Quartz crystal microbalance
QCM-D	Quartz crystal microbalance with dissipation monitoring
SD-OCT	Spectral domain optical coherence tomography
SEM	Scanning electron microscopy
SI-ATRP	Surface-initiated atom transfer radical polymerization
SL	Smoluchowski Levich
SPR	Surface plasmon resonance
UPEC	uropathogenic *E. coli*
UTI	Urinary tract infections
UV-vis	Ultraviolet–visible
VBNC	Viable but nonculturable
xDLVO theory	Extended Derjaguin, Landau, Verwey, Overbeek theory

Symbols

γ^{LW}	Lifshitz van der Waals components (mJ/m^2)
γ^-	Electron donor components (mJ/m^2)
$\gamma+$	Electron acceptor character (mJ/m^2)
$\boldsymbol{\gamma_l^{Tot}}$	Total surface energy (mJ/m^2)
$\boldsymbol{\gamma^{AB}}$	Lewis acid-base components (mJ/m^2)
$\boldsymbol{\Delta G}$	Surface hydrophobicity (mJ/m^2)
$\boldsymbol{\Delta G^{Adh}}$	Free energy of adhesion (mJ/m^2)
$\boldsymbol{R_a}$	Average roughness (nm)
Re	Reynolds number (dimensionless)
$\boldsymbol{\Upsilon}$	Wall shear rate (1/s)
$\boldsymbol{Pe}$	Péclet number (dimenssionless)
Q	Volumetric flow rate (m^3/s)
$\boldsymbol{h_0}$	Height of the rectangular flow channel (m)
$\boldsymbol{w_0}$	Width of rectangular channel (m)
$\boldsymbol{D_\infty}$	Diffusion coefficient (around 10^{-13} for microorganisms)
ρ	Fluid density (kg/m^3)
$\boldsymbol{\eta}$	Absolute viscosity (10^{-13} kg/m.s)
$\boldsymbol{v_{av}}$	Average flow velocity (m/s)
$\boldsymbol{R_b}$	Microbial radius (m)
$\boldsymbol{j_0^*}$,	Initial deposition rate (1/cm^2. s)
$\boldsymbol{C_b}$,	Bacterial concentration (cell/m^3)
$\boldsymbol{x}$,	Distance along the flow from the inlet (m)
$\boldsymbol{\tau_w}$	Wall shear stress (Pa)
$\mathbf{Re}_c$	Local Reynolds number (dimensionless)
$\boldsymbol{\theta_w}$	Contact angles with water (°)
$\boldsymbol{\theta_F}$	Contact angles with formamide (°)
$\boldsymbol{\theta_B}$	Contact angles with α-bromonaphthalene (°)

1. General overview

1.1. Relevance and motivation

Bacterial biofilms can be described as biological communities of microorganisms, usually living attached to surfaces and embedded in a self-produced matrix of extracellular polymeric substances (EPS) [1]. The EPS protects the biofilm, acting as a barrier to antibiotic penetration, and that is strongly influenced by the substratum on which the biofilm forms and the bulk phase which flows over the biofilm [2, 3]. Biofilm formation entails high costs and health risks since it has been estimated that as much as 80% of all human bacterial infections are biofilm-associated [4, 5]. Moreover, biomaterial-associated infections (BAIs) are expected to increase as the use of medical devices, such as catheters, artificial heart valves, prosthetic joints, as well as other implants, has increased drastically over the past century and is expected to continue alongside the aging of our society. This is due to an ever-improving technology within the medical field, and the demand for medical devices to restore function and quality of life is higher than ever.

Overall, most of the biofilm-related infections are associated with indwelling medical devices [6, 7] and among these, urinary tract infections (UTIs) are one of the most common affecting around 150 million people each year worldwide [8, 9] and are one of the major reasons for antibiotic use [10]. *Escherichia coli*, a universal bowel inhabitant, is the most common causative agent in UTIs that causes up to 90% of outpatient of the hospital-acquired infections [11, 12]. It is known that bacteria in biofilms behave differently from planktonic bacteria, particularly in response to antibiotic treatment [13, 14]. *E. coli* has also been found to persist and re-emerge after antibiotic exposure, due to many factors including reduced penetration of antibiotics in biofilms [15].

The so-called "race for the surface" reported in 1987 by Gristina, suggests that tissue cell integration and bacterial adhesion compete for a spot on the surface of the implant [16]. Great efforts in surface engineering have been made to prevent or mitigate the risk of infection since the physicochemical surface properties of biomaterials, such as the surface charges (hydrophobicity and or hydrophilicity), play an important role in the initial bacterial adhesion process. These new approaches include nanoparticles, polymer brushes, antifouling self-assembly monolayers, and hydrogels to be applied to contact lenses, shunts, endotracheal tubes and urinary catheters [17-21]. It should be highlighted, however, that most studies trying to unravel the key factors of bacterial adhesion of these surfaces have been carried out in static conditions focusing mainly on thermodynamic considerations. This neglects the importance of flow and shear in delivering the bacteria close to the surface, where the Lifshitz–van der Waals interactions are stronger [22]. Flow

is important in various engineering and biomaterial applications [2, 3, 23-26]. Specifically, *in vitro* systems such as flow cells, are used to assess the effect of shear stress in bacterial adhesion for different strains [27-31] and studies tried to correlate the extent of fouling with the energy of adhesion [27, 30, 32]. It has been shown that bacterial adhesion does not always correlate with surface properties but notoriously with the shear stress as later demonstrated by Moreira et al [3, 33]. Several designs of flow cells have been used, however presenting some limitations, such as the area that can be used for adhesion studies and the limitations of the flow range [34]. In this sense, a parallel plate flow cell (PPFC) was designed by our research team [3] to study biofilm development in dynamic conditions, enabling a better understanding of the factors affecting the initial bacterial adhesion, which is the onset of the biofilm development. This platform enables the study of real-time adhesion (single-cell visualization) and biofilm observation in a non-destructive way [3, 35], under controlled hydrodynamic conditions that mimic physiologically relevant conditions, studying a wide range of microorganisms and surfaces with different properties [3]. Nevertheless, despite all the information provided by all the studies in the last decades, understanding the role of the survival biofilm mechanics continues to be crucial to open new research paths that might help the design of new strategies for biofilm prevention and control.

1.2. Aims and outline of the thesis

The main aim of this thesis is the development and characterization of a standardized *in vitro* assay based on a PPFC system to investigate how the initial bacterial adhesion process unfolds, using as a bacterial model the *E. coli* JM109(DE3) given its relevance in industrial and biomedical settings. Additionally, the antifouling performance of modified surfaces was studied regarding their effectiveness under a broad range of hydrodynamic conditions. The shear stress range covered in this study was previously determined by computational fluid dynamics (CFD) and can be found in the human body and industrial scenarios [3]. The combined effects of strain type, nutritional conditions, surface properties and hydrodynamic conditions are also analysed regarding cell adhesion, biofilm formation and biofilm resistance to a common antibiotic. These features are extremely important since in most of the studies the response of the microorganisms to changes in the mechanical force of the fluid shear has not been considerate or elucidated and it is known that has important implications for pathogens during *in vivo* infection. The results obtained in this work may provide a better understanding of how the bacterial adhesion event occurs, providing important clues to devise strategies to inhibit or delay this event.

This thesis is structured into 8 chapters as follows:

C**hapter 2** provides a brief literature review describing the state-of-the-art on the biofilm development process and the main factors controlling its formation. A description of the *in vitro* platforms that are currently used for biofilm studies and an explanation of the one used in this thesis is also presented in more detail. Particular emphasis is given to hydrodynamic conditions that are relevant for biomedical scenarios as well as the study of the surface properties as a strategy to reduce or inhibit bacterial adhesion.

The following two chapters provide a detailed characterization of a small-scale flow cell for real-time observation of *E. coli* adhesion on a model surface, polydimethylsiloxane (PDMS, a type of silicone) widely used in industrial and biomedical settings.

Chapter 3 presents a simple method to identify the occurrence of hydrodynamic blocking using two-dimensional (2D) histograms showing the density probability function. The initial adhesion of *E. coli* was assessed, and the shear rate range covered in this study had been previously determined by CFD as previously described. The proposed image analysis is convenient to determine if blocking is occurring and masking the real adhesion behavior of the cells. In that case, the operational parameters may be tuned to prevent its occurrence.

Chapter 4 evaluates the contribution of cell sedimentation and detachment to the observed initial adhesion rates. The main purpose of this study was to unravel the major hydrodynamic related factors affecting biofilm development in flow conditions. It is known that PPFC systems are highly prone to sedimentation. The proposed image analysis is suitable to evaluate sedimentation and detachment by real-time image analysis and thus determine the "real" adhesion rates to a specific surface for different hydrodynamic conditions.

Following the characterization of the PPFC system, we proceed to the development of a standardized *in vitro* assay for testing the initial adhesion of *E. coli* to different antifouling surfaces at physiological shear values. Citrate buffer was used to enable a more accurate thermodynamic analysis of the adhesion phenomenon (Chapters 5 and 6) and a more complex medium to study the effect of the surrounding fluid on the performance of the modified surfaces (Chapter 5).

In **Chapter 5**, the performance of a tripeptide that self-assembles into an antifouling coating was evaluated under a broad range of hydrodynamic conditions that can be found in many biomedical applications. The surface coating was characterized by different techniques, and the effect of the surrounding medium composition was evaluated regarding the initial bacterial adhesion. This work follows a previous report in which this antifouling surface was tested under static conditions. The findings suggest critical features that should be considered when developing surfaces for biomedical purposes.

In **Chapter 6**, two polymer brushes with antifouling properties, poly[oligo(ethyleneglycol) methyl ether methacrylate] (poly(MeOEGMA)) and the poly[N-2-hydroxypropyl) methacrylamide] (poly(HPMA)) brushes, were studied at different shear stresses that can be found in the human body and medical devices. The brushes were grafted from glass using atom transfer radical polymerization. The PPFC was used, enabling the control of the shear stress by modifying the flow rate of the bacterial suspension. The amount and rate of bacterial attachment were measured and correlated to the surface energy. The study suggests that these surfaces can potentially be used in biomedical devices.

After the initial screening, the surfaces with the best performance to reduce the initial adhesion process were evaluated regarding the conditions that mimic a specific physiological scenario for a longer period (24 h) (Chapters 7 and 8). The resistance of the biofilms to shear stress and chemical treatment with an antibiotic was assessed (Chapter 8).

In **Chapter 7**, a combined shear rate of the urinary catheters (15/s) and the effect of a more complex medium (synthetic urine medium) was evaluated regarding the antifouling performance of poly(HPMA) brushes. Synthetic urine was used as a culture medium in longer assays since it has been reported that in clinical situations, such as the development of *E. coli* biofilms in urinary catheters, biofilms are completely mature after 24 h. The antifouling behavior was shown to be maintained during biofilm maturation and even in a simulated post-bladder infection period. Biofilms were shown to adapt their architecture during that period and viable but nonculturable (VBNC) cells were adsorbed weakly on the brushes and as a consequence completely washed away. These results suggest that the use of this brush in urinary tract devices (e. g. catheters and stents) may reduce biofilm formation and possibly render the formed biofilms more susceptible to antibiotic treatment and with reduced infectivity potential.

In **Chapter 8**, the performance of antifouling poly(MeOEGMA) brushes was evaluated on *E. coli* biofilm formation. This polymer brush was selected due to its resistance to protein adsorption and bacterial adhesion. The study aims to evaluate the antifouling properties of surface tested towards complex biological medium under a controlled shear rate and their impact on biofilm development as well as the resistance of the biofilms formed to chemical treatment with ampicillin. Importantly, the antifouling performance demonstrated by the polymer brush in previous work using citrate buffer (Chapter 6) was maintained here for a long period, during biofilm maturation and enhanced regarding cell removal after ampicillin exposure. The ability of this brush to significantly delay *E. coli* biofilm formation when compared to PDMS, makes it a very promising surface to prevent infections in urinary tract devices.

Finally, **Chapter 9** presents the main conclusions of this work and proposes future research lines to improve knowledge in the field.

1.3. References

1. Davey, M. E.; O'toole, G. A., Microbial biofilms: from ecology to molecular genetics. *Microbiology and Molecular Biology Reviews* **2000,** *64* (4), 847-867.
2. Teodósio, J.; Simões, M.; Melo, L.; Mergulhão, F., Flow cell hydrodynamics and their effects on *E. coli* biofilm formation under different nutrient conditions and turbulent flow. *Biofouling* **2011,** *27* (1), 1-11.
3. Moreira, J.; Araújo, J.; Miranda, J. M.; Simões, M.; Melo, L.; Mergulhão, F., The effects of surface properties on *Escherichia coli* adhesion are modulated by shear stress. *Colloids and Surfaces B: Biointerfaces* **2014,** *123*, 1-7.
4. Miquel, S.; Lagrafeuille, R.; Souweine, B.; Forestier, C., Anti-biofilm activity as a health issue. *Frontiers in Microbiology* **2016,** *7*.
5. Römling, U.; Balsalobre, C., Biofilm infections, their resilience to therapy and innovative treatment strategies. *Journal of Internal Medicine* **2012,** *272* (6), 541-561.
6. Hancock, V.; Ferrières, L.; Klemm, P., Biofilm formation by asymptomatic and virulent urinary tract infectious *Escherichia coli* strains. *FEMS Microbiology Letters* **2006,** *267* (1), 30-37.
7. Lo, E.; Nicolle, L. E.; Coffin, S. E.; Gould, C.; Maragakis, L. L.; Meddings, J.; Pegues, D. A.; Pettis, A. M.; Saint, S.; Yokoe, D. S., Strategies to prevent catheter-associated urinary tract infections in acute care hospitals: 2014 update. *Infection Control & Hospital Epidemiology* **2014,** *35* (5), 464-479.
8. Stamm, W. E.; Norrby, S. R., Urinary tract infections: disease panorama and challenges. *The Journal of Infectious Diseases* **2001,** *183* (Supplement_1), S1-S4.
9. Arciola, C. R.; Campoccia, D.; Montanaro, L., Implant infections: adhesion, biofilm formation and immune evasion. *Nature Reviews Microbiology* **2018,** *16* (7), 397.
10. Sihra, N.; Goodman, A.; Zakri, R.; Sahai, A.; Malde, S., Nonantibiotic prevention and management of recurrent urinary tract infection. *Nature Reviews Urology* **2018**, 1.
11. Flores-Mireles, A. L.; Walker, J. N.; Caparon, M.; Hultgren, S. J., Urinary tract infections: epidemiology, mechanisms of infection and treatment options. *Nature Reviews Microbiology* **2015,** *13* (5), 269-84.
12. Forde, B. M.; Roberts, L. W.; Phan, M.-D.; Peters, K. M.; Fleming, B. A.; Russell, C. W.; Lenherr, S. M.; Myers, J. B.; Barker, A. P.; Fisher, M. A.; Chong, T.-M.; Yin, W.-F.; Chan, K.-G.; Schembri, M. A.; Mulvey, M. A.; Beatson, S. A., Population dynamics of an *Escherichia coli* ST131 lineage during recurrent urinary tract infection. *Nature Communications* **2019,** *10* (1), 3643.
13. Chen, M.; Yu, Q.; Sun, H., Novel strategies for the prevention and treatment of biofilm related infections. *International Journal of Molecular Sciences* **2013,** *14* (9), 18488-18501.
14. Ito, A.; Taniuchi, A.; May, T.; Kawata, K.; Okabe, S., Increased antibiotic resistance of *Escherichia coli* in mature biofilms. *Applied and Environmental Microbiology* **2009,** *75* (12), 4093-4100.
15. Koseoglu, H.; Aslan, G.; Esen, N.; Sen, B. H.; Coban, H., Ultrastructural stages of biofilm development of *Escherichia coli* on urethral catheters and effects of antibiotics on biofilm formation. *Urology* **2006,** *68* (5), 942-946.
16. Gristina, A. G., Biomaterial-centered infection: microbial adhesion versus tissue integration. *Science* **1987,** *237* (4822), 1588-1595.

17. Busscher, H. J.; van der Mei, H. C.; Subbiahdoss, G.; Jutte, P. C.; van den Dungen, J. J.; Zaat, S. A.; Schultz, M. J.; Grainger, D. W., Biomaterial-associated infection: locating the finish line in the race for the surface. *Science Translational Medicine* **2012,** *4* (153), 153rv10-153rv10.

18. Kirschner, C. M.; Brennan, A. B., Bio-inspired antifouling strategies. *Annual Review of Materials Research* **2012,** *42*, 211-229.

19. Banerjee, I.; Pangule, R. C.; Kane, R. S., Antifouling coatings: recent developments in the design of surfaces that prevent fouling by proteins, bacteria, and marine organisms. *Advanced Materials* **2011,** *23* (6), 690-718.

20. van Hengel, I. A.; Riool, M.; Fratila-Apachitei, L. E.; Witte-Bouma, J.; Farrell, E.; Zadpoor, A. A.; Zaat, S. A.; Apachitei, I., Selective laser melting porous metallic implants with immobilized silver nanoparticles kill and prevent biofilm formation by methicillin-resistant *Staphylococcus aureus*. *Biomaterials* **2017,** *140*, 1-15.

21. Azeredo, J.; Azevedo, N. F.; Briandet, R.; Cerca, N.; Coenye, T.; Costa, A. R.; Desvaux, M.; Di Bonaventura, G.; Hébraud, M.; Jaglic, Z., Critical review on biofilm methods. *Critical Reviews in Microbiology* **2017,** *43* (3), 313-351.

22. Rodesney, C. A.; Roman, B.; Dhamani, N.; Cooley, B. J.; Katira, P.; Touhami, A.; Gordon, V. D., Mechanosensing of shear by *Pseudomonas aeruginosa* leads to increased levels of the cyclic-di-GMP signal initiating biofilm development. *Proceedings of the National Academy of Sciences* **2017,** *114* (23), 5906-5911.

23. Nuzzo, R. G., Biomaterials: stable antifouling surfaces. *Nature Materials* **2003,** *2* (4), 207-208.

24. Rodriguez-Emmenegger, C.; Brynda, E.; Riedel, T.; Houska, M.; Šubr, V.; Alles, A. B.; Hasan, E.; Gautrot, J. E.; Huck, W. T., Polymer brushes showing non-fouling in blood plasma challenge the currently accepted design of protein resistant surfaces. *Macromolecular Rapid Communications* **2011,** *32* (13), 952-957.

25. Teodósio, J. S.; Simões, M.; Alves, M. A.; Melo, L. F.; Mergulhão, F. J., Setup and validation of flow cell systems for biofouling simulation in industrial settings. *Scientific World Journal* **2012,** *2012*, 361496.

26. Tirrell, M.; Kokkoli, E.; Biesalski, M., The role of surface science in bioengineered materials. *Surface Science* **2002,** *500* (1-3), 61-83.

27. Pratt-Terpstra, I. H.; Weerkamp, A. H.; Busscher, H. J., Adhesion of oral streptococci from a flowing suspension to uncoated and albumin-coated surfaces. *Journal of General Microbiology* **1987,** *133* (11), 3199-3206.

28. Barton, A. J.; Sagers, R. D.; Pitt, W. G., Bacterial adhesion to orthopedic implant polymers. *Journal of Biomedical Materials Research: an official Journal of The Society for Biomaterials and The Japanese Society for Biomaterials* **1996,** *30* (3), 403-410.

29. Millsap, K.; Reid, G.; Van der Mei, H.; Busscher, H., Adhesion of *Lactobacillus* species in urine and phosphate buffer to silicone rubber and glass under flow. *Biomaterials* **1997,** *18* (1), 87-91.

30. Bruinsma, G.; Van der Mei, H.; Busscher, H., Bacterial adhesion to surface hydrophilic and hydrophobic contact lenses. *Biomaterials* **2001,** *22* (24), 3217-3224.

31. Busscher, H. J.; van der Mei, H. C., Microbial adhesion in flow displacement systems. *Clinical Microbiology Reviews* **2006,** *19* (1), 127-141.

32. Nauman, E. A.; Ott, C. M.; Sander, E.; Tucker, D. L.; Pierson, D.; Wilson, J. W.; Nickerson, C. A., Novel quantitative biosystem for modeling physiological fluid shear stress on cells. *Applied and Environmental Microbiology* **2007,** *73* (3), 699-705.

33. Moreira, J. M.; Simões, M.; Melo, L. F.; Mergulhão, F. J., *Escherichia coli* adhesion to surfaces – a thermodynamic assessment. *Colloid and Polymer Science* **2015,** *293* (1), 177-185.

34. Bakker, D.; Van der Plaats, A.; Verkerke, G.; Busscher, H.; Van der Mei, H., Comparison of velocity profiles for different flow chamber designs used in studies of microbial adhesion to surfaces. *Applied and Environmental Microbiology* **2003,** *69* (10), 6280-6287.

35. Li, J.; Busscher, H. J.; Norde, W.; Sjollema, J., Analysis of the contribution of sedimentation to bacterial mass transport in a parallel plate flow chamber. *Colloids and Surfaces B: Biointerfaces* **2011,** *84* (1), 76-81.

1.4. Scientific outputs

The results presented in this thesis are partially published/submitted in:

Papers in peer-reviewed journals

Alves P, Moreira, JM, Mergulhão FJ, Miranda JM (**2020**) Analysing the initial bacterial adhesion to evaluate the performance of antifouling surfaces. Antibiotics 2020, 9(7), 421. https://doi.org/10.3390/antibiotics9070421 **(Chapter 3)**

Alves P, Nir S, Reches M, & Mergulhão F (**2018**) The effects of fluid composition and shear conditions on bacterial adhesion to an anti-fouling peptide-coated surface. MRS Communications,1-9. https://doi.org/10.1557/mrc.2018.160 **(Chapter 5)**

Lopez-Mila B, **Alves P**, Riedel T, Dittrich B, Mergulhão F, Rodriguez-Emmenegger C (**2018**) Effect of shear stress on the reduction of bacterial adhesion to antifouling polymers. Bioinspiration & Biomimetics. https://doi.org/10.1088/1748-3190/aadcc2 **(Chapter 6)**

Alves P, Gomes LC, Vorobii M, Rodriguez-Emmenegger C, Mergulhão FJ (**2020**) The potential advantages of using a poly (HPMA) brush in urinary catheters: effects on biofilm cells and architecture. Colloids and Surfaces B: Biointerfaces, 191, 110976. https://doi.org/10.1016/j.colsurfb.2020.110976 **(Chapter 7)**

Alves P, Gomes LC, Rodríguez-Emmenegger C, Mergulhão FJ (**2020**) Efficacy of a poly(MeOEGMA) brush on the prevention of *Escherichia coli* biofilm formation and susceptibility. Antibiotics, 9(5), 216. https://doi.org/10.3390/antibiotics9050216 **(Chapter 8)**

Alves P, Miranda JM, Mergulhão FJ (2020) The effects of sedimentation and detachment on initial bacterial adhesion studies. (*in preparation*) **(Chapter 4)**

Communications at Scientific Meetings

Oral presentations

Alves P, Mergulhão F, Evaluation of *Escherichia coli* biofilms in controlled hydrodynamic conditions using flow cells, in BEL workshop, Faculty of Engineering at the University of Porto, 12th April **2018**, Porto, Portugal;

Alves P, Lopez-Mila B, Riedel T, Dittrich B, Rodriguez-Emmenegger C, Mergulhão F, Effect of shear stress on the reduction of bacterial adhesion to antifouling polymers, in COST AMiCI Meeting, 7th March **2019**, Riga, Latvia;

Alves P, Mergulhão F, Reduction of *Escherichia coli* biofilms using antifouling surfaces, in SCELSE meeting, Nanyang Technological University campus from 25th June 2019 to 12th July **2019**, Singapore;

Alves P, Mergulhão F, Antifouling surfaces for medical and industrial applications, in BEL workshop, Faculty of Engineering at the University of Porto, 12th June **2019**, Porto, Portugal;

Alves P, Mergulhão F, Performance assessment of antifouling peptide coating for reducing bacterial attachment using a parallel plate flow cell, in DeLNAM workshop, from 16th to 20th November **2019**, Ghent, Belgium.

Posters

Romeu, MJ, **Alves P**, Morais J, Vasconcelos V, Mergulhão FJ (**2017**) Biofilm formation by *Leptolyngbya mycoidea* LEGE 06118: surface effect, in Biofilms7, Porto, Portugal, 26-28 June 2016.

Moreira JMR, **Alves P**, Fulgêncio R, Oliveira F, Machado I, Bialuch I, Melo LF, Simões M, Mergulhão FJ (**2016**) Evaluation of SICAN and SICON® surfaces for biofouling mitigation in the food industry, in Biofilms7, Porto, Portugal, 26-28 June 2016;

Alves P, Moreira JMR and Mergulhão FJ (**2017**) Evaluation of bacterial adhesion to biomedical surfaces in controlled hydrodynamic conditions, in 2nd Doctoral Congress of Engineering 2017 (DCE17), Porto, Portugal, 8-9th June 2017;

Romeu MJ, **Alves P**, Morais J, Ramos V, Vasconcelos V, Mergulhão FJ **(2017)** Biofilm formation by cyanobacterium *Leptolyngbya mycoidea* LEGE 06118: surface effect, in 2nd Doctoral Congress of Engineering 2017 (DCE17), Porto, Portugal, 8-9th June 2017;

Alves P, Lopez-Mila B, Riedel T, Dittrich B, Rodriguez-Emmenegger C, Mergulhão FJ (**2019**) Effect of shear stress on the reduction of bacterial adhesion to antifouling polymers, COST AMiCI Meeting, Riga, Latvia, 7th March 2019;

Alves P, Mergulhão FJ (**2019**) Effect of shear stress on the reduction of bacterial adhesion to antifouling polymers, 14th International Triennial Conference on the Science and Technology of Adhesion and Adhesives (Adhesion'19), Bristol, United Kingdom, 3-5th September 2019;

Alves P, Mergulhão FJ (**2019**) Performance assessment of antifouling peptide coating for reducing bacterial attachment using a parallel plate flow cell, DeLNAM Meeting, Ghent, Belgium, 16-20th November 2019.

2. Literature review

2.1. Brief history of biofilm engineering

The accumulation of surface-adhered microorganisms has been a research interest since the early decades of the XX century. Indeed, it has been found that any surface, namely a rock, a tooth, the walls of a tube and a medical implant, in contact with an aqueous medium will be covered with a film formed by adhered microorganisms enclosed in a matrix of self-produced macromolecules, constituting what is currently called *biofilm* [1, 2]. The study of these structures gained visibility from the 1970s in the areas of health, biological reactors used in the treatment of liquid effluents, undesirable biofilms in industrial processes and ecology. After a few decades, the relevance of biofilms in the scientific, technological and medical communities has solidified. Nowadays, it is recognized that biofilms are ubiquitous in nature and constitute the most common form of organization in detriment of the free life form, as planktonic cells [3].

With the technological progress, the formation of undesirable deposits of microorganisms, sometimes encompassing inorganic particles, called *biofouling*, began to take place at an industrial level. The formation of these deposits causes several problems, namely the increased thermal resistance on heat transfer surfaces, increased pressure losses requiring higher pumping power, detachment of deposits leading to product contamination, particularly in the food industries. The adverse economic consequences stimulated the study to understand how these microbial communities were formed to control their development [4, 5].

The engineers wanted to develop models that would allow them to take predictive and preventive action on biofilm formation. However, given the complexity of the phenomena involved (physical, chemical and biological), it was quickly recognized that only multidisciplinary collaboration could help create the necessary knowledge. Thus, studies were initiated in different fields, namely the mechanisms of cell transport to the surface, the interaction forces between microorganisms and the surface, modeling of biofilm formation and population dynamics; modeling of spatial nutrient gradients within the biofilm and nutrient consumption kinetics; matrix composition and structure and population analysis [6].

Biofilm science and engineering had reached, in the early 1990s, a dynamic phase of youth and was in full development, but still in a relatively restricted environment. Although there was already considerable knowledge of the adhesion of microorganisms at this point, particularly in preventing the formation of dental plaque responsible for dental caries, biofilms were still largely ignored by the medical community in general [7]. Nevertheless, technological advances

applied to medicine have made it common practice to use invasive medical devices, such as prostheses, implants, catheters, shunts, stents, contact lenses, among others, which have multiplied the cases and infection associated with highly undesirable biofilms [8]. In fact, despite the care of asepsis in surgical interventions for the insertion of abiotic surfaces in the human body, contamination by commensal microorganisms of the skin is extremely frequent, and after being in a different habitat, they become pathogens, with the aggravation of developing biofilms that are a way of life in which microorganisms have a much higher tolerance to antimicrobial agents being 100 to 1000 times greater than the planktonic cells [9].

In the 1990s and 2000s, along with the extension to the world of molecular biotechnology, the science of biofilms benefited from decisive advances in the field of computer simulation, focusing on discrete programming methods, such as those based on the cellular automata techniques, which allowed the simulation of the temporal and spatial development of the biofilm architecture and contributed to the biofilm dynamics [10].

Nowadays, the complex development of biofilm and the tolerance to commonly prescribed drugs, imposes great challenges for the use of conventional antimicrobials and indicates the need for combined or multi-targeted therapies [11]. In this sense, the study of strategies capable of preventing bacterial adhesion through modification of surface properties, making them, for instance, anti-adhesive may be one of the simplest and potentially most economical ways to delay the formation of biofilm and subsequent infections [12, 13]. However, there are few studies evaluating the effectiveness of these new surfaces in conditions that mimic real scenarios, particularly regarding hydrodynamics. This becomes a critical step in translating research into practical applications.

2.1.1. Understanding biofilms: definition and structure

The attachment process and consequent development of the biofilm mechanisms on surfaces is a very complex phenomenon. This process is based on colloid chemistry and surface-surface interactions [14].

Biofilms can be composed of populations derived from a single species or a community of diverse species but, in both cases, the development of biofilm behavior requires the multistage approach described below [15]. Although the function and appearance of biofilms in several environments may be different, many species including *E. coli* have been shown to originate from the same sequence of events [16], which include an initial adhesion to the surface, formation of the microcolonies, ripening microcolonies in the developing matrix thereby allowing the maturation of biofilm and dispersion of sessile bacteria (Figure 2.1).

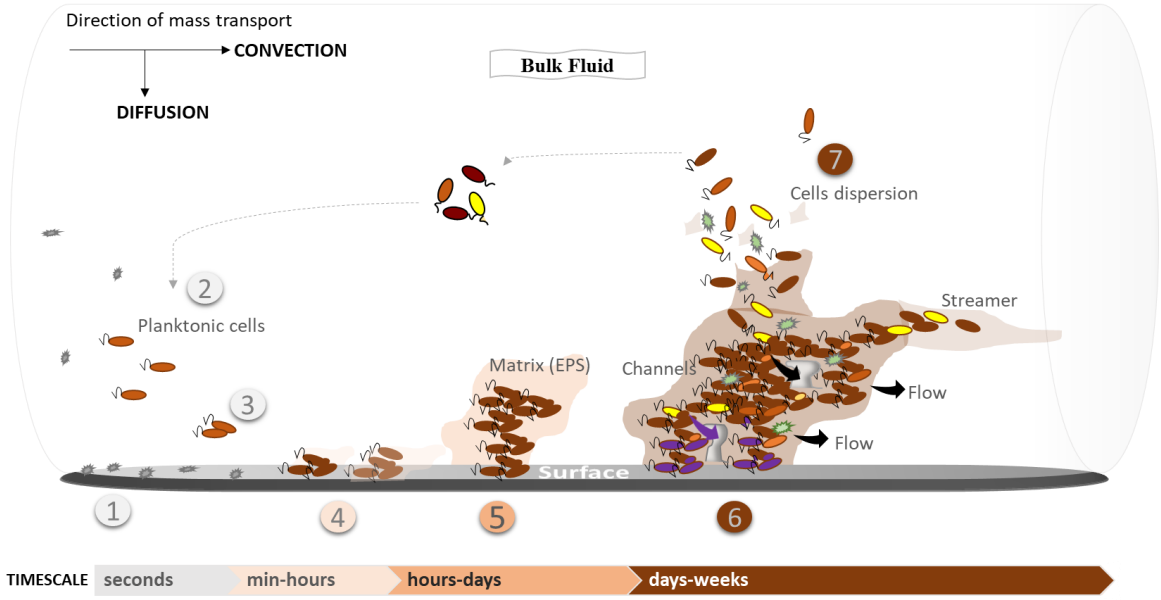

Figure 2.1. Representation of the stages of microbial biofilm formation. (1) Substratum pre-conditioning by ambient molecules; (2) Free-floating bacteria (planktonic cells) in the bulk fluid; (3) Coaggregation, cell-cell adhesion; (4) Microcolonies formation, initial reversible attachment leading to proliferation; (5) Irreversible attachment that includes the production of an extracellular polysaccharides substances (EPS) matrix; (6) Development of biofilm architecture with the water channels and the convective flow within these channels leading to the biofilm maturation; (7) Mature biofilms including detachment and dispersion of cells from the biofilm into the surrounding environment and the cycle repeats.

This model describes the initial mass transport from the aqueous environment in which organic matter is present (e.g. seawater, milk, tear fluid, urine, blood or saliva) on the surface, originating a conditioning film before the bacterial adhesion. Transport of microorganisms towards a substratum surface, as the second step in biofilm formation where a reversible cell attachment occurs [17].

The cells involved in the initial colonization start forming a porous structure where the microbial cells initiate glycocalyx (exopolysaccharide) production. During this stage, microcolonies get involved in extracellular matrix polymers originating three-dimensional (3D) structures being able to concentrate products of their own metabolism and regulate their effective contact with the fluid phase [18]. This polymeric matrix consists of several components including proteins, nucleic acids, other extracellular polymeric substances (EPS) and water (the major element of the biofilms, up to 97%, being responsible for nutrient flow inside the biofilm matrix) [15], representing approximately 85% of the biofilm [19]. The synthesis of this polymer matrix appears to be regulated by a variety of factors of which surface-attachment appears to be critical. The exopolymers serve two primary functions within the biofilm: first, the polysaccharides such as β-1,6-N-acetyl-D-glucosamine polymer, colanic acid, and cellulose, have been detected in the

biofilm matrix of *E. coli* [20] are produced in large amounts after initial fixation of the cell surface, likely to act as cement with which bacteria can reinforce the primary mechanisms of adhesion [21]. Then, the existence of the EPS [22] provides stability for these structures protecting the biofilm from the outer environment and impacts [23-25]. Bacteria living in biofilms are able to evade the host defense mechanisms [18, 26, 27]. The remarkable feature of the pedestal-like structures, water channels and pores have been explored in some detail [28, 29] showing that these structures are formed to enable the convective and diffusive transport of oxygen and nutrients that penetrate to all levels of the biofilm [30, 31]. It is believed that the biofilm formation starts when certain environmental factors trigger the fluctuations in cell-population density through a mechanism called *quorum sensing*. This mechanism allows the cells in the biofilm to better adapt their phenotype and gene expression to changes in the surrounding environment. Many bacteria use this mechanism to regulate a diverse array of physiological activities including symbiosis, virulence, competence, conjugation, motility and biofilm formation [32].

The forces present around the biofilm are very important since they promote cell attachment but also cell dispersion from the biofilm, leading to migration of these cells to new areas of the surface where they can form new biofilm structures (Figure 2.1). Detachment can be classified into erosion, sloughing, abrasion and grazing, but only the first two processes are assumed to be significantly affected by shear stress. Erosion is defined as the removal of the single cells or small particles from the surface of the biofilm detaching into the bulk fluid. Sloughing, in contrast, refers to the detachment of relatively large portions of the biofilm as a result of rapid changes or depletion of oxygen and nutrients. Thus, when the balance between growth and detachment is achieved, reaching a maximum average thickness of biofilm, the system is considered at the pseudo-steady state [33, 34].

It is known that biofilm formation is affected by different factors, such as surface properties, nutrient availability, hydrodynamics, temperature, pH and microbial cell properties [35] (Table 2.1). The bacterial structure is also very important since the presence of external filamentous appendages as flagella, pili and fimbriae, in addition to EPS, have been reported as critical for the initiation of *E. coli* biofilm formation [36], the model organism used in this thesis. Among these factors, the surface properties, the hydrodynamics and nutrient availability will be addressed in detail in this thesis.

Table 2.1. Variables involved in cell attachment and biofilm formation. Adapted from Donlan [35], Campoccia et al. [37], Richter et al. [38]

Properties of the adhesion surface (morphometry and physico-chemical properties)	Texture or roughness Surface energy Hydrophilicity/superhydrophilicity Hydrophobicity/superhydrophobicity Conditioning film
Properties of the bulk liquid (environmental conditions)	Flow velocity Temperature Host proteins/host adhesins Shear rate [a]/fluid viscosity Fluid flow rate [b] pH
Properties of the cell	Gram-positive/ Gram-negative Genus/Species Bacterial shape Cell surface hydrophobicity Extracellular appendages (e.g. fimbriae, flagella, pilli) Signaling molecules (e.g. cyclic diguanylic acid; Antigen 43)

2.1.2. Biofilms in the environment, industry and health

Since microorganisms are ubiquitous in nature, often interfering with human activity, it is perfectly logical that their ability to form biofilms has a pronounced impact on various contexts of interest such as environmental, industrial and biomedical [39] (Table 2.2). The biomedical area will be described in more detail since it is the one that received the greatest attention in the thesis.

In the environment, biofilms can damage civic and industrial infrastructure, causing harm to the environment. The so-called *biofouling* is a common feature on all submerged surfaces in aquatic environments, building the basis for later development of mature fouling communities [40]. Their detrimental impacts have serious implications on the efficiency of shipping, aquaculture and coastal industries in general [41]. Intense efforts have been undertaken to control biofouling on a wide range of surfaces, such as ship hulls [49]. This fouling phenomenon increases the surface roughness of the ship hulls, hence increasing their frictional resistance when the vessel moves through the water. As a result, speed is known to be reduced by 10%, leading to higher fuel

[a] The shear rate is the derivative of the velocity in the perpendicular direction from the wall. In this system, the shear rate gives an indication of the drag force felt by adhering cells and it is also a measurement of the frequency at which cells contact the wall. Mathematically, the shear stress in Newtonian fluids is proportional to the shear strain rate in the fluid, where the viscosity is the constant of proportionality.

[b] The (volumetric) flow rate, usually indicated as Q. Preferably expressed in m^3/s, or sometimes for practical reasons in ml/min or ml/s. Describes the volume of fluid passing through the system, regardless of its dimensions. The resulting average velocity of the flow, v_{av} (m/s), on the other hand, is greatly dependent on the cross-sectional area of the flow system and can be simply obtained by dividing the flow rate by the cross-section.

consumption and associated emissions of exhaust fumes (around 40%) [40]. Immersed offshore structures (cages, netting and pontoons), onshore equipment and structures such as pumps, pipelines, filters and holding tanks are the most affected areas by this process, due to physical damage, increased drag and accelerated biocorrosion. In the European Union, up to 10% of the total aquaculture industry expenditure concerns biofouling-related problems [42].

Table 2.2. Biofilms: context and the action type on human activity

BIOFILMS CONTEXT [c]	ACTION TYPE		Refs.
	Beneficial	**Harmful (Concerns/Specific process and result)**	
Environment 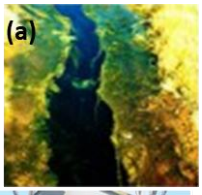 	Particularly in aquatic ecosystems, they contribute to sustaining food chains made up of various animal and plant species, as well as to nutrient recycling.	Implications on the efficiency of shipping, aquaculture and coastal industries. Affected areas such as the immersed offshore structures (cages, netting and pontoons), onshore equipment and structures (pumps, pipelines, filters and holding tanks). Increase drag and accelerate biocorrosion. Infection of plants and animals can cause serious disturbances in ecosystems.	4, 39-42
Industry 	In bioremediation and wastewater treatment, they allow better control of man-made pollution. Production of various compounds in reactors.	Biological fouling in food industry leads to an increase in maintenance costs, decreases operational efficiencies and promotes food contamination. Dissemination of foodborne pathogens - contamination and spoilage of processed foods, surface corrosion and deterioration of equipment components. Massive annual cost for the industry.	4, 43-45
Health 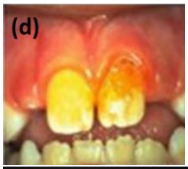 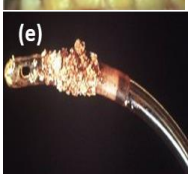	Biofilm formation in the teeth or vagina by commensal microorganisms prevents pathogenic microorganisms from forming biofilms themselves.	Infections caused by colonization of insertion of medical devices such as catheters or prostheses leads to higher healthcare costs, including deaths. Its formation directly in tissues of immunocompromised patients or with genetic abnormalities (in the case of cystic fibrosis) causes severe infections. Higher healthcare costs.	4, 11, 27, 46-48

[c] Biofilms are present everywhere: (a) natural biofilms growing in and around a stream; (b) a ship hull colonized by various fouling and invasive marine species; (c) biofouling in industrial pipes; (d) teeth with biofilm and (e) catheter with biofilm.

Biological fouling in the food industry also leads to an increase in maintenance costs, decreases operational efficiencies and promotes food contamination leading to economic losses and the dissemination of foodborne pathogens [43]. Since bacteria are able to colonize a wide variety of surfaces including those found in food industry settings (e.g. food processing equipment, walls and floors of the workspaces, storage and transport tanks) biofilm development on such surfaces often occurs [44]. This event can lead to contamination and spoilage of processed foods, surface corrosion and deterioration of equipment components [45] with emphasis on product contamination, being a special matter of concern since it presents a hazard to human health [50]. On the other hand, surface corrosion and equipment damage also imply a massive annual cost for the industry [43].

According to the National Institutes of Health, the development and persistence of surface-attached microbial communities, are responsible for about 75% of human bacterial infections [27]. Biomedical infections related to biofilm formation affect 17 million Americans per year, causing higher healthcare costs including more than half a million deaths [47, 48]. Regarding Europe, The European Center for Disease Prevention and Control reported that, annually, the number of patients with at least one nosocomial infection (NI) is superior than 4 million. Additionally, approximately 4.5 million NIs are directly responsible for about 37 000 deaths leading as well to a further 111 000 fatalities. Healthcare-associated infections (HCAI) in Europe is responsible for an estimated 16 million extra days spent in the hospital every year and accounts for roughly 25% of adverse events suffered by hospital patients, amounting to estimated direct costs of about €7 billion [51]. The source of the microorganisms causing these infections might be the skin of hospitalized patients or health-care workers and the hospital environment, which requires a hospital organization, management, and structure for prevention of HCAI [52].

2.2. Biomaterial-associated infections: a clinical problem

Biomaterial-associated infections (BAI) are expected to increase as the use of medical devices, such as catheters, artificial heart valves, prosthetic joints, as well as other implants, since has increased drastically over the past century and is expected to continue alongside the aging of our society. This is related to the fact that we have an ever-improving technology within the medical field, and the demand for medical devices to restore function and quality of life is higher than ever.

Overall, most of the biofilm-related infections are associated with indwelling medical devices (IMD) such as in intravenous catheters [53], prosthetic heart valves [54], urinary catheters [55], orthopedic devices [56], cardiac pacemakers [57], intrauterine devices [58], biliary tract stents [59], breast implants [60], contact lenses [61] and voice prosthesis [62] (Figure 2.2).

DEVICE-RELATED INFECTIONS
Ventricular derivations
Contact lenses
Endotracheal tubes
Central vascular catheters
Prosthetic cardiac valves; pacemakers
Breast implants
Peripheral vascular catheters
Urinary catheters
Orthopedic implants

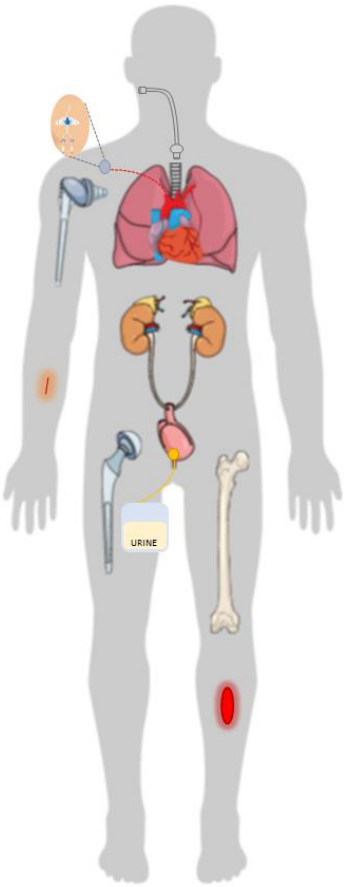

TISSUE-RELATED INFECTIONS
Chronic sinusitis
Chronic dental plaque and laryngitis
Endocarditis
Lung infection (cystic fibrosis)
Kidney stones
Biliary tract infections
Urinaru tract infections
Osteomyelitis
Chronic wounds

Figure 2.2. Biofilm-related infections. Adapted from Lebeaux et al. [63].

Urinary tract infections (UTIs) are one of the most common affecting around 150 million people each year worldwide [8, 64] and are one of the major reasons for antibiotic use [65]. The major risk factor for UTIs is the use of urinary catheters. The process of catheterization occurs via the urethra into the bladder enabling the measurement of the urine output. Catheter-associated urinary tract infection (CAUTI) is the most common HCAI in the USA and worldwide. Besides, it has been reported that patients with CAUTIs might develop other complications, leading to longer hospital stays and increased mortality [65, 66].

The surface of IMDs offers a favorable environment for the colonization and growth of a large number of microorganisms, with a predominance of Gram-negative and Gram-positive bacterial species, as shown in table 2.3.

Table 2.3. Microorganisms commonly found in indwelling medical devices-associated biofilm infections

Indwelling medical devices	Prevalent causative microorganisms	References
Urinary catheters	*Escherichia coli, Enterococcus faecalis, Enterobacter sp., Preoteus mirabilis, Pseudomonas aeruginosa, Klebsiella pneumoniae, Acinetobacter baumannii*	[67, 68]
Contact lenses	*P. aeruginosa, Staphylococcus aureus, Staphylococcus epidermidis, E. coli, Candida* sp., *Acanthamoeba* spp., *and Fusarium* spp., *Achromobacter, Stenotrophomonas, Delftia*	[69, 70]
Intrauterine devices	*S. aureus, C. albicans, Lactobacillus spp., Enterobacteriaceae, Enterococcus faecalis, Prevotella* sp., *Bacteroides* spp., *E. coli, Gardnerella vaginalis*	[58, 71, 72]
Biliary tract stents	*Enterococcus* spp., *E. coli, Klebsiella* spp., *Clostridium* spp., *Streptococcus* spp., *Staphylococcus* spp., *Candida* sp., *Pseudomonas* spp.	[73-75]
Breast implants	*E. coli, S. epidermidis, Propionibacterium acnes, peptostreptococci, C. perfringens, Ralstonia* spp.	[76-78]

2.2.1. *Escherichia coli* pathogenesis

The initially adhering microorganisms are of pivotal importance as they create the link between the implant surface and the biofilm entity. *E. coli*, a universal bowel inhabitant, present in several medical device-associated infections (Table 2.3), is the most common causative agent in UTIs [26, 79, 80]. *E. coli*, a Gram-negative and facultative anaerobic bacteria, is undoubtedly the most investigated bacterial species being used as model organism for the study of surfaces colonization [81]. These bacteria possess specialized virulence factors such as adhesins, toxins, iron-acquisition systems, polysaccharide coats and invasins for their pathogenicity [81]. From a genetic and clinical perspective, *E. coli* strains can be broadly categorized as commensal strains, intestinal pathogenic (such as enteric or diarrheagenic) strains, and extraintestinal pathogenic *E. coli* (ExPEC) or uropathogenic *E. coli* (UPEC) on the basis of their enhanced ability to cause extraintestinal disease, including UTIs [81-83] and bloodstream infection, resulting in the systemic inflammatory response syndrome (SIRS) [84], that contributes to billions of health care dollars and hundreds of thousands of lives lost each year [85].

Adherence to host cells is the initial step of an *E. coli* infection being essential for invasion and depends mainly of specific cell surface structures such as pili, or fimbriae, that recognize specific ligands on the substrate [86] it is well established that adhesin molecules help maintain biofilm structure and function as major components of the biofilm matrix [87]. For example, the FimH adhesin protein present at the tip of type I pili in *E. coli* experiences conformational changes that enable the cells to attach firmly to the surface under high flow [88]. For instance, shear forces

induced by rapid urine flow induce a mechanism known as a catch-bond conformation that prevents pathogen elimination in the urine stream [89]. Other example of cellular components in *E.coli* includes curli fibres in which the main CsgA subunit exhibits flexible local regions that contain aromatic residues promoting hydrophobic interactions, which strengthen adhesion to surfaces [90]. In general, *E. coli* strains demonstrate motility driven by flagella, an adhesin, that provides a physical contact with the surface having also a crucial role in initial bacterial attachment [3] as well as the type I pili in *E. coli*, have specific receptors that bind to specific substrates [91]. It is reported that *E. coli* harbouring flagella improve the adhesion on rougher surfaces compared with flat surfaces, probably because flagella can access crevices and initiate adhesion [92]. Although, this is not an absolute requirement as nonmotile bacteria can still form biofilms under certain conditions, as shown for *E. coli* [93]. In these cases, if the expression of strong adhesion factors are superior, the presence of flagellum is dispensable for the attachment of bacteria to the surface and consequently form biofilm [20].

In the last decades, *E. coli* has also been found to persist and re-emerge after the use of antimicrobial treatments commonly prescribed, such as ampicillin [81, 83]. This is due to many factors including reduced penetration of antibiotics in biofilms and/or cellular extrusion of the drugs [94]. As described, biofilm cells produce EPS matrix that protects the biofilm, acting as a barrier to antibiotic penetration, and that is strongly influenced by the substratum and the bulk phase [95, 96]. These complications have led to the development of a new area of biofilm studies: disinfection and control. Similar to the control of planktonic microorganisms by antibiotics, for which the minimum inhibitory concentration (MIC) has been defined, there are now some methods for determining the minimum biofilm eradication concentration (MBEC), which represents the minimum antibiotic concentration required for eradication of biofilm and is always superior to MIC [97]. The dimension of this problem worldwide is enormous and the fact that bacteria associated with biofilms are more resistant than their planktonic counterparts is a global healthcare concern [25]. Despite the solid knowledge that has been accumulated about the later stages of biofilm formation, little is known about the initial stages. Thus, it becomes essential to understand the adhesion mechanisms, since eliminating sessile bacteria is problematic. This is due to their extreme resistance not only to antibiotics but also to hydrodynamic shear forces (since the interaction forces between the implant surface and the microorganisms need to be strong enough to withstand shear-off) [98, 99].

2.3. Strategies to prevent or delay biofilm formation

Rising rates of antimicrobial resistance, fuelled by the overuse of antibiotics in humans,

are a serious threat to global public health. Alternatives to antibiotics for the prevention of recurrent infection, like UTI, are attractive options to reduce the risks of antimicrobial resistance.

The most studied nonantibiotic management options as preventive or to eliminate biofilms include mechanical or chemical cleaning as well as material replacement in industry or medical device replacement in the biomedical field. This process entails high costs and they are not always effective [100, 101]. Research on microbial biofilms is proceeding on many fronts; however, understanding the factors that affect the adhesion process continues to be the key to prevent or control biofilm formation. These factors are described below and include surface properties, hydrodynamics and platforms for *in vitro* studies, in more detail the use of flow cells.

2.3.1. The role of surface properties

It is proven that the physicochemical properties of the surface may exert a strong influence on the attachment process [102, 103]. The fate of adhesion is dictated by the sum of attractive as well as repulsive forces between the cell and the surface of a material. Bacteria experience several forces when moving from the liquid environment to the surface that is affected by a set of physicochemical, thermodynamic and microbiological phenomena. There are some theories that allow quantifying variations of the interaction energy between the surfaces involved. However, they only consider the physicochemical and thermodynamic aspects of adhesion, omitting the fact that microorganisms are "living surfaces".

The physicochemical interactions include the Lifshitz van der Waals (which are generally attractive), electrostatic (which are modulated by ionic strength and pH of the liquid environment) and Lewis acid-base hydrophobic interactions (which are attractive or repulsive depending on the environment, bacterium and surface chemistries) [17, 23, 104]. The surface of a cell or substrate has a surface energy that is a measure of the attractive interfacial forces. Thus, a surface can be classified into hydrophilic ($\Delta G > 0$ mJ/m^2) or hydrophobic ($\Delta G < 0$ mJ/m^2) if the interaction between the two entities is stronger than the interaction of each entity with water [105]. This physicochemical analysis has been used intensively since convenient and fast methods such as contact angle measurement are available [106, 107]. Contact angle measurement studies the wettability of a surface that is related to the surface energy, and it is determined by the contact angle of a sessile drop of liquid on a solid surface. Depending on the hydrophobicity level of the bacteria and the material surfaces, bacteria can adhere differently. It is reported that hydrophobic surfaces are more suitable for bacterial adhesion than hydrophilic ones. This occurs due to a physical barrier known as hydration layer resulting from hydrogen bonding between functional groups at the surface and water molecules from the surrounding fluid [108, 109].

The prediction of whether bacteria will adhere to a surface occurs through the variation

of Gibbs energy. Some theories concerning the forces involved during the process were developed. The thermodynamic approach includes the Lifshitz van der Waals forces and the Lewis acid-base interactions and, the Derjaguin, Landau, Verwey, Overbeek (DLVO) theory assumes that the system energy is the sum of the Lifshitz van der Waals forces and electrostatic interactions, both depending on the separation distance between particles [110]. In the first model, the electrostatic interactions and the interactions mediated by the exopolymers as well as extracellular appendices are not considered. The thermodynamic theory quantifies the energy involved in the adhesion and thus quantitatively predicts the possibility of establishing an interface between the bonding surface and the microorganism. Bacterial cell and liquid or solid surface thermodynamics are described by the surface tension parameters [111]. The DLVO theory explains the adhesion of microorganisms considering the interactions of the colloidal particles and despises all microbiological aspects of adhesion. In this theory, the forces of interaction are particularly long-range forces, and therefore only predict if microorganisms approach a certain distance from the surface. However, this theory neglects the Lewis acid-base interactions and thus currently, an extended DLVO (xDLVO) theory was developed considering the three interaction energies. Nowadays, the thermodynamic theory and xDLVO have been applied to predict bacterial adhesion to different surfaces [17, 110]. The characteristics of the two interacting surfaces, such as hydrophobicity, electric charge, and environmental conditions affect all the adhesion process and consequent biofilm formation. Understanding the thermodynamics of microbial adhesion is important as it enables us to predict whether the adhesion of a bacterium is favorable on different surfaces.

With the knowledge of the physicochemical parameters of the surface, it is possible to develop new strategies that make the surface less attractive to microorganisms. Several studies have tried to correlate bacterial adhesion with the physicochemical properties of the surface such as the study of the ratio between apolar Lifshitz van der Waals components (γ^{LW}) and electron donor components (γ^-) although with limited success [112-114]. A recent study correlating the *E. coli* adhesion with the γ^{LW}/γ^- ratio, shows that bacterial adhesion is reduced in surfaces with lower γ^{LW}/γ^- and enhanced otherwise [114]. This finding could be helpful in the manipulation of the surface energy and charge of the materials under study to promote the design of new coatings controlling these components or in the selection of existing materials, but also taking into consideration the forces that will be applied [104, 115, 116].

In model organisms, such as *E. coli* surface properties are very important in the adhesion process [117]. It has been shown that bacteria tend to bind preferentially to surfaces patterns in the micrometer range, rather than smooth surfaces. Contradictory, studies report conflicting results

regarding on the relationship between the nanometer-scale surfaces (nanopatterning) and bacterial adhesion [118, 119]. It has been demonstrated that although these surfaces prevent the initial adhesion of *Sthaphylococcus epidermidis*, the same did not happen with *E. coli*. This result can be explained with the cell shape and characteristics of the bacterial surface [120].

Thus, it is important to study the relationship between the surface of bacterial cells and the surface properties of the material to which they adhere. Generally, bacteria are negatively charged in aquous suspension, and these cells readily colonize the material surfaces with positive to neutral charges [121]. Also, the effect of surface hydrophobicity on bacterial adhesion depends on the hydrophobicity of the bacterial cell and is reported that hydrophobic bacteria preferentially colonize hydrophobic materials and vice versa [121]. Although, these conclusions are not linear since the process is complex and depends on several factors, such as the characteristics of the bacteria, the target material surface, and the environmental factors (e.g. presence of serum proteins or antibacterial substances [3].

Many advances have been made on surface modifications for the construction of artificial surfaces to modulate biological responses as well as improve device performance [122]. In this sense, is important to analyse surfaces after their treatment based on their topographic and chemical characterization, composition and surface energy. Thus, technology has been evolving to obtain a complete surface analysis. Some of these techniques are described in table 2.4 and are based on the study of the impact of high energy particles or X-rays under ultra-high vacuum spectroscopy, adsorption or emission, depth of analysis, sensitivity and resolution.

Table 2.4. The most common surface characterization techniques. Adapted from Nosonovsky & Bhushan [123], Singh et al. [124], Agarwal et al. [125]

Technique	Principle/ Operation	Provided information
Contact Angle Goniometry	Liquid wetting of surfaces; Angle at the interface where water, air and solid meet. This value is a measure of how the surface is wetted by water.	Wetting properties; Roughness.
Quartz Crystal Microbalance (QCM)/ Surface Acoustic Waves (SAW)	Liquid wetting of surfaces; Mass perturbations mechanisms which occur on the sensing film.	Change in mass upon deposition.
Infrared attenuated total reflection (ATR-IR) Spectroscopy	Infrared light; Vacuum; Light undergoes multiple internal reflections in the crystal of high refractive index. The sample is in contact with the crystal.	Functional groups, orientation (surface composition).
UV-vis Spectroscopy	Examining analyte interactions with molecularly imprinted polymers (MIPs); The change in absorbance is measured as a function of wavelength.	Packing density; Molecular footprint.
Fluorescence Spectroscopy	Absorption of photons allows a chromophore to reach an excited state. The photon absorption induces excitation and can be measured; The concentration of the analyte is directly proportional to the intensity of the emission.	Packing density; Molecular footprint.

Table 2.4. (Continued)

Technique	Principle/ Operation	Provided information
Ellipsometry	Reflected light beam; Light undergoes some change in polarization when it is reflected off the surface of a material. The polarization change is characteristic of the surface structure of the sample.	Film thickness; Refraction index.
Surface Plasmon Resonance (SPR)	Resonant oscillation of conduction electrons at the interface between negative and positive permittivity material stimulated by incident light. Measuring adsorption of material onto planar metal (typically gold or silver) surfaces or onto the surface of metal nanoparticles.	Film thickness; Refractive index of thin films upon analyte interaction.
X-ray Photoelectron Spectroscopy (XPS)	X-rays cause emission of photoelectron with characteristic energies; Vacuum; Measures the elemental composition, empirical formula, chemical state as well electronic state of the elements that exist within a material.	Elemental composition – surface chemistry (quantitative analysis).
Auger Electron Spectroscopy (AES)	Vacuum; Auger electrons emission caused by electron bombardment. These electrons are directed into an electron multiplier for analysis.	Elemental composition (surface conductivity needed).
Ion Scattering Spectroscopy (ISS)	Vacuum; A beam of ions is scattered by a surface and the kinetic energy is measured. The peaks observed corresponds to elastic scattering of ions from atoms at the surface of the sample.	Elemental composition (surface composition).
X-Ray Reflectivity (XRR)	Reflect a light beam of X-rays from a flat surface measuring the intensity of X-rays reflected in the specular direction.	Surface-sensitive analytical technique (thickness, roughness).
Near Edge X-ray Absorption Fine Structure (NEXAFS)	Absorption of an X-ray photon by a core level of an atom in a solid and the consequent emission of a photoelectron.	Chemical identity; Molecular orientation.
Spectroscopy Secondary Ion Mass Spectrometry (SIMS)	Vacuum; The surface is sputtered with a focused primary ion beam that causes a secondary ion emission. The ions ejected are collected and analysed.	Elemental, isotopic and molecular composition.
Atomic Force Microscopy (AFM) Scanning	A cantilever is used with a tip to scan over a sample surface.	Structure; Topography;
Scanning Tunneling Microscopy (STM)	Measures topography of surface electronic states using a tunneling current that is dependent on the separation between the probe tip and a sample surface. When a conducting tip is carried very near to the surface to be examined, a bias (voltage difference) applied between the tip and the sample can allow electrons to tunnel through the vacuum between them. Observation: This technique served as the groundwork for the subsequent advancement to Atomic Force Microscopy (AFM).	Morphology; Structure;
Scanning Electron Microscopy (SEM)	The electrons interact with the sample producing various signals containing information about the surface topography and sample composition. The electron beam is scanned, and the position of the beam is combined with the signal strength detected to produce an image.	Imaging; Grain structure.
Transmission Electron Microscopy (TEM)	A high energy beam of electrons is used through a very thin sample. The interactions between the electrons and the atoms can be used to observe the crystal structure as well dislocations and grain boundaries features.	Atomic structure; Chemical bonding.

Despite the fact that different approaches of surface modification are beginning to emerge, it is necessary to advance to a point that is possible to satisfy the most demanding applications, bearing in mind that chemical and structural stability and chemical selectivity are the most pressing issues [126, 127].

Table 2.5 reports a broad list of the effect of the surface properties on cell adhesion that have been developed in the last 37 years. In these studies, different materials (polymeric, coatings, plasma-treated surfaces, metallic surfaces, etc), were evaluated considering different contexts (environment, industry and health). Some of these applications include the reduction of protein adsorption and thrombogenicity, control of bacterial adhesion, growth and differentiation, improved wear and/or corrosion resistance, and potentiation of electrical conductivity [128]. The experiments were performed under different hydrodynamic conditions, temperature, time, culture medium and microorganisms using different platforms, in which the flow cells and agitated microtiter plates were the most used. Additionally, it is possible to conclude that the production of modified surfaces falls into two general groups, physicochemical modifications and surface coatings. The first involves alterations to the atoms, compounds or molecules as well as the surface topography. These modifications include chemical reactions, such as oxidation, reduction, acetylation, etching and mechanical roughening/polishing and patterning. Surface coatings can be composed of grafting including tethering of biomolecules, noncovalent and covalent coatings and thin-film deposition. These approaches have as critical requirement the stability which is linked to mechanical durability (resistance to cracking, delamination, etc) and chemical stability, particularly in a physiological environment [125].

In Table 2.5 are listed 77 studies and it is possible to observe that in some of them it was not possible to find a correlation between surface physicochemical properties and bacterial adhesion. Despite that fact, the parameters most often used in the studies were the surface hydrophobicity (ΔG) and the free energy of adhesion (ΔG^{Adh}). For the remaining studies, where a correlation between biofilm formation and surface properties was found, a unique parameter was not identified to correlate all the data, as other factors such as the hydrodynamics, bacterial strains and the surrounding environment, could interfere. In addition to chemistry, even the morphology of a surface can be structured and targeted to reduce the adherence of bacteria. Thus, several *in vitro* and very few, *in vivo* investigations have attempted to elucidate whether adequate morphology at micro and nanometric levels could be used to decrease the rate of BAIs [129]. A study performed on glass surfaces with different nanostructures has shown that surface topography can determine different bacterial behavior not only in terms of adhesion but also in terms of cell metabolism. Smoother topography down to nanometre levels is associated *in vitro* with lower

adhesion of Gram-positive and Gram-negative bacteria [130]. This study supports the various observations in previous studies reporting that rough and porous interfaces generally increase interactions with bacteria, enhancing bacterial adhesion [37].

In conclusion, the compilation in table 2.5 highlights the difficulty in controlling bacterial adhesion by manipulation of the surface properties. Additionally, the majority of these studies are focused in the reduction of the biofilm formation, showing that these authors are looking for surfaces with antibacterial properties. It is also known that the devices have to maintain the desirable interactions under the simulated physiological conditions. However, it is possible to observe that there are only few studies that attempt to mimic the real conditions in which the materials will be inserted. This brings serious limitations to the performance assessment of the best antiadhesive surfaces when correlating the *in vitro* and *in vivo* results.

Table 2.5. Examples of developed work in the last four decades in which different surfaces (polymeric surfaces; anti-adhesive; anti-bacterial coatings based on disinfectants and bactericidal substances; intrinsically bioactive material) were used under different operational conditions to evaluate the performance of surfaces on bacterial adhesion or biofilm process in different contexts (environment, industry and health). The microorganism's legend is described at the end of the table

Surfaces	Microorganism		Platform	Medium	T (°C)	Hydrodynamics	Assay Time	Parameters evaluated	Concluding remarks	Refs.
	G -	G +								
Environmental & Industrial application										
Glass treated with Si-(3-aminopropyltriethoxylane (APTES)) coupled with acid chlorides or carboxylic acids to the amine groups; Poly(ethyleneoxide) (PEO) - Food industry	EC ST	LM SA	Capped bottles	Sterile MOPS	37	Gentle shaking	24 h	Protein adsorption; Contact angle measurements; Surface chemistry	• Hydrophilic uncharged surfaces showed the greatest resistance to protein adsorption and so may be the best method for preventing cell adsorption to synthetic substrates.	131
Glass; Metal-oxide coated glass - Natural and engineered systems	EC BC PA	BS	Microbial adhesion to glass (MAG) test	Luria broth (Miller)	n.d.	Shaking conditions	n.d.	Contact angle measurements; Zeta potential; Surface roughness	• Increasing the ionic strength increased adhesion; • Adhesion was not significantly correlated with bacterial charge and contact angle; • Surface energy was a much better predictor of adhesion to different surfaces.	132
Glass - Bioremediation		PF	Glass tubes	n.d	n.d.	n.d.	1 h	Biofilm age; Nutrient concentration; Suspended cell concentration; Surface roughness	• Increasing glucose concentration, suspended cell concentration, surface roughness, and fluid velocity caused an increase in the adhesive strength; • Biofilms generally grew as a more compact pattern at the higher fluid velocity.	133
Polyethylene; Polypropylene; Granite - Kitchen surfaces applications	SE		6-well microtiter plate (MTP)	Phosphate-buffered saline (PBS)	25	100 rpm	1 h	Contact angle measurement; Surface roughness; Bacterial adhesion	• The adhesion could not be explained in terms of surface hydrophobicity and roughness of the materials tested. • The adhesion is strongly strain dependent, and this can constitute a factor of virulence among the different serotypes.	134
ASI 304 and 316 stainless steel; Copper; Polyvinyl chloride; Polypropylene; Polyethylene; Silicone; Glass – Drinking water distribution networks	Isolates from drinking water (Heterotrophic bacteria)		24-well MTP	PBS	RT	150 rpm	2 h	Thermodynamic parameters; Bacterial adhesion	• The mechanisms of adhesion, other than cellular physicochemical surface properties may play a determinant role on bacterial adhesion. • Surface physicochemical properties and thermodynamic approaches did not provide conclusive results.	135

Table 2.5. (Continued)

Surfaces	Microorganism		Platform	Medium	T (°C)	Hydrodynamics	Assay Time	Parameters evaluated	Concluding remarks	Refs.
	G -	G +								
Polysulfone; Polysulphone; Polyethersulfone; Regenerated cellulose ultrafiltration membranes – Water treatment	EC PP AC		n.d.	Distilled sterile water	20	Shaken	1-4 h	Contact angle measurement; Bacterial adhesion	• The adhesion of relatively hydrophilic EC to membrane surfaces is essentially lower comparing with the adhesion of more hydrophobic PP, or AC cells; • The adhesion to hydrophobic surfaces was higher than to hydrophilic cellulose one; • Membranes with deposited TiO2 particles under ultraviolet (UV) irradiation demonstrates a strong photobactericidal effect.	136
Ni-P nanocomposite coatings with TiO_2 and PTFE; Stainless steel – Metal used in heat exchangers, ship hulls and pipelines	PF CM VA		Static tank; Dynamic PPFC	Sea salt peptone (SSP)	28	Static; Shear stresses: $5.2x10^{-6}$ N/m^2 -$2.1x10^{-4}$ N/m^2	6, 12 and 24 h (bacterial adhesion – static immersion); dynamic (10 days)	Extended DLVO (Derjaguin, Landau, Verwey and Overbeek) theory; Surface free energy; Chen and Qi (CQ) ratio (γ^{LW}/γ^{-}); Bacterial adhesion	• The interaction energy has a strong correlation with the CQ ratio; • For the design of the antifouling release coatings use the lowest CQ ratio approach.	112, 137
Glass; PVC; Glass coated with beef extract, casein, and homogenised and unhomogenised mil – Food industry		LM	CoverWell perfusion chamber	Tryptic soya broth (TSB)	37	0.0505 and 0.7620 Pa	30 min	Contact angle measurements; Initial adhesion rate (IAR); Flow rate	• The IAR was affected by flow rate as the adhesion decrease at higher shear stress for most strains; • No correlation between surface hydrophobicity and IAR was observed.	138
Nylon; Melamine; High-density-polyethylene [HDPE]; Acetal polymeric plastic – Waste water treatment	Activated sludge		Aerobic reactor	Integrated fixed film activated sludge (IFAS)	17-22	230000 m^3/d	8 days	Contact angle measurements; Surface energy	• Surface hydrophilicity and surface energy were positively correlated with total biomass attachment.	139
Oligo(ethylene glycol) – Natural and engineered systems	CM		Flow cell	n.d.	n.d.	1 mL/min	2 h	Contact angle measurements (free energy of adhesion, ΔG^{Adh}); Surface energy	• The values of ΔG^{Adh} calculated do not correlate with the bacterial adhesion.	140

Table 2.5. (Continued)

Surfaces	Microorganism		Platform	Medium	T (°C)	Hydrodynamics	Assay Time	Parameters evaluated	Concluding remarks	Refs.
	G -	G +								
Glass; Copper; Stainless steel – food industry	EC		6-well MTP; Flat-bottomed MTP	Mueller-Hinton; Low nutrient medium	30	Shaking conditions (115 rpm, 0.27 Pa, Reynolds number (*Re* of 2400)	30 min (adhesion); 6 h (biofilm)	Nutrient; Hydrodynamic conditions; Contact angle measurements; Bacterial adhesion	• Adhesion/biofilm formation are correlated with surface hydrophobicity; • Effect of surface properties is dependent on the nutrient load and shear stress; • Initial attachment performance is a good predictor of biofilm formation.	141
AISI316 stainless steel; Polymethyl methacrylate (PMMA) – Food industry	PF	BC	48-well MTP (adhesion); Rotating cylinder reactor (biofilm)	Diluted nutrient medium	n.d.	Transitional agitation flow (*Re* of 2400)	2 h (adhesion); 7 days (biofilm)	Thermodynamic theory; Effect of the biocide benzyldimethyldodecyl ammonium chloride (BDMDAC) on the removal of biofilms	• It was not possible to correlate adhesion with the thermodynamic theory; • The combined action of BDMDAC and the different hydrodynamic conditions were not effective to stop the bacterial adhesion.	142
Diamond-Like Carbon (DLC) coating modified by incorporation of silicon (aC:H:Si or SICAN) and SICON® (a-C:H:Si:O); Staineless steel (SS) – Food industry	EC Natural flora present in industrial water (from a salad washing line)		6-well MTP; Flat bottomed MTP (adhesion); Flow cell system (biofilm formation)	Low nutrient medium; Industrial water spiked with EC	5; 30 (adhesion); 30 (Biofilm formation)	0.25 Pa	0.5; 2 and 6 h (adhesion); 5 days (biofilm); 6, 18 and 24 h (regrowth)	Contact angle measurements; Bacterial adhesion; Cleanability	• Biofilm formation was reduced on SICAN and SICON® and this may be explained by the lower ratio between the Lifshitz-van der Waals apolar component and the electron donor component. • A higher hygienic status can be attained if SICAN and SICON is used instead of SS until 6 h.	143, 144
Cell extracts (Total cell extract (TCE); Cytoplasm with cellular debris (CCDE); Periplasmic extract (PE)) to conditioning the surface; Polystyrene coupons – Food industry	EC		96-well MTP; Parallel plate flow chamber (PPFC)	Citrate buffer (CB)	30	0.07 Pa	1 h (adhesion); 24 h (biofilm formation)	Contact angle measurements; Multifractal analysis; Surface roughness; Bacterial adhesion	• MTP assays demonstrated that TCE and CCDE decreased initial biofilm formation. • The reduction in biofilm formation upon conditioning was not caused by the change in surface roughness. • Biofilm formation was dependent on the conditioning film concentration. • Under flow conditions all conditioning films reduced biofilm formation.	145

Table 2.5. (Continued)

Surfaces	Microorganism		Platform	Medium	T (°C)	Hydrodynamics	Assay Time	Parameters evaluated	Concluding remarks	Refs.
	G -	G +								
Pipe materials (Polyvinyl chloride; Polypropylene; structured wall high-density Polyethylene and solid wall high-density Polyethylene) - Drinking water distribution systems	Natural flora present in drinking water		Flow cells	Local (Cardiff, UK) drinking water distribution system	14.8–15.6	0.13 and 0.24 Pa	100 days	Surface roughness; Bacterial adhesion	• The surface roughness on biofilm development was seemingly greater than the impact of flow hydrodynamics. • The concentrations of bacteria were lower in the high flow assay on the smoother coupons than in the low flow assay on the rougher coupons.	146
Superhidrophobic surfaces with different microstructure topography-features - Aircrafts, heat exchangers, air conditioners, and turbine blades	n.d.		Cooling stage in a closed laboratory	80% humidity	-20 to 25	n.d.	0 to 260 s	Surface characterization; Contact angle measurements; Coverage (ImageJ software)	• The superhydrophobic surfaces significantly contributed to enhance the defrosting efficiency and the coverage fraction of remained water was only 8.5%.	147
Glass; Perspex - Aquatic environments and marine applications	*Nodosilinea* sp. LEGE 06020 (cyanobacteria)		12-well MTP	Z8 medium supplemented with 25 g/L of synthetic sea salts and B12 vitamin	25	4 and 40 s^{-1}	7 weeks (49 days)	Determination of the shear rate field by computational fluid dynamics (CFD); Contact angle mesurements; Biofilm architecture by Optical coherence tomography (OCT)	• Hydrodynamics play a crucial role in the biofilm maturation rather than during the initial adhesion phase. • The effect of surface hydrophobicity was less important than the hydrodynamic effect; • Biofilm formation was higher under low shear conditions and different shear rates can affect biofilm architecture.	148
Static mixers (Colloidal silica) - Mitigate fouling in tubular membranes	n.d.		Static mixers	Liquid water; Colloidal silica in phosphate buffer	50	10 s^{-1} to 100 s^{-1}	n.d.	CFD anaysis; Viscosity measurements	• Application of twisted tapes is possible and proven in heat transfer as well as for enhance mass transfer and improve fouling mitigation in tubular membrane systems.	149
Biomedical application										
Polymeric surfaces (Teflon; Polyethylene, Polystyrene; Acetal and sulfonated polystyrene) – Biomedical devices	EC	SA SP LM	Wells formed from agarose	Hanks balanced salt solution	21	static	30 min	Thermodynamic parameters (surface tension determinations); Bacterial adhesion	• The surface tension values obtained from bacterial adhesion are in agreement with those obtained from direct contact angle measurement on layers of bacteria.	113

Table 2.5. (Continued**)**

Surfaces	Microorganism		Platform	Medium	T (°C)	Hydrodynamics	Assay Time	Parameters evaluated	Concluding remarks	Refs.
	G -	G +								
Pluronic surfactants [copolymers of Poly(ethylene oxide) (PEO); Poly(propylene oxide) (PPO)] – Biomedical devices		SEa	Glass Petri dishes	PBS	37	static	1 h	Bacterial adhesion; Surfactants effects; Surface modification	• Surfaces modified with surfactants reduces the adhesion of the clinical isolates tested.	150
Benzalkonium chloride - Coating of central venous catheter		SEa	Fermenter with catheters inside	Nutrient broth	37	n.d.	4 h	Measurement of hydrophobicity; Bacterial adhesion	• The antimicrobial hydrophilic catheter is effective in preventing colonisation of both the external and internal surfaces.	151
Polyethylene; Polypropylene; Polythylenterephthalate; Polyetheruthane,; Poly(tetrafluorethylene-cohexafuopropylene) – Biomedical devices		SEa	n.d.	PBS	RT	Gentle shaking	3 h	Contact angle measurements (ΔG^{Adh}); Surface roughness and charge density; Bacterial adhesion	• No influence of surface roughness and charge density on bacterial adhesion was noticed. • A correlation between the ΔG^{Adh} and adhesion was observed.	152
Poly(orthoester); Poly(L-lactic acid); Polysulfone, polyethylene; Poly(ether ketone) - Orthopedic implant polymers	PA EC	SEa	PPFC	TSB; PBS	37	1.9 s^{-1}	1 h	Contact angle measurements (ΔG^{Adh}); Surface chemistry analysis; Bacterial adhesion	• ΔG^{Adh} was correlated with the amount of adherent PA but not for SEa and EC. • Compared to PBS, the TBS has properties that significantly decrease adhesion. • The ΔG^{Adh}, may play a significant role in the adhesion of some, but not all species of bacteria.	153
Glass; Silicone rubber – Coating of catheter material	*L.*		PPFC	Buffer; Urine	RT	15 s^{-1}	3 h	Contact angle measurements; Zeta potentials; Nutrients load effect; Bacterial adhesion	• Adhesion to surfaces differs with strain hydrophobicity and charge; • Urinary components can affect the ability of hydrophilic *L.* strains to adhere to the surface, thus should preferably be studied in urine solution.	154
Polyurethane (PU) with modified Poly(ethylene glycol) (PEG) - PEG1k) carrying terminal hydroxyl, amino and sulfonate groups and PEG3.4k) and PEG3.4k-heparin – Biomedical devices	EC	SEa	n.d.	TSB; Brain Heart Infusion (BHI); Human plasma	37	Constant swirling	24 h	Surface modification; Contact angle measurements; Bacterial adhesion	• All PEG modified surfaces reduced bacterial adhesion significantly and the degree of adhesion differs depending on surfaces as well as media.	155

Table 2.5. (Continued**)**

Surfaces	Microorganism		Platform	Medium	T (°C)	Hydrodynamics	Assay Time	Parameters evaluated	Concluding remarks	Refs.
	G -	G +								
Bioactive glass S53P4 – Tooth-care product for oral health	AN PG	AA SM SS	n.d.	Brewer hioglycollate Medium	37	n.d.	50 min	Ion release from the bioactive glass paste; Antibacterial effect	• The bioactive glass paste appears to possess a broad antimicrobial effect on microorganisms.	156
Glass coated with different PU (Pellethane, sulfonated Pellethane, phosphonated Pellethane, a zwitterionic phosphonated polyurethane, and quaternized amine PU) – Biomaterials surfaces		SA	Sterile plastic test tubes	PBS	37	Shaker bath	1 h	Protein adsorption (fibrinogen and high molecular weight kininogen); Bacterial adhesion	• Decreases in bacterial adhesion were observed on all the polymcrs except the quaternized amine polyurethanes.	157
PU (Biospan) matrix; Polyetherurethane (PEU) base matrix radiofrequency glow discharge plasma deposited with triethylene glycol dimethyl ether (triglyme); Poly(butyl methyacrylate) (pBMA) - Biomedical devices	PA		PPFC	Minimal salts medium with glucose	RT	20.3 dynes/cm^2	2, 4, 6, 8, 20 and 24 h	Rate of initial bacterial adhesion; Sustained release of antibiotic	• The pBMA-coated PEU contained and released ciprofloxacin in a controlled manner; • The rate of adherent cell accumulation was zero for the pBMA-coated PEU releasing ciprofloxacin	158
Sulfonated PEG-acrylate copolymer - Coating and blending of biomaterials	EC	SEa	n.d.	TSB; BHI; Fresh citrated (0.37%) human plasma containing media	37	Constant swirling	24 h	Contact angle measurements; Protein adsorption; Bacterial adhesion	• The modified surfaces using acrylate copolymers demonstrated increased hydrophilicity; • All copolymer surfaces reduced bacterial adhesion significantly, less platelet adhesion than the controls. • The adhesion level differs depending on surfaces as well as media.	159
Phosphorylcholine-coated fluoroplastic tympanostomy tube; Plain fluoroplastic and Silver oxide-impregnated fluoroplastic – Biomedical devices	PA	SA	Armstrong Tympanostomy tube styles	TSB	37	n.d.	5 days	Surface treatment on bacterial adhesion	• Only PA formed biofilm on the untreated fluoroplastic tubes. • The silver oxide-impregnated tubes developed biofilms from both SA and PA. • The treatment inhibits biofilm formation by both microorganisms.	160
Low density polyethylene; Cellulose diacetate (CDA) modified by deacetylation and phosphorylation – Biomedical devices		SEa	Sterile borosilicate glass tubes	PBS	37	Gentle shaking	1 h	Contact angle measurements; Surface tension and hydrophobicity; Surface roughness	• Adhesion was significantly lower using the more hydrophilic CDA, compared to a hydrophobic polymer.	161

Table 2.5. (Continued**)**

Surfaces	Microorganism		Platform	Medium	T (°C)	Hydrodynamics	Assay Time	Parameters evaluated	Concluding remarks	Refs.
	G -	G +								
Poly(ethylene oxide) (PEO)-brushes – Biomaterials	EC PA	SA SEa SSa	PPFC	PBS	n.d.	10 s^{-1}	4 h	Contact angle measurements; Surface chemistry; Bacterial adhesion	• Bacterial adhesion to PEO-brushes in a PPFC is greatly decreased comparing to glass, except for hydrophobic bacteria; • This result may be due by an attenuation in Lifshitz–Van der Waals attractive energies.	162
2-methacryloyloxyethyl phosphorylcholine (MPC) co-polymer – Biomedical devices	PA	SA SM	Contiguous denture surface; 24-well MTP	BHI; Luria–Bertani broth (LB); PBS	37	n.d.	1 and 24 h	Contact angle measurements; Microbial retention assays	• All microorganisms were found to bind significantly less well to MPC-coated surfaces than to non-coated surfaces; • The effect could be attributed to the superhydrophilicity of MPC-coated surfaces, whereas hydrophobic surfaces are well known to reduce bacterial retention.	163
Poly(L-lysine)/ poly(L-glutamic acid) (PLL/PGA) multilayers ending by several PLL/PGA-g-PEG bilayers; Bare silica surface - Biomaterials	EC		Plated on the polyelectrolyte multilayers	LB selected with ampicillin	n.d.	n.d.	30 min	Protein adsorption; Bacterial adhesion	• A multilayer of PLL/PGA-g-PEG significantly improves the anti-microbial protection; • The results show the ability of PGA-g-PEG to be inserted into multilayer films and to drastically reduce both protein adsorption and bacterial adhesion.	164
Poly(epsilon-caprolactone) (PCL)/PEG copolymer - Biomaterials	BS		24-well MTP	n.d.	37	100 rpm	12 h	Contact angle measurements; Surface topography; Protein adsorption; Bacterial adhesion	• Surface hydrophilicity improved with the increased PEG segments in diblock copolymers; • Bacterial adhesion was inhibited by increased PEG contents; • Surface nanotopography could influence cell adhesion and growth as well as platelet and monocyte activation.	165
Bare titanium surfaces; Titanium with monomolecular coatings of peptide-functionalized poly(L-lysine)-grafted-poly(ethylene glycol) (PLL-g-PEG/PEG-RGD) - Biomaterials		SA	Test flasks	BHI	37	Stationary	1, 2, 4 and 24 h	Surface chemistry; Protein adsorption	• Bare coating titanium surfaces significantly decreased the adhesion; • The surfaces coated with PLL-g-PEG/PEG-RGD have the ability to attach cells such as fibroblasts and osteoblasts while showing reduced SA adhesion.	166

Table 2.5. (Continued**)**

Surfaces	Microorganism		Platform	Medium	T (°C)	Hydrodynamics	Assay Time	Parameters evaluated	Concluding remarks	Refs.
	G -	G +								
Heparin and Chitosan deposited onto aminolyzed poly(ethylene terephthalate) (PET) films – Cardiovascular devices	EC		Sterile test tube; Well plates (antibacterial tests)	PBS	37	Shaken	4 h	Bacterial adhesion; pH; Antibacterial properties; Bacterial adhesion	• Bacterial adhesion was greater onto the PET control than onto the chitosan/heparin multilayer films; • The adherence of bacteria decreased with a decrease in assembly pH. The assembly pH has a remarkable effect on the antibacterial property of the multilayer.	167
Nitric oxide (NO)-releasing xerogel coatings on silicone surface; Bare silicone - Biomaterials		SA	Male rats (*in vivo*)	-	37	n.d.	8 days	Detection of NO release; Histology; Bacterial adhesion	• The number of infected implants was significantly reduced with the NO-releasing coating. • Histology revealed that the capsule formation around infected bare silicone rubber controls was immunoactive and that a biofilm may have formed; • Capsule formation in response to NO-releasing implants had greater vascularity in comparison with uninoculated or untreated controls.	168
Glass; Indium Tin Oxide (ITO)-coated glass - biomaterials	PS	SEa	Flow chamber	PBS	RT	6 s^{-1}	2 h	xDLVO adhesion energy; Bacterial adhesion	• The Gram + bacteria adhere more strongly to the surfaces and irreversibly than the Gram - bacteria; • Adhesion of both bacteria was higher onto hydrophobic coated surface.	169
Acrylic polymethyl methacrylates; Improved methacrylates; Bisacrylate composite resins) – Fixed prosthodontic materials		SM	48-well MTP	PBS	37	n.d.	n.d.	Surface roughness; Contact angle measurements; Bacterial adhesion	• The bacterial adhesion differed significantly among the assessed surfaces; • No correlation was found between bacterial adhesion and surface roughness or hydrophobicity; • Bisacrylate composite resins and acrylic polymethyl methacrylates had significantly lower adhesion potentials than improved methacrylates.	170
Polymer brushes (Surface-Grafted Polyacrylamide (PAAm) brushes) - biomaterials		SSa SA	PPFC	PBS; Physiological fluids	n.d.	10 s^{-1}	4 h	Surface chemistry; Physiological fluids; Protein adsorption; Bacteriala dhesion	• Reduction in microbial adhesion to the surface-grafted PAAm brush was observed; • PAAm brush coating did not cause surface deterioration and decreased microbial adhesion, even after 1-month exposure to physiological fluids.	171, 172

Table 2.5. (Continued**)**

Surfaces	Microorganism		Platform	Medium	T (°C)	Hydrodynamics	Assay Time	Parameters evaluated	Concluding remarks	Refs.
	G -	G +								
Helium plasma treated polyethylene terephthalate (PET); Bare PET – Biomedical devices		SEa	Well tissue-culture plates; Radial flow chamber	PBS	37	Static; 5; 50; 200 s^{-1}	2.5 h	Thermodynamic theory parameters; Surface energy; Bacterial adhesion; Hydrodynamics	• Plasma treatments are shown to significantly reduce bacterial adhesion; • The decrease in the surface free energy of the surfaces with time favor bacterial adhesion and aggregation. • There was a strong correlation between the thermodynamic predictions and the bacterial adhesion under static conditions. Under flow conditions, the increased shear rate restrict the predictability of the thermodynamic models.	173
Si and N doped diamond-like carbon coatings (DLC) – Biomedical devices	PA		Conical flask	PBS	37	20 rpm	1 h	Contact angle measurements; Surface energy; Surface morphology	• The results showed that the addition of N or Si in DLC coatings had a significant influence on bacterial adhesion; • The bacterial adhesion was correlated with the thermodynamic theory.	174
L-tryptophan-based hydrogels of amino acid-based cationic amphiphiles – biomedical application	EC PA KA	BS ML SA	Test tubes (antibacterial assays); 96-well MTP (cytotoxicity assays – HeLa cells)	LB; Dulbecco's modified Eagle's medium (DMEM)	37	Laminar flow (n.d)	5 to 7 h (antibacterial assays) followed by 24 h of incubation on agar plates; 3h (cytotoxicity assays)	Hydrophobicity; Antimicrobial activity; Cytotoxicity assays	• L-tryptophan based cationic amphiphilic hydrogelators with different hydrophobicities exhibited remarkable bactericidal activity against wide range of Gram+ and - bacteria; • Antimicrobial efficacy of the amphiphiles was greatly influenced by their alkyl chain length. • The surfaces remain biocompatible to the mammalian cells.	175
Silk sericin-functionalized titanium surfaces; bare titanium surfaces – Osseointegration		SA SEa	24-well MTP	PBS	37	n.d.	5 h	Surface chemistry; Bacterial adhesion	• The brushes significantly reduce the bacterial adhesion; • The silk sericin-immobilized surfaces promote osteoblast cells adhesion and proliferation.	176
Poly(oxy(acetylaminoundecyl esterthiomethyl)ethylene) (PAUTE) – Several biomedical devices especially blood contacting devices	EC PA	SA SEa EF	Mice (*in vivo*); Conical tubes	PBS	37	n.d. (implanted); gentle shaking (200 rpm)	1, 2, 4 and 8 h; 12 (weeks post-implantation); 15, 30, 60, 120, and 240 min (*in vivo* bacterial adhesion)	Contact angle measurements; Protein adsorption; Platelet adhesion; Bacterial adhesion; Bactericidal effect	• The brushes exhibit excellent water wettability being hydrophilic surfaces; • These brushes repel fibrinogen molecules and platelets from their surfaces and showed bactericidal effects on bacteria; • The surfaces are found to provide comfortable surface to anchor and growth of HEp-2 cells, and to exhibit excellent biocompatibility in mice.	177, 178

Table 2.5. (Continued**)**

Surfaces	Microorganism		Platform	Medium	T (°C)	Hydrodynamics	Assay Time	Parameters evaluated	Concluding remarks	Refs.
	G -	G +								
Glass with alkyl silane monolayers (methyl, amino and hydrodyl terminals) - Biomaterials		SEa	PPFC	PBS	37	50, 500, 1000, 2000 s^{-1}	2 h	Zeta potential measurements; DLVO theory; Surface free energy evaluation; Surface roughness	• The increase in the ionic strength significantly enhanced adhesion to the different surfaces, in accordance with the DLVO theory under low shear rates. The increase in the shear rate restricted the predictability of the theory.	179
SiO_2–MgO–Al_2O_3–K_2O–B_2O_3–F^- glass ceramic - Biomaterials	EC	SEa	n.d.	LB	37	n.d.	4 h	Bacterial adhesion; Antimicrobial properties	• The microstructure and base glass composition play an important role in enhancing the cellular functionality and antimicrobial properties.	180
Staineless steel, silver coatings – Biomedical devices	PA		Beaker	n.d.	37	20 rpm	1 h	Contact angle measurements; Surface energy; DLVO theory; Bacterial adhesion	• Surface energy had significant influence on initial bacterial adhesion at low corrosion rate; • There was a strong correlation between total surface energy and bacterial adhesion; • The number of bacteria attached to the surfaces decreases linearly with total interaction energy increasing, which is consistent with the extended DLVO theory.	181
Tunable bioadhesive hydrogel of thermoresponsive N-isopropylacrylamide (NIPAAm) containing zwitterionic sulfobetaine methacrylate (SBMA) – Biomedical applications	EC	SEa	24-well MTP	Medium containing 3.0 mg/mL beef extract and with 5.0 mg/mL peptone	37	100 rpm	24 h	Protein adsorption; Bacterial adhesion; Temperature resistance	• The polySBMA-rich hydrogels exhibited evident antimicrobial properties when they were incubated with Gram + and Gram- bacteria; • The tunable-bioadhesive behavior of temperature-sensitive poly(NIPAAm-co-SBMA) makes this biocompatible hydrogel.	182
Superhydrophobic xerogel coating from a mixture of nanostructured fluorinated silica colloids, fluoro-alkoxysilane, and a backbone silane – Biomedical applications	PA	SA	PPFC	TSB	37	0.2 mL/min	1.5 h	Contcat angle measurements; Bacterial adhesion	• The adhesion was reduced independent of the strain tested; • The superhydrophobic coating synthesis may be applied to any surface, regardless of geometry.	183

Table 2.5. (Continued**)**

Surfaces	Microorganism		Platform	Medium	T (°C)	Hydrodynamics	Assay Time	Parameters evaluated	Concluding remarks	Refs.
	G -	G +								
N,N,N-Trimethyl O-(2-hydroxy-3-trimethylammonium propyl) chitosans (TMHTMAPC) – Biomedical applications	EC	SA	n.d.	Nutrient medium	35	n.d.	24 and 48 h	Surface characterization; Antibacterial activity	• The existence of 100 mM Na+ slightly reduced the antibacterial activity of both chitosan and its quaternary ammonium derivatives, because Na+ and the chitosan derivatives formed a complex that reduced the binding force between the surfaces and bacteria.	184
Poly(vinyl alcohol) (PVA)/Chitosan-based hydrogels -Bbiomaterials	EC	BS	Piece of sterile discs of hydrogels	Nutrient Both (NB)	30	n.d.	24 h	Swelling behavior; Gel content; Morphological structure of the blend; Bacterial adhesion	• Chitosan was more effective in inhibiting growth of Gram + bacteria than the Gram - ; • The chitosan content as well as its molecular weight has a direct influence on bacteria growth inhibition; • The higher the chitosan content in the blend and the higher its initial molecular weight, the larger was the inhibition zone diameter.	185
Chitosan–γ-poly (glutamic acid) (c-PGA) polyelectrolyte complex hydrogel (PEC) – Drug carriers and artificial tissue scaffolds	EC	SA	Shake flask testing (antibacterial ability); 24-well MTP (biocompatibility assays)	NB; DMEM F-12	37	n.d.	4 h	Surface chemistry; Biocompatibility; Antibacterial effect	• The chitosan–c-PGA PEC hydrogels exhibited antibacterial ability against the microorganisms tested; • Biocompatibility studies revealed that the chitosan–c-PGA PEC hydrogel had good affinity for 3T3 fibroblast cells, especially the positive-charged ones (chitosan-dominated).	186
AIodine-supported titanium ($Ti–I_2$); Stainless steel; Titanium controls – Orthopedic implants	EC	SA	Petri dishes; Rabbits (*in vivo* effects)	BHI; LB (antimicrobial tests); Alpha-minimum essential medium (a-MEM) (cytocompatibility assays)	37	n.d.	2, 6 and 24 h (antimicrobial tests); 1 week (cytocompatibility assays); 14 days (remove implants)	Antimicrobial properties; Cytocompatibility properties; Surface properties (roughness; charge)	•$Ti–I_2$ clearly inhibited bacterial colonization more than the control metals; •$Ti–I_2$ has antimicrobial activity, exhibits cytocompatibility as well as exhibited good biocompatibility: colony formation of normal fibroblasts was observed; • Physical properties of the surfaces does not affect bacterial adhesion.	187
Silver/Hydroxyapatite composite coatings on porous titanium surfaces - Biomaterials	EC	SAa	Flat-bottom test tubes	LB; PBS	36	200 rpm	12 h	Surface characterization; Antibacterial activity; Biocompatibility - cell culture of osteoblasts	• The characterization revealed that silver particles uniformly distributed in the coatings without agglomeration; • High antibacterial ratio, > 95%, against EC and SAa and good biocompatibility was expressed by the silver-containing coatings (composite coatings with 0.8 wt %).	188

Table 2.5. (Continued**)**

Surfaces	Microorganism		Platform	Medium	T (°C)	Hydrodynamics	Assay Time	Parameters evaluated	Concluding remarks	Refs.
	G -	G +								
Poly(ethylene glycol) (PEG); Poly(ethylene glycol)-co-acrylic acid (PEG-AA) microgels - Biomaterials		SEa	Petri dishes	Fresh modified TSB	37	static	2, 6 and 10 h	Self-assembly; Patterning; Antifouling properties; Bacterial adhesion	• Consistent with macroscopic gels, a pH dependence of both zeta potential and hydrodynamic diameter was observed in AA-containing microgels but not in pure PEG microgels; • The microgel surface density could be controlled via the deposition time and the microgel concentration in the parent suspension; •Postdeposition L5 peptide loading into microgels further reduced bacterial attachment.	189
Titanium (Ti); Polyether-ether-ketone (PEEK); Silicon nitride (Si_3N_4) – Spinal implants	EC PA	SA SEa *Enterococcus*	n.d.	LB	37	n.d.	4, 24, 48 and 72 h	Nanostructure; Bacterial adhesion; Protein adsorption	• Decreased biofilm formation and bacterial colonization were demonstrated on both as fired and polished Si_3N_4 in comparison with Ti or PEEK Si_3N_4 resisted bacterial proliferation under these conditions, despite the absence of antibiotic pharmaceutical agents; • The unique surface chemistry and nanostructured features of Si_3N_4 may contribute to the favorable antibacterial properties of this bioceramic material.	190
PDMS; Glass; Titanium – Biomaterials	EC		Petri dish; Microfluidic flow cells	PBS	RT	Static; Flow conditions (10 µl/min)	2 h (static)	Contact angle measurements; Surface roughness; Bacterial adhesion	• Bacterial adhesion to all surfaces was most affected by the surface energy of these materials; • The roughness of the surface was not correlated with bacterial attachment; • Adhesion was observed to be strongly dependent upon the topographical features under both static and microfluidic flow conditions - the highest attachment density was observed on flat, un-patterned surfaces, while linear patterned surfaces showed greatly reduced cell attachment.	191

Table 2.5. (Continued**)**

Surfaces	Microorganism		Platform	Medium	T (°C)	Hydrodynamics	Assay Time	Parameters evaluated	Concluding remarks	Refs.
	G -	G +								
Polystyrene coated with surfactant pluronic F127 - Biomaterials	PA	SEa	96-well MTP	TSB	37	n.d.	24 h	Surface topography; Contact angle measurements; Bacterial adhesion	• Surface roughness and bacterial surface polarity does not influence the adhesion of SE; however, the material coated surface became extremely hydrophilic.	192
Silicone (SIL); Stainless steel (SS); Polyvinyl chloride (PVC); Glass as control - Biomaterials	EC		12-well MTP	MH broth	37	static	0.5, 4, 8, 12, 16., 20, 24 h	Contact angle measurements; Antibiotic effect (biofilm MIC; SEM); Quantification of EPS	•Hydrophobic materials, such as SIL, SS, and PVC, showed higher bacterial colonization than the hydrophilic GLA. SIL was the surface with the greatest bacteriala adhesion and the biofilms formed on this material were also less susceptible to both antibiotics; • Antibiotics can alter the morphology of EC.	193
Glass; Polydimethylsiloxane (PDMS) – Biomedical devices	EC		PPFC	Citrate buffer (CB) 0.05 M	37	0.005 to 0.07 Pa	0.5 h	CFD; Contact angle measurements; Bacterial adhesion	• The EC adhesion to hydrophobic PDMS and hydrophilic glass surfaces is modulated by shear stress with surface properties having a stronger effect at the lower and highest flow rates tested; • Negligible effects at intermediate flow rates.	96
Poly[oligo(ethylene glycol)methyl ether methacrylate] (poly(MeOEGMA)); Poly[N-(2-hydroxypropyl)methacrylamide] (poly(HPMA)) brushes - Biomaterials	PA		Custom-made biofilm reactors (n.d.)	Casein–soja–pepton–agar (CASO) medium; BM2 mineral medium; M9-medium; DMEM with 10% FBS.	n.d.	2 L/h	7 days	Surface characterization; Contact angle measurements; Antibiotic resistance	• PA in mineral media as well as CASO medium resulted in no biofilm formation, while a decrease of the biofilm formation on the brushes was observed when the medium was rich in nutrients and proteins. • Biofilm formation was observed using an antibiotic multi-resistant PA strain on both brushes. • Protein fouling was fully prevented on both brushes.	194
Self-assembly of a tripeptide (third amino acid of the peptide is 3,4-dihydroxy-L-phenylalanine (DOPA)); Bare titanium surface - Health care, marine and water treatment	EC PA		n.d.	n.d.	n.d.	Static	9; 96 h	Surface characterization; Protein adsorption; Contact angle measurement; Bacterial adhesion	• The peptide design includes the amino acid DOPA as the adsorption motif, the diphenylalanine as the element that directs the self-assembly process and fluorine atoms as the antifouling agents; • The formation of a coating on various substrates and presented its ability to disrupt the process of biofouling.	195

Table 2.5. (Continued**)**

Surfaces	Microorganism		Platform	Medium	T (°C)	Hydrodynamics	Assay Time	Parameters evaluated	Concluding remarks	Refs.
	G -	G +								
Cellulose acetate; Glass, Poly-L-lactide; Polydimethylsiloxane – Biomedical devices	EC		Micro and macro flow systems (microchannel; PPFC)	CB 0.05 M	37	0.022 Pa (32 s^{-1})	30 min	Thermodynamic theory; CFD; Bacterial adhesion	• Similar results were obtained in the two platforms; • Average wall shear stress may be a good scale-up factor between different systems.	196
Polystyrene; Poly-L-lactide; Cellulose acetate; Polydimethylsiloxane - Biomaterials	EC		PPFC	CB	37	0.01 Pa	30 min	Thermodynamic paramenters; Surface properties; Bacterial adhesion	• Bacterial adhesion is reduced in surfaces with lower γ^{LW}/γ^{-} and enhanced otherwise.	114
Poly(MeOEGMA); Poly(hydroxyethyl methacrylate) (poly (HEMA)); poly(HPMA); Poly(carboxybetaine acrylamide) (poly(CBAA)) brushes - Blood contacting devices	n.d.		Flow cell (protein fouling)	Undiluted human BP; Model solutions of plasma proteins; Human serum albumin	n.d.	25 mL/min	15 min	Surface characterization; Protein adsorption; Bacterial adhesion; Antifouling properties	• All brushes decreased the fouling from blood plasma over 95% and prevented the adhesion of platelets, erythrocytes, and leukocytes.	197
Poly(HEMA); poly(MeOEGMA); poly(CBAA); poly(HPMA) - Antithrombogenic surface	n.d.		PPFC	Undiluted human blood plasma	n.d.	2100 s^{-1} (assessment of atifouling properties); 1000 s^{-1} (assessment of thrombogenicity)	n.d.; 10 min (thrombogenicity)	Electromagnetic piezoelectric acoustic sensor (EMPAS); Assessment of thrombogenicity under flow; Antifouling; Protein adsortion	•The antifouling brushes were found to be capable of drastically reducing fouling from full human blood plasma; •The platelet aggregation and thrombus formation were largely reduced when the surfaces were exposed to whole human blood in a perfusion chamber under dynamic conditions.	198
Smooth surface moulding technique of silicone rubber – Indwelling voice prostheses		SA SEa SSa RD	Modified Robbins device made of stainless steel (artificial throat)	Growth medium (n.d.); PBS	37	n.d.	7 days	Surface roughness; Bacterial adhesion; Analysis of the clinical *in situ* lifetime;	•Use of a smoother mould and less viscous silicone rubber yielded a decrease in surface roughness that promotes the reduction in the prevalence of bacteria in *in vitro* formed biofilms; • The clinical lifetime was significantly increased suggesting that the choice of material and in particular its surface properties, may be determining factors to the clinical lifetime of the implants.	103

Table 2.5. (Continued**)**

Surfaces	Microorganism		Platform	Medium	T (°C)	Hydrodynamics	Assay Time	Parameters evaluated	Concluding remarks	Refs.
	G -	G +								
Graphene onto medical grade titanium: an atom-thick multimodal coating – Biomedical devices	Typical microbial composition in the oral cavity	SM EF	24-well MTP	BHI; Fresh saliva	37	80 rpm	24 h	Surface characterization; Biocompatibility; Mineralization potential; Bacterial adhesion	•The graphene-coated titanium is cytocompatible, did not induce cell membrane damage, induced human osteoblast maturation and increased the deposition of mineralized matrix; • Graphene decreased the formation of biofilms from the bacteria.	199
Natrelle (Smooth); SmoothSilk/SilkSurface (Silk); VelvetSurface (Velvet); Siltex; Biocell – Breast implants	PA RP	SEa	CDC Biofilm Reactor	Growth medium (10%-strength BHI broth with 0.5% adult bovine serum)	37	Continuous flow (2.7 ml/min)	2 h (adhesion); 24 h (biofilm formation) and stirring (125 rpm)	Surface roughness; Bacterial adhesion	• Surface areas increased with roughness and were similar among the three least rough implants (Smooth, Silk, and Velvet) and among the roughest implants (Siltex and Biocell); • Implant surfaces with rougher texture, resulting in more surface area, harbored greater biofilm loads than those with smoother surfaces.	78
Biomimetic polyurethane (PU) films with surface texturing and nitric oxide (NO) release - Biomaterials	PA	SEa SA	12-well MTP	50% human plasma; PBS	37	static	2 h	Biomimetic; Surface properties; NO release; Anticoagulation; Antibacteria	• The biomimetic modification with surface texturing and NO release provides an effective approach to improve the biocompatibility of polymeric materials in combating thrombosis and microbial infection.	200
Minocycline-loaded-niosomes; Titanium – Coatings for dental implants	PG		Dental implants (antibacterial activity); 96-well MTP (susceptibility and cytotoxicity assays)	Anaerobic broth; Blood broths; MEM medium (*in vitro* cytotoxicity)	37	Shaking conditions	1, 3, 5 and 7 days; 24 h (cytotoxicity assays)	Surface properties; Layer-by-layer spray coating; Drug release profile, activity and cytotoxicity against osteoblast cells	• Minocycline-loaded niosomes were successfully optimized and coated on dental implants by layer-by-layer spray coating; • The coating had the ability to sustain and prolong drug release for over 1 week and had antibacterial activity; • The coated implants were biocompatible and non-toxic to osteoblast cells.	201

Legend:

n.d., not disclosed; **RT**, room temperature

Bacteria:

AA, *Actinobacillus actinomycetemcomitans*; **AC**, *Acinetobacter calcoaceticus*; **AN**, *Actinomyces naeslundii*; **AX**, *Achromobacter xylosoxidans*; **BC**, *Burkholderia cepacian*; **BS**, *Bacillus subtilis*; **CM**, *Cobetia marina*; **DT**, *Delftia tsuruhatensis*; **EC**, *Escherichia coli*; **EF**, *Enterococcus faecalis*; **KA**, *Klebsiella aerogenes*; **L.,** *Lactobacillus;* **ML**, Micrococcus luteus; **PA**, *Pseudomonas aeruginosa*; **PF**, *Pseudomonas fluorescens*; **PP**, *Pseudomonas putida*; **PS**, *Pseudomonas stutzeri*; **PG**, *Porphyromonas gingivalis*; **RD**, *Rothia dentocariosa*; **RN**, *Ralstonia pickettii*; **SA**, *Staphylococcus aureus*; **SE**, *Salmonella* Enteritidis; **SEa**, *Staphylococcus epidermidis*; **SAa**, *Staphylococcus albus*; **SAb**, *Staphylococcus aureus*; **SM**, *Streptococcus mutans*; **SS**, *Streptococcus sanguis*; **SSa**, *Streptococcus salivarius*; **ST**, *Salmonella typhimurium*; **VA**, *Vibrio alginolyticus*

2.3.2. Impact of hydrodynamics

Bacteria in natural or man-made environments are exposed, more often than not, to flow conditions. It is known that a simple change in the fluid flow around the biofilm structure influences the rate of adhesion through mass transport processes, such as convection, diffusion, or sedimentation [202-204]. The predominant force acting on the biofilm is a shear force exerted in the flow direction determined by velocity on a given system [205].

It has been observed that, additionally, to the relevant role that flow hydrodynamics has on bacterial attachment, it is also one of the most decisive factors in biofilm maturation [206, 207]. Such factors can cause desorption, detachment and dispersion [208, 209]. Additionally, when the fluid flow exceeds a critical limit, the resulting shear stress may prevent bacterial adhesion [210, 211] and high shear stresses often lead to thinner, denser and stronger biofilms [212]. Researchers have been studying the flow of a fluid that can be described by numerical simulations in relation to the conservation of mass, momentum and energy [213]. Computational fluid dynamics (CFD) has been used to assess the applicability of different platforms in the simulation of the hydrodynamics of relevant scenarios, such as industrial and biomedical [196, 214-216].

In the industrial field, shear forces have been used as an effective tool in cleaning in place (CIP) procedures and for biofilm control [212, 217]. A study conducted by Teodósio et al. [218] reports the use of semi-circular flow cells to simulate the biofilm formation in industrial pipes. They tested two different shear stresses (0.183 and 0.511 Pa) on *E. coli* biofilm formation and used CFD to assess whether the flow in pipe systems can be simulated by this platform. The authors have shown that a semi-circular flow cell can efficiently simulate the flow obtained in a pipe with circular section when Reynolds numbers (*Re*) are comprised between 10 to 1000 and 3500 to 10000. Results demonstrated that at a higher flow rate, a thinner biofilm was obtained being important information for the prevention and control of industrial biofouling. The effect of shear stress and mass transfer on the development of *E. coli* biofilms was also demonstrated using a flow cell that mimics industrial piping settings. Authors verified that high flow rates are required at all times to reduce the build-up of bacterial biofilms, since increasing the shear stresses will promote biofilm detachment and potentiate the effect of cleaning agents due the increased mass transfer from the bulk fluid to the surface [219].

In the biomedical field, the shear stress generated is dependent on specific physiological conditions and should be considered since these parameters can affect the attachment of the bacteria and consequently biofilm development, structure and susceptibility [193, 196, 214, 220]. For example, the efficiency of *E. coli* to approach the surface can be affected by flow and shear rates. The swimming behavior of single *E. coli* K12 cells over a surface was shown to be affected by high

flow and high shear. This effect was observed using microfluidic chambers where different hydrodynamic conditions were applied [221]. For the low flow conditions the *E. coli* cells demonstrated random trajectories and under moderate shear rates (approximately 6/s) it was observed a positive rheotaxis, showing a greater upstream mobility against the flow direction contributing to the efficient propagation of *E. coli* such as in medical catheters. On the contrary, when under high flows the cells are removed [221]. Additionally, Gomes et al. [214] used a 96-wells microtiter plate to investigate the influence of nutrient concentration and flow conditions on biofilm formation by *E. coli* simulating relevant biomedical scenarios. CFD was used to assess the applicability of this platform showing that this system simulates a variety of biomedical scenarios. Other study using a different platform, PPFC, reported on the combined effects of surface properties (glass and PDMS were used as different physicochemical surfaces) and hydrodynamics on *E. coli* adhesion [96]. Five different flow rates and CFD were used to characterize the system. The results demonstrate that the surface properties were affected at the lowest and highest shear stresses, suggesting that the material selection for biomaterials should consider local hydrodynamics. The use of PPFC was shown to be adequate for the simulation of shear stresses found in several biomedical applications (e.g. circulatory and urinary systems) [96].

Given the importance of hydrodynamic forces in bacterial fixation, table 2.6 includes some studies in which shear stresses and shear rates found in different environments were considered. In the industrial field is possible to achieve shear rates between 10 and 21000/s and in a natural environment, a shear rate range between 4 and 125000/s can be obtained. Regarding the human body shear conditions and depending on the medical apparatus application, the shear stress range can vary between 0.0007 and 88.3 Pa.

Table 2.6. Characteristic shear conditions found in industry, environment, biomedical devices and human body

Area	Phenomenon	Shear strain rate (1/s)	Shear stress (Pa)	Refs.
Industry	Surface heat exchangers	< 40		222
	Wall of a planetary mixer during cake batters	20-500		223
	Flow of a film over a vertical plate	0.1		224
	Drinking water distribution systems	1000-10000	0.13 – 9.10	146, 225
	Reverse osmosis membrane	10000-21000		226
	Milk vat		<0.5	227
	Tubular membranes	10-100		149
	Mix proof valve		<9	228
	Model plumbing system		0.00063-5.08	229
	Cleaning in place (Pipes, pumps, corners, valves in food production lines)		0.01-5.32	143, 230

Table 2.6. (Continued)

Environment	Tumbling or poring	10-100		[224]
	Ship navigation (turbulent flow)	125000		[224]
	Ship in harbor	50		[224]
	Marine environments	4 and 40		[148]
	Channels within a biofilm	60-300		[224]
Human body	Blinking of an eye	0.35		[224]
	Fluid flow in the oral cavity	0.1 - 50		[224]
	On teeth, while biting an apple	200		[224]
	Salivary mucosal secretions		0.08	[231]
	Blood flow (BF) in carotid		0.33-1.6	[232, 233]
	Inner medullary collecting ducts (urine flow-induced shear stress from normal to high flow rate)		0.02 - 2	[234]
	BF in veins	50	0.1-0.6	[235-237]
	Peroneal veins		0.009–3	[238]
	BF in arteries	1.5 to 650	1-7	[235-237]
	BF in the little blood vessels	2600		[235]
	BF in aorta	45 - 305		[239]
	On osteocytes in bones	<263		[239]
	Kidney collecting duct cells		0.02–2	[240]
	Initiation of intracranial aneurism		>15	[241]
	Cerebral circulation	> 100		[241]
	Reproductive system (uterus)		<0.1	[242]
Biomedical devices	Urinary Flow in a catheter	15		[224, 243, 244]
	On eye contact lens motion	1000		[245]
	Niagara Hemodialysis Catheter (arterial luminal tip)	20 000 – 80 000		[246]
	Arterial luminal tip (Niagara cateter)		52.6-88.3	[247]
	Mitral jellyfish prosthetic valves		0.08-37.59	[248]
	Catheter sheath introducer		0.03	[249]
	Bjork-Shiley tilting-disk (mono) prosthetic valve		0.06-27.84	[248]
	Endovascular aneurysm sealing (EVAS) (different stented models– Endurant, AFX, Nellix		0.06-2.27	[250]
	Prosthetic femoral-popliteal bypass graft		0.5	[251]
	Femoropopliteal arteries stent		≤ 0.4	[252]
	Endothelialized Small-Diameter Vascular Grafts		0.007 – 1.45	[253]

2.4. Platforms for *in vitro* studies

Microtiter plates are one of the most widely used platforms for the screening of bacterial

adhesion and biofilm development to different surfaces in static or agitated conditions (see Table 2.5) [254]. These platforms enable high-throughput operation using a small working volume and allow the test of antibiofilm compounds to analyse antibiotic susceptibility (Table 2.7). Despite the widespread use, there is a lack of a standard methodology regarding the reported results of bacterial adhesion [24]. The normal process after the adhesion time is to wash the surface to remove the non-adherent bacteria and then quantify the sessile cells through direct or indirect measurements. Although, the impact of washing is a relevant step since loosely attached biofilm may not be measured correctly (Table 2.7). However, such methodology has been used, but it remains inadequate as it raises several questions such as the magnitude of the rinsing forces applied and the percentage of the total adhering bacteria removed after the process [24]. In addition, the hydrodynamic conditions inside these plates are poorly understood and there are few studies analysing these parameters on 12- and 96-well microtiter plates [148, 214].

The importance of research on the effect of hydrodynamic conditions on bacterial adhesion to surfaces has encouraged the development of different types of platforms [254, 255] which are listed in table 2.7. The presented platforms, such as the Center for Disease Control (CDC) Biofilm Reactor (CBR), flow cell, microfluidic, among other models, contributed to the current knowledge about the biofilm physiology within biofilm-related infections. Biofilm reactors are widely used to perform *in vitro* assays on biofilm formation under flow conditions. The choice of the platform is crucial to determine what kind of data can be extracted as well as the conditions to be mimicked, depending on the purpose of the study (e.g. industry, environment or biomedical). All platforms present advantages and limitations that are described in table 2.7. In the biomedical field, for example, although there are standardized methods such as ASTM E2871-13 and ASTM 2562-12 for the CDC biofilm reactor, the operation has specific limitations such as the geometry of the coupon is fixed and determined by the reactor design (coupon holder) and presented reduced sampling areas. Additionally, most of the biofilm reactors are basically stirred containers where the flow pattern changes within the surface and consequently does not mimic the flow characteristic of a urinary catheter, for example [255, 256]. Unfortunately, until now, there are no standardized platforms to test surfaces for the urinary tract. However, the platforms often used to perform these assays are flow systems such as the Robbins device and flow cells, because they are able to mimic the hydrodynamics of a specific environment [96, 255]. Despite the Robbins device has the advantage of evaluating surfaces under well-defined hydrodynamic conditions does not allow *in situ* online inspection of biofilms. Contrary to the small-scale flow cells that are built for microscopic observation of bacterial adhesion process. A recent study reports a designed *in vitro* urinary catheter using commercial silicone catheters exposing them to human urine and

E. coli to evaluate the biofilm formation in the intraluminal side under flow [257]. However, the authors did not consider the shear operating in the *in vitro* system described. Hydrodynamics determines the rate of transport of cells and nutrients to the surface. The flow rate by itself, without considering the geometry of the described flow system, provides little information about shear in the system and therefore it is not known whether the real conditions are being mimicked. It is important that the system is studied in such a way that the shear stress of the wall or the shear rate are determined and the system properly characterized [96]. In addition, the urinary system developed has other limitations due to the impossibility of *in situ* and real-time observation of the adhesion process as well as the biofilm development. Additionally, the evaluation of the biofilm structure is not possible as they cut the catheter to quantify the biofilm, destroying the structure of the biofilm.

In sum, there are three main parameters taking into account when studying bacterial adhesion in flow displacement systems: mass transport processes such as convection, diffusion, or sedimentation; wall shear rates, the main source of fluid flow forces on adhering organisms that acts parallel to the surface and depends on the viscosity of the suspension and the microbial dimensions; and artifacts, that are most easily created in microbial adhesion experiments, of which the "slight rinsing" and "dipping" artifacts are the most notorious. The surface tension forces acting on adherent microorganisms from a substrate can lift the adherent organism. Unlike wall shear forces, these surface tension detachment forces work perpendicularly to the substrate surface and therefore are directly opposed to adhesion forces [24].

The focus of this thesis is the use of a flow cell system, which is the best-suited platform to study adhesion and biofilm formation under controlled hydrodynamic conditions, and therefore, will be described in more detail in the following section.

Table 2.7. Main applications of standard platforms for in vitro biofilm studies and respective advantages and limitations. Adapted from Gomes et al. [256], Lebeaux et al. [258], Azevedo et al. [259]

Static systems

Platforms	Main applications	Main advantages	Main disadvantages
Microtiter Plate (MTP) 	Screening for biofilm formation capacity (bacteria attach to well surfaces); Test of antibiofilm compounds (biofilm antibiotic tolerance and resistance, efficiency of antibiofilm/antimicrobial products).	High throughput (simple to run) Inexpensive; Advanced equipment apart from plate reader is no needed; Non-invasive imaging (microscopic-grade microplates).	Not suitable for the study of early stages of biofilm formation; Direct observation can be complicated under the microscope; Loosely attached biofilm may not be measured correctly (can be detached during washing steps); Possible interference with liquid–air interface; Sometimes poor reproducibility; Operator dependent; Assessment possible only at a sufficiently high cell density.
Biofilm Ring Test (BRT)  Each well with microbeads	Immobilization of magnetic beads; Screening for biofilm formation ability; Test of antibiofilm molecules.	High throughput; Requires very few manipulations; Better reproducibility than the microtiter plates; Allows for a rapid monitoring of biofilm formation. Well-designed to investigate early stage of biofilm formation; Quick and automatic analysis; Easy-handling method (no washing, fixation or staining steps); Applicable to loosely attached biofilm Highly reproducible, not person/laboratory dependent.	Not fully tested nor automated; Requires specific equipment (magnetic device and scanner); Not intended to investigate late stages of biofilm formation; Not adapted for biofilms at the air-liquid interface; Possible restriction due to the growth medium.
Calgary biofilm device (CBD) 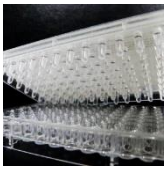	Biofilm antibiotic resistance and tolerance, efficiency of antibiofilm/ antimicrobial products.	Commercially available system; Pegs can be removed individually without opening the system avoiding contaminations; Consistent shear force across all pegs; Allow direct observation and quantification of biofilm overtime; High-Throughput; Easy to control the environmental conditions; Less sensitive to sedimentation; No need for advanced equipment apart from plate reader.	Each change of medium requires that pegs pass through the liquid–air interface; Loosely attached biofilm may not be measured correctly; Direct observation difficult; End-point measurement; Difficulty to collect individual pegs for enumeration; Sonication may not remove firmly attached cells; Usually only short-term experiments; Not suitable for investigating early stages of biofilm formation; Limited to single substrate materials (no coupons); Operation in batch mode; Unable to study high shear stress conditions.

Table 2.7. (Continued)

Dynamic Systems

Platforms	Main applications	Main advantages	Main disadvantages
Modified Robbins Device (MRD) 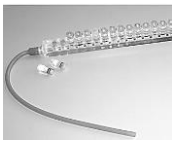	Mimic throat conditions and evaluate the efficiency of different products in rubber trachea-oesophageal prostheses; Screening of biofilm supporting surfaces; Suitable for in-line flow experiments (e.g. utility water systems).	Substratum coupons can be extracted or exchanged during the experiment; Can run for very long periods without intervention; Well defined hydrodynamic conditions; Operation at continuous culture conditions.	Low- to medium throughput; Expensive; Requires pumps or flow systems; Does not allow *in situ* online inspection of biofilms; Requires prior knowledge of the flow dynamics inside the device which can limit the operational range.
Flow Cell 	Flat walled transparent chambers with culture media flow under the microscope; Costly and expertise is needed. System is automatized and available for image analysis; Suitable for growing smaller number of biofilms; Can be used to study growth physiology, response to stresses (e.g. antibiotics), evaluation of efficiency of antibiofilm/antimicrobial products, flow conditions; Can in some extent be used to mimic natural flow conditions (e.g. in the body or in other natural environments).	Enables for non-destructive real-time adhesion and biofilm observation (single cell visualization); Excellent image quality; Can be designed with glass or other surfaces.	Low throughput; Does not allow direct access to the biofilm cells individually; Requires peristaltic pumps and other special equipment.
Center for Disease Control (CDC) Biofilm Reactor (CBR) 	Evaluation of biofilm formation, biofilm antibiotic resistance and tolerance; Biofilm control with new materials and antimicrobial agents; Mimicking indwelling devices (e.g. catheters and implantable cardiac devices); model of oral and wounds biofilms.	Commercially available system; Easy sampling at different time points. Possibility to study different materials simultaneously; Reliable system; Easy to control the hydrodynamic conditions.	Biofilm formed on a flat surface; The geometry of the coupon is fixed and determined by the reactor design (coupon holder); The flow pattern changes in the boundaries of the coupons. Lack of sampling surface area.
Drip Flow Biofilm Reactor (DFBR) 	Visualization and quantification of biofilm formation on coupons at low shear stress; Wound biofilm model. Tested for antimicrobial efficiency bacteriophage reduction of biofilms and other antibiofilm strategies; study biofilm heterogeneity; Model of biofilms present in oral cavity, catheters and wounds.	Low shear and high gas transfer; Allows for both solid/liquid and solid/air biofilm establishment; Compatible with different coupons (geometry); Non-invasive analysis of cell adhesion and biofilm formation; Allows the operation in continuous mode.	Heterogeneity of biofilm development on the coupons; Limited to low shear stress applications; Reduced volume and number of sampling surfaces; Difficult to control the environmental condition.

Table 2.7. (Continued)

Platforms	Main applications	Main advantages	Main disadvantages
Rotating Disc Reactor (RDR) 	Evaluation of antimicrobial and antifouling treatments; Used to study multispecies biofilms.	Liquid shear forces over the coupons can be varied.	The flow pattern changes in the boundaries of the coupons; Lack of sampling surface area; Biofilm formed on a flat surface.
Microfluidics 	Mimicking air-liquid interfaces provide *in situ* mixing of reagents.	Can be custom made for specific purposes; Versatile; Compatible with single cells analysis.	Requires special equipment for manufacturing and running systems; Can be expensive; Clogging can occur due to small dimensions.

2.4.1. Flow cell system

Amongst the diverse platforms created to study biofilms, researchers have been elected the flow cells for more than 30 years. These systems can be divided into different varieties, the one containing removable coupons, usually referred as large-scale flow cells (Figure 2.3a) [216, 260], and the one used in the studies through this thesis, that is particularly well-suited for real-time non-destructive microscopic analysis, usually small-scale flow cells (Figure 2.3b) [196]. Due to these features, flow cells have been used since the 1990s [261]. Although these devices are usually custom-made, some commercial alternatives are available, and even though they exist in a variety of shapes and sizes, flow cell systems are typically composed by pumps and tubes to circulate the cellular suspension and the growth medium through a chamber containing the test coupons made of different materials on which the microorganisms will adhere [262].

For instance, the semi-circular flow cells have been used as a platform to mimic the scale of industrial settings since turbulent flow is can be generated (Figure 2.3a) [216]. This system enables direct access to the coupons with the biofilm formed, usually after several days. However, these coupons must be removed from the system for analysis. Regarding the small flow cells models, such as flat plate flow cells, are able to evaluate different surfaces although the low amount of biofilm produced may include further analysis (chemical or biochemical) [255].

Ideally, the design of a flow displacement system should allow the fluid flow to be completely developed [24, 96].

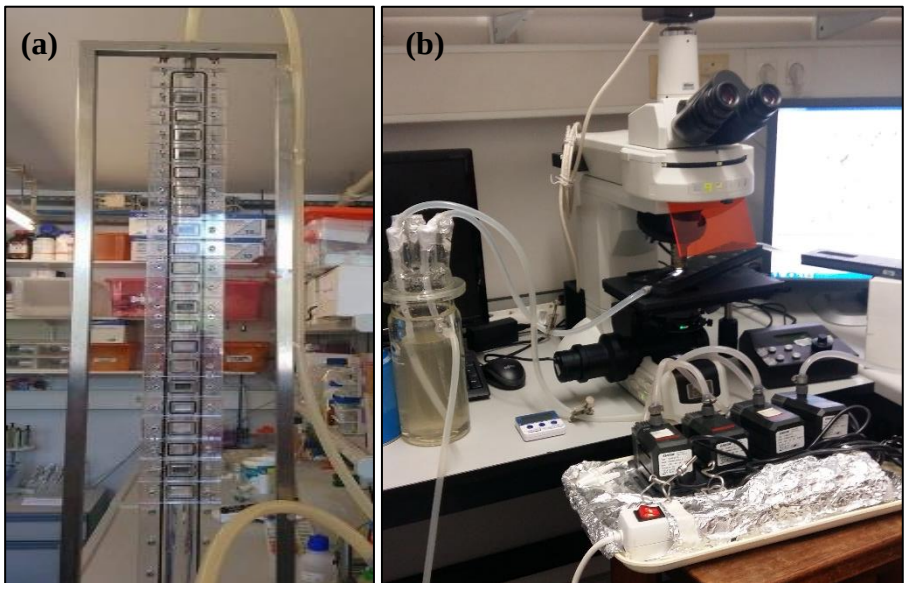

Figure 2.3. Illustrative photographs of flow cell systems: **(a)** semi-circular flow cell described by Teodósio et al. [216]; **(b)** parallel plate flow chamber (PPFC) described by Moreira et al. [96].

2.4.1.1. *Parallel plate flow cell (PPFC)*

The most widespread flow system to study adhesion is the PPFC developed by Bos et al.[17]. Adhesion can be operated in controlled hydrodynamic conditions that mimic physiologically relevant conditions, studying a wide range of microorganisms and surfaces with different properties. This platform enables the assessment of adhesion in real-time, allowing measurements of other experimental parameters such as the initial adhesion rate or removal rate after the passage of an air-liquid interface [24]. This system is easy to handle, requiring low volumes and consequently has reduced cost, enabling non-destructive real-time adhesion (single cell visualization) and biofilm observation [96, 263]. Several designs of these platforms have been used, however presenting some limitations, such as the area that can be used for adhesion studies and the limitations of the flow range [224].

The PPFC used to perform the studies reported in this thesis is represented in Figure 2.4. and was previously developed and described by our research group [96]. This platform has a rectangular cross section of 0.8 × 1.6 cm and a length of 25.42 cm. The inlet and outlet tubes have a diameter of 0.2 cm.

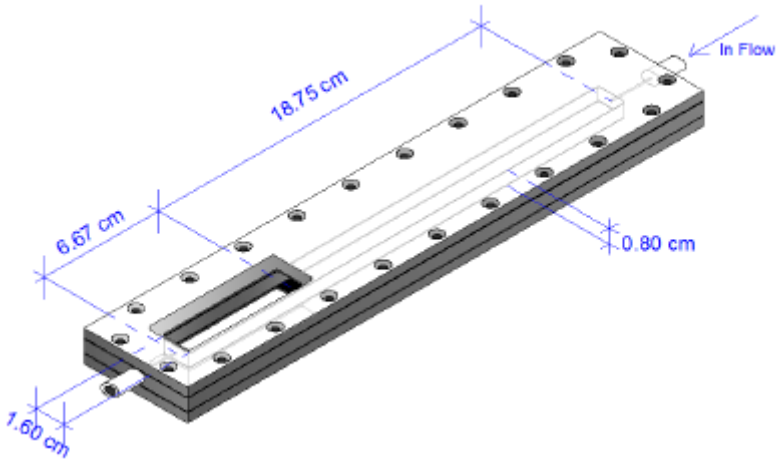

Figure 2.4. Schematic representation of the parallel plate flow cell.

In general, in order to mimic the shear for a specific condition in a PPFC, the dimensions of the flow cell or the flow rate should be adjusted [96, 255] to approach the required shear rates that can be achieved by the equations described in table 2.8.

Table 2.8. Equations required for wall shear rates, Reynolds (*Re)* and Péclet Number (*Pe*), and approximated Smoluchowski Levich **(**SL) solution at a distance x from the flow system inlet valid for rectangular flow displacement systems such as parallel plate flow cell (PPFC). Adapted from Busscher & van der Mei [24]

	Equation	Description
Wall shear rate, Υ(1/s)	$\frac{3Q}{(2h_0/2)^2 w_0}$	Derivative of the velocity in the perpendicular direction from the wall. Measurement of the frequency at which cells contact the wall.
Reynolds number, *Re*	$\frac{\rho Q}{(w_0 + h_0)\eta}$	Dimensionless quantity in fluid mechanics used to help predict flow patterns in different fluid flow situations.
Péclet number, *Pe*	$\frac{3v_{av}{R_b}^3}{2(h_0/2)^2 D_\infty}$	Represents the ratio between the convective and diffusional mass transport for the parallel plate configuration.
Smoluchowski Levich (SL) approximation, j_0^*	$0.538\frac{D_\infty C_b}{R_b}\left(\frac{Pe\, h_0}{x}\right)^{1/3}$	Determine the mass transport in flow displacement systems. It is assumed that the substratum surface acts as a perfect sink (e.g. all microorganisms sufficiently close to the surface adhere irreversibly).
Nomenclature of the terms used in the equations, (units)		
Q, volumetric flow rate (m^3/s)		
h_0, height of the rectangular flow channel (m)		
w_0, width of rectangular channel (m)		
D_∞, diffusion coefficient (around 10^{-13} for microorganisms)		
ρ, fluid density (kg/m^3)		
η, absolute viscosity (10^{-13} kg/m.s)		
v_{av}, average flow velocity (m/s)		
R_b, microbial radius (m)		
j_0^*, initial deposition rate ($1/cm^2$. s)		
C_b, bacterial concentration ($cell/m^3$)		
x, distance along the flow from the inlet (m)		

Measurement of microbial adhesion

PPFCs provide adequate control of the mass transport mechanisms and has been developed for real-time enumeration of microorganisms adhering to surfaces using microscopic techniques through automated image analysis [263]. The surfaces may or may not be transparent and, for transparent surfaces, light microscopy is the best option [96, 138]; otherwise, fluorochromes are used with epifluorescent microscopy [264].

The automated image analysis consists on the elaboration of a file that extracts the number of microorganisms adhering to the surface as a function of time [265]. The images are treated, and the adhered cells are distinguished from the background (surface). For that, it is necessary to apply a threshold to the sequence of images obtained [266]. This step, however, can lead to operator errors and therefore influence the result. Automated enumeration can only be used for adhesion analysis where cells are isolated on the surface. In addition, it is possible to extract the arrival and departure times of each adhering organism, in case of desorption analysis. However, this methodology requires an exact match of different images, such as a smaller

displacement of the field of view [24, 267].

The use of these methodologies allowed an advance in the study of bacterial adhesion in conditions more similar to those found in real scenarios [7, 19, 20]. However, despite the importance of mechanical forces in the establishment of biofilms in nature, their contributions to bacterial adhesion are poorly understood. There is a need of a more developed methodology able to study what happens for each instant of the adhesion process, contributing to a more reasonable interpretation of bacterial deposition in the PPFC system.

Measurement of biofilms

The extent of the biofilm developed can be measured using several methodologies that can be divided into macroscopic and microscopic methods (Table 2.9 and 2.10). The traditional approach to microbial quantification is based on plate counting. For this, biofilm cells are removed from the surface by sonication (bacteria adhered to the bottom and walls of the microtiter plate) or they can be detached from the surface by scraping and vortexing (bacteria adhered to coupons placed in the wells of the microtiter plates). However, plating is a labour-intensive and time-consuming, and can underestimate the number of viable cells due to the presence of viable but nonculturable cells (VBNCs).

Alternative techniques have been developed for the quantification of biofilms, including techniques to determine the total biofilm biomass (EPS as well as live/dead cells), the number of viable sessile cells only, or the amount of extracellular polymers in the biofilm matrix (Table 2.9). In the early ages of biofilm research, much focus was placed on the analysis of the amount and thickness of biofilms. These parameters are still of current interest in research using flow cell systems, however, in combination with the study of biofilm components, function and structure. Chemical methods using dyes or fluorochromes are also used to bind or adsorb to biofilm components. Crystal violet (CV) staining for biofilm quantification remains the most frequently used quantification technique in microplate assays [254]. These assays acts on living and dead cells, as well as some components present in the biofilm matrix, and are thus suitable for quantifying the total biofilm biomass [268]. However, this technique requires washing steps aimed at removing non-adherent bacteria as well as an excess dye, which may affect the detachment of some sessile cells and thereby affect measurements [269].

Colorimetric methods, such as the use of XTT (2,3-bis- (2-methoxy-4-nitro-5-sulfophenyl) -2H-tetrazolium-5-carboxanilide) or TTC (2,3,5-triphenyl-2H chloride) internal salt tetrazolium salts), which are tetrazolium and resazurin salts (also known as Alamar Blue), were also used to evaluate cell physiology in biofilms, allowing quantification of metabolic activity in biofilms. Resazurin has several advantages compared to tetrazolium salt assays since it is possible to

visually monitor the conversion of non-fluorescent blue to pink resazurin. It is non-toxic to eukaryotic cells and prokaryotes and is inexpensive [254]. Colorimetric methods that quantify exopolysaccharides, total proteins and carbohydrates were applied to quantify biofilm biomass. However, amounts of EPS components do not always correlate with biofilm biomass. To avoid this, it was suggested to measure phospholipids, which are universally distributed cellular components expressed at a relatively constant level among the microbial community. However, the determination of phospholipids is limited due to their recovery rate, amount of background lipid contamination and sensitivity of analytical equipment [270].

Despite the emergence of techniques for the macroscopic characterization of biofilms, the combination of microscopy with various labeling techniques and digital image acquisition/analysis software is extremely useful for the study of heterogeneity of biofilm [271].

Several imaging modalities have been used to detect biofilm biomass and cell viability. Brightfield or phase contrast microscopy remains a useful base-line technique to provide visual identification of biofilm formation. Light microscopy is advantageous because it requires simple sample preparation and is cheap and easy to perform. However, it can only be used on samples of biofilm grown on thin transparent surfaces, since the methodology requires the passage of a light beam through the sample. Therefore, more appropriate techniques for the study of biofilms have been used, such as Confocal Laser Scanning Microscopy (CLSM), Optical Coherence Tomography (OCT) and Scanning Electron Microscopy (SEM). Table 2.10 presents several microscopy approaches, highlighting their advantages and limitations. The methodologies described are important tools for assessing biofilm biomass properties as they allow describing biofilm spatial organization, their heterogeneities and links with the community functions in a more direct way.

- ***Optical coherence tomography (OCT)***

OCT is a non-destructive tool, is rapid and real-time, *in situ* imaging method for biofilm study [272]. For that, it is not required staining, contrary to what happens when using CLSM. Through this technique is possible to measure the thickness of the biofilm formed in a PPFC. This result is obtained by selecting different cross-sections under the surface and then 2D-cross sectional scans of the field of view are created (Figure 2.5a) [272]. From that, the surface and biofilm are delimited, and a maximum and minimum height are determined. An average from these points provides information about the biofilm thickness. The biofilm structure is thus obtained based on the signal strength distributions in the OCT images. Additionally, OCT can perform roughness analysis and obtain 3D-biofilm images of the tested surface (Figure 2.5b) and, therefore, obtain information about biofilms formed under different hydrodynamic conditions[148].

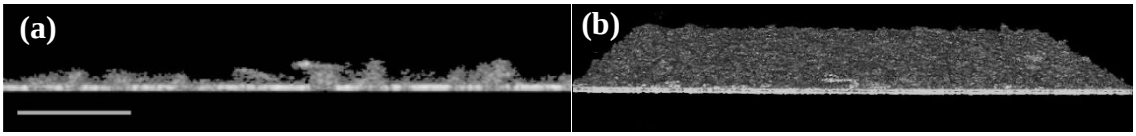

Figure 2.5. Representative images obtained by optical coherence tomography (OCT) of *Escherichia coli* JM109(DE3) biofilms formed in 24 h on polydimethylsiloxane (PDMS): **(a)** 2D cross-sectional OCT images (Scale bar = 200 μm); **(b)** 3D- OCT images of the biofilms were obtained from the 2D scans by selecting different zones of the samples with the same captured volume (3.66 x 1.52 x 2.98 mm^3 corresponding to 509 x 313 x 1024 $pixels^3$). Biofilm was formed at shear rate prevalent in urinary catheter (15/s).

Table 2.9. Methods used for biofilm quantification, such as biofilm biomass, viability and extracellular polymeric substances (EPS) measurements. Adapted from Azeredo et al. [254]

Method	Application	Advantages	Limitations
Microtiter plate dye-staining for total biomass (Crystal violet or safranin assay)	Indirect measurement of biofilm biomass	Versatility (different microorganisms) High throughput Does not require removal of the biofilm if it has been formed in a microtiter plate	Lack of reproducibility Lack of sensitivity Overestimation or underestimation of biofilm biomass, depending on the washing step A standardized protocol is not available
Microtiter plate dye-staining for biomass metabolic activity (Resazurin assay; XTT, TTC assay)	Indirect measurement of biofilm metabolic activity by chemical reduction of a dye	Versatility (applicable to a broad range of microorganisms) High throughput Does not require removal of the biofilm if it has been formed in a microtiter plate	Low detection limit ($>10^3$–10^8 CFU/biofilm) Difficult to use in polymicrobial biofilms (due to the different metabolic rates)
Cation-exchange resin – Dowex resin / Phenol sulphuric method (polysaccharide quantification); Lowry modified method (protein quantification)	Analyze EPS composition	Deciphering sugar and protein composition of EPS	Intracellular content contaminations
Digital micrometer Light microscope -- Confocal Laser Scanning Microscopy (CLSM) Optical Coherence Tomography (OCT)	Biofilm thickness and architecture measurements	Simple sample preparation Cheap and easy to perform -- Reconstruction of 3D images of a sample	Operator dependent Limited magnification and resolution -- Use of fluorophores is required Time consuming
Indirect measurement of biofilm by dry or wet weight	Physical methods to measure the weight	Easy to perform Non-destructive	Time consuming
Colony Formation Units (CFU) ATP bioluminescence assay Epifluorescence microscope (DAPI, Live/Dead BacLight bacterial viability kit)	Biofilm cells quantification	Available in all microbiology labs Easy to perform	Only detects the culturable fraction of the biofilm population (dormant, viable but nonculturable cells are not detected) Limited to microorganisms that develop colonies on agar plates Underestimates the number of culturable cells due to microbial aggregation time-consuming

Table 2.10. Relevant microscopy techniques applied to the study of biofilms. Adapted from Azeredo et al. [254], Sen & Yadav [273].

Method	Application	Advantages	Limitations
Light microscopy	Visual identification of biofilm formation Quantitative assessment of biofilm biomass Useful combination with transmission electron microscopy or scanning electron microscopy	Simple sample preparation Cheap and easy to perform Imaging of larger parts of a sample compared to electron microscopy	Limited magnification and resolution Sample staining necessary Morphotype differentiation relatively gross Lacking discriminatory detail
Epifluorescence microscopy	Distribution and enumeration of biofilm cells on the surface	Easy to perform Less expensive	2D imaging only Not applicable to thick biofilms The use of fluorochromes is necessary for viewing bacteria
Atomic force microscopy (AFM)	Quantitative biofilm analysis used to confirm findings obtained with other quantitative or imaging techniques Biofilm topography and morphological in *situ* imaging	Non-destructive technique Works under ambient conditions, which minimizes pre-treatments and artifacts even on liquid surfaces (enables *in situ* imaging) Same resolution along and perpendicular to the surface 3D-reconstruction Qualitative and quantitative assessment of living biofilms under physiological-like conditions	Inability to obtain a large area survey scan Sample damage or artifacts caused by tip shape and size (although generally considered negligible)
Confocal laser scanning microscopy (CLSM)	Biofilm visualization and quantification of structural parameters Biofilm spatial structure Spatial distribution of viable bacteria, localized cell death Antimicrobials effect on cell viability	Resolution compatible with single cell visualization Reconstruction of 3D-images of a sample No need for extensive computer processing	Use of fluorophores is required Limited number of reporter molecules (i.e. no universal matrix probes exist) Interference of local properties of the biofilm with the fluorescence probes Natural auto-fluorescence may hide signal of interest
Scanning electron microscopy (SEM)	Study of the biofilm spatial structure Evaluation of the effects of exposure to antibiofilm drugs Biofilm formation kinetics assessment Qualitative support for findings from quantification methods (high correlation) Possible quantitative analysis using dedicated imaging software	Resolution higher than other imaging techniques (resolves surface details) Good depth of field Ability to image complex shapes Wide range of magnifications (20x to 30000x)	Tedious and time-consuming sample preparation Lacks vertical resolution Preparation processes (fixation, dehydration, and coating with a conductive material) can destroy sample structure or cause artifacts

- ***Confocal laser scanning microscopy (CLSM)***

CLSM emerged in the early 1990s as the most versatile and powerful microscopic technique for studying the spatial structure of biofilm and its associated functions [254, 274]. Through the technique, it is possible to acquire multiple images designated as a "stack" (series of digital *xy* optical planes) at different depths of the sample. Combining these plans makes possible to reconstruct the 3D architecture of the biofilm (Figure 2.6) as well to extract quantitative structural parameters such as biovolume, thickness, and roughness of the biofilm [275]. CLSM biofilm images can be obtained with a range of fluorescent probes with unique specificities, the most common being cell-permeant nucleic acid dyes, SYTO™ 9, SYTO™ 61 and SYBR-Green [254, 276].

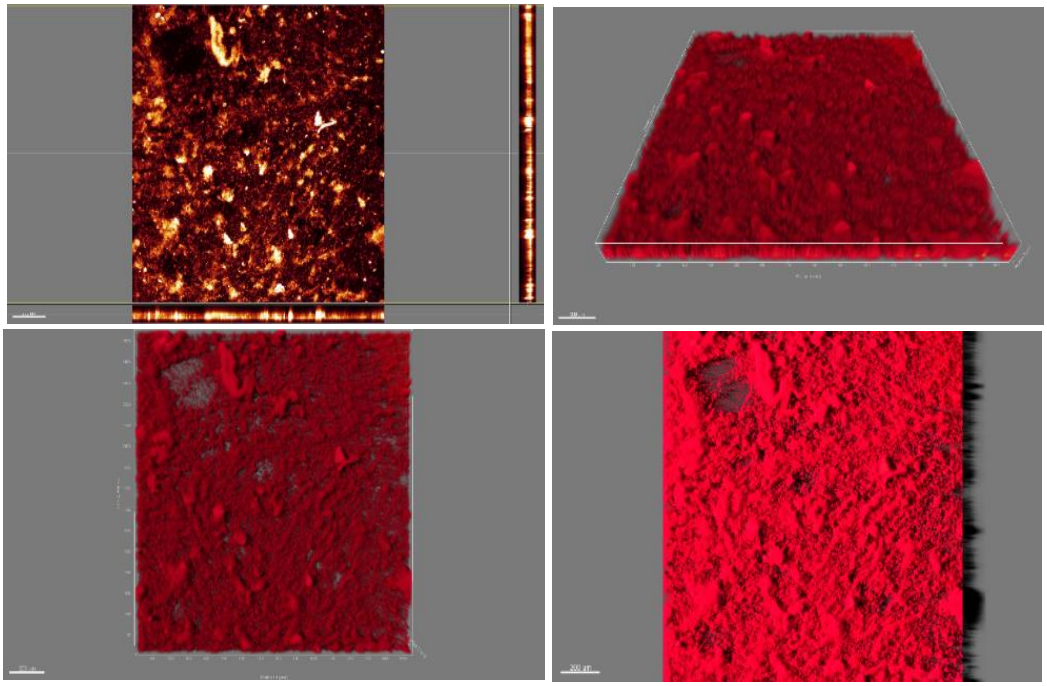

Figure 2.6. 3D projections of *Escherichia coli* JM109(DE3) biofilms on glass obtained from confocal *z* stacks using IMARIS software. Biofilm samples were counterstained in red with Syto™ 61, a cell-permeant fluorescent nucleic acid stain. The representative images present an aerial view of the biofilms formed in 24 h (shadow projection on the right). The white bar corresponds to 200 μm.

Specific microorganisms within a complex community can be localized using specific oligonucleotides employing *in situ* fluorescent hybridizations (FISH) approaches, and the study of biofilm structure is also possible [277]. The use of genetically engineered bacteria to make them fluorescent, for example, by expressing green fluorescent protein (GFP) [275] is also a possibility. Another possibility offered by CLSM is the analysis of cell death in a biofilm. Several fluorescent dyes are used in CLSM images, the live/dead mix being one of the most popular. This procedure

couples green SYTO™ 9 and red propidium iodide, so that bacteria with a compromised membrane appear yellow or red, while viable cells appear green. This labeling can be used, for example, to analyze the spatial distribution of viable bacteria, to observe the existence of localized cell death in biofilms and their regulation, and to evaluate the effect of various antimicrobials on the cell viability. However, live/dead color in CLSM imaging should be carefully analysed, as the differentiation between red or green channels is often influenced by the intensity of the lasers used. Despite the intrinsic limitations associated with the need for fluorophores, CLSM remains a method of choice for biofilm visualization and quantification [254].

Image processing software is often used for instance with images extracted from CLSM. Such programs enable quantitative analysis of biofilm images, such as Imaris®, that was designed to generate 3D images with shadow projection, cross-sections and 3D images (Figure 2.6).

However, since some software packages are rather costly, some research groups prefer to use alternative public domain software packages. Among these is the popular image processing software ImageJ, an open system to which independent software developers can make plugins for qualitative and quantitative purposes [278]. Another very popular free software for non-commercial purposes is the Daime image processing package [279], which enables both visualization of image data and some analytical processing. Contrary to the ImageJ plugins, this package was created with biofilm images in mind and can be used for visualization and analysis.

For quantitative purposes, it is important to know how to use biofilm images to quantitate biomass, biofilm thickness, roughness coefficient, and fractal dimension. In CLSM, the raw data is extracted from confocal microscopy stack images, a range of individual images (slices) is recorded from focal planes at specified positions. One of the most commonly used software to quantify these parameters is the Comstat package, originally created as a MATLAB script [280] and later rewritten as a plugin (Comstat2) for ImageJ [281]. Similar packages are the MATLAB script PHLIP [282] and ISA3D, which is a compiled MATLAB script [283]. Daime [281] is an alternative software, designed for data presentation not being dedicated to, but capable of extracting quantitative data. ImageJ, general-purpose software can also, be used for quantitative purposes [284] with plugins, ImagePro Plus, Imaris and Volocity. However, it should be noted that quantification programs have some typical inherent problems, being the main one the determination of the threshold value. Still, unless special conditions are applied, the most advanced automatic threshold mechanisms provide comparable and acceptable results [285]. In experiments with biofilms, there is a variation of results that is common to all analysis techniques making statistical analysis necessary to validate the results [286].

- ***Scanning electron microscopy (SEM)***

SEM is a well-established microscopic technique based on surface scattering and absorption of electrons [254]. SEM micrographs have a large depth of field yielding a 3D rendering of the biofilm surface. Although this technique lacks vertical resolution, it can reveal the morphology of bacteria adhered to a surface, the surface morphology as well the relation between both [287] (Figure 2.7a). Accordingly, SEM has been a preferred method for visualizing biofilms since it provides information about the spatial structure and detects the presence of EPS [288] (Figure 2.7b). It is an extremely useful tool for comparative analysis in biofilm research. SEM imaging has been generally performed to qualitatively support findings from other quantification methods showing a high correlation [287].

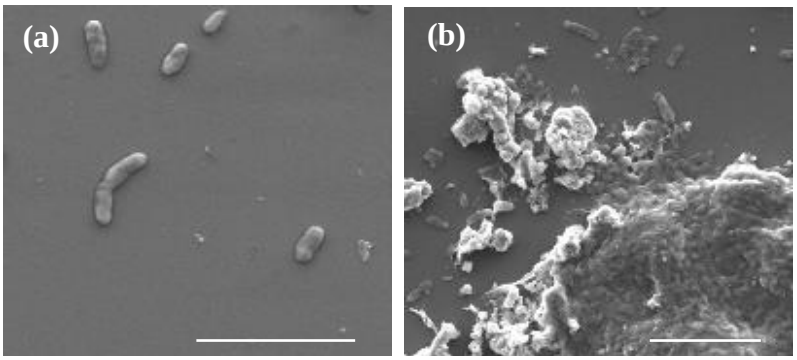

Figure 2.7. Scanning electron microscopy (SEM) analysis of *Escherichia coli* JM109(DE3) biofilms formed in artificial urine medium after 24 h of development on polydimethylsiloxane (PDMS): **(a)** representative micrographs of single cell adhesion (magnification: 10000x; bars = 5 μm); **(b)** representative micrographs of biofilm structure (magnification: 5000x; bars = 10 μm).

In sum, it is well known that the study of biofilms has been undergoing a great evolution. The physiology of single cells and interactions within a biofilm has been analysed at an ever-increasing level of detail. For this, the development of new and better hardware tools such as microfluidics and high-resolution microscopy was essential.

2.5. References

1. Costerton, J. W.; Geesey, G.; Cheng, K., How bacteria stick. *Scientific American* **1978,** *238* (1), 86-95.
2. Zobell, C. E.; Allen, E. C., The significance of marine bacteria in the fouling of submerged surfaces. *Journal of Bacteriology* **1935,** *29* (3), 239.
3. Berne, C.; Ellison, C. K.; Ducret, A.; Brun, Y. V., Bacterial adhesion at the single-cell level. *Nature Reviews Microbiology* **2018,** *16* (10), 616.
4. Characklis, W., Bioengineering report. Fouling biofilm: a process analysis. *Biotechnology and Bioengineering* **1981,** *23*, 1923-1960.
5. Bott, T.; Pinheiro, M., Biological fouling - velocity and temperature effects. *The Canadian Journal of Chemical Engineering* **1977,** *55* (4), 473-474.
6. Marshall, K. C.; Breznak, J. In *Microbial adhesion and aggregation*, Dahlem Workshop on Microbial Adhesion and Aggregation (1984), Springer-Verlag: 1984.
7. Gibbons, R.; Nygaard, M., Interbacterial aggregation of plaque bacteria. *Archives of Oral Biology* **1970,** *15* (12), 1397-IN39.
8. Arciola, C. R.; Campoccia, D.; Montanaro, L., Implant infections: adhesion, biofilm formation and immune evasion. *Nature Reviews Microbiology* **2018,** *16* (7), 397.
9. Ceri, H.; Olson, M.; Stremick, C.; Read, R.; Morck, D.; Buret, A., The Calgary Biofilm Device: new technology for rapid determination of antibiotic susceptibilities of bacterial biofilms. *Journal of Clinical Microbiology* **1999,** *37* (6), 1771-1776.
10. Picioreanu, C.; van Loosdrecht, M. C.; Heijnen, J. J., A new combined differential-discrete cellular automaton approach for biofilm modeling: application for growth in gel beads. *Biotechnology and Bioengineering* **1998,** *57* (6), 718-731.
11. Koo, H.; Allan, R. N.; Howlin, R. P.; Stoodley, P.; Hall-Stoodley, L., Targeting microbial biofilms: current and prospective therapeutic strategies. *Nature Reviews Microbiology* **2017,** *15* (12), 740-755.
12. Alves, P.; Nir, S.; Reches, M.; Mergulhão, F., The effects of fluid composition and shear conditions on bacterial adhesion to an antifouling peptide-coated surface. *MRS Communications* **2018,** *8* (3), 938-946.
13. Alves, P.; Gomes, L. C.; Rodríguez-Emmenegger, C.; Mergulhão, F. J., Efficacy of a poly(MeOEGMA) brush on the prevention of *Escherichia coli* biofilm formation and susceptibility. *Antibiotics (Basel, Switzerland)* **2020,** *9* (5).
14. Kaali, P.; Strömberg, E.; Karlsson, S., *Prevention of biofilm associated infections and degradation of polymeric materials used in biomedical applications*. INTECH Open Access Publisher: 2011.
15. Davey, M. E.; O'toole, G. A., Microbial biofilms: from ecology to molecular genetics. *Microbiology and Molecular Biology Reviews* **2000,** *64* (4), 847-867.
16. Camper, A. K.; Warnecke, M.; Jones, W.; McFeters, G., *Pathogens in model distribution system biofilms*. American Water Works Association: Denver, 1998.
17. Bos, R.; Van der Mei, H. C.; Busscher, H. J., Physico-chemistry of initial microbial adhesive interactions–its mechanisms and methods for study. *FEMS Microbiology Reviews* **1999,** *23* (2), 179-230.
18. Costerton, J., Overview of microbial biofilms. *Journal of Industrial Microbiology & Biotechnology* **1995,** *15* (3), 137-140.
19. Donlan, R. M.; Costerton, J. W., Biofilms: survival mechanisms of clinically relevant microorganisms. *Clinical Microbiology Reviews* **2002,** *15* (2), 167-193.

20. Beloin, C.; Roux, A.; Ghigo, J. M., *Escherichia coli* biofilms. *Current Topics in Microbiology and Immunology* **2008,** *322*, 249-289.

21. Limoli, D. H.; Jones, C. J.; Wozniak, D. J., Bacterial extracellular polysaccharides in biofilm formation and function. *Microbiol Spectr* **2015,** *3* (3), 10.1128/microbiolspec.MB-0011-2014.

22. Gilbert, P.; Das, J.; Foley, I., Biofilm susceptibility to antimicrobials. *Advances in Dental Research* **1997,** *11* (1), 160-167.

23. Dunne, W. M., Bacterial adhesion: seen any good biofilms lately? *Clinical Microbiology Reviews* **2002,** *15* (2), 155-166.

24. Busscher, H. J.; van der Mei, H. C., Microbial adhesion in flow displacement systems. *Clinical Microbiology Reviews* **2006,** *19* (1), 127-141.

25. Hall, C. W.; Mah, T.-F., Molecular mechanisms of biofilm-based antibiotic resistance and tolerance in pathogenic bacteria. *FEMS Microbiology Reviews* **2017,** *41* (3), 276-301.

26. Shunmugaperumal, T., *Biofilm eradication and prevention: a pharmaceutical approach to medical device infections*. John Wiley & Sons: Hoboken, New Jersey, 2010.

27. Miquel, S.; Lagrafeuille, R.; Souweine, B.; Forestier, C., Anti-biofilm activity as a health issue. *Frontiers in Microbiology* **2016,** *7*.

28. Costerton, J. W.; Lewandowski, Z.; Caldwell, D. E.; Korber, D. R.; Lappin-Scott, H. M., Microbial biofilms. *Annual Reviews in Microbiology* **1995,** *49* (1), 711-745.

29. Korber, D.; Lawrence, J.; Lappin-Scott, H.; Costerton, J., The formation of microcolonies and functional consortia within biofilms. In *Bacterial Biofilms*, Costerton, H. M. L.-S. J. W., Ed. Cambridge University Press: Cambridge, 1995; pp 15-45.

30. Stoodley, P.; Lewandowski, Z., Liquid flow in biofilm systems. *Applied and Environmental Microbiology* **1994,** *60* (8), 2711-2716.

31. Teodósio, J.; Simões, M.; Melo, L.; Mergulhão, F., The influence of the nutrient load on the formation of *Escherichia coli* biofilms. In *Advances in medicine and biology*, 1st Edition ed.; Berhardt, L. V., Ed. Nova Science Publishers, Inc: New York, 2011; Vol. 20, pp 153-168.

32. Miller, M. B.; Bassler, B. L., Quorum sensing in bacteria. *Annual Reviews in Microbiology* **2001,** *55* (1), 165-199.

33. Bryers, J. D., Modeling biofilm accumulation. In *Physiological Models in Microbiology*, 1s ed.; Bazin, M., Ed. CRC Press: Boca Raton, 1988; Vol. 2, pp 109-144.

34. Choi, Y.; Morgenroth, E., Monitoring biofilm detachment under dynamic changes in shear stress using laser-based particle size analysis and mass fractionation. *Water Science and Technology* **2003,** *47* (5), 69-76.

35. Donlan, R. M., Biofilms: microbial life on surfaces. *Emerging Infectious Diseases* **2002,** *8* (9), 881.

36. Van Houdt, R.; Michiels, C. W., Role of bacterial cell surface structures in *Escherichia coli* biofilm formation. *Research in Microbiology* **2005,** *156* (5-6), 626-633.

37. Campoccia, D.; Montanaro, L.; Arciola, C. R., A review of the biomaterials technologies for infection-resistant surfaces. *Biomaterials* **2013,** *34* (34), 8533-8554.

38. Richter, A. M.; Possling, A.; Malysheva, N.; Yousef, K. P.; Herbst, S.; von Kleist, M.; Hengge, R., Local c-di-GMP signaling in the control of synthesis of the *E. coli* biofilm exopolysaccharide pEtN-cellulose. *Journal of Molecular Biology* **2020**.

39. Gordon, V. D.; Davis-Fields, M.; Kovach, K.; Rodesney, C. A., Biofilms and mechanics: a review of experimental techniques and findings. *Journal of Physics D: Applied Physics* **2017,** *50* (22), 223002.

40. Almeida, E.; Diamantino, T. C.; de Sousa, O., Marine paints: The particular case of antifouling paints. *Progress in Organic Coatings* **2007,** *59* (1), 2-20.

41. Railkin, A. I., *Marine biofouling: colonization processes and defenses* CRC Press: Boca Raton, Florida, 2004; p 320.

42. Willemsen, P., Biofouling in European aquaculture: is there an easy solution? *European Aquaculture Society Special Publication* 2005, pp 82-87.

43. Brooks, J. D.; Flint, S. H., Biofilms in the food industry: problems and potential solutions. *International Journal of Food Science & Technology* **2008,** *43* (12), 2163-2176.

44. Srey, S.; Jahid, I. K.; Ha, S.-D., Biofilm formation in food industries: a food safety concern. *Food Control* **2013,** *31* (2), 572-585.

45. Arnold, J.; Boothe, D.; Suzuki, O.; Bailey, G., Multiple imaging techniques demonstrate the manipulation of surfaces to reduce bacterial contamination and corrosion. *Journal of Microscopy* **2004,** *216* (3), 215-221.

46. Hancock, V.; Ferrières, L.; Klemm, P., Biofilm formation by asymptomatic and virulent urinary tract infectious *Escherichia coli* strains. *FEMS microbiology letters* **2006,** *267* (1), 30-37.

47. Römling, U.; Kjelleberg, S.; Normark, S.; Nyman, L.; Uhlin, B. E.; Åkerlund, B., Microbial biofilm formation: a need to act. *Journal of Internal Medicine* **2014,** *276* (2), 98-110.

48. Perencevich, E. N.; Sands, K. E.; Cosgrove, S. E.; Guadagnoli, E.; Meara, E.; Platt, R., Health and economic impact of surgical site infections diagnosed after hospital discharge. *Emerging Infectious Diseases* **2003,** *9* (2), 196.

49. Hultberg, M.; Asp, H.; Marttila, S.; Bergstrand, K.-J.; Gustafsson, S., Biofilm formation by *Chlorella vulgaris* is affected by light quality. *Current Microbiology* **2014,** *69* (5), 699-702.

50. Pompermayer, D. M.; Gaylarde, C. C., The influence of temperature on the adhesion of mixed cultures of *Staphylococcus aureus* and *Escherichia coli* to polypropylene. *Food Microbiology* **2000,** *17* (4), 361-365.

51. Marschang, S.; Bernardo, G., Prevention and control of healthcare-associated infection in Europe: a review of patients' perspectives and existing differences. *Journal of Hospital Infection* **2015,** *89* (4), 357-362.

52. Zingg, W.; Holmes, A.; Dettenkofer, M.; Goetting, T.; Secci, F.; Clack, L.; Allegranzi, B.; Magiorakos, A.-P.; Pittet, D., Hospital organisation, management, and structure for prevention of health-care-associated infection: a systematic review and expert consensus. *The Lancet Infectious Diseases* **2015,** *15* (2), 212-224.

53. Smith, R. N.; Nolan, J. P., Central venous catheters. *British Medical Journal* **2013,** *347*, f6570.

54. Murdoch, D. R.; Corey, G. R.; Hoen, B.; Miró, J. M.; Fowler, V. G.; Bayer, A. S.; Karchmer, A. W.; Olaison, L.; Pappas, P. A.; Moreillon, P., Clinical presentation, etiology, and outcome of infective endocarditis in the 21st century: the International Collaboration on Endocarditis–Prospective Cohort Study. *Archives of Internal Medicine* **2009,** *169* (5), 463-473.

55. Barbadoro, P.; Labricciosa, F. M.; Recanatini, C.; Gori, G.; Tirabassi, F.; Martini, E.; Gioia, M. G.; D'Errico, M. M.; Prospero, E., Catheter-associated urinary tract infection: role of the setting of catheter insertion. *American Journal of Infection Control* **2015,** *43* (7), 707-710.

56. Campoccia, D.; Montanaro, L.; Arciola, C. R., The significance of infection related to orthopedic devices and issues of antibiotic resistance. *Biomaterials* **2006,** *27* (11), 2331-2339.

57. Inacio, R. C.; Klautau, G. B.; Murça, M. A. S.; da Silva, C. B.; Nigro, S.; Rivetti, L. A.; Pereira, W. L.; Salles, M. J. C., Microbial diagnosis of infection and colonization of cardiac implantable electronic devices by use of sonication. *International Journal of Infectious Diseases* **2015,** *38*, 54-59.

58. Auler, M. E.; Morreira, D.; Rodrigues, F. F.; Abr Ão, M. S.; Margarido, P. F.; Matsumoto, F. E.; Silva, E. G.; Silva, B. C.; Schneider, R. P.; Paula, C. R., Biofilm formation on intrauterine devices in patients with recurrent vulvovaginal candidiasis. *Medical Mycology* **2010,** *48* (1), 211-216.

59. Zhou, H.-F.; Huang, M.; Ji, J.-S.; Zhu, H.-D.; Lu, J.; Guo, J.-H.; Chen, L.; Zhong, B.-Y.; Zhu, G.-Y.; Teng, G.-J., Risk prediction for early biliary infection after percutaneous transhepatic biliary stent placement in malignant biliary obstruction. *Journal of Vascular and Interventional Radiology* **2019,** *30* (8), 1233-1241.e1.

60. Franchelli, S.; Pesce, M.; Baldelli, I.; Marchese, A.; Santi, P.; De Maria, A., Analysis of clinical management of infected breast implants and of factors associated to successful breast pocket salvage in infections occurring after breast reconstruction. *International Journal of Infectious Diseases* **2018,** *71*, 67-72.

61. Wu, Y. T.; Tam, C.; Zhu, L. S.; Evans, D. J.; Fleiszig, S. M. J., Human tear fluid reduces culturability of contact lens-associated *Pseudomonas aeruginosa* biofilms but induces expression of the virulence-associated type III secretion system. *The Ocular Surface* **2017,** *15* (1), 88-96.

62. van der Mei, H. C.; Buijssen, K. J.; van der Laan, B. F.; Ovchinnikova, E.; Geertsema-Doornbusch, G. I.; Atema-Smit, J.; van de Belt-Gritter, B.; Busscher, H. J., Voice prosthetic biofilm formation and *Candida morphogenic* conversions in absence and presence of different bacterial strains and species on silicone-rubber. *PloS One* **2014,** *9* (8), e104508.

63. Lebeaux, D.; Ghigo, J.-M.; Beloin, C., Biofilm-related infections: bridging the gap between clinical management and fundamental aspects of recalcitrance toward antibiotics. *Microbiology and Molecular Biology Reviews* **2014,** *78* (3), 510-543.

64. Stamm, W. E.; Norrby, S. R., Urinary tract infections: disease panorama and challenges. *The Journal of Infectious Diseases* **2001,** *183* (Supplement_1), S1-S4.

65. Sihra, N.; Goodman, A.; Zakri, R.; Sahai, A.; Malde, S., Nonantibiotic prevention and management of recurrent urinary tract infection. *Nature Reviews Urology* **2018**, 1.

66. Siddiq, D. M.; Darouiche, R. O., New strategies to prevent catheter-associated urinary tract infections. *Nature Reviews Urology* **2012,** *9* (6), 305.

67. Wi, Y. M.; Patel, R., Understanding biofilms and novel approaches to the diagnosis, prevention, and treatment of medical device-associated infections. *Infectious Disease Clinics* **2018,** *32* (4), 915-929.

68. Holá, V.; Ruzicka, F.; Horka, M., Microbial diversity in biofilm infections of the urinary tract with the use of sonication techniques. *FEMS Immunology & Medical Microbiology* **2010,** *59* (3), 525-528.

69. Wiley, L.; Bridge, D. R.; Wiley, L. A.; Odom, J. V.; Elliott, T.; Olson, J. C., Bacterial biofilm diversity in contact lens-related disease: emerging role of *Achromobacter*, *Stenotrophomonas*, and *Delftia*. *Investigative Ophthalmology & Visual Science* **2012,** *53* (7), 3896-3905.

70. Sankaridurg, P. R.; Sharma, S.; Willcox, M.; Naduvilath, T. J.; Sweeney, D. F.; Holden, B. A.; Rao, G. N., Bacterial colonization of disposable soft contact lenses is greater during corneal infiltrative events than during asymptomatic extended lens wear. *Journal of Clinical Microbiology* **2000,** *38* (12), 4420-4424.

71. Liu, Z.; Kong, Y.; Gao, Y.; Ren, Y.; Zheng, C.; Deng, X.; Chen, T., Revealing the interaction between intrauterine adhesion and vaginal microbiota using high-throughput sequencing. *Molecular Medicine Reports* **2019,** *19* (5), 4167-4174.

72. Pál, Z.; Urbán, E.; Dósa, E.; Pál, A.; Nagy, E., Biofilm formation on intrauterine devices in relation to duration of use. *Journal of Medical Microbiology* **2005,** *54* (12), 1199-1203.

73. Schneider, J.; Hapfelmeier, A.; Fremd, J.; Schenk, P.; Obermeier, A.; Burgkart, R.; Forkl, S.; Feihl, S.; Wantia, N.; Neu, B., Biliary endoprosthesis: a prospective analysis of bacterial colonization and risk factors for sludge formation. *PloS One* **2014,** *9* (10), e110112.

74. Donelli, G.; Guaglianone, E.; Di Rosa, R.; Fiocca, F.; Basoli, A., Plastic biliary stent occlusion: factors involved and possible preventive approaches. *Clinical Medicine & Research* **2007,** *5* (1), 53-60.

75. Basioukas, P.; Vezakis, A.; Zarkotou, O.; Fragulidis, G.; Themeli-Digalaki, K.; Rizos, S.; Polydorou, A., Isolated microorganisms in plastic biliary stents placed for benign and malignant diseases. *Annals of Gastroenterology* **2014,** *27* (4), 399.

76. Karau, M. J.; Greenwood-Quaintance, K. E.; Schmidt, S. M.; Tran, N. V.; Convery, P. A.; Jacobson, S. R.; Bite, U.; Clay, R. P.; Petty, P. M.; Johnson, C. H., Microbial biofilms and breast tissue expanders. *BioMed Research International* **2013,** *2013*.

77. Lynch, A. S.; Robertson, G. T., Bacterial and fungal biofilm infections. *Annual Review of Medicine* **2008,** *59*, 415-428.

78. James, G. A.; Boegli, L.; Hancock, J.; Bowersock, L.; Parker, A.; Kinney, B. M., Bacterial adhesion and biofilm formation on textured breast implant shell materials. *Aesthetic Plastic Surgery* **2019,** *43* (2), 490-497.

79. Flores-Mireles, A. L.; Walker, J. N.; Caparon, M.; Hultgren, S. J., Urinary tract infections: epidemiology, mechanisms of infection and treatment options. *Nature Reviews Microbiology* **2015,** *13* (5), 269-284.

80. Trautner, B. W.; Lopez, A. I.; Kumar, A.; Siddiq, D. M.; Liao, K. S.; Li, Y.; Tweardy, D. J.; Cai, C., Nanoscale surface modification favors benign biofilm formation and impedes adherence by pathogens. *Nanomedicine: Nanotechnology, Biology and Medicine* **2012,** *8* (3), 261-270.

81. Vila, J.; Sáez-López, E.; Johnson, J. R.; Römling, U.; Dobrindt, U.; Cantón, R.; Giske, C. G.; Naas, T.; Carattoli, A.; Martínez-Medina, M.; Bosch, J.; Retamar, P.; Rodríguez-Baño, J.; Baquero, F.; Soto, S. M., *Escherichia coli*: an old friend with new tidings. *FEMS Microbiology Reviews* **2016,** *40* (4), 437-463.

82. Manges, A. R.; Geum, H. M.; Guo, A.; Edens, T. J.; Fibke, C. D.; Pitout, J. D. D., Global Extraintestinal Pathogenic *Escherichia coli* (ExPEC) Lineages. *Clinical Microbiology Reviews* **2019,** *32* (3), e00135-18.

83. Asadi Karam, M. R.; Habibi, M.; Bouzari, S., Urinary tract infection: pathogenicity, antibiotic resistance and development of effective vaccines against Uropathogenic *Escherichia coli*. *Molecular Immunology* **2019,** *108*, 56-67.

84. McNamara, J. F.; Avent, M.; Stewart, A.; Kwan, C.; Paterson, D. L., Evaluation of quick sequential organ failure assessment and systemic inflammatory response syndrome in patients with gram negative bloodstream infection. *Infection, Disease & Health* **2020**.

85. Russo, T. A.; Johnson, J. R., Medical and economic impact of extraintestinal infections due to *Escherichia coli*: focus on an increasingly important endemic problem. *Microbes and Infection* **2003,** *5* (5), 449-456.

86. Biran, D.; Ron, E. Z., Extraintestinal pathogenic *Escherichia coli*. *Current topics in microbiology and immunology* **2018,** *416*, 149-161.

87. Flemming, H.-C.; Wingender, J.; Szewzyk, U.; Steinberg, P.; Rice, S. A.; Kjelleberg, S., Biofilms: an emergent form of bacterial life. *Nature Reviews Microbiology* **2016,** *14* (9), 563-575.

88. Klein, R. D.; Hultgren, S. J., Urinary tract infections: microbial pathogenesis, host–pathogen interactions and new treatment strategies. *Nature Reviews Microbiology* **2020,** *18* (4), 211-226.

89. Sauer, M. M.; Jakob, R. P.; Luber, T.; Canonica, F.; Navarra, G.; Ernst, B.; Unverzagt, C.; Maier, T.; Glockshuber, R., Binding of the bacterial adhesin FimH to its natural, multivalent high-mannose type glycan targets. *Journal of the American Chemical Society* **2019,** *141* (2), 936-944.

90. DeBenedictis, E. P.; Liu, J.; Keten, S., Adhesion mechanisms of curli subunit CsgA to abiotic surfaces. *Science advances* **2016,** *2* (11), e1600998.

91. Pratt, L. A.; Kolter, R., Genetic analysis of *Escherichia coli* biofilm formation: roles of flagella, motility, chemotaxis and type I pili. *Molecular microbiology* **1998,** *30* (2), 285-93.

92. Friedlander, R. S.; Vlamakis, H.; Kim, P.; Khan, M.; Kolter, R.; Aizenberg, J., Bacterial flagella explore microscale hummocks and hollows to increase adhesion. *Proceedings of the National Academy of Sciences* **2013,** *110* (14), 5624.

93. Reisner, A.; Haagensen, J. A.; Schembri, M. A.; Zechner, E. L.; Molin, S., Development and maturation of *Escherichia coli* K-12 biofilms. *Molecular microbiology* **2003,** *48* (4), 933-46.

94. Koseoglu, H.; Aslan, G.; Esen, N.; Sen, B. H.; Coban, H., Ultrastructural stages of biofilm development of *Escherichia coli* on urethral catheters and effects of antibiotics on biofilm formation. *Urology* **2006,** *68* (5), 942-946.

95. Teodósio, J.; Simões, M.; Melo, L.; Mergulhão, F., Flow cell hydrodynamics and their effects on *E. coli* biofilm formation under different nutrient conditions and turbulent flow. *Biofouling* **2011,** *27* (1), 1-11.

96. Moreira, J.; Araújo, J.; Miranda, J. M.; Simões, M.; Melo, L.; Mergulhão, F., The effects of surface properties on *Escherichia coli* adhesion are modulated by shear stress. *Colloids and Surfaces B: Biointerfaces* **2014,** *123*, 1-7.

97. Wu, H.; Moser, C.; Wang, H.-Z.; Høiby, N.; Song, Z.-J., Strategies for combating bacterial biofilm infections. *International Journal of Oral Science* **2015,** *7* (1), 1.

98. Hancock, V.; Witsø, I. L.; Klemm, P., Biofilm formation as a function of adhesin, growth medium, substratum and strain type. *International Journal of Medical Microbiology* **2011,** *301* (7), 570-576.

99. Koerner, R.; Butterworth, L.; Mayer, I.; Dasbach, R.; Busscher, H., Bacterial adhesion to titanium-oxy-nitride (TiNOX) coatings with different resistivities: a novel approach for the development of biomaterials. *Biomaterials* **2002,** *23* (14), 2835-2840.

100. Melo, L. F.; Flemming, H.-C., Mechanistic aspects of heat exchanger and membrane biofouling and prevention. In *The science and technology of industrial water treatment*, Amjad, Z., Ed. CRC press: New York, 2010; pp 365-380.

101. Busscher, H. J.; van der Mei, H. C.; Subbiahdoss, G.; Jutte, P. C.; van den Dungen, J. J.; Zaat, S. A.; Schultz, M. J.; Grainger, D. W., Biomaterial-associated infection: locating the finish line in the race for the surface. *Science Translational Medicine* **2012,** *4* (153), 153rv10-153rv10.

102. Fletcher, M.; Loeb, G., Influence of substratum characteristics on the attachment of a marine pseudomonad to solid surfaces. *Applied and Environmental Microbiology* **1979,** *37* (1), 67-72.

103. Buijssen, K. J.; Oosterhof, J. J.; Basil, L.; Waters, M.; Duits, M.-A.; Busscher, H. J.; Mei, H.; Laan, B., Influence of surface roughness on silicone rubber voice prostheses on in vitro biofilm formation and clinical lifetime in laryngectomised patients. *Clinical Otolaryngology* **2017**.

104. Ong, Y.-L.; Razatos, A.; Georgiou, G.; Sharma, M. M., Adhesion forces between *E. coli* bacteria and biomaterial surfaces. *Langmuir* **1999,** *15* (8), 2719-2725.

105. Van Oss, C., Hydrophobicity of biosurfaces - origin, quantitative determination and interaction energies. *Colloids and Surfaces B: Biointerfaces* **1995,** *5* (3-4), 91-110.

106. Cerca, N.; Pier, G. B.; Vilanova, M.; Oliveira, R.; Azeredo, J., Quantitative analysis of adhesion and biofilm formation on hydrophilic and hydrophobic surfaces of clinical isolates of *Staphylococcus epidermidis*. *Research in Microbiology* **2005,** *156* (4), 506-514.

107. Soon, C. F.; Omar, W. I. W.; Nayan, N.; Basri, H.; Narawi, M. B.; Tee, K. S., A bespoke contact angle measurement software and experimental setup for determination of surface tension. *Procedia Technology* **2013,** *11*, 487-494.

108. An, Y. H.; Friedman, R. J., Concise review of mechanisms of bacterial adhesion to biomaterial surfaces. *Journal of Biomedical Materials Research Part A* **1998,** *43* (3), 338-348.

109. Harding, J. L.; Reynolds, M. M., Combating medical device fouling. *Trends in Biotechnology* **2014,** *32* (3), 140-146.

110. Perni, S.; Preedy, E. C.; Prokopovich, P., Success and failure of colloidal approaches in adhesion of microorganisms to surfaces. *Advances in Colloid and Interface Science* **2014,** *206*, 265-274.

111. Strevett, K. A.; Chen, G., Microbial surface thermodynamics and applications. *Research in Microbiology* **2003,** *154* (5), 329-335.

112. Liu, C.; Zhao, Q., Influence of surface-energy components of Ni–P–TiO2–PTFE nanocomposite coatings on bacterial adhesion. *Langmuir* **2011,** *27* (15), 9512-9519.

113. Absolom, D. R.; Lamberti, F. V.; Policova, Z.; Zingg, W.; van Oss, C. J.; Neumann, A. W., Surface thermodynamics of bacterial adhesion. *Applied and Environmental Microbiology* **1983,** *46* (1), 90-97.

114. Moreira, J. M.; Simões, M.; Melo, L. F.; Mergulhão, F. J., *Escherichia coli* adhesion to surfaces–a thermodynamic assessment. *Colloid and Polymer Science* **2015,** *293* (1), 177-185.

115. Gallardo-Moreno, A. M.; Navarro-Pérez, M. L.; Vadillo-Rodríguez, V.; Bruque, J. M.; González-Martín, M. L., Insights into bacterial contact angles: difficulties in defining hydrophobicity and surface Gibbs energy. *Colloids and Surfaces B: Biointerfaces* **2011,** *88* (1), 373-380.

116. Baier, R.; Meyer, A.; Natiella, J.; Natiella, R.; Carter, J., Surface properties determine bioadhesive outcomes: methods and results. *Journal of Biomedical Materials Research Part A* **1984,** *18* (4), 337-355.

117. Helbig, R.; Günther, D.; Friedrichs, J.; Rößler, F.; Lasagni, A.; Werner, C., The impact of structure dimensions on initial bacterial adhesion. *Biomaterials Science* **2016,** *4* (7), 1074-8.

118. James, S. A.; Hilal, N.; Wright, C. J., Atomic force microscopy studies of bioprocess engineering surfaces – imaging, interactions and mechanical properties mediating bacterial adhesion. *Biotechnology Journal* **2017,** *12* (7), 1600698.

119. Hizal, F.; Rungraeng, N.; Lee, J.; Jun, S.; Busscher, H. J.; van der Mei, H. C.; Choi, C.-H., Nanoengineered superhydrophobic surfaces of aluminum with extremely low bacterial adhesivity. *ACS Applied Materials & Interfaces* **2017,** *9* (13), 12118-12129.

120. Bagherifard, S.; Hickey, D. J.; de Luca, A. C.; Malheiro, V. N.; Markaki, A. E.; Guagliano, M.; Webster, T. J., The influence of nanostructured features on bacterial adhesion and bone cell functions on severely shot peened 316L stainless steel. *Biomaterials* **2015,** *73*, 185-197.

121. An, Y. H.; Friedman, R. J., Concise review of mechanisms of bacterial adhesion to biomaterial surfaces. *Journal of biomedical materials research* **1998,** *43* (3), 338-348.

122. Hasan, J.; Crawford, R. J.; Ivanova, E. P., Antibacterial surfaces: the quest for a new generation of biomaterials. *Trends in Biotechnology* **2013,** *31* (5), 295-304.

123. Nosonovsky, M.; Bhushan, B., *Green Tribology: Biomimetics, Energy Conservation and Sustainability*. 1 ed.; Springer-Verlag Berlin Heidelberg: 2012; p 634.

124. Singh, V.; Mondal, P. C.; Singh, A. K.; Zharnikov, M., Molecular sensors confined on SiOx substrates. *Coordination Chemistry Reviews* **2017,** *330*, 144-163.

125. Agarwal, R.; García, A. J., Chapter 37 - Surface Modification of Biomaterials. In *Principles of Regenerative Medicine (Third Edition)*, Atala, A.; Lanza, R.; Mikos, A. G.; Nerem, R., Eds. Academic Press: Boston, 2019; pp 651-660.

126. Nuzzo, R. G., Biomaterials: stable antifouling surfaces. *Nature Materials* **2003,** *2* (4), 207-208.

127. Cheng, Y.; Feng, G.; Moraru, C. I., Micro- and nanotopography sensitive bacterial attachment mechanisms: a review. *Frontiers in Microbiology* **2019,** *10*, 191-191.

128. Ratner, B. D.; Hoffman, A. S.; Schoen, F. J.; Lemons, J. E., *Biomaterials science: an introduction to materials in medicine*. 2nd edition ed.; Elsevier Academic Press: California, USA, 2006; Vol. 31, p 59.

129. Moriarty, T. F.; Campoccia, D.; Nees, S. K.; Boure, L. P.; Richards, R. G., *In vivo* evaluation of the effect of intramedullary nail microtopography on the development of local infection in rabbits. *The International Journal of Artificial Organs* **2010,** *33* (9), 667-675.

130. Mitik-Dineva, N.; Wang, J.; Truong, V. K.; Stoddart, P.; Malherbe, F.; Crawford, R. J.; Ivanova, E. P., *Escherichia coli*, *Pseudomonas aeruginosa*, and *Staphylococcus aureus* attachment patterns on glass surfaces with nanoscale roughness. *Current Microbiology* **2009,** *58* (3), 268-273.

131. Cunliffe, D.; Smart, C.; Alexander, C.; Vulfson, E., Bacterial adhesion at synthetic surfaces. *Applied and Environmental Microbiology* **1999,** *65* (11), 4995-5002.

132. Li, B.; Logan, B. E., Bacterial adhesion to glass and metal-oxide surfaces. *Colloids and Surfaces B: Biointerfaces* **2004,** *36* (2), 81-90.

133. Chen, M.; Zhang, Z.; Bott, T., Effects of operating conditions on the adhesive strength of *Pseudomonas fluorescens* biofilms in tubes. *Colloids and Surfaces B: Biointerfaces* **2005,** *43* (2), 61-71.

134. Oliveira, K.; Oliveira, T.; Teixeira, P.; Azeredo, J.; Henriques, M.; Oliveira, R., Comparison of the adhesion ability of different *Salmonella Enteritidis* serotypes to materials used in kitchens. *Journal of Food Protection* **2006,** *69* (10), 2352-2356.

135. Simões, L. C.; Simões, M.; Oliveira, R.; Vieira, M. J., Potential of the adhesion of bacteria isolated from drinking water to materials. *Journal of Basic Microbiology* **2007,** *47* (2), 174-183.

136. Kochkodan, V.; Tsarenko, S.; Potapchenko, N.; Kosinova, V.; Goncharuk, V., Adhesion of microorganisms to polymer membranes: a photobactericidal effect of surface treatment with TiO2. *Desalination* **2008,** *220* (1-3), 380-385.

137. Liu, C.; Zhao, Q., The CQ ratio of surface energy components influences adhesion and removal of fouling bacteria. *Biofouling* **2011,** *27* (3), 275-85.

138. Szlavik, J.; Paiva, D. S.; Mørk, N.; van den Berg, F.; Verran, J.; Whitehead, K.; Knøchel, S.; Nielsen, D. S., Initial adhesion of *Listeria monocytogenes* to solid surfaces under liquid flow. *International Journal of Food Microbiology* **2012,** *152* (3), 181-188.

139. Khan, M. M. T.; Chapman, T.; Cochran, K.; Schuler, A. J., Attachment surface energy effects on nitrification and estrogen removal rates by biofilms for improved wastewater treatment. *Water Research* **2013,** *47* (7), 2190-2198.

140. Ista, L. K.; López, G. P., Thermodynamic analysis of marine bacterial attachment to oligo (ethylene glycol)-terminated self-assembled monolayers. *Biointerphases* **2013,** *8* (1), 24.

141. Moreira, J.; Gomes, L.; Simões, M.; Melo, L.; Mergulhão, F., The impact of material properties, nutrient load and shear stress on biofouling in food industries. *Food and Bioproducts Processing* **2015,** *95*, 228-236.

142. Lemos, M.; Gomes, I.; Mergulhão, F.; Melo, L.; Simões, M., The effects of surface type on the removal of *Bacillus cereus* and *Pseudomonas fluorescens* single and dual species biofilms. *Food and Bioproducts Processing* **2015,** *93*, 234-241.

143. Moreira, J.; Fulgêncio, R.; Alves, P.; Machado, I.; Bialuch, I.; Melo, L.; Simões, M.; Mergulhão, F., Evaluation of SICAN performance for biofouling mitigation in the food industry. *Food Control* **2016,** *62*, 201-207.

144. Moreira, J.; Fulgêncio, R.; Oliveira, F.; Machado, I.; Bialuch, I.; Melo, L.; Simões, M.; Mergulhão, F., Evaluation of SICON® surfaces for biofouling mitigation in critical process areas. *Food and Bioproducts Processing* **2016,** *98*, 173-180.

145. Moreira, J.; Gomes, L.; Whitehead, K.; Lynch, S.; Tetlow, L.; Mergulhão, F., Effect of surface conditioning with cellular extracts on *Escherichia coli* adhesion and initial biofilm formation. *Food and Bioproducts Processing* **2017,** *104*, 1-12.

146. Cowle, M. W.; Webster, G.; Babatunde, A. O.; Bockelmann-Evans, B. N.; Weightman, A. J., Impact of flow hydrodynamics and pipe material properties on biofilm development within drinking water systems. *Environmental Technology* **2019**.

147. Shen, Y.; Jin, M.; Wu, X.; Tao, J.; Luo, X.; Chen, H.; Lu, Y.; Xie, Y., Understanding the frosting and defrosting mechanism on the superhydrophobic surfaces with hierarchical structures for enhancing anti-frosting performance. *Applied Thermal Engineering* **2019,** *156*, 111-118.

148. Romeu, M. J.; Alves, P.; Morais, J.; Miranda, J. M.; de Jong, E.; Sjollema, J.; Ramos, V.; Vasconcelos, V.; Mergulhão, F., Biofilm formation behaviour of marine filamentous cyanobacterial strains in controlled hydrodynamic conditions. *Environmental Microbiology* **2019**.

149. Armbruster, S.; Stockmeier, F.; Junker, M.; Schiller-Becerra, M.; Yüce, S.; Wessling, M., Short and spaced twisted tapes to mitigate fouling in tubular membranes. *Journal of Membrane Science* **2020,** *595*, 117426.

150. Bridgett, M.; Davies, M.; Denyer, S. P., Control of staphylococcal adhesion to polystyrene surfaces by polymer surface modification with surfactants. *Biomaterials* **1992,** *13* (7), 411-416.

151. Tebbs, S.; Elliott, T., Modification of central venous catheter polymers to prevent *in vitro* microbial colonisation. *European Journal of Clinical Microbiology and Infectious Diseases* **1994,** *13* (2), 111-117.

152. Jansen, B.; Kohnen, W., Prevention of biofilm formation by polymer modification. *Journal of Industrial Microbiology* **1995,** *15* (4), 391-396.

153. Barton, A. J.; Sagers, R. D.; Pitt, W. G., Bacterial adhesion to orthopedic implant polymers. *Journal of biomedical materials research* **1996,** *30* (3), 403-410.

154. Millsap, K.; Reid, G.; Van der Mei, H.; Busscher, H., Adhesion of *Lactobacillus* species in urine and phosphate buffer to silicone rubber and glass under flow. *Biomaterials* **1997,** *18* (1), 87-91.

155. Park, K. D.; Kim, Y. S.; Han, D. K.; Kim, Y. H.; Lee, E. H. B.; Suh, H.; Choi, K. S., Bacterial adhesion on PEG modified polyurethane surfaces. *Biomaterials* **1998,** *19* (7-9), 851-859.

156. Stoor, P.; Söderling, E.; Salonen, J. I., Antibacterial effects of a bioactive glass paste on oral microorganisms. *Acta Odontologica Scandinavica* **1998,** *56* (3), 161-165.

157. Flemming, R. G.; Proctor, R. A.; Cooper, S. L., Bacterial adhesion to functionalized polyurethanes. *Journal of Biomaterials Science, Polymer Edition* **1999,** *10* (6), 679-697.

158. Hendricks, S. K.; Kwok, C.; Shen, M.; Horbett, T. A.; Ratner, B. D.; Bryers, J. D., Plasma-deposited membranes for controlled release of antibiotic to prevent bacterial adhesion and biofilm formation. *Journal of biomedical materials research* **2000,** *Journal of Biomedical Materials Research* (2), 160-70.

159. Lee, H. J.; Park, K. D.; Park, H. D.; Lee, W. K.; Han, D. K.; Kim, S. H.; Kim, Y. H., Platelet and bacterial repellence on sulfonated poly(ethylene glycol)-acrylate copolymer surfaces. *Colloids and Surfaces B: Biointerfaces* **2000,** *18* (3), 355-370.

160. Berry, J. A.; Biedlingmaier, J. F.; Whelan, P. J., In vitro resistance to bacterial biofilm formation on coated fluoroplastic tympanostomy tubes. *Otolaryngology - Head and Neck Surgery* **2000,** *123* (3), 246-251.

161. Fonseca, A.; Granja, P.; Nogueira, J.; Oliveira, D.; Barbosa, M., *Staphylococcus epidermidis* RP62A adhesion to chemically modified cellulose derivatives. *Journal of Materials Science: Materials in Medicine* **2001,** *12* (6), 543-548.

162. Roosjen, A.; Kaper, H. J.; van der Mei, H. C.; Norde, W.; Busscher, H. J., Inhibition of adhesion of yeasts and bacteria by poly (ethylene oxide)-brushes on glass in a parallel plate flow chamber. *Microbiology* **2003,** *149* (11), 3239-3246.

163. Hirota, K.; Murakami, K.; Nemoto, K.; Miyake, Y., Coating of a surface with 2-methacryloyloxyethyl phosphorylcholine (MPC) co-polymer significantly reduces retention of human pathogenic microorganisms. *FEMS Microbiology Letters* **2005,** *248* (1), 37-45.

164. Boulmedais, F.; Frisch, B.; Etienne, O.; Lavalle, P.; Picart, C.; Ogier, J.; Voegel, J. C.; Schaaf, P.; Egles, C., Polyelectrolyte multilayer films with pegylated polypeptides as a new type of anti-microbial protection for biomaterials. *Biomaterials* **2004,** *25* (11), 2003-2011.

165. Hsu, S.-H.; Tang, C.-M.; Lin, C.-C., Biocompatibility of poly(ε-caprolactone)/poly(ethylene glycol) diblock copolymers with nanophase separation. *Biomaterials* **2004,** *25* (25), 5593-5601.

166. Harris, L.; Tosatti, S.; Wieland, M.; Textor, M.; Richards, R., *Staphylococcus aureus* adhesion to titanium oxide surfaces coated with non-functionalized and peptide-functionalized poly (L-lysine)-grafted-poly (ethylene glycol) copolymers. *Biomaterials* **2004,** *25* (18), 4135-4148.

167. Fu, J.; Ji, J.; Yuan, W.; Shen, J., Construction of anti-adhesive and antibacterial multilayer films via layer-by-layer assembly of heparin and chitosan. *Biomaterials* **2005,** *26* (33), 6684-6692.

168. Nablo, B. J.; Prichard, H. L.; Butler, R. D.; Klitzman, B.; Schoenfisch, M. H., Inhibition of implant-associated infections via nitric oxide release. *Biomaterials* **2005,** *26* (34), 6984-6990.

169. Bayoudh, S.; Othmane, A.; Mora, L.; Ouada, H. B., Assessing bacterial adhesion using DLVO and XDLVO theories and the jet impingement technique. *Colloids and Surfaces B: Biointerfaces* **2009,** *73* (1), 1-9.

170. Buergers, R.; Rosentritt, M.; Handel, G., Bacterial adhesion of *Streptococcus mutans* to provisional fixed prosthodontic material. *The Journal of Prosthetic Dentistry* **2007,** *98* (6), 461-469.

171. Cringus-Fundeanu, I.; Luijten, J.; van der Mei, H. C.; Busscher, H. J.; Schouten, A. J., Synthesis and characterization of surface-grafted polyacrylamide brushes and their inhibition of microbial adhesion. *Langmuir* **2007,** *23* (9), 5120-5126.

172. Fundeanu, I.; van der Mei, H. C.; Schouten, A. J.; Busscher, H. J., Polyacrylamide brush coatings preventing microbial adhesion to silicone rubber. *Colloids and Surfaces B: Biointerfaces* **2008,** *64* (2), 297-301.

173. Katsikogianni, M.; Amanatides, E.; Mataras, D.; Missirlis, Y., *Staphylococcus epidermidis* adhesion to He, He/O2 plasma treated PET films and aged materials: Contributions of surface free energy and shear rate. *Colloids and Surfaces B: Biointerfaces* **2008,** *65* (2), 257-268.

174. Liu, C.; Zhao, Q.; Liu, Y.; Wang, S.; Abel, E., Reduction of bacterial adhesion on modified DLC coatings. *Colloids and Surfaces B: Biointerfaces* **2008,** *61* (2), 182-187.

175. Roy, S.; Das, P. K., Antibacterial hydrogels of amino acid-based cationic amphiphiles. *Biotechnology and Bioengineering* **2008,** *100* (4), 756-764.

176. Zhang, F.; Zhang, Z.; Zhu, X.; Kang, E.-T.; Neoh, K.-G., Silk-functionalized titanium surfaces for enhancing osteoblast functions and reducing bacterial adhesion. *Biomaterials* **2008,** *29* (36), 4751-4759.

177. Kim, G.; Park, S.; Jung, J.; Heo, K.; Yoon, J.; Kim, H.; Kim, I. J.; Kim, J. R.; Lee, J. I.; Ree, M., Novel brush polymers with phosphorylcholine bristle ends: synthesis, structure, properties, and biocompatibility. *Advanced Functional Materials* **2009,** *19* (10), 1631-1644.

178. Kim, G.; Rho, Y.; Park, S.; Kim, H.; Son, S.; Kim, H.; Kim, I. J.; Kim, J. R.; Kim, W. J.; Ree, M., The biocompatibility of self-assembled brush polymers bearing glycine derivatives. *Biomaterials* **2010,** *31* (14), 3816-3826.

179. Katsikogianni, M.; Missirlis, Y., Interactions of bacteria with specific biomaterial surface chemistries under flow conditions. *Acta biomaterialia* **2010,** *6* (3), 1107-1118.

180. Kalmodia, S.; Molla, A. R.; Basu, B., *In vitro* cellular adhesion and antimicrobial property of SiO2–MgO–Al2O3–K2O–B2O3–F glass ceramic. *Journal of Materials Science: Materials in Medicine* **2010,** *21* (4), 1297-1309.

181. Shao, W.; Zhao, Q., Effect of corrosion rate and surface energy of silver coatings on bacterial adhesion. *Colloids and Surfaces B: Biointerfaces* **2010,** *76* (1), 98-103.

182. Chang, Y.; Yandi, W.; Chen, W.-Y.; Shih, Y.-J.; Yang, C.-C.; Chang, Y.; Ling, Q.-D.; Higuchi, A., Tunable bioadhesive copolymer hydrogels of thermoresponsive poly (N-isopropyl acrylamide) containing zwitterionic polysulfobetaine. *Biomacromolecules* **2010,** *11* (4), 1101-1110.

183. Privett, B. J.; Youn, J.; Hong, S. A.; Lee, J.; Han, J.; Shin, J. H.; Schoenfisch, M. H., Antibacterial fluorinated silica colloid superhydrophobic surfaces. *Langmuir* **2011,** *27* (15), 9597-9601.

184. Xu, T.; Xin, M.; Li, M.; Huang, H.; Zhou, S.; Liu, J., Synthesis, characterization, and antibacterial activity of *N,O*-quaternary ammonium chitosan. *Carbohydrate Research* **2011,** *346* (15), 2445-2450.

185. Tahtat, D.; Mahlous, M.; Benamer, S.; Khodja, A. N.; Youcef, S. L.; Hadjarab, N.; Mezaache, W., Influence of some factors affecting antibacterial activity of PVA/Chitosan based hydrogels synthesized by gamma irradiation. *Journal of Materials Science: Materials in Medicine* **2011,** *22* (11), 2505-2512.

186. Tsao, C. T.; Chang, C. H.; Lin, Y. Y.; Wu, M. F.; Wang, J.-L.; Han, J. L.; Hsieh, K. H., Antibacterial activity and biocompatibility of a chitosan–γ-poly (glutamic acid) polyelectrolyte complex hydrogel. *Carbohydrate Research* **2010,** *345* (12), 1774-1780.

187. Shirai, T.; Shimizu, T.; Ohtani, K.; Zen, Y.; Takaya, M.; Tsuchiya, H., Antibacterial iodine-supported titanium implants. *Acta Biomaterialia* **2011,** *7* (4), 1928-1933.

188. Qu, J.; Lu, X.; Li, D.; Ding, Y.; Leng, Y.; Weng, J.; Qu, S.; Feng, B.; Watari, F., Silver/hydroxyapatite composite coatings on porous titanium surfaces by sol-gel method. *Journal of Biomedical Materials Research Part B: Applied Biomaterials* **2011,** *97* (1), 40-48.

189. Wang, Q.; Uzunoglu, E.; Wu, Y.; Libera, M., Self-assembled poly(ethylene glycol)-co-acrylic acid microgels to inhibit bacterial colonization of synthetic surfaces. *ACS Applied Materials & Interfaces* **2012,** *4* (5), 2498-2506.

190. Gorth, D. J.; Puckett, S.; Ercan, B.; Webster, T. J.; Rahaman, M.; Bal, B. S., Decreased bacteria activity on Si3N4 surfaces compared with PEEK or titanium. *International Journal of Nanomedicine* **2012,** *7*, 4829.

191. Graham, M. V.; Mosier, A. P.; Kiehl, T. R.; Kaloyeros, A. E.; Cady, N. C., Development of antifouling surfaces to reduce bacterial attachment. *Soft Matter* **2013,** *9* (27), 6235-6244.

192. Treter, J.; Bonatto, F.; Krug, C.; Soares, G. V.; Baumvol, I. J. R.; Macedo, A. J., Washing-resistant surfactant coated surface is able to inhibit pathogenic bacteria adhesion. *Applied Surface Science* **2014,** *303*, 147-154.

193. Gomes, L.; Silva, L. N.; Simões, M.; Melo, L.; Mergulhão, F., *Escherichia coli* biofilm formation and antibiotic susceptibility on biomedical materials. **2014**.

194. Rodriguez-Emmenegger, C.; Decker, A.; Surman, F.; Preuss, C. M.; Sedlakova, Z.; Zydziak, N.; Barner-Kowollik, C.; Schwartz, T.; Barner, L., Suppressing *Pseudomonas aeruginosa* adhesion via non-fouling polymer brushes. *Rsc Adv* **2014,** *4* (110), 64781-64790.

195. Maity, S.; Nir, S.; Zada, T.; Reches, M., Self-assembly of a tripeptide into a functional coating that resists fouling. *Chemical Communications* **2014,** *50* (76), 11154-11157.

196. Moreira, J.; Ponmozhi, J.; Campos, J.; Miranda, J. M.; Mergulhão, F., Micro-and macro-flow systems to study *Escherichia coli* adhesion to biomedical materials. *Chemical Engineering Science* **2015,** *126*, 440-445.

197. Surman, F.; Riedel, T.; Bruns, M.; Kostina, N. Y.; Sedlakova, Z.; Rodriguez-Emmenegger, C., Polymer brushes interfacing blood as a route toward high performance blood contacting devices. *Macromolecular Bioscience* **2015,** *15* (5), 636-646.

198. de los Santos Pereira, A.; Sheikh, S.; Blaszykowski, C.; Pop-Georgievski, O.; Fedorov, K.; Thompson, M.; Rodriguez-Emmenegger, C., Antifouling polymer brushes displaying antithrombogenic surface properties. *Biomacromolecules* **2016,** *17* (3), 1179-1185.

199. Dubey, N.; Ellepola, K.; Decroix, F. E.; Morin, J. L.; Castro Neto, A.; Seneviratne, C. J.; Rosa, V., Graphene onto medical grade titanium: an atom-thick multimodal coating that promotes osteoblast maturation and inhibits biofilm formation from distinct species. *Nanotoxicology* **2018,** *12* (4), 274-289.

200. Xu, L.-C.; Meyerhoff, M. E.; Siedlecki, C. A., Blood coagulation response and bacterial adhesion to biomimetic polyurethane biomaterials prepared with surface texturing and nitric oxide release. *Acta Biomaterialia* **2019,** *84*, 77-87.

201. Wongsuwan, N.; Dwivedi, A.; Tancharoen, S.; Nasongkla, N., Development of dental implant coating with minocycline-loaded niosome for antibacterial application. *Journal of Drug Delivery Science and Technology* **2020,** *56*, 101555.

202. Korber, D. R.; Lawrence, J. R.; Zhang, L.; Caldwell, D. E., Effect of gravity on bacterial deposition and orientation in laminar flow environments. *Biofouling* **1990,** *2* (4), 335-350.

203. Marshall, K. C., Mechanisms of bacterial adhesion at solid-water interfaces. In *Bacterial Adhesion*, Savage, D. C.; Fletcher, M., Eds. Springer: Boston, MA, 1985; pp 133-161.

204. van Loosdrecht, M. C.; Lyklema, J.; Norde, W.; Zehnder, A. J., Bacterial adhesion: a physicochemical approach. *Microbial Ecology* **1989,** *17* (1), 1-15.

205. Stoodley, P.; Dodds, I.; Boyle, J.; Lappin-Scott, H., Influence of hydrodynamics and nutrients on biofilm structure. *Journal of Applied Microbiology* **1998,** *85* (S1).

206. Stoodley, P.; Lewandowski, Z.; Boyle, J. D.; Lappin-Scott, H. M., Structural deformation of bacterial biofilms caused by short-term fluctuations in fluid shear: an *in situ* investigation of biofilm rheology. *Biotechnology and Bioengineering* **1999,** *65* (1), 83-92.

207. Tallawi, M.; Opitz, M.; Lieleg, O., Modulation of the mechanical properties of bacterial biofilms in response to environmental challenges. *Biomaterials Science* **2017,** *5* (5), 887-900.

208. Farrell, D.; Morrissey, I.; De Rubeis, D.; Robbins, M.; Felmingham, D., A UK multicentre study of the antimicrobial susceptibility of bacterial pathogens causing urinary tract infection. *Journal of Infection* **2003,** *46* (2), 94-100.

209. Vieira, M. J.; Melo, L. F.; Pinheiro, M. M., Biofilm formation: hydrodynamic effects on internal diffusion and structure. *Biofouling* **1993,** *7* (1), 67-80.

210. Morisaki, H., Measurement of the force necessary for removal of bacterial cells from a quartz plate. *Microbiology* **1991,** *137* (11), 2649-2655.

211. Rutter, P.; Vincent, B., Attachment mechanisms in the surface growth of microorganisms. In *Physiological Models in Microbiology*, Bazin, M. J.; Prosser, J. I., Eds. CRC Press: Boca Raton, Florida, 1988; Vol. 2, pp 87-107.

212. Liu, Y.; Tay, J.-H., The essential role of hydrodynamic shear force in the formation of biofilm and granular sludge. *Water Research* **2002,** *36* (7), 1653-1665.

213. Scott, G.; Richardson, P., The application of computational fluid dynamics in the food industry. *Trends in Food Science & Technology* **1997,** *8* (4), 119-124.

214. Gomes, L.; Moreira, J.; Teodósio, J.; Araújo, J.; Miranda, J.; Simões, M.; Melo, L.; Mergulhão, F., 96-well microtiter plates for biofouling simulation in biomedical settings. *Biofouling* **2014,** *30* (5), 535-546.

215. Halder, P.; Nasabi, M.; Lopez, F. J. T.; Jayasuriya, N.; Bhattacharya, S.; Deighton, M.; Mitchell, A.; Bhuiyan, M. A., A novel approach to determine the efficacy of patterned surfaces for biofouling control in relation to its microfluidic environment. *Biofouling* **2013,** *29* (6), 697-713.

216. Teodósio, J. S.; Simoes, M.; Alves, M. A.; Melo, L. F.; Mergulhao, F. J., Setup and validation of flow cell systems for biofouling simulation in industrial settings. *The Scientific World Journal* **2012,** *2012*.

217. Shi, X.; Zhu, X., Biofilm formation and food safety in food industries. *Trends in Food Science & Technology* **2009,** *20* (9), 407-413.

218. Teodósio, J. S.; Silva, F. C.; Moreira, J. M.; Simões, M.; Melo, L. F.; Alves, M. A.; Mergulhão, F. J., Flow cells as quasi-ideal systems for biofouling simulation of industrial piping systems. *Biofouling* **2013,** *29* (8), 953-966.

219. Moreira, J.; Simões, M.; Melo, L.; Mergulhão, F., The combined effects of shear stress and mass transfer on the balance between biofilm and suspended cell dynamics. *Desalination and Water Treatment* **2015,** *53* (12), 3348-3354.

220. Gomes, L. C.; Moreira, J. M. R.; Miranda, J. M.; Simões, M.; Melo, L. F.; Mergulhão, F. J., Macroscale versus microscale methods for physiological analysis of biofilms formed in 96-well microtiter plates. *Journal of Microbiological Methods* **2013,** *95* (3), 342-349.

221. Kaya, T.; Koser, H., Direct upstream motility in Escherichia coli. *Biophys J* **2012,** *102* (7), 1514-1523.

222. Yataghene, M.; Pruvost, J.; Fayolle, F.; Legrand, J., CFD analysis of the flow pattern and local shear rate in a scraped surface heat exchanger. *Chemical Engineering and Processing: Process Intensification* **2008,** *47* (9), 1550-1561.

223. Chesterton, A.; Moggridge, G.; Sadd, P.; Wilson, D., Modelling of shear rate distribution in two planetary mixtures for studying development of cake batter structure. *Journal of Food Engineering* **2011,** *105* (2), 343-350.

224. Bakker, D.; Van der Plaats, A.; Verkerke, G.; Busscher, H.; Van der Mei, H., Comparison of velocity profiles for different flow chamber designs used in studies of microbial adhesion to surfaces. *Applied and Environmental Microbiology* **2003,** *69* (10), 6280-6287.

225. Mathieu, L.; Bertrand, I.; Abe, Y.; Angel, E.; Block, J.; Skali-Lami, S.; Francius, G., Drinking water biofilm cohesiveness changes under chlorination or hydrodynamic stress. *water Research* **2014,** *55*, 175-184.

226. Shi, W.; Benjamin, M. M., Effect of shear rate on fouling in a Vibratory Shear Enhanced Processing (VSEP) RO system. *Journal of Membrane Science* **2011,** *366* (1-2), 148-157.

227. Konuklar, G.; Gunasekaran, S., Rennet-induced milk coagulation by continuous steady shear stress. *Journal of Colloid and Interface Science* **2002,** *250* (1), 149-158.

228. Jensen, B. B.; Friis, A., Predicting the cleanability of mix-proof valves by use of wall shear stress. *Journal of Food Process Engineering* **2005,** *28* (2), 89-106.

229. Liu, Z.; Lin, Y.; Stout, J.; Hwang, C.; Vidic, R.; Yu, V., Effect of flow regimes on the presence of *Legionella* within the biofilm of a model plumbing system. *Journal of Applied Microbiology* **2006,** *101* (2), 437-442.

230. Lelièvre, C.; Legentilhomme, P.; Gaucher, C.; Legrand, J.; Faille, C.; Bénézech, T., Cleaning in place: effect of local wall shear stress variation on bacterial removal from stainless steel equipment. *Chemical Engineering Science* **2002,** *57* (8), 1287-1297.

231. Thomas, W. E.; Trintchina, E.; Forero, M.; Vogel, V.; Sokurenko, E. V., Bacterial adhesion to target cells enhanced by shear force. *Cell* **2002,** *109* (7), 913-23.

232. Augst, A.; Ariff, B.; McG. Thom, S.; Xu, X.; Hughes, A. D., Analysis of complex flow and the relationship between blood pressure, wall shear stress, and intima-media thickness in the human carotid artery. *American Journal of Physiology-heart and Circulatory Physiology* **2007,** *293* (2), H1031-H1037.

233. Giddens, D.; Zarins, C.; Glagov, S., The role of fluid mechanics in the localization and detection of atherosclerosis. *Journal of Biomechanical Engineering* **1993,** *115* (4B), 588-594.

234. Lee, Y.-H.; Lai, C.-W.; Cheng, Y.-C., Fluid shear stress induces cell cycle arrest in human urinary bladder transitional cell carcinoma through bone morphogenetic protein receptor-Smad1/5 pathway. *Cellular and Molecular Bioengineering* **2018,** *11* (3), 185-195.

235. Inauen, W.; Baumgartner, H. R.; Bombeli, T.; Haeberli, A.; Straub, P. W., Dose-and shear rate-dependent effects of heparin on thrombogenesis induced by rabbit aorta subendothelium exposed to flowing human blood. *Arteriosclerosis, Thrombosis, and Vascular Biology* **1990,** *10* (4), 607-615.

236. Paszkowiak, J. J.; Dardik, A., Arterial wall shear stress: observations from the bench to the bedside. *Vascular and Endovascular Surgery* **2003,** *37* (1), 47-57.

237. Fernandes, D. C.; Araujo, T. L. S.; Laurindo, F. R. M.; Tanaka, L. Y., Chapter 7 - Hemodynamic forces in the endothelium: from mechanotransduction to implications on development of atherosclerosis. In *Endothelium and Cardiovascular Diseases*, Da Luz, P. L.; Libby, P.; Chagas, A. C. P.; Laurindo, F. R. M., Eds. Academic Press: 2018; pp 85-95.

238. Wang, Y.; Pierce, I.; Gatehouse, P.; Wood, N.; Firmin, D.; Xu, X. Y., Analysis of flow and wall shear stress in the peroneal veins under external compression based on real-time MR images. *Medical Engineering & Physics* **2012,** *34* (1), 17-27.

239. Ymele-Leki, P.; Ross, J. M., Erosion from *Staphylococcus aureus* biofilms grown under physiologically relevant fluid shear forces yields bacterial cells with reduced avidity to collagen. *Applied and Environmental microbiology* **2007,** *73* (6), 1834-41.

240. Cai, Z.; Xin, J.; Pollock, D. M.; Pollock, J. S., Shear stress-mediated NO production in inner medullary collecting duct cells. *American Journal of Physiology-Renal Physiology* **2000,** *279* (2), F270-F274.

241. Singh, P. K.; Marzo, A.; Howard, B.; Rufenacht, D. A.; Bijlenga, P.; Frangi, A. F.; Lawford, P. V.; Coley, S. C.; Hose, D. R.; Patel, U. J., Effects of smoking and hypertension on wall shear stress and oscillatory shear index at the site of intracranial aneurysm formation. *Clinical Neurology and Neurosurgery* **2010,** *112* (4), 306-313.

242. Nauman, E. A.; Ott, C. M.; Sander, E.; Tucker, D. L.; Pierson, D.; Wilson, J. W.; Nickerson, C. A., Novel quantitative biosystem for modeling physiological fluid shear stress on cells. *Applied and Environmental Microbiology* **2007,** *73* (3), 699-705.

243. Velraeds, M. M.; Van de Belt-Gritter, B.; Van der Mei, H.; Reid, G.; Busscher, H., Interference in initial adhesion of uropathogenic bacteria and yeasts to silicone rubber by a *Lactobacillus acidophilus* biosurfactant. *Journal of Medical Microbiology* **1998,** *47* (12), 1081-1085.

244. Ramstedt, M.; Ribeiro, I. A.; Bujdakova, H.; Mergulhão, F. J.; Jordao, L.; Thomsen, P.; Alm, M.; Burmølle, M.; Vladkova, T.; Can, F., Evaluating efficacy of antimicrobial and antifouling materials for urinary tract medical devices: challenges and recommendations. *Macromolecular Bioscience* **2019,** *19* (5), 1800384.

245. Tran, V. B.; Fleiszig, S. M.; Evans, D. J.; Radke, C. J., Dynamics of flagellum-and pilus-mediated association of *Pseudomonas aeruginosa* with contact lens surfaces. *Applied and Environmental Microbiology* **2011,** *77* (11), 3644-3652.

246. Mareels, G.; De Wachter, D. S.; Verdonck, P. R., Computational fluid dynamics-analysis of the Niagara hemodialysis catheter in a right heart model. *Artificial Organs* **2004,** *28* (7), 639-648.

247. Mareels, G. Experimental and numerical modeling of flow and mass transport in a bioartificial liver PhD, Ghent University, 2007.

248. Morsi, Y.; Kogure, M.; Umezu, M., Relative blood damage index of the jellyfish valve and the Bjork-Shiley tilting-disk valve. *Journal of Artificial Organs* **1999,** *2* (2), 163-169.

249. Frumento, R. J.; Hirsh, A. L.; Parides, M. K.; Bennett-Guerrero, E., Differences in arterial and venous thromboelastography parameters: potential roles of shear stress and oxygen content. *Journal of Cardiothoracic and Vascular Anesthesia* **2002,** *16* (5), 551-554.

250. Boersen, J. T.; Groot Jebbink, E.; Versluis, M.; Slump, C. H.; Ku, D. N.; de Vries, J.-P. P. M.; Reijnen, M. M. P. J., Flow and wall shear stress characterization after endovascular aneurysm repair and endovascular aneurysm sealing in an infrarenal aneurysm model. *Journal of Vascular Surgery* **2017,** *66* (6), 1844-1853.

251. O'Brien, T. P.; Grace, P.; Walsh, M.; Burke, P.; McGloughlin, T., Computational investigations of a new prosthetic femoral-popliteal bypass graft design. *Journal of Vascular Surgery* **2005,** *42* (6), 1169-1175.

252. Desyatova, A.; Poulson, W.; MacTaggart, J.; Maleckis, K.; Kamenskiy, A., Cross-sectional pinching in human femoropopliteal arteries due to limb flexion, and stent design optimization for maximum cross-sectional opening and minimum intramural stresses. *Journal of The Royal Society Interface* **2018,** *15* (145), 20180475.

253. Uzarski, J. S.; Cores, J.; McFetridge, P. S., Physiologically modeled pulse dynamics to improve function in *in vitro*-endothelialized small-diameter vascular grafts. *Tissue Engineering Part C: Methods* **2015,** *21* (11), 1125-1134.

254. Azeredo, J.; Azevedo, N. F.; Briandet, R.; Cerca, N.; Coenye, T.; Costa, A. R.; Desvaux, M.; Di Bonaventura, G.; Hébraud, M.; Jaglic, Z., Critical review on biofilm methods. *Critical Reviews in Microbiology* **2017,** *43* (3), 313-351.

255. Ramstedt, M.; Ribeiro, I. A. C.; Bujdakova, H.; Mergulhão, F. J. M.; Jordao, L.; Thomsen, P.; Alm, M.; Burmølle, M.; Vladkova, T.; Can, F.; Reches, M.; Riool, M.; Barros, A.; Reis, R. L.; Meaurio, E.; Kikhney, J.; Moter, A.; Zaat, S. A. J.; Sjollema, J., Evaluating efficacy of antimicrobial and antifouling materials for urinary tract medical devices: challenges and recommendations. *Macromolecular Bioscience* **2019,** *19* (5), 1800384.

256. Gomes, I. B.; Meireles, A.; Gonçalves, A. L.; Goeres, D. M.; Sjollema, J.; Simões, L. C.; Simões, M., Standardized reactors for the study of medical biofilms: a review of the principles and latest modifications. *Critical Reviews in Biotechnology* **2018,** *38* (5), 657-670.

257. Chua, R. Y. R.; Lim, K.; Leong, S. S. J.; Tambyah, P. A.; Ho, B., An in-vitro urinary catheterization model that approximates clinical conditions for evaluation of innovations to prevent catheter-associated urinary tract infections. *The Journal of hospital infection* **2017,** *97* (1), 66-73.

258. Lebeaux, D.; Chauhan, A.; Rendueles, O.; Beloin, C., From *in vitro* to *in vivo* models of bacterial biofilm-related infections. *Pathogens* **2013,** *2* (2), 288-356.

259. Azevedo, N. F.; Lopes, S. P.; Keevil, C. W.; Pereira, M. O.; Vieira, M. J., Time to "go large" on biofilm research: advantages of an omics approach. *Biotechnology Letters* **2009,** *31* (4), 477-485.

260. Azevedo, A. S.; Almeida, C.; Gomes, L. C.; Ferreira, C.; Mergulhão, F. J.; Melo, L. F.; Azevedo, N. F., An *in vitro* model of catheter-associated urinary tract infections to investigate the role of uncommon bacteria on the *Escherichia coli* microbial consortium. *Biochemical Engineering Journal* **2017,** *118*, 64-69.

261. Wolfaardt, G.; Lawrence, J.; Robarts, R.; Caldwell, S.; Caldwell, D., Multicellular organization in a degradative biofilm community. *Applied and Environmental Microbiology* **1994,** *60* (2), 434-446.

262. Coenye, T.; Nelis, H. J., *In vitro* and *in vivo* model systems to study microbial biofilm formation. *Journal of Microbiological Methods* **2010,** *83* (2), 89-105.

263. Li, J.; Busscher, H. J.; Norde, W.; Sjollema, J., Analysis of the contribution of sedimentation to bacterial mass transport in a parallel plate flow chamber. *Colloids and Surfaces B: Biointerfaces* **2011,** *84* (1), 76-81.

264. Skovager, A.; Whitehead, K.; Siegumfeldt, H.; Ingmer, H.; Verran, J.; Arneborg, N., Influence of flow direction and flow rate on the initial adhesion of seven *Listeria monocytogenes* strains to fine polished stainless steel. *International Journal of Food Microbiology* **2012,** *157* (2), 174-181.

265. Sjollema, J.; Busscher, H. J.; Weerkamp, A. H., Real-time enumeration of adhering microorganisms in a parallel plate flow cell using automated image analysis. *Journal of Microbiological Methods* **1989,** *9* (2), 73-78.

266. Meinders, J. M.; Van der Mei, H. C.; Busscher, H. J., *In situ* enumeration of bacterial adhesion in a parallel plate flow chamber - elimination or in focus flowing bacteria from the analysis. *Journal of Microbiological Methods* **1992,** *16* (2), 119-124.

267. Wit, P. J.; Noordmans, J.; Busscher, H. J., Tracking of colloidal particles using microscopic image sequence analysis Application to particulate microelectrophoresis and particle deposition. *Colloids and Surfaces A: Physicochemical and Engineering Aspects* **1997,** *125* (1), 85-92.

268. Pitts, B.; Hamilton, M. A.; Zelver, N.; Stewart, P. S., A microtiter-plate screening method for biofilm disinfection and removal. *Journal of Microbiological Methods* **2003,** *54* (2), 269-276.

269. Gómez-Suárez, C.; Busscher, H. J.; van der Mei, H. C., Analysis of bacterial detachment from substratum surfaces by the passage of air-liquid interfaces. *Applied and Environmental Microbiology* **2001,** *67* (6), 2531-2537.

270. Pinkart, H.; Ringelberg, D.; Piceno, Y.; Macnaughton, S.; White, D., Biochemical approaches to biomass measurements and community structure analysis. In *Manual of Environmental Microbiology*,

Second Edition ed.; Hurst, C. J.; Crawford, R. L., Eds. DC: ASM Press: Washington, 2002; Vol. 2, pp 101-113.

271. Stewart, P. S.; Franklin, M. J., Physiological heterogeneity in biofilms. *Nature Reviews Microbiology* **2008,** *6* (3), 199-210.

272. Hou, J.; Wang, C.; Rozenbaum, R. T.; Gusnaniar, N.; de Jong, E. D.; Woudstra, W.; Geertsema-Doornbusch, G. I.; Atema-Smit, J.; Sjollema, J.; Ren, Y.; Busscher, H. J.; van der Mei, H. C., Bacterial Density and Biofilm Structure Determined by Optical Coherence Tomography. *Scientific Reports* **2019,** *9* (1), 9794.

273. Sen, M.; Yadav, P., Modern methods in microscopy for the assessment of biofilms. In *Biofilms in human diseases: treatment and control.*, Kumar, S.; Chandra, N.; Singh, L.; Hashmi, M. Z.; Varma, A., Eds. Springer, Cham: Cham, Switzerland, 2019.

274. Lawrence, J.; Korber, D.; Hoyle, B.; Costerton, J. W.; Caldwell, D., Optical sectioning of microbial biofilms. *Journal of Bacteriology* **1991,** *173* (20), 6558-6567.

275. Gomes, L.; Deschamps, J.; Briandet, R.; Mergulhão, F., Impact of modified diamond-like carbon coatings on the spatial organization and disinfection of mixed-biofilms composed of *Escherichia coli* and *Pantoea agglomeran*s industrial isolates. *International Journal of Food Microbiology* **2018,** *277*, 74-82.

276. Alves, P.; Gomes, L. C.; Vorobii, M.; Rodriguez-Emmenegger, C.; Mergulhão, F. J., The potential advantages of using a poly(HPMA) brush in urinary catheters: effects on biofilm cells and architecture. *Colloids and Surfaces B: Biointerfaces* **2020,** *191*, 110976.

277. Olsen, I., Organization of supragingival plaque at the micron scale. *Journal of Oral Microbiology* **2018,** *10* (1), 1438722.

278. van de Linde, S., Single-molecule localization microscopy analysis with ImageJ. *Journal of Physics D: Applied Physics* **2019**, 52 (20), 203002.

279. Daims, H.; Lücker, S.; Wagner, M., Daime, a novel image analysis program for microbial ecology and biofilm research. *Environmental Microbiology* **2006**, 8 (2), 200-213.

280. Heydorn, A.; Nielsen, A. T.; Hentzer, M.; Sternberg, C.; Givskov, M.; Ersbøll, B. K.; Molin, S., Quantification of biofilm structures by the novel computer program COMSTAT. *Microbiology* **2000**, 146 (10), 2395-2407.

281. Vorregaard, M. Comstat2-a modern 3D image analysis environment for biofilms. Citeseer, Technical University of Denmark, **2008**.

282. Mueller, L. N.; De Brouwer, J. F.; Almeida, J. S.; Stal, L. J.; Xavier, J. B., Analysis of a marine phototrophic biofilm by confocal laser scanning microscopy using the new image quantification software PHLIP. *BMC Ecology* **2006**, 6 (1), 1.

283. Beyenal, H.; Donovan, C.; Lewandowski, Z.; Harkin, G., Three-dimensional biofilm structure quantification. *Journal of Microbiological Methods* **2004**, 59 (3), 395-413.

284. Abràmoff, M. D.; Magalhães, P. J.; Ram, S. J., Image processing with ImageJ. *Biophotonics International* **2004**, pp 36-42.

285. Zielinski, J. S.; Zielinska, A. K.; Bouaynaya, N.; Vaughan, J. G.; Smeltzer, M. S. *In Automated biofilm region recognition and morphology quantification from confocal laser scanning microscopy imaging*, Proceedings of the 2011 Biomedical Sciences and Engineering Conference: Image Informatics and Analytics in Biomedicine, IEEE: 2011; pp 1-4.

286. Heydorn, A.; Ersbøll, B.; Kato, J.; Hentzer, M.; Parsek, M. R.; Tolker-Nielsen, T.; Givskov, M.; Molin, S., Statistical analysis of *Pseudomonas aeruginosa* biofilm development: impact of mutations in genes

involved in twitching motility, cell-to-cell signaling, and stationary-phase sigma factor expression. *Applied and Environmental Microbiology* **2002**, 68 (4), 2008-2017.

287. Gomes, L. C.; Mergulhão, F. J., SEM analysis of surface impact on biofilm antibiotic treatment. *Scanning* **2017**, 2017.

288. Hung, C.; Zhou, Y.; Pinkner, J. S.; Dodson, K. W.; Crowley, J. R.; Heuser, J.; Chapman, M. R.; Hadjifrangiskou, M.; Henderson, J. P.; Hultgren, S. J., *Escherichia coli* biofilms have an organized and complex extracellular matrix structure. *mBio* **2013**, 4 (5), e00645-13.

3. Analysing the initial bacterial adhesion to evaluate the performance of antifouling surfaces [d]

Abstract

The aim of this work was to study the initial events of *Escherichia coli* adhesion to polydimethylsiloxane, which is critical for the development of antifouling surfaces.

A parallel plate flow cell was used to perform the initial adhesion experiments under controlled hydrodynamic conditions (shear rates ranging between 8 and 100/s), mimicking biomedical scenarios. Initial adhesion studies capture more accurately the cell-surface interactions as in later stages, incoming cells may interact with the surface but also with already adhered cells. Adhesion rates were calculated and results shown that after some time (between 5 and 9 minutes), these rates decreased (by 55% on average), from the initial values for all tested conditions. The common explanation for this decrease is the occurrence of hydrodynamic blocking, where the area behind each adhered cell is screened from incoming cells. This was investigated using a pair correlation map from which two-dimensional histograms showing the density probability function were constructed. The results highlighted a lower density probability (below 4.0×10^{-4}) of the presence of cells around a given cell under different shear rates irrespectively of the radial direction. A shadowing area behind the already adhered cells was not observed, indicating that hydrodynamic blocking was not occurring and therefore it could not be the cause for the decreases in cell adhesion rates. Afterward, cell transport rates from the bulk solution to the surface were estimated using the Smoluchowski-Levich approximation and values in the range of 80-170 cells/cm^2.s were obtained. The drag forces that adhered cells have to withstand were also estimated and values in the range of 3-50 $\times 10^{-14}$ N were determined. Although mass transport increases with the flow rate, drag forces also increase and the relative importance of these factors may change in different conditions. This work demonstrates that adjustment of operational parameters in initial adhesion experiments may be required to avoid hydrodynamic blocking, in order to obtain reliable data about cell-surface interactions that can be used in the development of more efficient antifouling surfaces.

[d] The content of this chapter was adapted from the following publication:

Alves P, Moreira JM, Mergulhão FJ, Miranda JM (**2020**) Analysing the initial bacterial adhesion to evaluate the performance of antifouling surfaces. *Antibiotics* 2020, 9(7), 421. Doi: 10.3390/antibiotics9070421

3.1. Introduction

Bacterial adhesion to a surface triggers a series of events that may lead to biofilm formation and fouling of that surface. Biofilms are bacterial cell communities that are embedded in a self-produced and highly hydrated matrix of extracellular polymeric substances (EPS). Living in biofilms is the most common state for bacteria in natural environments [1], and biofilms can be composed of single or multiple species that interact with each other [2]. Biofilms can cause deterioration of industrial equipment, food spoilage and disease [3, 4] but they are also used in wastewater treatment systems and have been investigated for the production of valuable molecules including recombinant proteins [5, 6].

The first step in biofilm formation is the surface adsorption of molecules from the surrounding medium. This originates a conditioning film that can affect subsequent bacterial adhesion [7]. Initially, bacterial adhesion is reversible, but then the adhered organisms start to produce EPS and to anchor themselves irreversibly, leading to the development of the biofilm structure. Then, biofilms mature and release bacteria, often leading to serious bacterial transmission issues [1]. Microorganisms that adhere first have a pivotal role in linking the biofilm to the surface, and their retention is crucial to maintain the biofilm on that surface when it is challenged by shear forces [8]. Thus, a better understanding of the initial adhesion process may provide clues to the development of antifouling surfaces.

One of the most promising strategies to prevent or delay biofilm formation on a given surface is to use a coating. In both medical and industrial settings, different types of antifouling coatings have been developed to prevent adhesion, which operate by contact killing or that release biocidal agents [9]. Release systems may promote the development of different types of resistance, and contact killing surfaces may originate a layer of dead cells and cellular debris that can serve as anchoring points for subsequent cell adhesion [7]. In that case, newly adhered cells can be protected from the biocidal agent by the layer formed by dead cells and debris. Anti-adhesion systems are, therefore, an attractive way of preventing or delaying biofilm formation [10]. The development of anti-adhesion coatings is an intense area of research, but these coatings have to be tested in environmental conditions that mimic their application scenario. Since medical and industrial biofilms often develop in areas where significant fluid motion exists, fluid displacement systems have been used to study these initial bacterial-surface interactions [11]. One of the most commonly used platforms for adhesion studies is the parallel plate flow cell (PPFC), which enables real-time monitoring of bacterial adhesion when the system is mounted on a microscope stage coupled to an image acquisition system [11].

A typical initial adhesion experiment performed in a PPFC with continuous monitoring

of the number of adhered cells generates a pattern where a linear trajectory can be identified first, followed by a decrease in slope where adhesion seems to be leveling off [8]. It has been proposed that during the linear phase, cells arriving at the surface interact solely with the surface and that the rate at which organisms adhere in this phase is truly representative of the affinity of that organism to that surface [8]. It is also believed that at later stages, when the surface is partially covered, an arriving cell will interact with the surface but also with other adhered cells and that the observed adhesion rates level off due to hydrodynamic blocking [8]. As a consequence, these second adhesion rates would not be truly representative of the interaction between a single cell and the surface, as data would reflect contributions from different interactions that are hard to separate [8].

It has been demonstrated that hydrodynamic blocking can reduce the adhesion of cells by screening the surface behind already adhered cells [12]. If the surface is entirely free of cells, an incoming cell can freely attach as long as it can withstand the shear forces. However, when cells start to attach irreversibly, an incoming cell can no longer attach immediately behind an already adhered cell because that area is effectively screened. This creates a shadow where cell adhesion is prohibited (Figure 3.1). During colloidal particle deposition, it has been shown that the area blocked by one particle can represent 8 to 675 times the cross-sectional area of that particle [13, 14]. In general, blocking is more likely to occur at high surface coverages, but local flow effects can introduce anisotropy in cell adhesion [12].

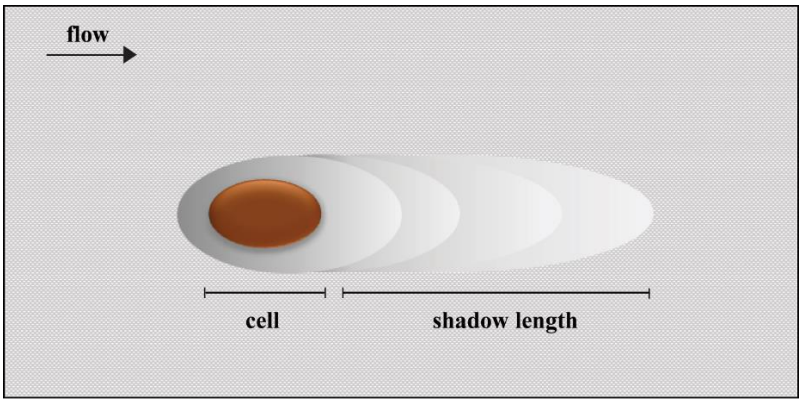

Figure 3.1. The hydrodynamic blocking effect. The area blocked by an adhered cell where further cell adhesion is prohibited is represented by the shadow.

A detailed analysis of the hydrodynamic blocking has been presented in several works by Adamczyk and co-workers [15-17], but this approach is not straightforward to many researchers, and this may explain why a blocking analysis is absent from many studies dealing with adhesion under flow conditions. In a study by van Loenhout et al. [12], the hydrodynamic blocking effect on particle adsorption was assessed by performing experiments in laminar flow and Monte Carlo

simulations to evaluate the effect of the hydrodynamic shadow on particle distribution. The spatial distribution and anisotropy were analysed through a two-dimensional (2D) map of a pair correlation function that was obtained from image analysis. This enabled the observation of the exclusion zone originating from the hydrodynamic blocking. The position of the adhered particles could be calculated and revealed the density of particles adhering around a given particle when compared to the overall density.

The arrival of cells to the surface is dictated by mass transport, and in flow systems, this transport is achieved by convection and diffusion. Although solutions for the convective-diffusion equation can be obtained by complicated mathematical procedures, there are approximate solutions such as the Smoluchowski-Levich (SL) approximation that assumes that all microorganisms sufficiently close to a surface will adhere irreversibly [8]. On the other hand, adhered cells have to withstand hydrodynamic forces that may cause cell desorption, and therefore the adhesion rates observed in initial adhesion experiments are a balance between all these effects. It has also been shown that initial adhesion experiments can produce valuable data for the development of antifouling surfaces [10, 18], and therefore the correct interpretation of that data is critical.

In this study, we have monitored in real-time the initial adhesion of *Escherichia coli* to a polydimethylsiloxane (PDMS) coating. *E. coli* was chosen as a model organism due to its relevance in both clinical and industrial settings, and PDMS is a very versatile polymer commonly used in both scenarios [19]. An interpretation of the events unfolding during initial adhesion is provided, showcasing the relative importance of cell transport to the surface, hydrodynamic blocking, and desorption forces.

3.2. Materials and methods

3.2.1. Bacteria and culture conditions

E. coli JM109(DE3) from Promega (USA) was selected for this study because it has been used in previous works from our group for the evaluation of initial adhesion in antifouling surfaces [10, 18, 20, 21] and because it has was shown to have similar biofilm formation behavior to different clinical isolates, including *E. coli* CECT 434 [22].

The inoculum was prepared as previously described [23]. Briefly, 500 µl of a glycerol stock (kept at -80 ºC) was added to a total volume of 0.2 L of the inoculation medium composed by 5.5 g/L glucose (Chem-Lab nv, Belgium), 2.5 g/L peptone (Oxoid, UK), 1.25 g/L yeast extract (Merck KGaA, Germany) in phosphate buffer (1.88 g/L KH_2PO_4 and 2.60 g/L Na_2HPO_4; Chem-Lab nv, Belgium) at pH 7.0. The culture was incubated overnight at 37 °C, with orbital agitation (160

rpm in a shaker: IKA KS 130 basic, Germany). Subsequently, this culture was centrifuged (at 3202 *g* for 10 min at 25 °C) to harvest the cells, and these were washed twice with 0.05 M of citrate buffer (composed by citric acid, Scharlau, Spain; pH 5.0) to remove any traces of the culture medium [24]. Cells were again harvested by centrifugation and resuspended in citrate buffer by vortexing in order to reach an optical density of 0.1 ($OD_{610\ nm}$). A calibration curve was used to determine the cell density (7.6 x 10^7 cells/mL). This suspension was used to perform adhesion experiments.

3.2.2. Surface preparation

Adhesion experiments were performed in a PPFC, as described by Moreira et al. [25]. The PPFC used in the present work has a rectangular cross-section of 0.8 × 1.6 cm and a length of 25.42 cm. Briefly, glass slides (7.6 x 2.6 x 0.1 cm, VWR, Portugal) were washed with a 0.5% detergent solution (Sonasol Pril, Henkel Ibérica SA, Spain) for 30 min and then the detergent was rinsed with distilled water. Subsequently, the surfaces were immersed in 3% sodium hypochlorite for 30 min. Finally, the surfaces were rinsed with distilled water and prepared for coating.

PDMS (Sylgard 184 Part A, Dow Corning; viscosity=1.1 cm^2/s; specific density=1.03, USA) was prepared by performing the following steps: i) the curing agent (Sylgard 184 Part B, Dow Corning) was added to the PDMS at a 1:10 ratio; ii) the mixture was placed in the vacuum chamber in which the pump was turned on and off periodically thus changing the pressure and collapsing air bubbles that may have formed. Subsequently, the mixture was used to coat glass slides by spin-coating (Spin150 PolosTM, Netherlands) at 4000 rpm for 60 s in order to obtain a thickness of 10 μm. PDMS slides were then cured overnight at 80 °C.

3.2.3. Adhesion experiments

A PPFC was used to monitor *E. coli* adhesion to PDMS, as previously described [25]. Briefly, the PPFC was coupled to a jacketed tank connected to centrifugal pumps. This system was sterilized by recirculating a sodium hypochlorite solution (3% v/v; 3 cycles of 15 min each). Subsequently, it was washed with sterile water and placed inside a laminar flow chamber for UV sterilization (30 min). Citrate buffer was introduced in the system and passed through in order to prefill the tubes and purge air from the system. The PDMS slides were also sterilized by UV and fixed aseptically to the bottom and top plates of the PPFC contained an opening area for introducing the test surfaces as previously described [25]. Then, the PPFC system was properly mounted in a microscope stage to monitor cell attachment. The bacterial suspension was recirculated through the PPFC system for 30 min at different flow rates (1, 2, 4, 6, 8 and 10 ml/s). The flow rates were adjusted with a valve.

Cell attachment was monitored in real-time for 30 min through brightfield microscopy. The temperature was kept constant at 37 °C using a recirculating water bath connected to the tank jacket to mimic human body conditions (Figure 3.2). Imaging conditions (e.g., exposure time, light intensity, magnification, condenser height and approximate positioning of the slide) were maintained between experiments. Three independent experiments were performed for each surface and condition tested. Images were acquired every 60 s with a camera (Nikon DS-Ri 1, Japan) connected to a microscope (Nikon Eclipse LV100, Japan) and stored for further analysis. Obtained images were processed using ImageJ (version 1.38e) software [26] and for each flow rate tested, the number of adhered cells per unit area was determined as a function of time (Code 1 – section 3.6.4., supplementary material).

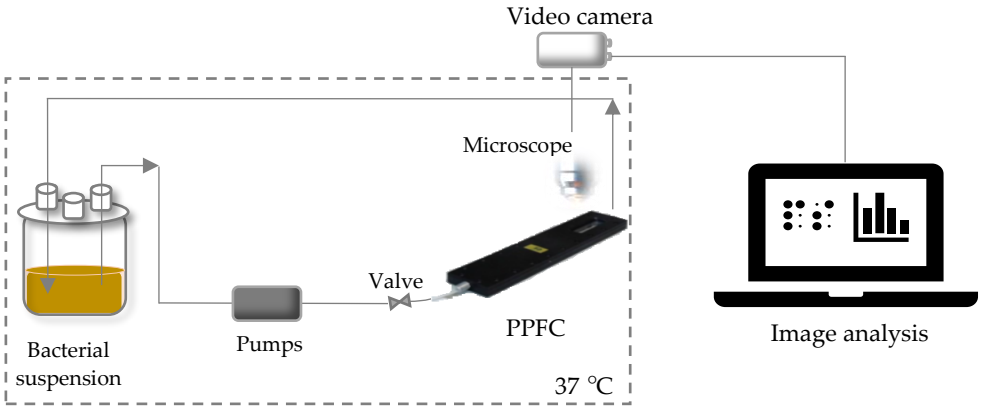

Figure 3.2. Schematic representation of the experimental set-up used. The parallel plate flow cell (PPFC) was accoupled to the pumps and the tank jacket to recirculate the bacterial suspension. The temperature was kept constant at 37 °C using a recirculating water bath connected to the tank jacket to mimic human body conditions. Images were acquired every 60 s with a camera (Nikon DS-Ri 1, Japan) connected to a microscope (Nikon Eclipse LV100, Japan) and stored for further analysis.

Initial adhesion rates were obtained by linear regression analysis of initial points. After some time, from 5 to 9 minutes, the adhesion rate decreased, and the remaining points were subjected to a second linear regression. The difference between the first and second slopes was analysed. Standard deviations on the triplicate sets were calculated for all analysed parameters. Graph production and statistical analysis were performed using GraphPad Prism 6.01 (La Jolla, USA). The differences between the slopes as well as the variation of the adhesion rates with the shear conditions were evaluated using one-way analysis of variance (one-way ANOVA, Tukey's post-hoc test). All statistical analysis used a 95% confidence limit, so that *P* values equal to or greater than 0.05 were not considered statistically significant.

The percentage area fraction covered by *E. coli* cells was determined for different flow rates (1 to 10 ml/s). For this, ImageJ macro scripts were created to convert the images to an 8-bit greyscale file format and thresholds were applied to determine the occupied area (Code 2 – section 3.6, supplementary material).

3.2.4. Blocking analysis

After each 30 min trial, 5 images were taken in different regions of the surface to obtain a large set of adhered cells. Using ImageJ, the images were inverted, and the maxima detected (Figure S3.1). Each maximum corresponds to a cell. The respective coordinates were obtained and a pair correlation map was constructed [12]. Results are presented in the form of a 2D density probability function. The probability density function can be used to calculate, by integration, the probability of a cell being found around another cell at a region defined by Δx and Δy, where x and y are the coordinates centered in the reference cell. The probability density function was calculated using an R language script (see R scripts – section 3.6, supplementary material). To find the probability density function, a threshold R_{max} was defined. Pairs at a distance larger than R_{max} were not considered to construct the probability density function.

3.2.5. Mass transfer and drag force

The theoretical mass transport was estimated though the SL equation (approximate solution) [8] for each flow rate is determined by the Equation 3.1:

$$SL = 0.538 \frac{D_\infty C_b}{R_b} \left(\frac{Pe\, h_0}{x}\right)^{1/3}, \quad (3.1)$$

where D_∞ is the diffusion coefficient (approximately 4.0 x 10^{-13} m^2/s for *E. coli* [27]), C_b is the bacterial concentration (7.6 x 10^{13} cell/m^3), h_0 is the height of the rectangular channel (0.08 m) and x is the distance for which an average velocity variation below 15% was determined (m) as detailed in Moreira et al. [25]. R_b corresponds to the microbial radius (4.5 x 10^{-7} m) assuming that *E. coli* has a cylindrical shape estimated accordingly to the equation [15]:

$$R_b = \frac{1}{\ln\left(\frac{L}{b}\right) - 0.11} \left(\frac{L}{2}\right), \quad (3.2)$$

where L and b are the length and the diameter of the *E. coli* used in this study, respectively.

The SL equation also includes the Péclet number (*Pe*) which represents the ratio between convective and diffusional mass transport, given for the parallel plate configuration as:

$$Pe = \frac{3 v_{av} {R_b}^3}{2(h_0/2)^2 D_\infty}, \quad (3.3)$$

where v_{av} is the average flow velocity (m/s) determined in Moreira et al. [25].

It is assumed that gravity effects and hydrodynamic lift are negligible compared to the drag force [28] which was estimated by the following equations (Equations 3.4 and 3.5) [28] :

$$D = 32.0\tau_w R_b^2 + O(\mathrm{Re}_c), \quad (3.4)$$

where τ_w corresponds to the wall shear stress.

The flow within the near-wall region can be characterized using the local Reynolds number (Re_c), based on the shear rate, Υ, [28], as follows:

$$\mathrm{Re}_c = \rho \Upsilon R_b^2 / \mu\,, \quad (3.5)$$

where ρ , is the density (993.37 kg/m^3), and μ, the dynamic viscosity of the fluid (0.000694 kg/m.s). The values for τ_w and Υ, were obtained by computational fluid dynamics as described in Moreira et al. [25] and are listed in table S3.1 (supplementary material).

Re_c is always lower than 1, as $R_b \ll h_0$, and so the inertial effects are negligible in the near-wall region and terms of higher order, $O(\mathrm{Re}_c)$, in Equation (3.4) are negligible [28].

3.3. Results and discussion

Bacterial adhesion experiments were performed at different flow rates yielding a range of shear rates between 8 and 100/s, similar to relevant biomedical scenarios (Table S3.1, supplementary material) [22, 25].

Figure 3.3 shows the number of cells adhered to the PDMS surface during the experimental time at different flow rates. In all tested conditions, an initial adhesion rate was determined by linear regression of the first experimental points (Figure 3.3, blue dashed line), and it was observed that after some time (between 5 and 9 minutes), the experimental points did not fit this initial regression. Thus, a second linear regression was made with the remaining points (Figure 3.3, red dashed line) so that a second adhesion rate could be determined. It was found that this second adhesion rate was lower (on average 55%) than the value determined with the first regression (in blue) (Figure 3.4a), but the most significant reduction was observed for the lower and higher flow rates (on average 76%; $P < 0.05$, Figure 3.4a). The flow rate 2 ml/s presents the lowest reduction in the adhesion rate with a decrease of 20% (Figure 3.4a). Additionally, the adhesion rates were statistically different when comparing the results for the lower and the higher flow rates (1 and 2 ml/s with 8 and 10 ml/s, respectively) ($P < 0.05$).

It has been hypothesized that the main cause for this reduction in adhesion rate could be due to hydrodynamic blocking as arriving cells would interact with either already adhered cells or with the free surface [8]. Since the blocking effect is commonly evaluated as a function of the

surface area coverage [12, 29], this value was determined for the time were the slope decreased at each flow rate. Values between 0.8 to 1.8% were obtained, indicating low surface coverage at that time.

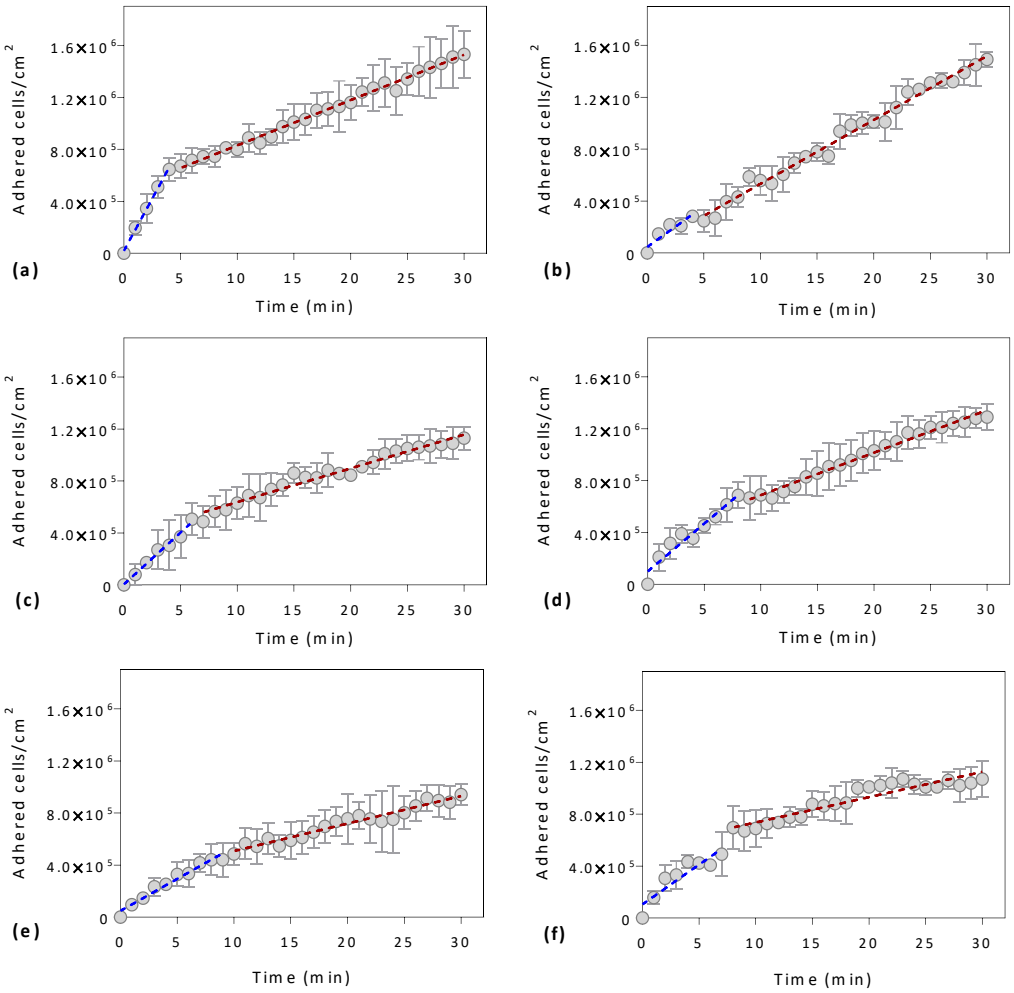

Figure 3.3. Number of *Escherichia coli* JM109(DE3) cells adhered to polydimethylsiloxane (PDMS) as a function of time. The dashed line indicates the best fit to a linear function for the initial adhesion rate (blue) and final adhesion rate (red) of the experiments. The adhesion assays were performed during 30 min at different flow rates: **(a)** 1 ml/s, **(b)** 2 ml/s, **(c)** 4 ml/s, **(d)** 6 ml/s, **(e)** 8 ml/s and **(f)** 10 ml/s corresponding to shear rates of 7.5/s, 15.0/s, 33.7/s, 51.6/s, 80.3/s and 100.8/s, respectively, in a PPFC. Error bars indicate the standard deviation from three independent experiments.

In order to assess if hydrodynamic blocking was occurring, we have performed an image analysis for each flow rate at the end of the adhesion assay (30 min), where surface coverage is at its highest value. It is precisely in those situations that blocking would be most likely to occur in our assays [12, 29]. The image analysis revealed that the final surface coverage was similar for all tested flow rates (Figure 3.4b) and was below 4%.

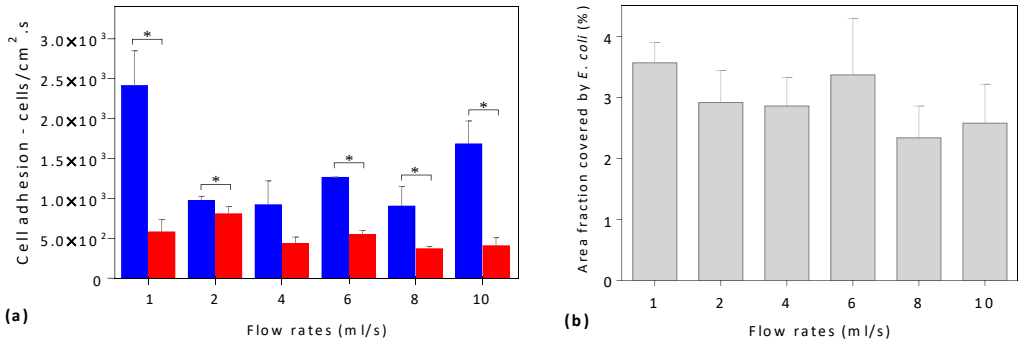

Figure 3.4. (a) Initial adhesion rates of *Escherichia coli* JM109(DE3) determined by linear regression of the first experimental points (blue bar) and for the remaining points (red bar) at different flow rates: 1 ml/s, 2 ml/s, 4 ml/s, 6 ml/s, 8 ml/s and 10 ml/s, corresponding to shear rates of 7.5/s, 15.0/s, 33.7/s, 51.6/s, 80.3/s and 100.8/s. Statistical significance between the adhesion rates and the different flow rates was evaluated by one-way analysis of variance (one-way ANOVA, Tukey's post-hoc test) (*, $P < 0.05$); **(b)** Area fraction covered by *E. coli* cells at the end of adhesion assay (30 min) on PDMS for the same hydrodynamic conditions.

Afterward, a pair correlation map was used to establish if significant areas were blocked by already adhered cells. 2D histograms were created, showing the probability density function of the presence of cells around a given cell (Figure 3.5). The central cell was excluded from the calculations, which explains the low probability in the center of the image. Cells at a distance larger than 50 pixels (30.5 μm) were also excluded from the analysis as it has been shown that blocking is more effective at distances shorter than the cut-off value used in this work [30]. If hydrodynamic blocking was occurring, the pair correlation map should show a low probability of cell adhesion along the flow direction, as demonstrated in previous studies [12]. However, in our experiments, the pair correlation maps are symmetrical, as the density probability of the presence of a cell around a given cell was uniform (Figure 3.5) and had no directional bias. This demonstrates that hydrodynamic blocking was not occurring during our experiments. Not at the end of the assay and surely not at the time point where the adhesion rates decreased.

In a previous study, it was shown that the size of the blocked area is a function of the dimensionless Péclet number [31]. In the present work, the Péclet number was below 0.4, which is much lower than the scenarios simulated in that study (2 to 100). Indeed, the size of the blocked area was shown to increase at higher shear rates and large particle sizes [12], and this may also explain why a shadow area was not observed in our work. Additionally, the low surface coverage may also have prevented the occurrence of blocking as it has been reported that even at surface coverages of about 10%, the blocking effect may not be significant [29].

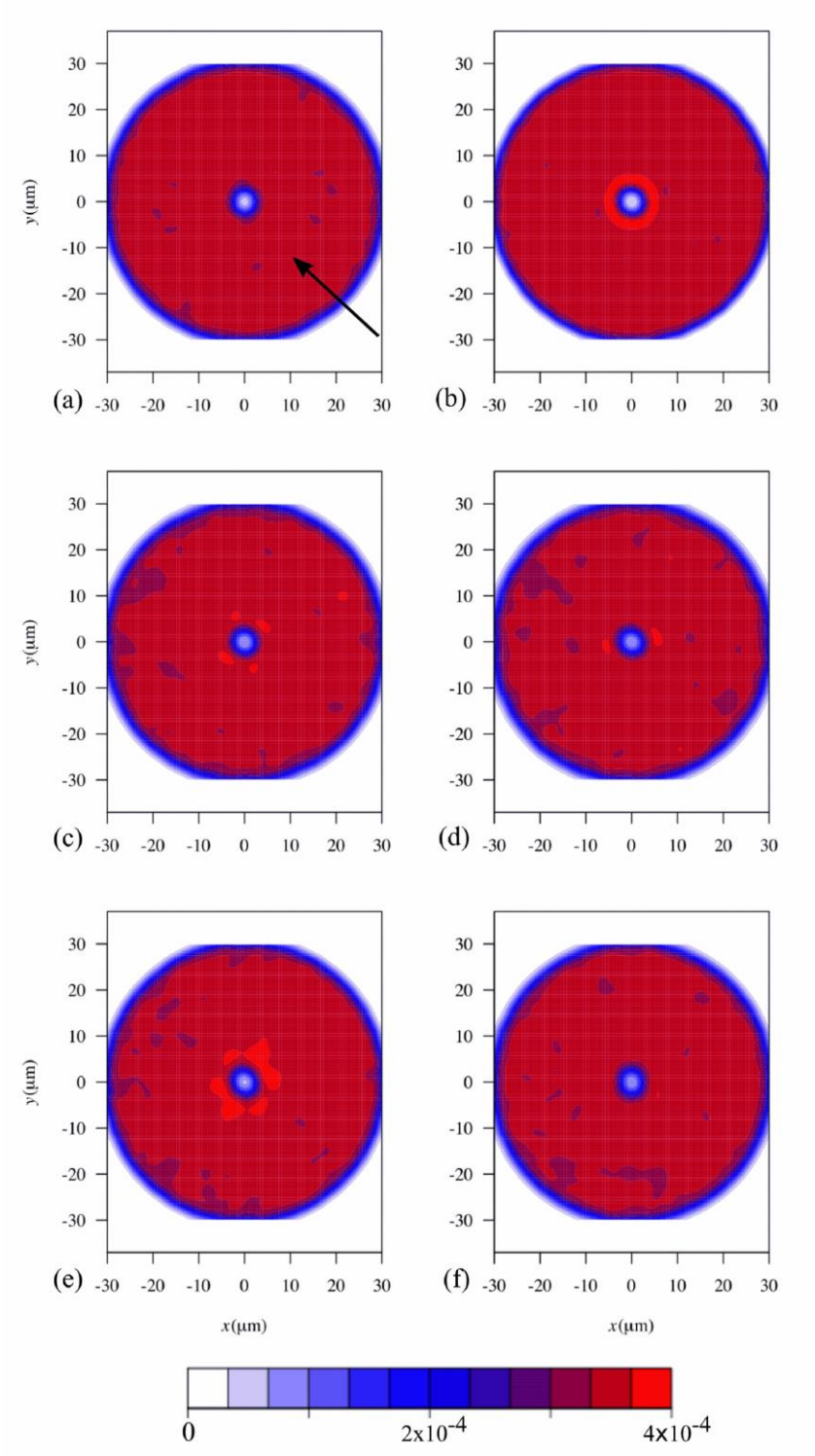

Figure 3.5. 2D histograms representing the probability density function of the presence of a cell around a given cell (reference cell is in the center). Results for different flow rates are shown: **(a)** 1 ml/s, **(b)** 2 ml/s, **(c)** 4 ml/s, **(d)** 6 ml/s, **(e)** 8 ml/s and **(f)** 10 ml/s corresponding to shear rates of 7.5/s, 15.0/s, 33.7/s, 51.6/s, 80.3/s and 100.8/s, respectively, in a PPFC. The number of independent cells measured for each flow rate was **(a)** 1.53 x 10^6 ± 1.84 x 10^5 cells/cm^2; **(b)** 1.49 x 10^6 ± 6.14 x 10^4 cells/cm^2; **(c)** 1.13 x 10^6 ± 8.87 x 10^4 cells/cm^2; **(d)** 1.29 x 10^6 ± 9.84 x 10^4 cells/cm^2; **(e)** 9.41 x 10^5 ± 8.25 x 10^4 cells/cm^2 and **(f)** 1.07 x 10^6 ± 1.37 x 10^5 cells/cm^2. The direction of the flow in all histograms is depicted by an arrow located on panel **(a)**.

Since hydrodynamic blocking was not occurring, other factors may explain the reduction in adhesion rates that we have observed (Figure 3.3). Higher flow velocities increase the number of contacts between planktonic cells and the surface, but the increased shear forces may also prevent adhesion or promote desorption [32, 33]. In order to ascertain the effect of flow rate variation on the transport of cells from the bulk solution to the surface, the SL approximation was used [8]. Figure 3.6 shows that as the flow rate increases, mass transport is favored, and since the SL approximation considers that all cells in close proximity to the surface will adhere, higher adhesion rates are expected at higher flow rates. However, as the flow rate increases, the wall shear stress also increases, and therefore higher drag forces are expected (Figure 3.6). It has been shown that sufficiently high shear stresses cause adhering bacteria to slide and roll over a surface, which may lead to desorption [34].

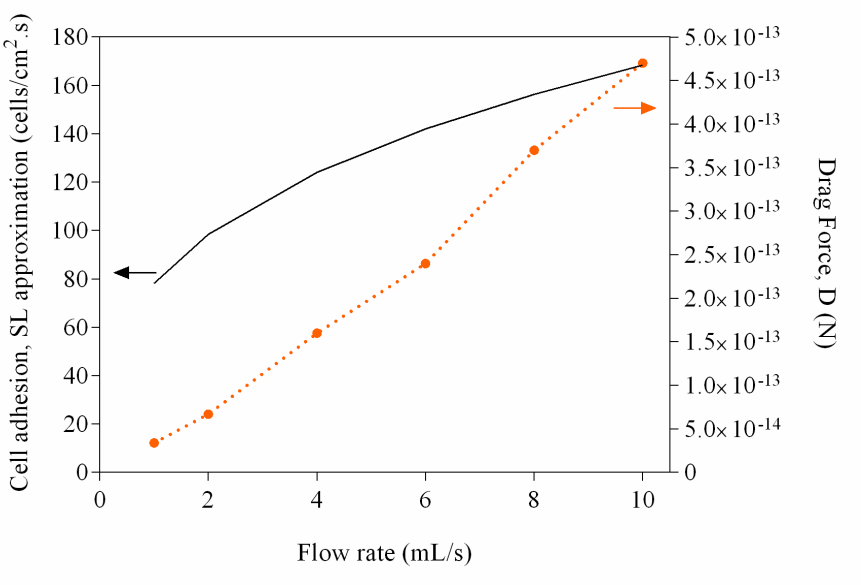

Figure 3.6. Variation of the drag force (D) and values obtained with the Smoluchowski-Levich (SL) approximation as a function of the flow rates: 1 ml/s, 2 ml/s, 4 ml/s, 6 ml/s, 8 ml/s and 10 ml/s, corresponding to shear rates of 7.5/s, 15.0/s, 33.7/s, 51.6/s, 80.3/s and 100.8/s. The full line represents the predicted adhesion rate using the SL approximation and the dashed line represents the drag force.

It is known that the strength of adhesion can depend on the history of the contact between a bacterium and a surface and that factors like the residence time and the shear applied during adhesion are strong modulators [35, 36]. Additionally, these forces are strongly dependent on chemistry [37] and mechanical properties of the surface [38]. It is likely that for each experimental condition tested, the relative importance of mass transport and desorption changes, and this may induce variations in the observed cell adhesion. In any case, since blocking is not occurring, the experimental values obtained at this second stage are also a reflection of the interaction between

single cells and the surface.

3.4. Conclusions

Bacterial adhesion studies are important not only because they provide an understanding of the early stages of biofilm formation but also because they may provide clues for the development of more efficient antifouling surfaces. These studies should be performed in conditions that mimic the real-life scenario not only regarding the surfaces and bacteria under evaluation but also in defined hydrodynamic conditions prevailing on that scenario. When real-time monitoring of initial adhesion is performed, a decrease in the initial adhesion rates is often observed along the experimental time. This decrease is often associated with hydrodynamic blocking, which can occur at significant surface coverage values. For low surface coverage situations, this decrease is most likely caused by cell desorption, which occurs when the force exerted on a single bacterium overcomes the adhesion force between the cell and that surface. Initial adhesion experiments should, therefore, be conducted so that low surface coverage values are obtained (by adapting the test conditions, namely the assay time), and the absence of blocking should be verified so that reliable results can be obtained. This enables the performance evaluation of different coatings so that more efficient antifouling surfaces can be developed.

3.5. References

1. Gusnaniar, N.; van der Mei, H. C.; Qu, W.; Nuryastuti, T.; Hooymans, J. M. M.; Sjollema, J.; Busscher, H. J., Physico-chemistry of bacterial transmission versus adhesion. *Advances in Colloid and Interface Science* **2017,** *250*, 15-24.

2. Costa, A. M.; Mergulhão, F. J.; Briandet, R.; Azevedo, N. F., It is all about location: how to pinpoint microorganisms and their functions in multispecies biofilms. *Future microbiology* **2017,** *12* (11), 987-999.

3. Brooks, J. D.; Flint, S. H., Biofilms in the food industry: problems and potential solutions. *International journal of food science & technology* **2008,** *43* (12), 2163-2176.

4. Miquel, S.; Lagrafeuille, R.; Souweine, B.; Forestier, C., Anti-biofilm activity as a health issue. *Frontiers in microbiology* **2016,** *7*, 592.

5. Soares, A.; Azevedo, A.; Gomes, L. C.; Mergulhão, F. J., Recombinant protein expression in biofilms. *AIMS microbiology* **2019,** *5* (3), 232-250.

6. Soares, A.; Gomes, L. C.; Mergulhão, F. J., Comparing the recombinant protein production potential of planktonic and biofilm cells. *Microorganisms* **2018,** *6* (2).

7. Moreira, J.; Gomes, L.; Whitehead, K.; Lynch, S.; Tetlow, L.; Mergulhão, F., Effect of surface conditioning with cellular extracts on *Escherichia coli* adhesion and initial biofilm formation. *Food and Bioproducts Processing* **2017,** *104*, 1-12.

8. Busscher, H. J.; van der Mei, H. C., Microbial adhesion in flow displacement systems. *Clinical Microbiology Reviews* **2006,** *19* (1), 127-141.

9. Ramstedt, M.; Ribeiro, I. A. C.; Bujdakova, H.; Mergulhão, F. J. M.; Jordao, L.; Thomsen, P.; Alm, M.; Burmølle, M.; Vladkova, T.; Can, F.; Reches, M.; Riool, M.; Barros, A.; Reis, R. L.; Meaurio, E.; Kikhney, J.; Moter, A.; Zaat, S. A. J.; Sjollema, J., Evaluating efficacy of antimicrobial and antifouling materials for urinary tract medical devices: challenges and recommendations. *Macromolecular Bioscience* **2019,** *19* (5), e1800384.

10. Lopez-Mila, B.; Alves, P.; Riedel, T.; Dittrich, B.; Mergulhão, F.; Rodriguez-Emmenegger, C., Effect of shear stress on the reduction of bacterial adhesion to antifouling polymers. *Bioinspiration & Biomimetics* **2018,** *13* (6), 065001.

11. Azeredo, J.; Azevedo, N. F.; Briandet, R.; Cerca, N.; Coenye, T.; Costa, A. R.; Desvaux, M.; Di Bonaventura, G.; Hébraud, M.; Jaglic, Z., Critical review on biofilm methods. *Critical reviews in microbiology* **2017,** *43* (3), 313-351.

12. van Loenhout, M. T.; Kooij, E. S.; Wormeester, H.; Poelsema, B., Hydrodynamic flow induced anisotropy in colloid adsorption. *Colloids and surfaces A: Physicochemical and engineering aspects* **2009,** *342* (1-3), 46-52.

13. Meinders, J.; Noordmans, J.; Busscher, H., Simultaneous monitoring of the adsorption and desorption of colloidal particles during deposition in a parallel plate flow chamber. *Journal of colloid and interface science* **1992,** *152* (1), 265-280.

14. Dabroś, T.; Van de Ven, T., Kinetics of coating by colloidal particles. *Journal of Colloid and Interface Science* **1982,** *89* (1), 232-244.

15. Adamczyk, Z., Modeling adsorption of colloids and proteins. *Current opinion in colloid & interface science* **2012,** *17* (3), 173-186.

16. Adamczyk, Z.; Warszyński, P.; Szyk-Warszyńska, L.; Weroński, P., Role of convection in particle deposition at solid surfaces. *Colloids and Surfaces A: Physicochemical and Engineering Aspects* **2000,** *165* (1-3), 157-187.

17. Adamczyk, Z., Particle adsorption and deposition: role of electrostatic interactions. *Advances in Colloid and Interface Science* **2003,** *100*, 267-347.

18. Alves, P.; Gomes, L. C.; Vorobii, M.; Rodriguez-Emmenegger, C.; Mergulhão, F. J., The potential advantages of using a poly(HPMA) brush in urinary catheters: effects on biofilm cells and architecture. *Colloids and Surfaces B: Biointerfaces* **2020,** *191*, 110976.

19. Gomes, M.; L.C. Gomes; Teixeira-Santos, R.; Mergulhao, F., PDMS in urinary tract devices: applications, problems and potential solutions. In *Polydimethylsiloxane: Structure and Applications* Carlsen, P. N., Ed. Nova Science Publishers, Inc.: Hauppauge, USA, 2020.

20. Alves, P.; Gomes, L. C.; Rodríguez-Emmenegger, C.; Mergulhão, F. J., Efficacy of a poly(MeOEGMA) brush on the prevention of *Escherichia coli* biofilm formation and susceptibility. *Antibiotics (Basel)* **2020,** *9* (5).

21. Alves, P.; Nir, S.; Reches, M.; Mergulhão, F., The effects of fluid composition and shear conditions on bacterial adhesion to an antifouling peptide-coated surface. *MRS Communications* **2018,** *8* (3), 938-946.

22. Gomes, L.; Moreira, J.; Teodósio, J.; Araújo, J.; Miranda, J.; Simões, M.; Melo, L.; Mergulhão, F., 96-well microtiter plates for biofouling simulation in biomedical settings. *Biofouling* **2014,** *30* (5), 535-546.

23. Teodósio, J.; Simões, M.; Melo, L.; Mergulhão, F., Flow cell hydrodynamics and their effects on *E. coli* biofilm formation under different nutrient conditions and turbulent flow. *Biofouling* **2011,** *27* (1), 1-11.

24. Simões, M.; Simões, L. C.; Cleto, S.; Pereira, M. O.; Vieira, M. J., The effects of a biocide and a surfactant on the detachment of *Pseudomonas fluorescens* from glass surfaces. *International journal of food microbiology* **2008,** *121* (3), 335-341.

25. Moreira, J.; Araújo, J.; Miranda, J. M.; Simões, M.; Melo, L.; Mergulhão, F., The effects of surface properties on *Escherichia coli* adhesion are modulated by shear stress. *Colloids and Surfaces B: Biointerfaces* **2014,** *123*, 1-7.

26. Schneider, C. A.; Rasband, W. S.; Eliceiri, K. W., NIH Image to ImageJ: 25 years of image analysis. *Nature methods* **2012,** *9* (7), 671.

27. Xia, Z.; Woo, L.; van de Ven, T. G., Microrheological aspects of adhesion of *Escherichia coli* on glass. *Biorheology* **1989,** *26* (2), 359-75.

28. Boulbene, B.; Morchain, J.; Bonin, M. M.; Janel, S.; Lafont, F.; Schmitz, P., A combined computational fluid dynamics (CFD) and experimental approach to quantify the adhesion force of bacterial cells attached to a plane surface. *AIChE Journal* **2012,** *58* (12), 3614-3624.

29. van der Mei, W. N.; Krom, B.; Sjollema, J., Analysis of the contribution of sedimentation to bacterial mass transport in a parallel plate flow chamber Part II: Use of fluorescence imaging. *Colloids and Surfaces B: Biointerfaces* **2011,** *87*, 427-432.

30. Sjollema, J.; Busscher, H., Deposition of polystyrene particles in a parallel plate flow cell. 2. Pair distribution functions between deposited particles. *Colloids and Surfaces* **1990,** *47*, 337-352.

31. Dabros, T., Interparticle hydrodynamic interactions in deposition processes. *Colloids and Surfaces* **1989,** *39* (1), 127-141.

32. Lecuyer, S.; Rusconi, R.; Shen, Y.; Forsyth, A.; Vlamakis, H.; Kolter, R.; Stone, H. A., Shear stress increases the residence time of adhesion of *Pseudomonas aeruginosa*. *Biophysical journal* **2011,** *100* (2), 341-350.

33. Dickinson, R. B.; Cooper, S. L., Analysis of shear‐dependent bacterial adhesion kinetics to biomaterial surfaces. *AIChE Journal* **1995,** *41* (9), 2160-2174.

34. Nejadnik, M. R.; van der Mei, H. C.; Busscher, H. J.; Norde, W., Determination of the shear force at the balance between bacterial attachment and detachment in weak-adherence systems, using a flow displacement chamber. *Applied and Environmental Microbiology* **2008,** *74* (3), 916.

35. Marshall, B. T.; Sarangapani, K. K.; Lou, J.; McEver, R. P.; Zhu, C., Force history dependence of receptor-ligand dissociation. *Biophysical Journal* **2005,** *88* (2), 1458-1466.

36. Xu, L. C.; Vadillo-Rodriguez, V.; Logan, B. E., Residence time, loading force, pH, and ionic strength affect adhesion forces between colloids and biopolymer-coated surfaces. *Langmuir* **2005,** *21* (16), 7491-500.

37. Garrett, T. R.; Bhakoo, M.; Zhang, Z., Bacterial adhesion and biofilms on surfaces. *Progress in Natural Science* **2008,** *18* (9), 1049-1056.

38. Lichter, J. A.; Thompson, M. T.; Delgadillo, M.; Nishikawa, T.; Rubner, M. F.; Van Vliet, K. J., Substrata mechanical stiffness can regulate adhesion of viable bacteria. *Biomacromolecules* **2008,** *9* (6), 1571-1578.

3.6. Supplementary material

3.6.1. Image processing and extraction of cell coordinates

After each 30 min trial, 5 images were taken in different regions of the surface to obtain a large set of adhered cells. Using ImageJ, the images were inverted, and the maxima detected (Figure S3.1). Each maximum corresponds to a cell. The respective coordinates were obtained, and a pair correlation map was constructed [1]. Results were presented in the form of a 2D density probability function. The probability density function was calculated using two R language scripts. The file with the cell coordinates (input file) and the R language scripts are presented in the following sections.

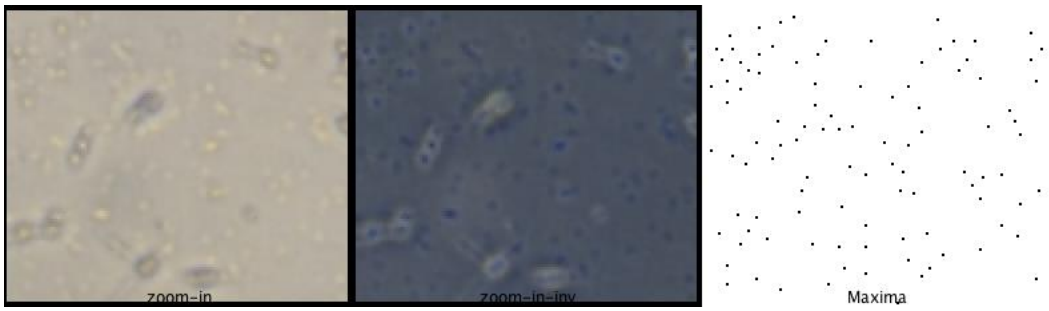

Figure S3.1. Steps of the method. From left to right: initial image, inverted image and maxima.

3.6.2. Input files

The input file for the R scripts that generate the 2D correlations maps has the following format (only the first 6 lines of the file are shown):

```
-------------
      X    Y
1   389   71
2   561  533
3  1191  539
4   417   63
5  1017  461
-------------
```

3.6.3. R scripts

Two R language scripts were used to generate 2D correlations plot, a script that calculates the relative position in relation to the reference cell from the coordinates of the cells and a script that generates the histogram.

3.6.3.1. Relative positions script

```
library(plotrix)
rm(list=ls(all=TRUE))
```

```
# base path
	dir0="/Users/jmiranda/Desktop/results/"
#	coordinate files are here
	dirSub="t/"

#	relative coordinates directory (output of this script will be saved here)
	dir_res_sub="t-res/"
	dir_res=paste(dir0,dir_res_sub,sep="")
	dir=paste(dir0,dirSub,sep="")
	text_t=character()
	ficheiros_nome=list.files(dir,pattern="*.txt",full.names = FALSE)
	ficheiro=paste(dir,ficheiros_nome[1],sep="/")
# cut off radius in pixels
	radius=50.0
	dados=read.table(ficheiro,header=TRUE,blank.lines.skip=FALSE)
for (temp in ficheiros_nome)
	{
# processes all available files
	aux=numeric()
	aux2=numeric()
	xx=numeric()
	yy=numeric()
	ficheiro=paste(dir,temp,sep="/")
	dados=read.table(ficheiro,header=TRUE,blank.lines.skip=FALSE)
	ficheiro_base=strsplit(temp,"\\.")[[1]]
	ficheiro_res0=paste(ficheiro_base[1],"res",sep="_")
	ficheiro_res0=paste(ficheiro_res0,"txt",sep=".")
	ficheiro_res=paste(dir_res,ficheiro_res0,sep="")
	xx=dados$X
	yy=dados$Y
	n=length(yy)
	xmax=max(xx)
	ymax=max(yy)

	for(i in (1:n))
		{
		if(xx[i]>radius & yy[i]>radius & xx[i]<(xmax-radius) & yy[i]<(ymax-radius))
		{
		for(j in (1:n))
		{
		if(j!=i)
		{

		xp0=xx[i]
		yp0=yy[i]
		xp=xx[j]
		yp=yy[j]

		dist=sqrt((xp-xp0)^2+(yp-yp0)^2)

		if(dist<radius )
```

```
                {
                aux=c(aux,xp-xp0)
                aux2=c(aux2,yp-yp0)
                }
                }}}}

  x <- data.frame(a = aux, b = aux2)
  write.table(x, file = ficheiro_res, sep = ",", col.names = NA,
 qmethod = "double")
  }
```

3.6.3.2. Histogram script

```
  library(plotrix)
  library(MASS)
  require(grDevices) # for colours
  rm(list=ls(all=TRUE))
#   base path
  dir0="/Users/jmiranda/Desktop/results/"
#   directory with the coordinates files
  dirSub="t-res/"
#   full path
  dir=paste(dir0,dirSub,sep="")
  ficheiros_nome=list.files(dir,pattern="*.txt",full.names = FALSE)
  temp=ficheiros_nome[1]
  count=numeric()
  for (temp in ficheiros_nome)
                {
                dir2=paste(dir0,"t-tif/",sep="")
                nome=paste(dir2,temp,sep="")
                nome=paste(nome,".tiff",sep="")
                tiff(filename = nome, , res = 300, width = 1600, height = 1600)
                ficheiro=paste(dir,temp,sep="/")

  dados=read.table(ficheiro,sep=",",header=FALSE,blank.lines.skip=FALSE,skip=1)

#               0.61 is the conversion factor from pixels to micrometers
                x=dados$V2*0.61
                y=-dados$V3*0.61

#               maximum and minimum values
                valmax=4e-4
                valmin=0

                df <- data.frame(x,y)
                k <- kde2d(x, y,n=50)
                clo=""
                rgb.palette <- colorRampPalette(c("white", "blue", "red"),space = "rgb")

                clo=rgb.palette(12)
                a=seq(valmin,valmax,(valmax-valmin)/12)
```

```
filled.contour(k, col= clo,levels = a , zlim=range(valmin,valmax),asp = 1,plot.title=title(main =
temp,
  xlab = expression(paste(italic(x),"(",symbol(m),"m)")), ylab =
expression(paste(italic(y),"(",symbol(m),"m)")) )  )
                dev.off()
                }
```

3.6.4. Code 1: Cell adhesion analysis

```
rename("Original");
run("8-bit");
run("Subtract Background...", "rolling=20 light stack");
run("Set Scale...", "distance=1000 known=110 unit=um");
setAutoThreshold("Default");
setOption("BlackBackground", false);
run("Convert to Mask", "method=Default background=Light calculate");
run("Analyze Particles...", "size=1-Infinity show=Outlines display exclude clear summarize
stack");
```

3.6.5. Code 2: Surface coverage

```
run("8-bit");
run("Invert""stack");
run("Subtract Background..."  "rolling=10 light stack");
run("Color Balance...");
setAutoThreshold("Default dark");
run("Threshold...");
call("ij.plugin.frame.ThresholdAdjuster.setMode"  "Red");
setAutoThreshold("Default");
run("NaN Background"  "stack");
run("NaN Background"  "stack");
run("Set Measurements..."  "area area_fraction limit redirect=None decimal=3");

run("Analyze Particles..." "show=Outlines display exclude clear summarize stack");
```

Table S3.1. Shear rate and wall shear stress at the different flow rates tested (determined by Computational Fluid Dynamics) and examples of biomedical scenarios where these shear rates can be found. Adapted from Alves et al. [2]

Flow rate (ml/s)	Wall shear stress (τ_w, Pa)	Shear rate (Υ, 1/s)	Biomedical scenarios
1	0.0052	7.5	Fluid flow in the oral cavity
2	0.0102	15.0	Urinary flow in a catheter
4	0.0237	33.7	Flow in femoral artery
6	0.0362	51.6	Blood flow in venous vessels
8	0.0566	80.3	Flow in ascending aorta
10	0.0719	100.8	Flow in ascending aorta

3.6.6. References

1. van Loenhout, M. T.; Kooij, E. S.; Wormeester, H.; Poelsema, B., Hydrodynamic flow induced anisotropy in colloid adsorption. *Colloids and surfaces A: Physicochemical and engineering aspects* **2009,** 342, (1-3), 46-52.

2. Alves, P.; Nir, S.; Reches, M.; Mergulhão, F., The effects of fluid composition and shear conditions on bacterial adhesion to an antifouling peptide-coated surface. *MRS Communications* **2018,** 8, (3), 938-946.

4. The effects of sedimentation and desorption on initial bacterial adhesion studies [e]

Abstract

Bacterial adhesion to biomaterials often occurs, despite the mechanical forces generated through the fluid contact with surfaces. Although the progress of the last years in the study of bacterium-surface interactions, the contribution of bacterial mass transport to cell adhesion is still poorly understood.

In this work, the mass transport mechanisms involved in the initial adhesion of *Escherichia coli* to polydimethylsiloxane (PDMS) surfaces were evaluated by *in situ* and real-time imaging using a parallel plate flow cell (PPFC) operating at different flow rates (1, 3, 7 and 9 ml/s). The contributions of sedimentation and desorption to the apparent adhesion rates were evaluated. Our results demonstrated sedimentation is the major effector for cell adhesion in the PPFC system, which had a strong influence on *E. coli* adhesion (on average 40%). Thus, higher adhesion rates are obtained due to the contribution of sedimentation and this is more noticeable at lower shear stresses. On the contrary, the desorption process was negligible in the range of shear stresses tested (0.0052, 0.016, 0.042 and 0.064 Pa). The analysis outlined in this work enables a better understand of the initial interactions between bacteria and a surface in a flow displacement system.

The content of this chapter is being prepared for publication:

[e] **Alves P**, Gomes LG, Miranda JM, Mergulhão FJ (**2020**) The effects of sedimentation and desorption on initial bacterial adhesion studies

4.1. Introduction

Attachment and accumulation of microorganisms occur on surfaces exposed to an aqueous environment, leading to the subsequent growth of biofilms. Adhered bacteria are generally exposed to a wide range of hydrodynamic forces created by the fluid flow [1]. Biofilm formation starts with bacterial mass transport, by which bacteria can be transported to a surface through sedimentation and diffusion (mostly under stagnant conditions) [2], or by combination of sedimentation, convection and diffusion (in flow displacement systems) when in an aqueous environment [3-5]. Convective mass transport prevails under turbulent flow conditions [6].

Over the past decades, extensive research on biofilm formation has been done, and the early stages of microbial adhesion have been particularly studied due to their relevance in the development of biofilms in industrial equipment and medical settings [7]. Several parameters affect the adhesion process such as the surface properties of microorganisms and substrates, the hydrodynamic conditions operating during the adhesion process, and external parameters such as gravity and the surrounding environment [6, 8]. All these parameters should be taken into account when designing an implant, for example, in order to reduce the susceptibility of the biomedical device to bacterial colonization and subsequent infection [9, 10].

The reversibility of microbial adhesion implies a continuous exchange between the microorganisms adhered to the surface and those floating in the bulk fluid. Adherent organisms can leave a surface when conditions become unfavorable [11, 12]. Bacterial cells can be removed from the biofilm through desorption, detachment, and dispersion processes. Desorption is the transfer of bacteria attached to a substrate to the bulk liquid and this is observed in the initial stages of the biofilm formation process. The detachment process is considered the main process that limits the accumulation of biofilm, including the processes of erosion and sloughing. Erosion describes the continuous removal of biomass, while sloughing involves the removal of intact parts of biofilm or the entire biofilm [13]. In order to determine the degree of reversible adhesion, several theories and experimental systems have been developed. However, theories to predict adhesion rates in particular flow systems have been applied mainly to colloidal particle [14-17]. For instance, a methodology based on the *in situ* microscopic observation of the adhesion process was described to further determine the adhesion and desorption rates of colloidal particles on collector surfaces in a parallel plate flow cell (PPFC) [15]. The researchers observed low desorption of adhering particles both during the adhesion process, as well as afterward when flowing with buffer, which suggests that the process of particle adhesion might be considered as reversible [15]. To gain a more comprehensive understanding of bacterial mass transport, Sjollema and his coworkers [18] described a PPFC system which enables the *in situ* and real-time counting of

adhering microorganisms using automated image analysis. This platform offers the opportunity to mimic *in vivo* hydrodynamic forces of felt by attached bacteria and, by regulating the applied fluid flow, the bacterial adhesion properties can be studied under conditions that are more similar to those found in real scenarios [7, 19, 20]. Later, a study conducted by Li et al. [3] reported a microscopy-based methodology to determine the gravitational contribution to bacterial mass transport in a PPFC taking into account the bacterial concentration over the height of the flow channel. For this, the authors adopted the Smoluchowski–Levich (SL) solution that assumes that the substratum acts as a perfect sink on which every particle/bacterium arriving at the surface adheres irreversibly. Adhesion efficiency was obtained through the ratio between the experimentally observed initial adhesion rates and the theoretical rates calculated by the SL-solution [3]. This indicates the fraction of bacteria that arrives at the surface that will adhere successfully under the influence of the interaction forces between the bacteria and the surface. The results of Li et al. [3] demonstrated that the SL-solution of the convective-diffusion equation was four-to-five-fold higher than unity for *Staphylococcus aureus* ATCC 12600. They concluded that sedimentation is the predominant contribution to mass transport in this platform.

Despite the importance of mechanical forces in the establishment of biofilms in nature, their contributions to bacterial adhesion are poorly understood. Most of the studies carried out focus on the study of the bacterial retention capacity after a certain period of adhesion, as they argue that bacterial retention is crucial for the maintenance of the entire biofilm on a surface and during periods of high shear forces [6]. In this sense, it has been suggested in the past that more studies should address bacterial retention and not the bacterial adhesion process. Consequently, many studies on microbial adhesion do not deal with adhesion, but with the capacity of adherent organisms to withstand the process of desorption (microbial retention) [6, 21, 22].

In this work, an experimental approach was developed to obtain the mass balance of *Escherichia coli* adhesion to a solid substratum (polydimethylsiloxane, PDMS) on a PPFC. This method allows a detailed study of the adhesion process, in which adhesion, desorption and sedimentation are addressed in real time as opposed to and endpoint analysis usually performed at later stages of biofilm development. Initial adhesion experiments are helpful to characterize the interaction of cells with the surface because, in dynamic assays, organisms that arrive at a substratum surface interact solely with the surface. At later stages of biofilm development, when the surface is already partially covered with adhering organisms, an adhering cell will have interactions with the substratum surface, but also with already adhered organisms, and these effects become harder to separate [6]. By performing a mass balance in real time, it is possible to

obtain a more accurate interpretation of the initial bacterial adhesion and its interactions with the surface.

4.2. Materials and methods

4.2.1. Bacterial strain and growth conditions

Escherichia coli JM109(DE3) from Promega (USA) was selected for this study as it had shown to adhere to different surfaces in the PPFC system [23-26]. The pre-culture was prepared and grown overnight at 37 °C as previously described (Chapter 3-section 3.2.1).

4.2.2. Surface preparation

PDMS was the material selected for these experiments since it is transparent and one of the most widely used surfaces in flow displacement systems [10, 27] particularly for biomedical applications. PDMS slides were prepared as fully described in Chapter 3-section 3.2.2.

4.2.3. Parallel plate flow cell experiments

The PPFC is a flow displacement system widely used in the study of bacterial adhesion to surfaces [9, 20, 28]. The PPFC system used in this work was completely characterized by our research group [20, 24] and has the advantage of allowing the establishment of desired hydrodynamic conditions and consequently the control of bacterial mass transport. Prior to use, the flow cell was disinfected as previously described in Chapter 3-section 3.2.3.

Subsequently, the system was mounted in a microscope stage to monitor bacterial adhesion and desorption, flowing in a closed circuit. Experiments were performed for 30 min at different flow rates: 1, 3, 7 and 9 ml/s that were adjusted with a valve. According to the Computational Fluid Dynamics (CFD) simulations previously performed [20], the average shear stresses corresponding to these flow rates are 0.0052, 0.016, 0.042 and 0.064 Pa. During the PPFC operation, the *E. coli* suspension was recirculated through a pump system at a controlled temperature of 37 °C. The bacterial adhesion and desorption from the PDMS surface were monitored for each flow rate with a brightfield microscope (Nikon Eclipse LV100, Japan) equipped with 20 × objective (NA = 0.4). Image acquisition was performed every 60 s with a camera (Nikon DS-Ri 1, Japan) at a defined field of the surface without moving the system, and high-quality images with 2592 x 1944 pixels were automatically stored.

4.2.4. Data analysis

Image analysis was performed using ImageJ (version 1.38e) software [29] and for each flow rate tested, the number of adhered bacteria per surface area was enumerated at each time-point

using a macro (Code 1 and 2-supplementary material, section 4.6). Images were converted to a 32-bit greyscale file format and thresholds were applied. Each image has a resolution of 2592 x 1944 pixels, with each pixel having 256 possible gray values (0 = black; 255 = white). This step allows differentiating the gray value of an adhering organism from the background [18, 30]. Then, the analysis of these images consisted on creating addition and a duplication image steps of the stored images. This enabled that the background gray value remained the same, as well as the values associated with bacteria that are adhering to the surface, contrary to moving bacteria that acquired different gray values. Comparison of successively taken images allowed the simultaneous determination of the number of adsorbed and desorbed cells, of cells that remained attached and of new cells arriving at the surface every 60 s.

The cumulative adhered cells were estimated for the bottom and top of the PPFC and are defined as the number of total cells that were observed *in situ* and that accumulate over time, and correspond to $n(t)$ in Equation (4.1):

$$n(t) = n_{old} + n_{new} + n_{des} \tag{4.1}$$

in which n_{old} represents the cumulative number of bacteria that remained adhered, n_{new} refers to the cumulative number of new cells that arrived at the surface, and n_{des} is the cumulative number of desorbed bacteria.

Adhesion kinetics expressed in terms of the initial adhesion rates, j_0 (cells/cm^2.min), were obtained from bottom and top planes of the PPFC by linear regression analysis of initial adhesion points (adhered cells/cm^2 in function of time) for each flow rate (Figure 4.2) according to Equation (4.2) [12]:

$$j_0 = \frac{dn(t)}{dt} \tag{4.2}$$

The data presented in Figure 4.2 represents an average of three independent results for each tested condition. To verify the statistical significance, the data was analysed using GraphPad Prism® 6.01 (La Jolla, CA, USA). Paired t-test analysis was performed based on confidence levels of 95% (differences are reported as significant for P values < 0.05 and are denoted by *).

Additionally, for sedimentation analysis, bacterial adhesion experiments were carried out under stagnant conditions, i.e. the adhering bacteria were monitored during the 30 min of the experiment and then, the flow was stopped after this time for each hydrodynamic condition evaluated. Then, were taken 6 different vertical planes (z), including the bottom and the top plane of the PPFC, in at least 5 different field of view (FOV) using a joystick (Prior Scientific Ltd, Cambridge, UK) coupled to the microscope. Three independent experiments were performed.

For each flow rate tested, the number of bacteria adhering per unit area was recorded as a function of time using the ImageJ software. The number of bacterial cells was then divided by the surface area of the FOV to obtain the number of cells per square centimeter (Figure 4.3).

Afterward, differential balances for the n_{new} and n_{des} were determined as n_{i+1}-n_i for each one of the variables to explore what happens at each instant during the 30 min of the adhesion experiment and for the flow rates tested (Figure 4.4). The sedimentation value was calculated considering the difference between the number of cells adhered to the bottom plate and the average value previously determined at each time point and flow rate. The cells that arrived at the surface by sedimentation, n_{sed}, were determined considering the difference between the sedimentation value and the n_{new} of the bottom plan (Figure 4.4).

4.3. Results and discussion

A macro script for ImageJ was developed in this work to automatically measure the number of attached cells as a function of time in a PPFC system operated at different flow rates. The PPFC system was selected since it was properly characterized [20].

The mass balance for *E. coli* cells was calculated for different flow rates (1 to 9 ml/s) over 30 min (Figure 4.1) considering the following parameters: the cumulative number of adhered cells ($n(t)$), the cumulative number of desorbed cells (n_{des}), and the cumulative number of cells that remained attached to the surface plus the new ones that arrive at the surface ($n_{old} + n_{new}$). The number of adhered cells is a balance between the cells that arrive at the surface and can initiate a reversible adhesion process and those that are desorbed from the surface due to shear. Looking at Figure 4.1, $n(t)$ and $n_{old} + n_{new}$ increased linearly with time for all tested shear conditions.

In general, increasing the flow rate resulted in a decrease in the number of bacteria attached to the surface (Figure 4.1), which can be justified by the increase in the number of desorbed cells (n_{des}). It is known that the increase in shear stress can lead to an increase in the number of contacts between the cells in the bulk and the surface, but the increased shear forces may also prevent adhesion or promote cell desorption [31, 32]. Since it has recently been proven that the hydrodynamic blocking phenomenon does not occur in this system for similar shear stresses (Chapter 3), the decrease in cell adhesion rates may be related to other phenomena such as desorption [13, 33] or sedimentation [3]. The results indicated an increased cell desorption in the initial minutes of the adhesion experiment (from 20 to 80% of desorption), depending on the flow rate and assay time (Figure 4.1). Different behaviors are observed as for the lowest flow rate (1 ml/s; Figure 4.1a), the desorption is very low throughout the experiment (from 3 to 9%), whereas higher values are obtained at higher flow rates. For the intermediate flow rate (3 ml/s; Figure 4.1b) and

the highest flow rate (9 ml/s; Figure 4.1d) tested, desorption increases over time and then decreases after 10 min. Interestingly, for the flow rate 7 ml/s (Figure 4.1c), an increase in the desorption percentage in the initial moments of the experiment is observed and then the desorption percentages decrease after 20 min.

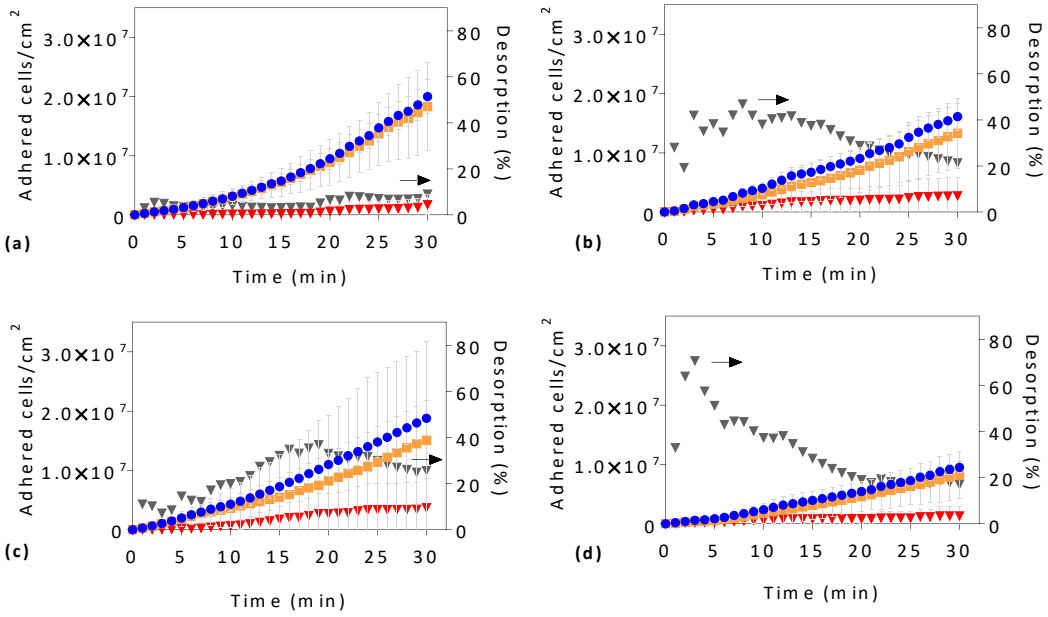

Figure 4.1. Global mass balance of *Escherichia coli* JM109(DE3) adhesion process to PDMS at different flow rates: **(a)** 1 ml/s; **(b)** 3 ml/s; **(c)** 7 ml/s and **(d)** 9 ml/s, corresponding to the shear stresses of 0.0052, 0.016, 0.042 and 0.064 Pa, respectively. The cumulative number of adhered cells, $n(t)$ (●), the cumulative number of desorbed cells, n_{des} (▼), the cumulative number of cells that remained attached to the surface plus the new ones that arrive at the surface, $n_{old} + n_{new}$ (■) is depicted in the x-axis; and the desorption (%) (▼) of the cells is depicted by an arrow located on panels (y-axis).

At higher flow rates, the depletion of cells near the surface and slower attachment lead to an accumulation of cells probably caused by sedimentation. In order to experimentally determine the contribution of sedimentation to the mass transport in the PPFC, the bacterial concentration at the bottom and top plate was first estimated. When initial adhesion rate (j_0), is shown as a function of the flow rate to the bottom and top planes of the PPFC, it is possible to conclude that *E. coli* cells were mostly present in the lower part of the PPFC ($P < 0.05$; Figure 4.2), probably due to sedimentation. Afterward, a microscopy-based method was introduced to measure the height-dependent bacterial concentration in the PPFC at the end of each experiment (Figure 4.3). The results corroborate the observations in Figure 4.2. In fact, the cells were shown to be closer to the bottom plane than the other planes, decreasing from the bottom to the top.

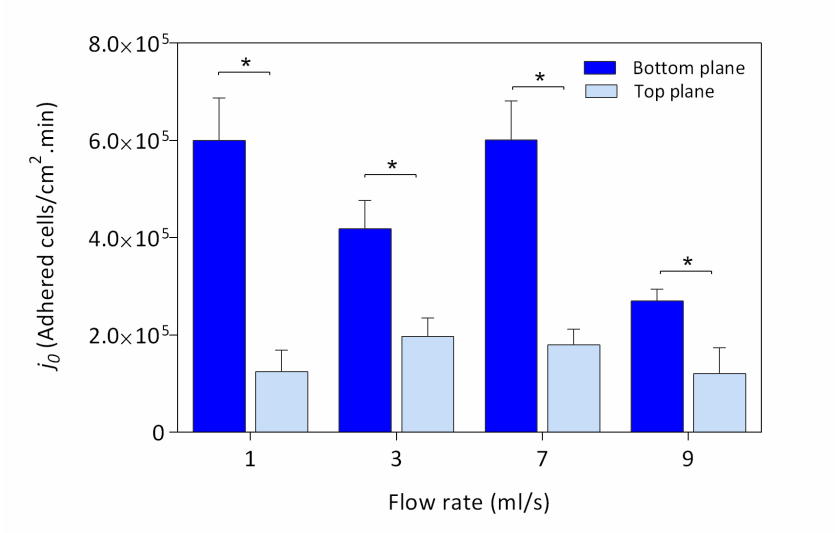

Figure 4.2. Initial adhesion rates (j_0) of *Escherichia coli* JM109(DE3) to the bottom (■) and top (■) planes of the parallel plate flow cell at different flow rates (1, 3, 7 and 9 ml/s corresponding to the shear stresses of 0.0052, 0.016, 0.042 and 0.064 Pa, respectively). The means ± SDs for three independent experiments are illustrated. Statistically significant differences obtained between the surfaces are indicated by * for $P < 0.05$.

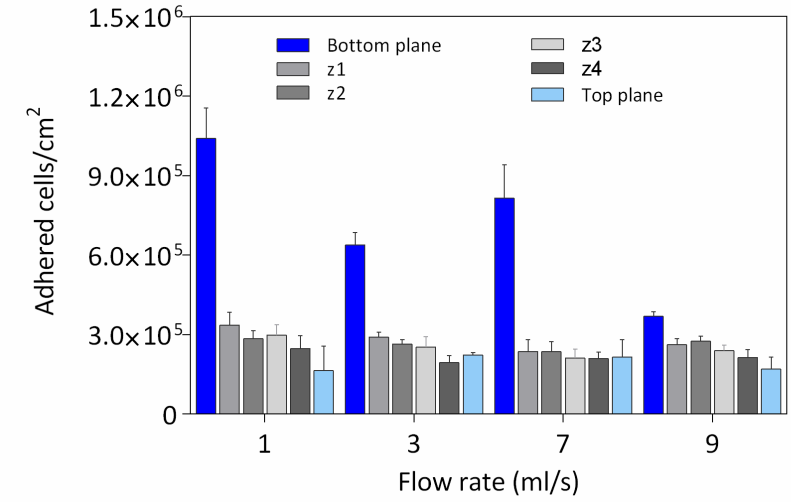

Figure 4.3. Height dependence of the *Escherichia coli* JM109(DE3) concentration at different flow rates: 1, 3, 7 and 9 ml/s, corresponding to the shear stresses of 0.0052, 0.016, 0.042 and 0.064 Pa, respectively. Each color corresponds to different heights inside the parallel plate flow cell: bottom plane (PDMS - 0 μm; ■), z1 (1552 μm; ■), z2 (3104 μm; ■), z3 (4656 μm; ■), z4 (6207 μm; ■) and top plane (PDMS - 7759 μm; ■).

Figure 4.4 presents the differential mass balance for the *E. coli* adhesion process at different flow rates, i.e, the new cells that arrived at the surface on a given instant as well as the desorbed cells. This analysis enables us to understand what happens at a given time-point of the 30-min assay. Then, the number of cells that arrived by sedimentation at the PDMS surface were

determined for the purpose of obtaining the sedimentation contribution (%) (Figure 4.4). It is possible to observe that sedimentation had a strong influence on bacterial adhesion for all tested conditions (on average 40%) and the desorption process is almost negligible when compared to the total adhesion rate. Not all bacteria that reach the bottom plate adhere firmly [34], namely the new cells arriving at the surface whose number increased with the increase of the shear forces acting upon them (Figure 4.4). This suggests that the residence time was not enough to promote strong cell-surface interactions and consequently promote the *E. coli* desorption from the PDMS surface. However, these non-adherent bacteria were probably transported along the surface by the flow, contributing to the increase in bacterial concentration near the bottom plate and to the adhesion efficiency, particularly at lower flow rates (Chapter 3-Figure 3.6). The relative contribution of sedimentation to bacterial mass transport did not depend on the flow rate, as observed in figure 4.4, since the average value was quite similar for all tested flow rates (40%).

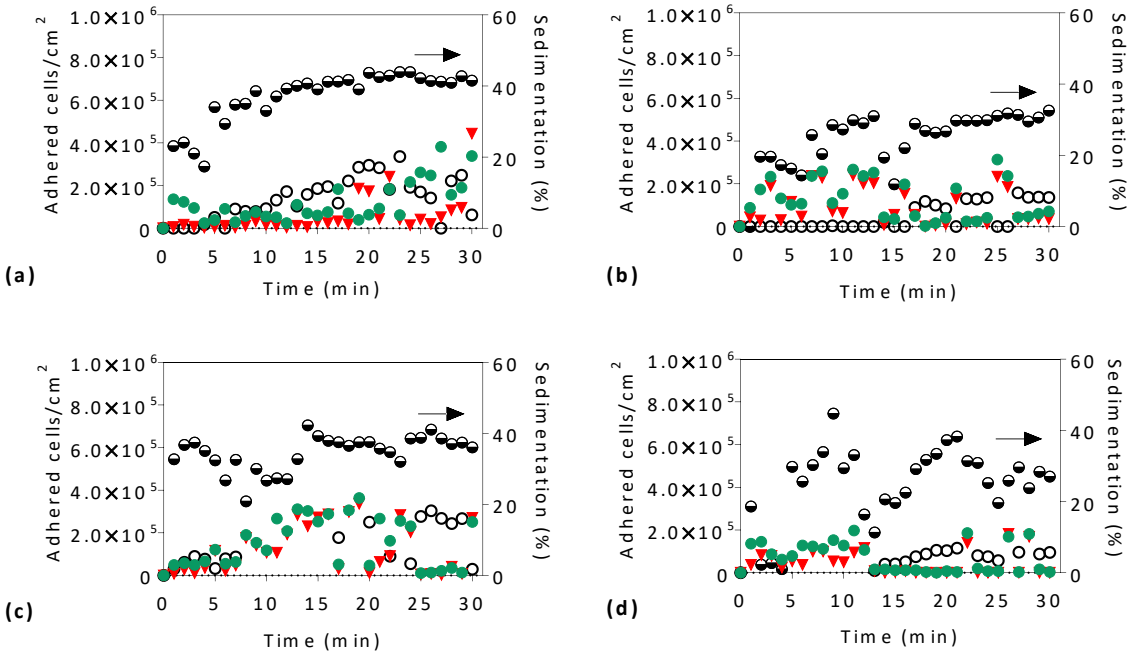

Figure 4.4. Differential balance plots for each time point at different flow rates: **(a)** 1 ml/s; **(b)** 3 ml/s; **(c)** 7 ml/s and **(d)** 9 ml/s, corresponding to the shear stresses of 0.0052, 0.016, 0.042 and 0.064 Pa, respectively. The desorbed cells, n_{des} (▼); the cells that arrived at the surface, n_{new} (●); the cells that arrived at the surface by sedimentation, n_{sed} (○) is depicted in the *x*-axis; and the sedimentation contribution (◒) is depicted by an arrow located on panels (*y*-axis).

The effect of shear stress on the adhesion of cells, bacteria, or colloidal particles to a surface has been thoroughly evaluated through fundamental theories as well as experimental assays [3, 17-19, 32, 35, 36]. However, most of the studies are based on the detachment analysis of the biofilms formed [37-39] or are interested in first fixing the cells to the surface and then applying

higher shear fluid forces, bubbles or surfactants to evaluate the detachment process in order to assess the retention capacity of adhered cells [34, 40-42]. A decrease in the total number of adhesion events as shear increases has often been reported, for example, for functionalized microspheres [33] and for bacteria [32, 43], in agreement with our observations. Although an increased flow rate results in increased mass transport, the decrease of cell sticking efficiency suggests the existence of an energy barrier forming a reversible binding state. Moreover, an increased shear rate leads to shorter binding events and so to higher desorption rates at short times [33]. Longer residence times can result in an increased number of bonds formed between the cell and the surface, or in the strengthening of these links. In the case of *E. coli*, shear-enhanced adhesion can be a consequence of specific catch-bonds formed between FimH, a protein present on *E. coli* type I pili, and mannose adsorbed on the substrate. The adhesion enhancement is triggered by a conformational change of FimH under fluid flow [44]. Another particularity is related to the surfaces; although initially bare, they can be quickly conditioned by the macromolecules present in the flowing medium, which could then act as specific binders [25, 45, 46]. In this study, citrate buffer (commonly used in adhesion assays) [20, 47], was chosen due to its minimal surface conditioning capacity in order to have only bacteria adhering to the surface and not a possible contaminant of a complex media.

4.4. Conclusions

An automated image-analysis method was developed in this study to quantify the contribution of sedimentation and desorption in flow displacement systems such as the PPFC. Sedimentation, rather than desorption, showed to be the major effector for cell adhesion in the PPFC system. The analysis of mass transport proposed here may be applicable to other bacterial strains. Moreover, it is a simple and reliable technique that does not require additional equipment to deepen the knowledge in such a complex process as bacterial adhesion under flow conditions.

4.5. References

1. Persat, A.; Nadell, C. D.; Kim, M. K.; Ingremeau, F.; Siryaporn, A.; Drescher, K.; Wingreen, N. S.; Bassler, B. L.; Gitai, Z.; Stone, H. A., The mechanical world of bacteria. *Cell* **2015,** *161* (5), 988-997.

2. Marmur, A.; Ruckenstein, E., Gravity and cell adhesion. *Journal of Colloid and Interface Science* **1986,** *114* (1), 261-266.

3. Li, J.; Busscher, H. J.; Norde, W.; Sjollema, J., Analysis of the contribution of sedimentation to bacterial mass transport in a parallel plate flow chamber. *Colloids and Surfaces B: Biointerfaces* **2011,** *84* (1), 76-81.

4. Vu, K.; Yang, G.; Wang, B.; Tawfiq, K.; Chen, G., Bacterial interactions and transport in geological formation of alumino-silica clays. *Colloids and Surfaces B: Biointerfaces* **2015,** *125*, 45-50.

5. Tran, V. B.; Fleiszig, S. M.; Evans, D. J.; Radke, C. J., Dynamics of flagellum-and pilus-mediated association of *Pseudomonas aeruginosa* with contact lens surfaces. *Applied and Environmental Microbiology* **2011,** *77* (11), 3644-3652.

6. Busscher, H. J.; van der Mei, H. C., Microbial adhesion in flow displacement systems. *Clinical Microbiology Reviews* **2006,** *19* (1), 127-141.

7. Azeredo, J.; Azevedo, N. F.; Briandet, R.; Cerca, N.; Coenye, T.; Costa, A. R.; Desvaux, M.; Di Bonaventura, G.; Hébraud, M.; Jaglic, Z., Critical review on biofilm methods. *Critical reviews in microbiology* **2017,** *43* (3), 313-351.

8. Ramstedt, M.; Ribeiro, I. A. C.; Bujdakova, H.; Mergulhão, F. J. M.; Jordao, L.; Thomsen, P.; Alm, M.; Burmølle, M.; Vladkova, T.; Can, F.; Reches, M.; Riool, M.; Barros, A.; Reis, R. L.; Meaurio, E.; Kikhney, J.; Moter, A.; Zaat, S. A. J.; Sjollema, J., Evaluating efficacy of antimicrobial and antifouling materials for urinary tract medical devices: challenges and recommendations. *Macromolecular Bioscience* **2019,** *19* (5), e1800384.

9. Alves, P.; Gomes, L. C.; Vorobii, M.; Rodriguez-Emmenegger, C.; Mergulhão, F. J., The potential advantages of using a poly(HPMA) brush in urinary catheters: effects on biofilm cells and architecture. *Colloids and Surfaces B: Biointerfaces* **2020,** *191*, 110976.

10. Alves, P.; Gomes, L. C.; Rodríguez-Emmenegger, C.; Mergulhão, F. J., Efficacy of a poly(MeOEGMA) brush on the prevention of *Escherichia coli* biofilm formation and susceptibility. *Antibiotics (Basel)* **2020,** *9* (5).

11. Rosenberg, E.; Mitchell, R., Microbial surfactants. *Critical Reviews in Biotechnology* **1985,** *3* (2), 109-132.

12. Meinders, J. M.; van der Mei, H. C.; Busscher, H. J., Deposition efficiency and reversibility of bacterial adhesion under flow. *Journal of Colloid and Interface Science* **1995,** *176* (2), 329-341.

13. Petrova, O. E.; Sauer, K., Escaping the biofilm in more than one way: desorption, detachment or dispersion. *Current opinion in microbiology* **2016,** *30*, 67-78.

14. Dąbroś, T.; Van de Ven, T., Kinetics of coating by colloidal particles. *Journal of Colloid Interface Science* **1982,** *89* (1), 232-244.

15. Meinders, J. M.; Noordmans, J.; Busscher, H. J., Simultaneous monitoring of the adsorption and desorption of colloidal particles during deposition in a parallel plate flow chamber. *Journal of Colloid and Interface Science* **1992,** *152* (1), 265-280.

16. Chari, K.; Rajagopalan, R., Transport of colloidal particles over energy barriers. *Journal of Colloid and Interface Science* **1985,** *107* (1), 278-282.

17. Adamczyk, Z.; Dabros, T.; Czarnecki, J.; Van De Ven, T. G., Particle transfer to solid surfaces. *Advances in Colloid Interface Science* **1983,** *19* (3), 183-252.

18. Sjollema, J.; Busscher, H. J.; Weerkamp, A. H., Real-time enumeration of adhering microorganisms in a parallel plate flow cell using automated image analysis. *Journal of Microbiological Methods* **1989,** *9* (2), 73-78.

19. Bakker, D. P.; Busscher, H. J.; van der Mei, H. C., Bacterial deposition in a parallel plate and a stagnation point flow chamber: microbial adhesion mechanisms depend on the mass transport conditions. *Microbiology* **2002,** *148* (2), 597-603.

20. Moreira, J.; Araújo, J.; Miranda, J. M.; Simões, M.; Melo, L.; Mergulhão, F., The effects of surface properties on *Escherichia coli* adhesion are modulated by shear stress. *Colloids and Surfaces B: Biointerfaces* **2014,** *123*, 1-7.

21. Bos, R.; van der Mei, H. C.; Gold, J.; Busscher, H. J., Retention of bacteria on a substratum surface with micro-patterned hydrophobicity. *FEMS Microbiol Lett* **2000,** *189* (2), 311-5.

22. Mayton, H. M.; White, D.; Marcus, I. M.; Walker, S. L., Influence of nano-CuO and -TiO2 on deposition and detachment of Escherichia coli in two model systems. *Environmental Science: Nano* **2019,** *6* (11), 3268-3279.

23. Moreira, J.; Ponmozhi, J.; Campos, J.; Miranda, J. M.; Mergulhão, F., Micro-and macro-flow systems to study *Escherichia coli* adhesion to biomedical materials. *Chemical Engineering Science* **2015,** *126*, 440-445.

24. Moreira, J. M. R.; Simões, M.; Melo, L. F.; Mergulhão, F. J., *Escherichia coli* adhesion to surfaces–a thermodynamic assessment. *Colloid and Polymer Science* **2015,** *293* (1), 177-185.

25. Moreira, J. M. R.; Gomes, L. C.; Whitehead, K. A.; Lynch, S.; Tetlow, L. A.; Mergulhão, F. J., Effect of surface conditioning with cellular extracts on *Escherichia coli* adhesion and initial biofilm formation. *Food and Bioproducts Processing* **2017,** *104*, 1-12.

26. Vagos, M. R.; Moreira, J. M. R.; Soares, O. S. G. P.; Pereira, M. F. R.; Mergulhão, F. J., Incorporation of carbon nanotubes in polydimethylsiloxane to control *Escherichia coli* adhesion. *Polymer Composites* **2019,** *40* (S2), E1697-E1704.

27. Siddiqui, S.; Chandrasekaran, A.; Lin, N.; Tufenkji, N.; Moraes, C., Microfluidic shear assays to distinguish between bacterial adhesion and attachment strength on stiffness-tunable silicone substrates. *Langmuir* **2019**.

28. Alves, P.; Nir, S.; Reches, M.; Mergulhão, F., The effects of fluid composition and shear conditions on bacterial adhesion to an antifouling peptide-coated surface. *MRS Communications* **2018,** *8* (3), 938-946.

29. Schneider, C. A.; Rasband, W. S.; Eliceiri, K. W., NIH Image to ImageJ: 25 years of image analysis. *Nature methods* **2012,** *9* (7), 671.

30. Meinders, J. M.; Van der Mei, H. C.; Busscher, H. J., In situ enumeration of bacterial adhesion in a parallel plate flow chamber - elimination or in focus flowing bacteria from the analysis. *Journal of Microbiological Methods* **1992,** *16* (2), 119-124.

31. Lecuyer, S.; Rusconi, R.; Shen, Y.; Forsyth, A.; Vlamakis, H.; Kolter, R.; Stone, H. A., Shear stress increases the residence time of adhesion of *Pseudomonas aeruginosa*. *Biophysical Journal* **2011,** *100* (2), 341-350.

32. Dickinson, R. B.; Cooper, S. L., Analysis of shear-dependent bacterial adhesion kinetics to biomaterial surfaces. *AIChE Journal* **1995,** *41* (9), 2160-2174.

33. Pierres, A.; Touchard, D.; Benoliel, A.-M.; Bongrand, P., Dissecting streptavidin-biotin interaction with a laminar flow chamber. *Biophysical journal* **2002,** *82* (6), 3214-3223.

34. Simões, M.; Simões, L. C.; Cleto, S.; Pereira, M. O.; Vieira, M. J., The effects of a biocide and a surfactant on the detachment of *Pseudomonas fluorescens* from glass surfaces. *International Journal of Food Microbiology* **2008,** *121* (3), 335-341.

35. Meinders, J.; Busscher, H., Adsorption and desorption of colloidal particles on glass in a parallel plate flow chamber - influence of ionic strength and shear rate. *Colloid and Polymer Science* **1994,** *272* (4), 478-486.

36. Sjollema, J.; Busscher, H. J.; Weerkamp, A. H., Experimental approaches for studying adhesion of microorganisms to solid substrata: applications and mass transport. *Journal of Microbiological Methods* **1989,** *9* (2), 79-90.

37. Fux, C.; Wilson, S.; Stoodley, P., Detachment characteristics and oxacillin resistance of *Staphyloccocus aureus* biofilm emboli in an in vitro catheter infection model. *Journal of Bacteriology* **2004,** *186* (14), 4486-4491.

38. van Loosdrecht, M. C.; Heijnen, J. J.; Eberl, H.; Kreft, J.; Picioreanu, C., Mathematical modelling of biofilm structures. *Antonie Van Leeuwenhoek* **2002,** *81* (1-4), 245-56.

39. Xavier Jde, B.; Picioreanu, C.; van Loosdrecht, M. C., A general description of detachment for multidimensional modelling of biofilms. *Biotechnology and Bioengineering* **2005,** *91* (6), 651-69.

40. Azeredo, J.; Pacheco, A. P.; Lopes, I.; Oliveira, R.; Vieira, M. J., Monitoring cell detachment by surfactants in a parallel plate flow chamber. *Water Science and Technology* **2003,** *47* (5), 77-82.

41. Adamczyk, Z., Modeling adsorption of colloids and proteins. *Current Opinion in Colloid & Interface Science* **2012,** *17* (3), 173-186.

42. Roosjen, A.; Boks, N. P.; van der Mei, H. C.; Busscher, H. J.; Norde, W., Influence of shear on microbial adhesion to PEO-brushes and glass by convective-diffusion and sedimentation in a parallel plate flow chamber. *Colloids and Surfaces B: Biointerfaces* **2005,** *46* (1), 1-6.

43. McClaine, J. W.; Ford, R. M., Characterizing the adhesion of motile and nonmotile *Escherichia coli* to a glass surface using a parallel-plate flow chamber. *Biotechnology and Bioengineering* **2002,** *78* (2), 179-189.

44. Forero, M.; Yakovenko, O.; Sokurenko, E. V.; Thomas, W. E.; Vogel, V., Uncoiling mechanics of *Escherichia coli* type I fimbriae are optimized for catch bonds. *PLoS biology* **2006,** *4* (9).

45. Bos, R.; van der Mei, H. C.; Busscher, H. J., Physico-chemistry of initial microbial adhesive interactions-its mechanisms and methods for study. *FEMS Microbiology Reviews* **1999,** *23* (2), 179-230.

46. Lorite, G. S.; Rodrigues, C. M.; de Souza, A. A.; Kranz, C.; Mizaikoff, B.; Cotta, M. A., The role of conditioning film formation and surface chemical changes on *Xylella fastidiosa* adhesion and biofilm evolution. *Journal of Colloid and Interface Science* **2011,** *359* (1), 289-95.

47. Lopez-Mila, B.; Alves, P.; Riedel, T.; Dittrich, B.; Mergulhão, F.; Rodriguez-Emmenegger, C., Effect of shear stress on the reduction of bacterial adhesion to antifouling polymers. *Bioinspiration & Biomimetics* **2018,** *13* (6), 065001.

4.6. Supplementary material

***CODE* 1** (quantification of the bacterial adhesion during 30 min of bacterial adhesion)*:*

```
rename("Original");
run("32-bit");
run("Subtract Background...", "rolling=20 light stack");
run("Set Scale...", "distance=1000 known=110 unit=um");
setAutoThreshold("Default");
setOption("BlackBackground", false);
run("Convert to Mask", "method=Default background=Light calculate");
run("Analyze Particles...", "size=1-Infinity show=Outlines display exclude clear summarize stack");
```

CODE 2 (quantification of desorbed cells during 30 min of bacterial adhesion):

```
rename("cells");
run("Fill Holes", "stack");
run("32-bit");
run("Duplicate...", "title=cells-TMIN1 duplicate range=2-61");
selectWindow("cells");
run("Duplicate...", "duplicate range=1-60");
imageCalculator("Subtract create stack", "cells-TMIN1","cells-1");
selectWindow("Result of cells-TMIN1");
run("Divide...", "value=2 stack");
run("Add...", "value=127.5 stack");
run("Color Balance...");
```

5. The effects of fluid composition and shear conditions on bacterial adhesion to an antifouling peptide-coated surface [f]

Abstract

Biofilms can damage implants and are difficult to treat. Here, we assessed the performance of a tripeptide that self-assembles into an antifouling coating over a broad range of shear conditions that are relevant to biomedical applications. Adhesion assays were performed using a parallel plate flow chamber. The results show that the coating can reduce *E. coli* adhesion up to 70% when compared with glass. At a shear rate of 15/s, typical for urinary catheters, the coating reduced the adhesion by more than 50%. These findings suggest critical features that should be considered when developing surfaces for biomedical purposes.

The content of this chapter is being prepared for publication:

[f] **Alves P**, Gomes LG, Miranda JM, Mergulhão FJ (**2020**) The effects of sedimentation and desorption on initial bacterial adhesion studies. *MRS Communications*, 1-9. Doi: 10.1557/mrc.2018.160

5.1. Introduction

In medical devices, biofouling is an undesirable process of bacterial colonization that occurs spontaneously, in temporary (e.g., contact lenses, endotracheal tubes as well as urinary and central venous catheters) and in permanently implanted devices (e.g., cardiac valves, vascular grafts and joint replacements), leading to biomaterial-associated infections (BAIs) [1]. Biofilms grown on biomaterials are responsible for 75% of human bacterial infections [2], and urinary tract infections (UTIs) are one of the most common bacterial infections, affecting around 150 million people each year worldwide [3]. *Escherichia coli* is the predominant uropathogen responsible for about 80% of all hospital-acquired infections and can adhere to biomedical surfaces and consequently, develop biofilms [4-6]. Delaying the biofilm onset may reduce the need for antimicrobial treatment and the costs associated with replacing the infected materials.

Antifouling surfaces have been extensively developed by altering the physical and/or chemical surface properties, mimicking natural antifouling surfaces and enhancing the surface resistance to biological contamination.[7] Great efforts in surface engineering have been made in order to prevent or mitigate bacterial adhesion and biofilm development using nanoparticles, polymer brushes, hydrogels and antifouling self-assembly monolayers [8-15]. Maity et al. [14] reported the self-assembly of a tripeptide into a functional coating that interferes with the first step of biofouling. The peptide design includes the amino acid, 3,4-dihydroxy-L-phenylalanine (DOPA), the main constituent of mussel adhesive proteins (MAPs), which promotes adhesion to any substrate. Diphenylalanine is the element that directs the self-assembly and modification of the benzene rings of phenylalanine with fluorine atoms provides the antifouling function. This peptide configuration displayed a reduction of up to 90% of the attached bacteria (*Pseudomonas aeruginosa* and *E. coli*) under static conditions [14]. Nevertheless, previous reports demonstrated that bacterial adhesion may not only be affected by the surface properties, but also by the shear forces existing in the system [12, 16, 17]. In the biomedical field, the fluid behavior is dependent on specific physiological conditions and can affect cell attachment, biofilm development, morphology and antimicrobial susceptibility [18-22]. One important parameter that describes the shear effects is the shear rate which is the derivative of the velocity in the perpendicular direction from the surface and it is also an indicator of the frequency at which cells contact the surface. Table 2.6 (Chapter 2 – section 2.3.2) lists several biomedical scenarios where the shear rate is within the range tested here (7 to 80/s). Experiments were performed using a parallel plate flow cell (PPFC), which is a widely used platform for studying biofilms under controlled hydrodynamic conditions [15, 23, 24].

The main goal of this study was to assess the antifouling performance of a peptide coating under a broad range of hydrodynamic conditions that can be found in many biomedical applications. The surface coating was characterized by various techniques and the effect of the surrounding medium composition was evaluated. This work follows a previous report in which this antifouling surface was tested under static conditions [14].

A scheme showing the interaction of *E. coli* with the surface can be seen in figure 5.1.

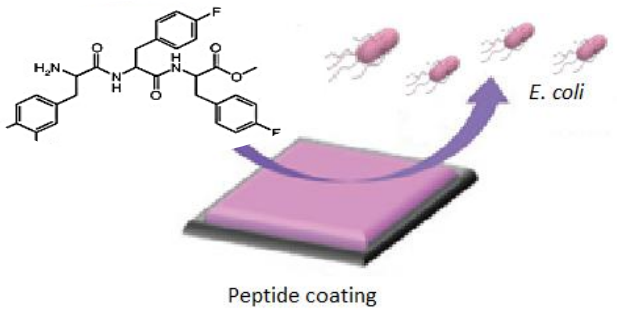

Figure 5.1. Scheme representing adhesion of *Escherichia coli* on a self-assembled tripeptide with antifouling properties were the chemical structure is represented.

5.2. Materials and methods

5.2.1. Preparation and characterization of surfaces

Sodium dodecyl sulfate (SDS) was obtained from MerckTM (Israel). Ethanol and methanol were obtained from Bio-lab (Israel). Glass microscope slides (W x D x H; 76 x 26 x 1 mm, VWR) were dipped in 2% SDS (w/w) for 30 min. Then, they were rinsed with triple-distilled water (TDW), transferred to methanol for an additional 30 min, dipped in ethanol for 30 min and dried under nitrogen. The clean slides were then placed in a ventilated hood and coated with peptide solution (0.5 mg/ml in ethanol) using a dual action spray airbrush (DuraPowers, CA, USA). Briefly, the peptide design (Figure 5.1) includes the amino acid DOPA (3, 4-dihydroxy-L-phenylalanine) as the adsorption motif (that the insertion of the amino acid DOPA into the peptide sequence acts as a glue and immobilizes the peptide on different substrates), the diphenylalanine as the element that directs the self-assembly process and fluorine atoms as the antifouling agents [7, 14]. Each slide was sprayed with the peptide solution for three times.

5.2.2. Attenuated total reflection (ATR) spectra were recorded using Fourier-transform infrared (FITR) spectroscopy analysis

Attenuated total reflection (ATR) spectra were recorded using Fourier-transform infrared spectroscopy (FITR) (Nicolet 6700 model, Thermo Scientific, MA, USA) with a Ge-ATR arrangement (VariGATR™, Harrick Scientific, NY, USA). For all the surfaces, spectra were collected with an applied force of 350 N at 4 cm^{-1} resolution with 3000 scans averaged signal and an incident angle of 65°. The absorbance maximal values were determined using the OMNIC™ analysis program (Thermo Scientific, MA, USA). Peak signals were enhanced by computing the second derivative of the spectrum.

5.2.3. Quartz crystal microbalance with dissipation monitoring (QCM-D) analysis

QCM-D (Q-sense, Biolin Scientific, Sweden) was used for studying peptide adhesion onto an SiO_2 surface. Measurements were performed in a flow module Explorer system. SiO_2 sensors with a fundamental resonant frequency of 5MHz were also purchased. Prior to each experiment, SiO_2 sensors were cleaned with Oxygen/Plasma (Atto, Diener Electronic, Germany), followed by rinsing with 2% SDS and TDW and finally dried under nitrogen. All QCM-D experiments were performed under flow-through conditions using a digital peristaltic pump (IsmaTec Cole-Parmer, Germany). The studied solutions were injected into the sensor crystal chamber at 0.1 ml/min. The peptide was dissolved in ethanol to a concentration of 0.5 mg/ml. All data was analysed using QTools software. Frequency data was fitted to the Sauerbrey equation and the adsorbed mass and layer thickness were calculated according to the linear relation [25]:

$$\Delta m = -\frac{C \cdot \Delta f}{n}, \tag{5.1}$$

where Δm is the adsorbed mass, Δf is the frequency change during adsorption, C is the sensitivity constant characteristic of the quartz crystal (17.7 $ng/cm^2 \cdot Hz$) and n is the overtone number. The reported values were averaged for overtones 5 and 7.

5.2.4. Ellipsometry

The thickness of the peptide-based coating was measured using the α-SE spectroscopic ellipsometer (J.A. Woollam, NE, USA). Measurements were carried out at wavelengths ranging from 380 to 900 nm at a 70° angle of incidence. The optical properties of the substrate were fitted using SiO_2. The thickness of the layers and refractive indices were fitted according to the Cauchy model [26] and an angle offset was permitted. Then, the parameters were allowed to be fitted to determine values

that are more accurate.

5.2.5. Atomic force microscopy (AFM) analysis

AFM images were taken in AC mode with a Si_3N_2 tip with a spring constant of 3 N/m (NanoWizard 3, JPK Instruments, Germany) and processed using JPK data processing software (JPK Instruments, Germany). Arithmetic roughness (*Ra*) and peak-valley values were calculated from a cross-section.

5.2.6. Bacterial culture

E. coli JM109(DE3) from Promega (Madison, WI, USA) was used in this study due to its ability to adhere to different surfaces in a diversity of platforms operated under different shear conditions [18, 27, 28]. Its genotype is [*end*A1, *rec*A1, *gyr*A96, *thi*, *hsd*R17 (r_k^- , m_k^+), *rel*A1, *sup*E44, λ^- Δ(lac-*pro*AB), [F′, *tra*D36, *pro*AB, *lac*I^q ZΔM15], λ(DE3)] [29] and this strain has shown a similar adhesion behavior when compared to a clinical isolate, *E. coli* CECT 434 [19]. Motility studies show that *E. coli* JM109(DE3) and CECT 434 have similar swarming and twitching motilities although the later has a higher swimming motility (Figure S5.1, supplementary material-section 5.6.1). indicating that flagella are active [30] in both strains.

An overnight culture was prepared as described in Chapter 3, section 3.2.1. Cells were harvested by centrifugation (for 10 min at 3200 *g*), and washed twice either in 0.05 mol/L of citrate buffer (CB; Sharlau, Spain), pH 5.0 [27] or in enriched nutrient medium (EM), pH 7.0. EM is a 1:100 dilution of the inoculation medium (described in Chapter 3, section 3.2.1) where the phosphate buffer concentration is maintained [31, 32]. EM was chosen since it was reported that higher nutrient levels can favour cell adhesion [19, 33]; however, the inoculation medium was still diluted to decrease cell division and to enable us to work with cells that would be in a more uniform physiological state. The pellet was resuspended in the corresponding medium and the cellular suspensions were adjusted to a final concentration of 7.6 x 10^7 cells/ml, assessed by optical density at 610 nm (OD = 0.1).

5.2.7. Surface hydrophobicity and free energy of adhesion

The hydrophobicity of the bare glass and peptide-coated glass was evaluated using the Lifshitz-van der Waals acid base approach [34, 35]. The contact angles were determined by the sessile drop method using a contact angle meter (OCA 15 Plus; Dataphysics, Filderstadt, Germany) and three pure liquids: water and formamide (polar solvents) and α-bromonaphthalene (nonpolar solvent) (Sigma-Aldrich Co., Portugal) [36]. The surface tension components were taken from the

literature [36]. Measurements of at least 10 drops on each surface with each reference liquid were performed at room temperature. The surface energy components of a solid surface (*s*) were obtained by measuring the contact angles (θ) with three reference liquids (*l*) with known surface tension components, followed by solving three equations of the type [34]:

$$(1 + cos\theta)\gamma_l^{Tot} = 2\left(\sqrt{\gamma_s^{LW}\,\gamma_l^{LW}} + \sqrt{\gamma_s^{+}\,\gamma_l^{-}} + \sqrt{\gamma_s^{-}\,\gamma_l^{+}}\right), \tag{5.2}$$

From the model proposed by van Oss,[37] the total surface energy (γ_l^{Tot}) of a pure substance is expressed as:

$$\gamma_l^{Tot} = \gamma^{LW} + \gamma^{AB}, \tag{5.3}$$

where γ^{LW} and γ^{AB} are the Lifshitz-van der Waals components of the surface free energy and Lewis acid-base components, respectively.

The polar AB component comprises the electron acceptor (γ^{+}) and electron donor (γ^{-}) parameters, given as:

$$\gamma^{AB} = 2\sqrt{\gamma^{+}\,\gamma^{-}}\,, \tag{5.4}$$

The degree of hydrophobicity of a given material is expressed as the free energy of interaction ΔG^{TOT} between two entities of the surface immersed in a polar liquid as water (*w*). In this approach, the ΔG value can be calculated through the surface tension components of the interacting entities according to:

$$\Delta G^{TOT} = -2\left(\sqrt{\gamma_s^{LW}} - \sqrt{\gamma_w^{LW}}\right)^2 + 4\left(\sqrt{\gamma_s^{+}\,\gamma_w^{-}} + \sqrt{\gamma_s^{-}\,\gamma_w^{+}} - \sqrt{\gamma_s^{+}\,\gamma_s^{-}} - \sqrt{\gamma_w^{+}\,\gamma_w^{-}}\right), \tag{5.5}$$

If ΔG < 0 mJ/m², the material is considered hydrophobic because the interaction between the two entities is stronger than the interaction of each entity with water. Conversely, if ΔG > 0 mJ/m², the material is hydrophilic.

When studying the interaction (free energy of adhesion) between surface *(s)* and bacteria *(b)* that are immersed in water, the total interaction energy, (ΔG^{Adh}), can be expressed as:

$$\Delta G^{Adh} = \gamma_{sb}^{LW} - \gamma_{sw}^{LW} - \gamma_{bw}^{LW} + 2\left[\sqrt{\gamma_w^{+}}\left(\sqrt{\gamma_s^{-}} + \sqrt{\gamma_b^{-}} - \sqrt{\gamma_w^{-}}\right) + \sqrt{\gamma_w^{-}}\left(\sqrt{\gamma_s^{+}} + \sqrt{\gamma_b^{+}} - \sqrt{\gamma_w^{+}}\right) - \sqrt{\gamma_s^{+}\,\gamma_b^{-}} - \sqrt{\gamma_s^{-}\,\gamma_b^{+}}\right] \tag{5.6}$$

Thermodynamically, if ΔG^{Adh} < 0 mJ/m², adhesion is favoured, whereas adhesion is not expected to occur if ΔG^{Adh} > 0 mJ/m². The contact angle measurements and the subsequent hydrophobicity and thermodynamic analysis was performed on the pristine surfaces (Table 5.1) and also after 30 min

incubation of the surfaces in CB or EM (Table S5.1, supplementary material).

5.2.8. Parallel plate flow chamber assays

A PPFC was used to monitor *E. coli* adhesion as described in Chapter 3 (section 3.2.3) to both bare glass and peptide-coated glass. All the surfaces were sterilized by spraying with absolute ethanol for 5 min prior to use. The bacterial suspension was recirculated for 30 min at different flow rates: 1 ml/s, 2 ml/s, 4 ml/s, 6 ml/s and 8 ml/s) that correspond to shear rate values of 7/s, 15/s, 30/s, 50/s and 80/s [23]. Cell attachment was monitored by brightfield microscopy as described in Chapter 3 (section 3.2.3), and three trials were performed for each flow rate and surface.

The microscopic images were analysed by ImageJ (version 1.38e) software [38] to determine the number of adherent cells per square centimetre as a function of time for each shear rate tested (Chapter 3, supplementary material-section 3.6.4,). Initial adhesion rates (IAR) were obtained from linear regression of the data presented in figure 5.3.

5.2.9. Statistical analysis

The data presented in figures 5.3 and 5.4 represents an average of three independent results for each tested condition. To verify the statistical significance, the data was analysed using GraphPad Prism® 6.01 (La Jolla, CA, USA). Paired t-test analysis was performed based on confidence levels of 95% (differences are reported as significant for P values < 0.05 and are denoted by **) and 90% (differences are reported as significant for P values < 0.1 and are denoted by *).

5.3. Results and discussion

5.3.1. Characterization of the peptide-based coating

Glass was coated since it has a flat transparent inexpensive surface that has been previously used with this flow system [12, 23].

The formulation evaluated here consists of a low-molecular-weight peptide that interferes with the first step of biofouling [14]. Unlike in the previous work where the peptide self-assembled on the surface by dip coating [14], here the peptide coated the surface by spraying and rapid evaporation of the solvent. ATR-FTIR results (Figure 5.2a) showed that despite the different coating process, the peptide preserved its surface orientation, mostly consisting of anti-parallel beta sheets with peaks at 1609 and 1670 cm^{-1}, as previously demonstrated [14].

QCM-D measurement followed the peptide adsorption onto a SiO_2 sensor, which is used as

the model system for glass [39]. Figure 5.2b depicts the QCM-D real-time monitoring of the process. Upon adding the peptide, the frequency decreased instantly to about -40 Hz. Then, it decreased at a more moderate rate, changing again after 5 h. At the end of the run, the sensor was washed with clean ethanol, the non-adsorbed peptide was removed, and the overall frequency change was ~45 Hz. From figure 5.2b, it can be concluded that the adsorption process can be divided into three steps, where the peptide bonding to SiO_2 decreases in each step. This may be related to the formation of the layers in which the first peptide layer formed immediately, resulting in a high frequency change (Figure S5.2-phase 1, supplementary material). Then, owing to the change in the sensor-solvent interface, the adsorption process slowed down and the amount of peptide adsorbed decreased (Figure S5.2-phase 2, supplementary material). Eventually, all binding sites were saturated and the peptide was adsorbed by a different mechanism, probably via non-specific interactions (Figure S5.2-phase 3, supplementary material). However, these interactions are weaker and the peptide was washed away at the end of the run. By fitting the frequency change to the Sauerbrey equation (Equation 5.1), it was possible to calculate the adsorbed mass. The loaded mass per surface area was found to be 901 ± 166 ng/cm^2 and the layer thickness was 9 ± 1 nm (Figure S5.3, supplementary material). This thickness value is similar to the one determined by ellipsometry (10.7 ± 0.5 nm).

AFM was used to characterize the nano- and micro-scale topographical structures of the bare glass and peptide-coated glass (Figure 5.2c). The images revealed that after deposition of the peptide onto the glass slide, the surface seems smoother and more homogeneous. Additionally, the average roughness (*Ra*) decreased from 490 ± 40 pm for the bare glass to 232 ± 1 pm for the peptide-coated glass.

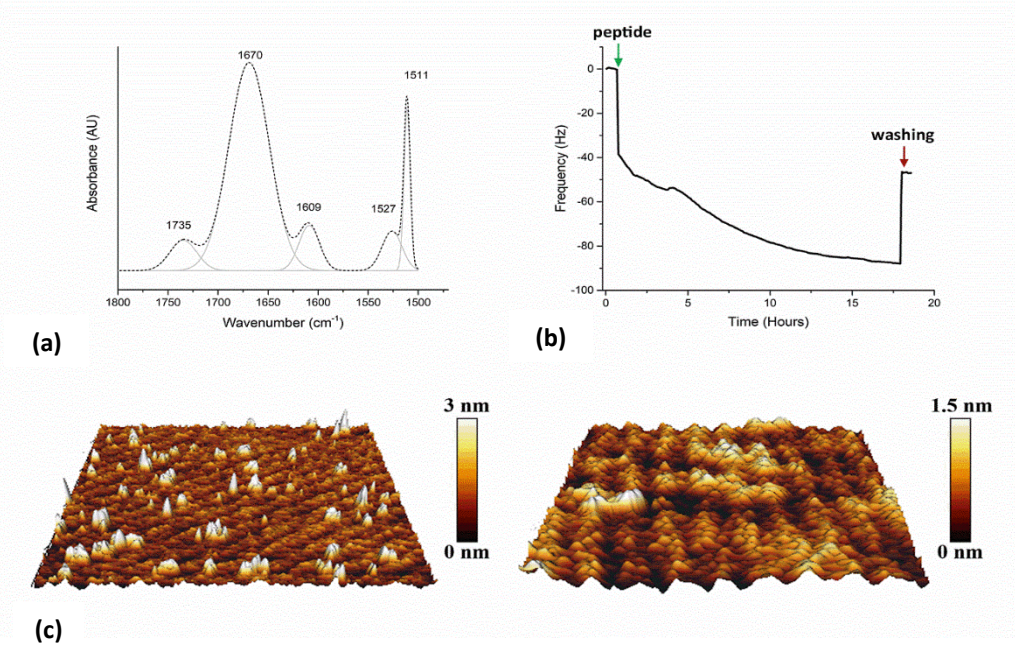

Figure 5.2. Characterization of the peptide-coated surface. **(a)** Attenuated total reflection-Fourier-transform infrared spectroscopy (ATR-FTIR) spectrum of the amide region: original measurement (the dashed line) and the second derivative fit (the grey line). **(b)** Real-time Quartz Crystal Microbalance with Dissipation (QCM-D) measurement. A fifth overtone is presented. **(c)** The surface topography of bare glass (on the left) and peptide-coated glass (on the right) (2 μm x 2 μm scan).

A thermodynamic analysis of the pristine surfaces and *E. coli* cells was performed, based on contact angle measurements (Table 5.1). It was observed that the bare glass and *E. coli* cells are hydrophilic ($\Delta G > 0$ mJ/m^2), whereas the peptide coating is hydrophobic ($\Delta G < 0$ mJ/m^2). Regarding the γ^+ and γ^- components, the bare and coated glass are both polar surfaces, being mostly electron donors with a small electron acceptor component. From a thermodynamic point of view, *E. coli* adhesion to both surfaces was not expected to occur ($\Delta G^{Adh} > 0$ mJ/m^2). Nevertheless, just considering the analysis of the pristine surfaces, *E. coli* adhesion to glass is predicted to be thermodynamically less favourable than to peptide because ΔG^{Adh} glass > ΔG^{Adh} peptide.

Table 5.1. Contact angles with water (θ_w), formamide (θ_F) and α-bromonaphthalene (θ_B); surface tension parameters (γ^{LW}, γ^+ and γ^-), hydrophobicity (ΔG) and free energy of adhesion (ΔG^{Adh}) between *Escherichia coli* JM109(DE3) and each surface

	Contact angle (°)			Surface tension parameters (mJ/m²)				Hydrophobicity (mJ/m²)	Free energy of adhesion (mJ/m²)
	Θ_w	θ_F	θ_B	γ^{LW}	γ^+	γ^-	γ^{AB}	ΔG	ΔG^{Adh}
Surface									
Glass	23.1 ± 2.4	29.3 ± 2.3	36.4 ± 3.5	36.1	0.8	54.8	13.1	35.6	73.0
Peptide coating	53.7 ± 1.7	43.6 ± 0.8	43.8 ± 0.7	32.9	1.0	26.6	10.4	-0.5	49.0
Bacteria									
E. coli	19.1 ± 0.9	73.3 ± 0.7	58.5 ± 2.0	25.7	0.0	123.2	0.0	121.9	n/a

Values are means ± SDs of three independent experiments.

5.3.2. Bacterial adhesion assays

The performance of an antifouling peptide-coated glass was evaluated under different hydrodynamic conditions (shear rates between 7 and 80/s) using two different media and *E. coli* as a model organism. The peptide formulation used here was the best configuration for biofilm reduction, as demonstrated in a previous study [14]. In that work, biofilms of *P. aeruginosa* and *E. coli* were formed under static conditions on bare titanium surfaces and titanium surfaces coated with different formulations of peptides. The peptide containing fluorinated phenylalanine enabled a 93% and 74% reduction in the biofilm biomass of *P. aeruginosa* and *E. coli*, respectively, as assayed by crystal violet staining. It is widely known that hydrodynamics affects biofilm formation on medical devices as a result of the fluid flow, which can modulate cell adhesion to a given surface [23, 24, 40]. To evaluate the performance of the same peptide under different hydrodynamic conditions, a PPFC was used.

Figure 5.3 presents the initial adhesion results obtained for each surface (glass and peptide coating) for 30 min on the PPFC, from which the initial adhesion rates (IARs) were calculated (Figure 5.4). The number of adherent bacteria increased with time for both surfaces and culture media (Fig. 5.3). In general, higher bacterial adhesion was obtained for glass (particularly in CB), which is the most hydrophilic surface material (Table 5.1). Previous studies have shown that *E. coli* adhesion is higher on hydrophobic surfaces than on hydrophilic surfaces [41, 42]. However, a correlation between surface hydrophobicity and bacterial adhesion was not found here probably due to other effects (biological and physical), which may be comparatively more important [12, 43].

In order to assess the effect of the assay media on surface hydrophobicity, the contact angles and the subsequent thermodynamic analysis were also performed after 30 min incubation of the

surfaces in CB or EM without the presence of bacterial cells (Table S5.1, supplementary material). It was found that the hydrophobicity of glass increased after incubation in CB and the predicted energy of adhesion decreased. A similar trend was observed for the peptide coating after it was immersed in EM; however, no significant changes were detected in these two parameters when glass was immersed on EM or the peptide incubated with CB. Thus, it seems that the model can predict a higher adhesion in glass after immersion in CB (higher hydrophobicity and lower energy of interaction) when compared with EM, but it fails to predict the observed behavior in the peptide coating. Apparently, the thermodynamic model is thus better suited to handle simple surfaces like glass [12] and fails to predict the results on more complex surfaces, such as the peptide coating where other interactions can be significant [44].

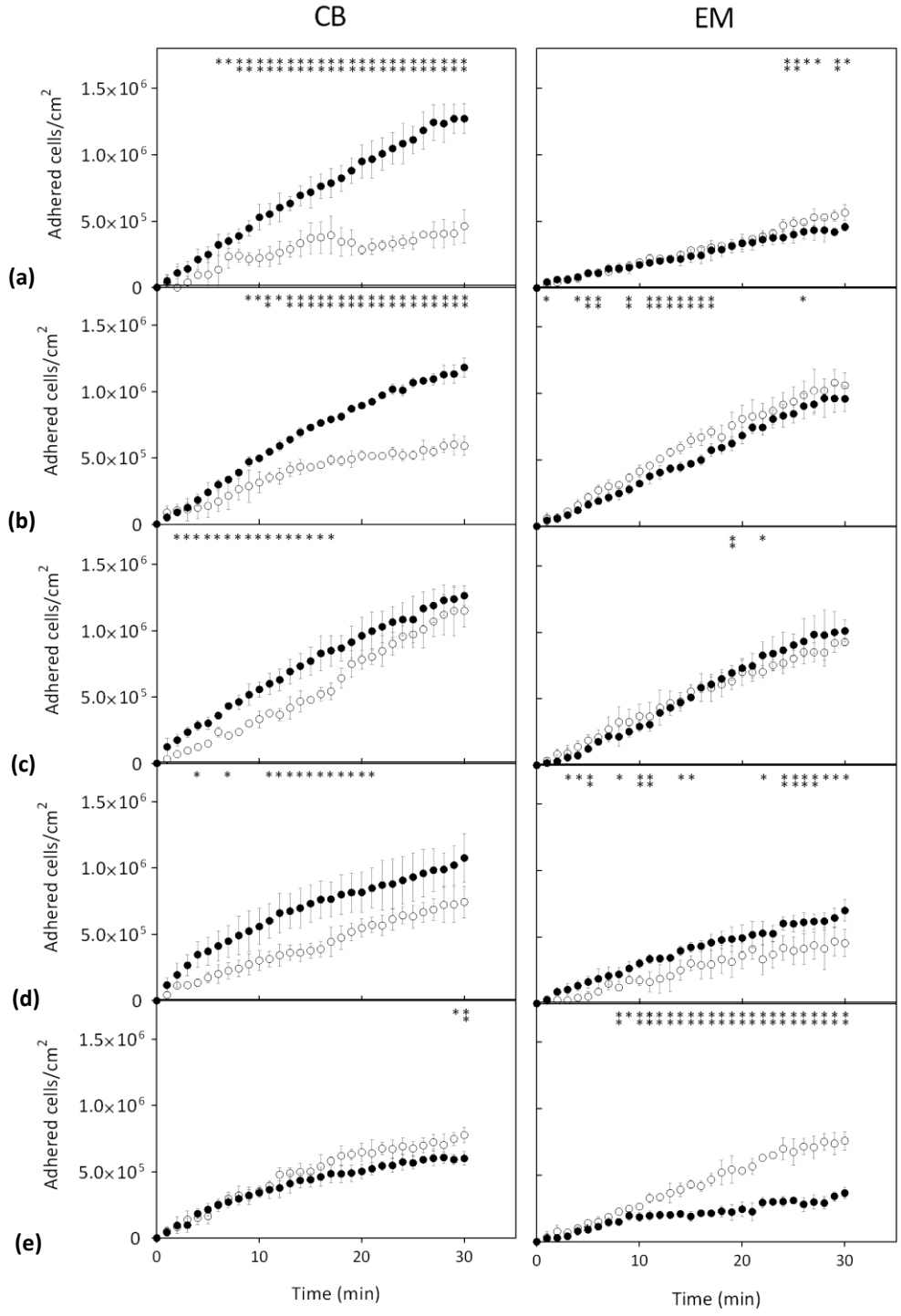

Figure 5.3. Adhesion of *Escherichia coli* JM109(DE3) on bare glass (●) and peptide-coated glass (○) for 30 min under different shear rates: **(a)** 7/s, **(b)** 15/s, **(c)** 30/s, **(d)** 50/s and **(e)** 80/s. Two different culture media were used: citrate buffer (CB) and enriched medium (EM). The means ± SDs for three independent experiments are illustrated. Statistically significant differences obtained between the surfaces are indicated by ** for $P < 0.05$ or * for $P < 0.1$ at the corresponding shear rate values.

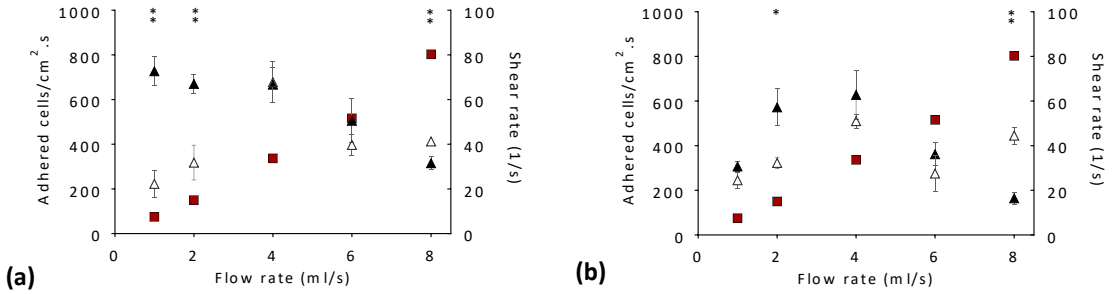

Figure 5.4. Initial adhesion rates for bare glass (▲) and peptide-coated glass (Δ) in function of the flow rate (1, 2, 4, 6 and 8 ml/s) and at each correspondent shear rate (7/s, 15/s, 30/s, 50/s and 80/s) (■). **(a)** Citrate buffer (CB) and **(b)** enriched medium (EM). Statistically significant differences obtained between the surfaces are indicated by ** for $P < 0.05$ or * for $P < 0.1$ at the corresponding shear rate values.

The IARs were higher on glass using CB (particularly at lower shear rates), exhibiting a decreasing trend as the shear rate increased (Figure 5.4a). With peptide-coated glass, the IARs increased until a shear rate of 30/s was reached and then decreased at higher shear rates (Figure 5.4a). Regarding the EM (Figure 5.4b), similar results were observed between glass and the peptide coating and the IAR evolution with increasing shear rates; this was similar to what was obtained for the coated peptide in CB. The best results were attained for the lower shear rates (7.5 and 15/s s) using CB (about 70% and 50% of adhesion reduction, compared with bare glass, $P < 0.05$), showing that the antifouling action of the peptide is enhanced when compared with glass under low nutrient conditions and lower shear rate values. Using EM, a maximum reduction of 40% was attained at a shear rate of 15/s on the peptide-coated surfaces, compared with bare glass (Figure 5.4b). The number of adherent cells represents a balance between the cells that arrive at the surface and can initiate a reversible adhesion process, and those that are desorbed from the surface due to shear forces [23]. A reduction in cell adhesion was only obtained for the glass surface in CB at the highest shear rates tested (Figure 5.4a). This was probably because the higher shear forces contribute to higher cell detachment (or hamper the process of initial reversible adhesion) [23, 45]. The performance of the peptide on CB was the opposite of what was determined for glass at low shear rates (7-30/s). It is likely that the detrimental effects on adhesion caused by the increased shear forces may be counterbalanced by an increased number of contacts with the surface per unit time. The relative importance of these two factors seems to be different for both surfaces under low nutrient conditions. Interestingly, when using EM (Figure 5.4b) both surfaces display the same behavior, with the beneficial effects of higher contact frequency being observed from 7.5 to 30/s and the deleterious effects of the increased shear

forces becoming dominant at higher shear rates. The similar behavior of the two surfaces may be related to the fact that very few materials can effectively resist non-specific protein adsorption from complex media and meet the challenges of medical implants [8, 46].

In order to evaluate the performance of the peptide-based antifouling coating we plotted the IAR obtained in this study with those obtained from a previous study [12]. That study was performed in the same PPFC and with the same strain and surrounding fluid (CB) at a shear rate of 15/s (which can be found in urinary catheters). Importantly, the comparison showed that the peptide coating is superior to other polymers such as polystyrene, poly-L-lactide and cellulose acetate (Figure 5.5), which are commonly used to manufacture different biomedical devices.

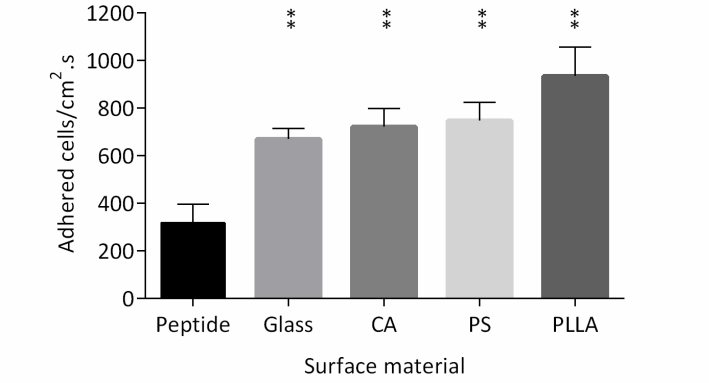

Figure 5.5. *Escherichia coli* JM109(DE3) adhesion rates on peptide, bare glass and on three polymeric surfaces: cellulose acetate (CA), polystyrene (PS) and poly-L-lactic acid (PLLA), obtained in the parallel plate flow cell for 30 min at a shear rate of 15/s using citrate buffer as the surrounding fluid. Results for polymeric surfaces were extracted from Moreira et al. [12]. Statistically significant differences obtained between the surfaces are indicated by ** for $P < 0.05$.

5.4. Conclusions

This study shows the importance of evaluating the antifouling properties of new surfaces under hydrodynamic conditions that are relevant for a particular application. In addition, the importance of the chemical composition of the surrounding fluid was highlighted because it can affect the performance of the surface. This is particularly important for biomedical applications where fluid compositions and flow dynamics can vary significantly. Although the results indicate considerable adhesion reduction under the conditions tested, longer-term studies under controlled hydrodynamic conditions are needed in order to evaluate the effects of surface chemistry and topography on bacterial adhesion and biofilm formation, using a surrounding fluid that is relevant

to a particular biomedical application. The tests performed so far support the beneficial properties of the peptide coating, and this may be considered as an initial screening step in evaluating *in vitro* surface performance for a broad range of biomedical applications.

5.5. References

1. Costerton, J. W.; Stewart, P. S.; Greenberg, E. P., Bacterial biofilms: a common cause of persistent infections. *Science* **1999,** *284* (5418), 1318-1322.

2. Miquel, S.; Lagrafeuille, R.; Souweine, B.; Forestier, C., Anti-biofilm activity as a health issue. *Frontiers in Microbiology* **2016,** *7*, 592.

3. Stamm, W. E.; Norrby, S. R., Urinary tract infections: disease panorama and challenges. *The Journal of Infectious Diseases* **2001,** *183* (Supplement_1), S1-S4.

4. Koseoglu, H.; Aslan, G.; Esen, N.; Sen, B. H.; Coban, H., Ultrastructural stages of biofilm development of *Escherichia coli* on urethral catheters and effects of antibiotics on biofilm formation. *Urology* **2006,** *68* (5), 942-946.

5. Stamm , W. E.; Hooton , T. M., Management of Urinary Tract Infections in Adults. *New England Journal of Medicine* **1993,** *329* (18), 1328-1334.

6. Shunmugaperumal, T., *Biofilm eradication and prevention: a pharmaceutical approach to medical device infections*. John Wiley & Sons: New Jersey, 2010.

7. Nir, S.; Reches, M., Bio-inspired antifouling approaches: the quest towards non-toxic and non-biocidal materials. *Current Opinion in Biotechnology* **2016,** *39*, 48-55.

8. Kirschner, C. M.; Brennan, A. B., Bio-inspired antifouling strategies. *Annual Review of Materials Research* **2012,** *42*, 211-229.

9. Banerjee, I.; Pangule, R. C.; Kane, R. S., Antifouling coatings: recent developments in the design of surfaces that prevent fouling by proteins, bacteria, and marine organisms. *Advanced Materials* **2011,** *23* (6), 690-718.

10. Li, B.; Logan, B. E., Bacterial adhesion to glass and metal-oxide surfaces. *Colloids and Surfaces B: Biointerfaces* **2004,** *36* (2), 81-90.

11. An, Y. H.; Friedman, R. J., Concise review of mechanisms of bacterial adhesion to biomaterial surfaces. *Journal of Biomedical Materials Research Part A* **1998,** *43* (3), 338-348.

12. Moreira, J. M.; Simões, M.; Melo, L. F.; Mergulhão, F. J., *Escherichia coli* adhesion to surfaces–a thermodynamic assessment. *Colloid and Polymer Science* **2015,** *293* (1), 177-185.

13. Nuzzo, R. G., Biomaterials: stable antifouling surfaces. *Nature Materials* **2003,** *2* (4), 207-208.

14. Maity, S.; Nir, S.; Zada, T.; Reches, M., Self-assembly of a tripeptide into a functional coating that resists fouling. *ChemComm* **2014,** *50* (76), 11154-11157.

15. Azeredo, J.; Azevedo, N. F.; Briandet, R.; Cerca, N.; Coenye, T.; Costa, A. R.; Desvaux, M.; Di Bonaventura, G.; Hébraud, M.; Jaglic, Z., Critical review on biofilm methods. *Critical Reviews in Microbiology* **2017,** *43* (3), 313-351.

16. Absolom, D. R.; Lamberti, F. V.; Policova, Z.; Zingg, W.; van Oss, C. J.; Neumann, A. W., Surface thermodynamics of bacterial adhesion. *Applied and Environmental Microbiology* **1983,** *46* (1), 90-97.

17. Liu, C.; Zhao, Q., Influence of surface-energy components of Ni–P–TiO2–PTFE nanocomposite coatings on bacterial adhesion. *Langmuir* **2011,** *27* (15), 9512-9519.

18. Gomes, L. C.; Silva, L. N.; Simoes, M.; Melo, L. F.; Mergulhao, F. J., *Escherichia coli* adhesion, biofilm development and antibiotic susceptibility on biomedical materials. *Journal of Biomedical Materials Research Part A* **2015,** *103* (4), 1414-23.

19. Gomes, L.; Moreira, J.; Teodósio, J.; Araújo, J.; Miranda, J.; Simões, M.; Melo, L.; Mergulhão, F., 96-well microtiter plates for biofouling simulation in biomedical settings. *Biofouling* **2014,** *30* (5), 535-546.

20. Ong, Y.-L.; Razatos, A.; Georgiou, G.; Sharma, M. M., Adhesion Forces between *E. coli* bacteria and biomaterial surfaces. *Langmuir* **1999,** *15* (8), 2719-2725.

21. Gallardo-Moreno, A. M.; Navarro-Pérez, M. L.; Vadillo-Rodríguez, V.; Bruque, J. M.; González-Martín, M. L., Insights into bacterial contact angles: Difficulties in defining hydrophobicity and surface Gibbs energy. *Colloids and Surfaces B: Biointerfaces* **2011,** *88* (1), 373-380.

22. Baier, R.; Meyer, A.; Natiella, J.; Natiella, R.; Carter, J., Surface properties determine bioadhesive outcomes: methods and results. *Journal of Biomedical Materials Research Part A* **1984,** *18* (4), 337-355.

23. Moreira, J.; Araújo, J.; Miranda, J. M.; Simões, M.; Melo, L.; Mergulhão, F., The effects of surface properties on *Escherichia coli* adhesion are modulated by shear stress. *Colloids and Surfaces B: Biointerfaces* **2014,** *123*, 1-7.

24. Busscher, H. J.; van der Mei, H. C., Microbial adhesion in flow displacement systems. *Clinical Microbiology Reviews* **2006,** *19* (1), 127-141.

25. Marx, K. A., Quartz crystal microbalance: a useful tool for studying thin polymer films and complex biomolecular systems at the solution− surface interface. *Biomacromolecules* **2003,** *4* (5), 1099-1120.

26. Tompkins, H. G.; McGahan, W. A., *Spectroscopic ellipsometry and reflectometry: a user's guide*. Wiley: New York, 1999.

27. Moreira, J.; Ponmozhi, J.; Campos, J.; Miranda, J. M.; Mergulhão, F., Micro-and macro-flow systems to study *Escherichia coli* adhesion to biomedical materials. *Chemical Engineering Science* **2015,** *126*, 440-445.

28. Teodósio, J.; Simões, M.; Melo, L.; Mergulhão, F., Flow cell hydrodynamics and their effects on *E. coli* biofilm formation under different nutrient conditions and turbulent flow. *Biofouling* **2011,** *27* (1), 1-11.

29. Teodósio, J.; Simões, M.; Mergulhao, F., The influence of nonconjugative *Escherichia coli* plasmids on biofilm formation and resistance. *Journal of Applied Microbiology* **2012,** *113* (2), 373-382.

30. Neidhardt, F. C., Motility and Chemotaxis. In *Escherichia coli and Salmonella typhimurium: cellular and molecular biology*, ASM Press: Washington, D.C., 1987; Vol. 1, pp 732-759.

31. Moreira, J.; Fulgêncio, R.; Alves, P.; Machado, I.; Bialuch, I.; Melo, L.; Simões, M.; Mergulhão, F., Evaluation of SICAN performance for biofouling mitigation in the food industry. *Food Control* **2016,** *62*, 201-207.

32. Moreira, J.; Gomes, L.; Simões, M.; Melo, L.; Mergulhão, F., The impact of material properties, nutrient load and shear stress on biofouling in food industries. *Food and Bioproducts Processing* **2015,** *95*, 228-236.

33. Frias, J.; Ribas, F.; Lucena, F., Effects of different nutrients on bacterial growth in a pilot distribution system. *Antonie Van Leeuwenhoek* **2001,** *80* (2), 129-138.

34. Van Oss, C., Hydrophobicity of biosurfaces-origin, quantitative determination and interaction energies. *Colloids and Surfaces B: Biointerfaces* **1995,** *5* (3-4), 91-110.

35. Van Oss, C. J.; Good, R. J.; Chaudhury, M. K., Additive and nonadditive surface tension components and the interpretation of contact angles. *Langmuir* **1988,** *4* (4), 884-891.

36. Janczuk, B.; Chibowski, E.; Bruque, J.; Kerkeb, M.; Caballero, F. G., On the consistency of surface free energy components as calculated from contact angles of different liquids: an application to the cholesterol surface. *Journal of Colloid and Interface Science* **1993,** *159* (2), 421-428.

37. Van Oss, C. J., *Interfacial forces in aqueous media*. CRC press: New York, 2006.

38. Schneider, C. A.; Rasband, W. S.; Eliceiri, K. W., NIH Image to ImageJ: 25 years of image analysis. *Nature Methods* **2012,** *9* (7), 671.

39. Ojovan, M. I., Glass formation in amorphous SiO 2 as a percolation phase transition in a system of network defects. *Journal of Experimental and Theoretical Physics* **2004,** *79* (12), 632-634.

40. Teodósio, J. S.; Silva, F. C.; Moreira, J. M.; Simões, M.; Melo, L. F.; Alves, M. A.; Mergulhão, F. J., Flow cells as quasi-ideal systems for biofouling simulation of industrial piping systems. *Biofouling* **2013,** *29* (8), 953-966.

41. Fletcher, M.; Loeb, G., Influence of substratum characteristics on the attachment of a marine pseudomonad to solid surfaces. *Applied and Environmental Microbiology* **1979,** *37* (1), 67-72.

42. Cerca, N.; Pier, G. B.; Vilanova, M.; Oliveira, R.; Azeredo, J., Quantitative analysis of adhesion and biofilm formation on hydrophilic and hydrophobic surfaces of clinical isolates of *Staphylococcus epidermidis*. *Research in Microbiology* **2005,** *156* (4), 506-514.

43. Oliveira, K.; Oliveira, T.; Teixeira, P.; Azeredo, J.; Henriques, M.; Oliveira, R., Comparison of the adhesion ability of different *Salmonella enteritidis* serotypes to materials used in kitchens. *Journal of Food Protection* **2006,** *69* (10), 2352-2356.

44. Bos, R.; Van der Mei, H. C.; Busscher, H. J., Physico-chemistry of initial microbial adhesive interactions–its mechanisms and methods for study. *FEMS Microbiology Reviews* **1999,** *23* (2), 179-230.

45. Bakker, D.; Van der Plaats, A.; Verkerke, G.; Busscher, H.; Van der Mei, H., Comparison of velocity profiles for different flow chamber designs used in studies of microbial adhesion to surfaces. *Applied and Environmental Microbiology* **2003,** *69* (10), 6280-6287.

46. Graham, M. V.; Mosier, A. P.; Kiehl, T. R.; Kaloyeros, A. E.; Cady, N. C., Development of antifouling surfaces to reduce bacterial attachment. *Soft Matter* **2013,** *9* (27), 6235-6244.

5.6. Supplementary material

5.6.1. *E. coli* motility assays and results

Since *E. coli* JM109(DE3) is a K-12 derived strain and there are no listed mutations on genes coding for adhesins it is likely that these are present. In order to verify the presence of flagella, motility assays [1] were performed with both strains. Bacterial motility is a crucial factor in the colonization of natural environments. *E. coli* has two flagella-driven motility types: swimming and swarming. Swimming motility consists of individual cell movement in liquid medium or soft semisolid agar, whereas swarming is a coordinated cellular behavior leading to a collective movement on semisolid surfaces. It is known that swimming motility can be influenced by several types of environmental stress [2].

It was shown that *E. coli* JM109(DE3) has swimming motility (albeit 40% less than the CECT strain) (Figure S5.1) which indicates that flagella are functional [3]. Interestingly the swarming and twitching motilities are similar in both strains.

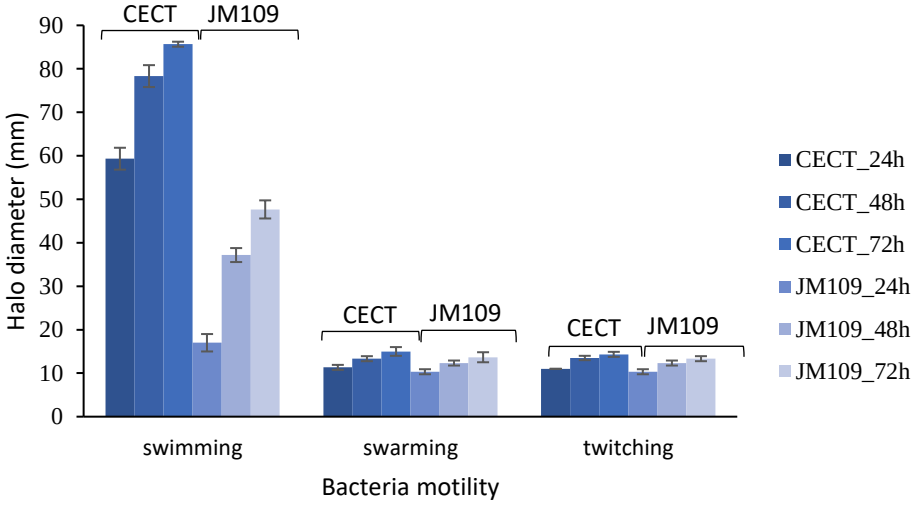

Figure S5.1. Motility (swimming, swarming, twitching) of *Escherichia coli* CECT 434 (control) and *Escherichia coli* JM109(DE3).

5.6.2. References

1. Borges, A.; Simões, L. C.; Saavedra, M. J.; Simões, M., The action of selected isothiocyanates on bacterial biofilm prevention and control. *International Biodeterioration & Biodegradation* **2014,** *86*, 25-33.

2. Gómez-Gómez, J., Manfredi, C., Alonso, J. et al. A novel role for RecA under non-stress: promotion of swarming motility in *Escherichia coli* K-12 . BMC Biol 5, 14 (2007).

3. Neidhardt, F. C., Motility and Chemotaxis. In *Escherichia coli and Salmonella typhimurium: cellular and molecular biology*, ASM Press: Washington, D.C., 1987; Vol. 1, pp 732-759.

5.6.3. Surface hydrophobicity and free energy of adhesion

Table S5.1. Contact angles with water (θ_w), formamide (θ_F) and α-bromonaphthalene (θ_B); surface tension parameters (γ^{LW}, γ^+ and γ^-), hydrophobicity (ΔG) and free energy of adhesion (ΔG^{Adh}) between *Escherichia coli* JM109(DE3)and each surface. Measurements were made before (top two rows) or after 30 min immersion in the testing media as indicated

Surface	Contact angle (º)			Surface Tension parameters (mJ/m^2)				Hydrophobicity (mJ/m^2)	Energy of adhesion (mJ/m^2)
	θ_w	θ_F	θ_B	γ^{LW}	γ^+	γ^-	γ^{AB}	ΔG^{TOT}	ΔG^{adh}
Glass	23.1 ± 2.4	29.3 ± 2.3	36.4 ± 3.5	36.1	0.8	54.8	13.1	35.6	73.0
Peptide coating	53.7 ± 1.7	43.6 ± 0.8	43.8 ± 0.7	32.9	1.0	26.6	10.5	-0.5	49.0
Glass in CB (30 min)	31.6 ± 3.8	18.3 ± 3.8	27.6 ± 3.1	39.5	1.5	39.8	15.6	14.0	57.6
Glass in EM (30 min)	20.7 ± 2.9	20.1 ± 3.3	23.9 ± 2.9	40.7	0.8	51.7	12.7	29.9	70.7
Peptide coating in CB (30 min)	46.9 ± 2.1	35.3 ± 3.1	31.0 ± 2.8	38.3	0.8	30.3	10	2.9	53.4
Peptide coating in EM (30 min)	79.0 ± 3.2	41.7 ± 1.8	26.2 ± 3.0	40.0	2.2	1.6	3.7	-59.5	3.8

5.6.4. QCM-D measurements

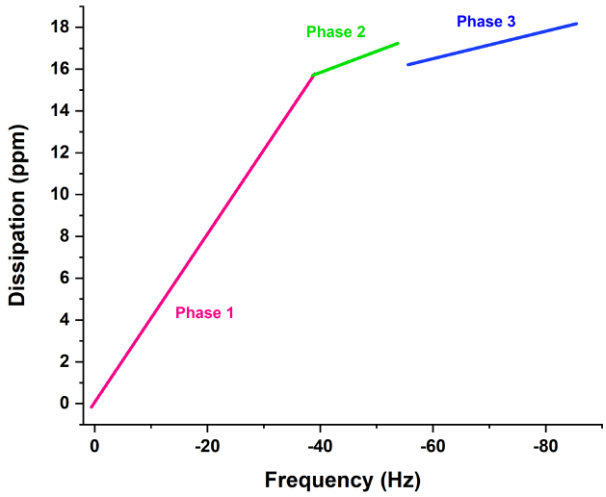

Figure S5.2. Dissipation *vs.* frequency of the fifth overtone. The adsorption behavior of the peptide changed throughout the run, suggesting different mechanisms of adsorption.

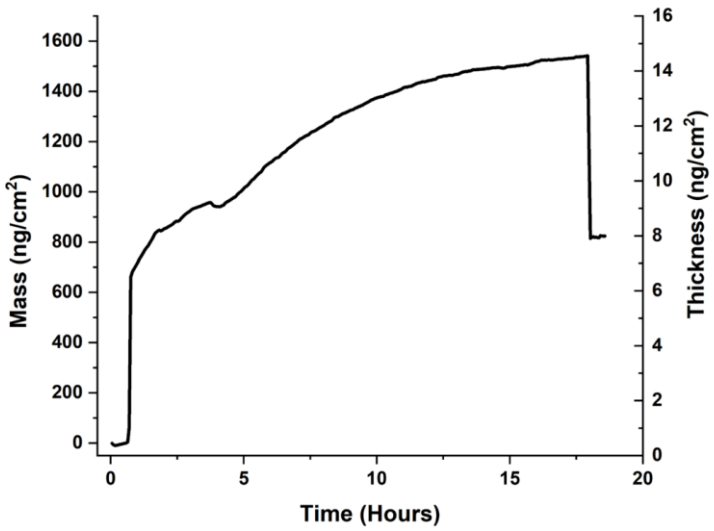

Figure S5.3. Mass accumulation on the quartz crystal microbalance with dissipation (QCM-D) sensor and layer thickness across time. After 17 h, the sensor was washed, the free peptide was removed, and the total mass and layer thickness decreased.

6. Effect of shear stress on the reduction of bacterial adhesion to antifouling polymers [g]

Abstract

In this work, two antifouling polymer brushes were tested at different shear stress conditions to evaluate their performance in reducing the initial adhesion of *Escherichia coli*. Assays were performed using a parallel plate flow chamber and a shear stress range between 0.005 and 0.056 Pa. These shear stress values are found in different locations in the human body where biomedical devices are placed. The poly(MeOEGMA) and poly(HPMA) surfaces were characterized and it was shown that they can reduce initial adhesion up to 90% when compared to glass. Importantly, the performance of these surfaces was not affected by the shear stress, which is an indication that they do not collapse under this shear stress range. The brushes displayed a similar behavior despite the differences in their chemical composition and surface energy. Both surfaces have shown ultra-low adsorption of macromolecules from the medium when tested with relevant biological fluids (urine and serum). This indicates that these surfaces can potentially be used in biomedical devices to reduce initial bacterial colonization and eventually reduce biofilm formation on these devices.

[g] The content of this chapter was adapted from the following publication:

Lopez-Mila B, Alves P, Riedel T, Dittrich B, Mergulhão F, Rodriguez-Emmenegger C (**2018**) Effect of shear stress on the reduction of bacterial adhesion to antifouling polymers. *Bioinspiration & Biomimetics*. Doi: 10.1088/1748-3190/aadcc2

6.1. Introduction

The adhesion of bacteria and colonization on various surfaces remains a significant challenge in industry, food safety and medicine. Upon adhesion to a surface, a series of processes begin leading to a change in cell phenotype that ultimately results in the formation of a microbial community termed biofilm [1, 2]. The individual cells recognize that the surface is suitable and modify their gene expression towards a sessile form [3]. A biofilm is a collection of bacteria attached to a surface, embedded in a matrix of excreted extracellular polymeric substances (EPS) [4].

Biofilms have many negative outcomes ranging from economic losses to life-threatening conditions [5-8]. Currently, device-related infections caused by bacteria adhering to biomaterials remain a significant challenge [9]. Topical devices (e.g. contact lenses) can be colonized immediately upon contact, transcutaneous devices (e.g. vascular catheters) are colonized more progressively by skin bacteria, and even orthopedic implants can be subjected to infection. Urinary catheters are among the ones with the highest incidence of bacterial infection accounting for as much as 30% of all nosocomial infections and 20% of bacteremia. A substantial number (70 to 80%) of such infections are associated with the use of a urethral catheter [10-12]. It is estimated that bacteria nested in biofilms are between 500 to 5000 times more resistant to biocides compared to when they are in a planktonic state [13, 14]. Consequently, inhibiting bacterial adhesion and thus preventing biofilm formation is a primary research focus.

The first step in the formation of a biofilm is the adsorption of macromolecules, primarily proteins, from the medium. Proteins are much smaller than bacteria and can diffuse to surfaces faster. They can be adsorbed via a series of weak interaction stemming from the different aminoacid residues. The adsorption of proteins and other macromolecules results in the formation of a new interface, known as the conditioning film, which may support the rapid binding of bacteria by resulting in more favorable adhesion energy or by exposing chemical groups for binding [1]. The second step comprises the adhesion of bacteria to the substrate [15, 16] which is followed by the secretion of EPS and formation of a biofilm matrix. The matrix provides protection from adverse chemical conditions and mechanical stability [15, 17, 18]. Thus, bacterial eradication becomes much more difficult. The interplay of both material and bacterial surfaces [19] further complicates this process. A number of polymer coatings have been developed aiming at reducing the adsorption of biomolecules and bacteria. The adhesion of bacteria onto hydrophobic surfaces (including a large number of polymeric materials) is mediated by the rapid adsorption of macromolecules that decrease the interfacial energy [20-22]. On the other hand, bacterial adhesion on hydrophilic surfaces is caused by (i) specific binding of ligand by receptors located at the bacterium surface (mainly adhesins) and (ii) several physicochemical interactions [23]. The main

component of the latter are the Lifshitz-van der Waals forces and forces originating from overlapping electrical double layers [24]. These attractive long-range interactions, which span over hundreds of Å, can be minimized by coating the surfaces with hydrophilic polymer brushes. They are an effective steric barrier keeping the bacterium at a sufficiently large distance where the Lifshitz-van der Waals interactions are low [25, 26]. Based on this simple physical principle the end-grafting grafting of poly(ethylene glycol) chains (PEG) to a surface was introduced [26]. However, only limited success was achieved [27, 28]. The grafting-to approach, typically only reaches low thicknesses (1 – 10 nm) which are not sufficient to ensure a steric barrier [24, 26, 29-31]. Furthermore, PEG-based coatings fail to prevent the adsorption of biomolecules from complex biological media such as blood plasma which supports biofilm formation [20, 22, 32]. The grafting-from method, *i.e.* using the surface directly to grow the polymer chains, results in densely grafted, longer polymer chains with a concomitant higher surface coverage yielding a more effective steric barrier with fewer defects. Typically, such brushes are produced by reversible-deactivation radical polymerization methods [33-38]. The polymerizable part of the monomers are selected to have relatively high enthalpy gain upon the addition to the growing chain. This enthalpy gain is used to overcome the entropic penalty of the highly stretched chains (less configurational entropy). Various brushes of oligo(ethylene glycol) methacrylate, zwitterionic betaines (sulfobetaine, carboxybetaine, phosphorycholine methacrylates), and *N*-(2-hydroxypropyl) methacrylamide were shown to be resistant to adsorption from biofluids [20, 39, 40] as well as to biofilm formation [19, 41-43]. Moreover, using single-cell force spectroscopy it was demonstrated that antifouling polymer brushes can prevent biofilm formation and also minimize the forces involved in bacterial colonization [44].

It should be highlighted, however, that the vast majority of studies trying to unravel the key factors of bacterial adhesion of polymer brushes have been carried out in static conditions focusing mainly in thermodynamic considerations. This neglects the importance of flow and shear in delivering the bacteria close to the surface, where the Lifshitz-van der Waals interactions are stronger [45]. In particular, flow is important in various engineering and biomaterial applications [46-50]. *In vitro* systems are used to assess the effect of shear stress in bacterial adhesion for different strains [51-55] and studies tried to correlate the extent of fouling with the energy of adhesion [51, 54, 56]. It has been shown that bacterial adhesion does not always correlates with surface properties but notoriously with the shear stress as later demonstrated by Moreira *et al* [46, 47].

In this work, the adhesion of *Escherichia coli* on antifouling polymer brushes is studied at different shear stresses. Poly[oligo(ethyleneglycol) methyl ether methacrylate], poly(MeOEGMA), and poly[*N*-2-hydroxypropyl) methacrylamide], poly(HPMA), brushes were

grafted from glass using atom transfer radical polymerization. For the purpose described, a parallel plate flow chamber (PPFC) was used enabling the control of the shear stress by modifying the flow rate of the bacterial suspension. The amount and rate of bacterial attachment were measured and correlated to the surface energy of the surfaces. The range of shear stresses was selected to match those that can be found in the human body and medical devices (see Table 2.6, Chapter 2-section 2.3.2).

A scheme showing the interaction of *E. coli* with the surfaces and the flow can be seen in figure 6.1.

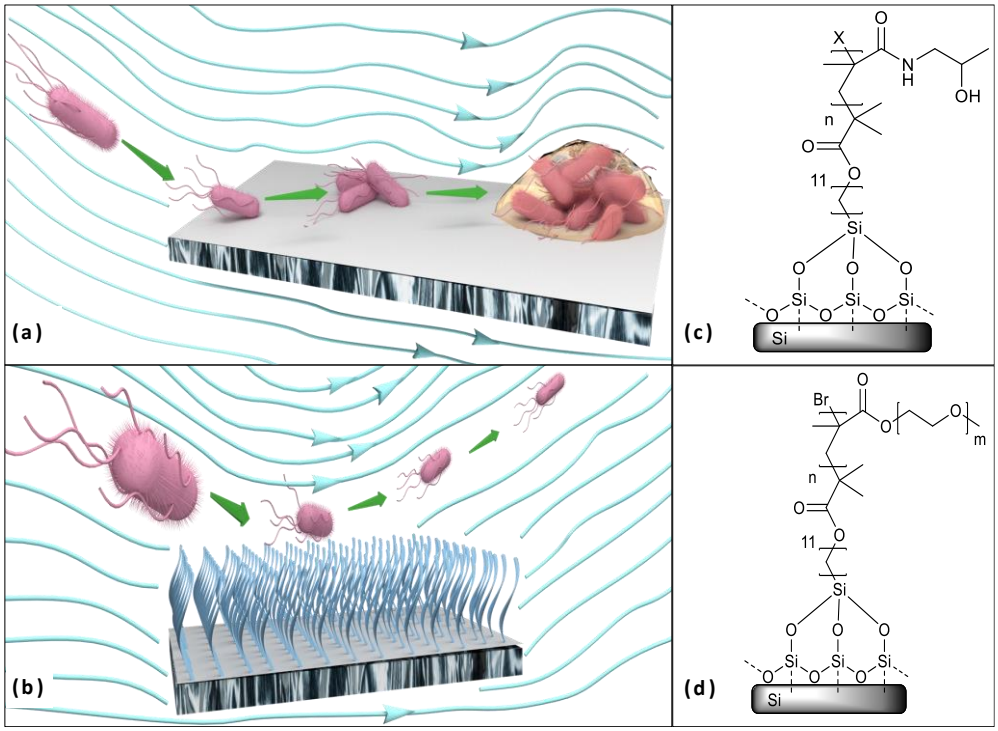

Figure 6.1. Scheme representing adhesion of *Escherichia coli* as a function of flow rate on **(a)** unfunctionalized surfaces and **(b)** coated with polymer brushes. The chemical structure of **(c)** poly(HPMA) and **(d)** poly(MeOEGMA) brushes are also depicted.

6.2. Materials and methods

6.2.1. Materials

Oligo(ethylene glycol) methyl ether methacrylate (M_n = 300 g/mol, MeOEGMA), catalysts $CuBr_2$ (99%), CuBr (99.99%), CuCl (≥99.99%), $CuCl_2$ (99.99%), ligands 2,2′- bipyridyl (99%), 1,4,8,11-tetramethyl-1,4,8,11-tetraazacyclotetradecane (Me_4Cyclam, 98%) were purchased from Sigma−Aldrich, Czech Republic. The initiators; ω-mercaptoundecyl bromoisobutyrate and 11-(trichlorosilyl)undecyl 2-bromo-2-methylpropanoate were synthesized according to

published procedures [44]. The monomer *N*-(2-hydroxypropyl) methacrylamide (HPMA) was prepared as previously described [44]. Purified water (Millipore, Milli-Q system) was used. Methanol, ethanol, acetone, and toluene were purchased from Lachner, Czech Republic.

6.2.2. Self-assembled monolayer of initiator

The self-assembled monolayer (SAM) of 11-(trichlorosilyl)undecyl 2-bromo-2-methylpropanoate initiator was assembled onto round glass slides (15 mm diameter) for bacterial adhesion, and onto silicon wafers (1 x 1 cm^2) for ellipsometry, atomic force microscopy (AFM) and grazing angle attenuated total reflection Fourier - transform infrared spectroscopy (GAATR – FTIR).

Glass and silicon samples were rinsed twice with ethanol and deionized Milli-Q water, blow-dried with nitrogen, and treated in UV/Ozone cleaner (Jelight) for 20 min. Subsequently, the samples were immersed in a freshly prepared solution of 1 mg/ml of 11-(trichlorosilyl)undecyl 2-bromo-2-methylpropanoate in anhydrous toluene for 3 h. During the incubation, the samples were kept in a desiccator to minimize humidity that could lead to undesired hydrolysis of the chlorosilane. Samples were then rinsed with a copious amount of toluene, acetone, ethanol and Milli-Q water, and blow-dried with nitrogen.

Initiator groups were also bound to gold coated substrates for subsequent evaluation of protein fouling via surface plasmon resonance (SPR). A SAM of ω-mercaptoundecyl bromoisobutyrate was formed on gold deposited on glass SPR chips. The SPR chips were cleaned using the same procedure as described above, transferred to a 1 mM solution of ω-mercaptoundecyl bromoisobutyrate in absolute ethanol and kept overnight at room temperature. They were rinsed with ethanol and water and blow-dried with nitrogen.

6.2.3. Preparation of the polymer brushes via surface – initiated atom transfer radical polymerization (SI-ATRP)

6.2.3.1. Poly(MeOEGMA) brushes

(1) Methanol, (2) MeOEGMA (39.8 g, 132.7 mmol) in 35 ml of water, and (3) 2,2´bipyridyl (1082.9 mg, 6.9 mmol), $CuBr_2$ (117.3 mg, 525 μmol) and CuBr (376.8 mg, 2.6 mmol) were deoxygenated separately by bubbling with Ar for 1 h. Methanol (35 ml) was then transferred using gas-tight syringes from flask 1 to flask 3 to generate the catalyst solution. The monomer solution, (flask 2) was transferred to flask 3 and mixed. Finally, the polymerization mixture was cannulated to the reactors containing the initiator-coated surfaces under Ar. The polymerization proceeded for 35 min at 30 °C [57]. The samples were stored in Milli-Q water.

6.2.3.2. Poly(HPMA) brushes

The solvent, methanol, 13 ml, was thoroughly degassed via five freeze – pump – thaw cycles and transferred to a previously degassed Schlenk flask containing CuCl (77.0 mg, 778 μmol), $CuCl_2$ (23.1 mg, 172 μmol), and Me_4Cyclam (266.5 mg, 1039 μmol). Simultaneously, a solution of HPMA (6.15 g, 42.9 mmol, in 26 ml of water and 13 ml of methanol) was degassed via five freeze – pump – thaw cycles. The blue catalyst solution was transferred to the monomer solution using a gastight syringe. When the polymerization mixture was homogenous, it was immediately cannulated to the reactors containing the samples. The polymerization was carried out at 30 °C for 2 h. The samples were taken out of the reactors, washed successively with water and stored in water.

6.2.4. Physicochemical characterization of polymer brushes

The dry thickness of the polymer layer was measured with a J.A. Woollam M-2000X Spectroscopic Ellipsometer. Data were acquired in air at room temperature in the wavelength range λ = 245–1000 nm at angles of incidence (AOI), of 60°, 65°, and 70° and fitted with Complete EASE software using a polymer on silicon model. Samples were measured at three points to verify the uniformity of the surface modification.

The morphology and roughness were studied using AFM Multimode Atomic Force Microscope NanoScope IIIa (Digital Instruments). The scans were carried out in tapping mode in air, using silicon probes OTESPA-R3 (Bruker) with a nominal spring constant of 26 N/m and a tip radius of 7 nm. Areas of 1 × 1 μm^2 (512 × 512 pixels) were scanned at a rate of 1 Hz. The scans were analyzed using Gwyddion software.

Grazing Angle Attenuated Total Reflection Fourier-Transform Infrared (GAATR-FTIR) spectra were obtained from the dry polymer brushes using a Nicolet Nexus 870 FTIR spectrometer (ThermoFisher Scientific) equipped with a VariGATR attachment (Harrick Scientific Products) under continuous purging with dry air. For the collection of the spectra, 256 scans were taken at a resolution of 2 cm^{-1}.

Protein fouling from human urine and fetal bovine serum was monitored using a custom -built SPR instrument (Institute of Photonics and Electronics, Academy of Sciences of the Czech Republic, Prague) [58]. The sensor response ($\Delta\lambda_{res}$) was obtained as the difference between the baselines in the buffer before and after the injection of the tested samples. From calibrations, $\Delta\lambda_{res}$ = 1 nm corresponds to a change in the deposited protein mass of 150 pg/mm^2.

6.2.5. Bacteria and culture conditions

Escherichia coli JM109(DE3) from Promega (Madison, WI, USA) was selected as it was

used in previous works [46, 47, 59]. An overnight culture and the bacterial suspension to use in the PPFC experiments were prepared as previously described in Chapter 3, section 3.2.1.

6.2.6. Surface hydrophobicity and free energy of adhesion

Bacterial hydrophobicity was evaluated by the contact angle method already described by Moreira *et al* [47]. Hydrophobicity of the surfaces was measured through contact angle measurements following the Van Oss approach [60, 61]. Contact angles were determined automatically using three solvents with different polarities, two polar solvents [formamide and water (Sigma-Aldrich Co., Portugal)] and one nonpolar solvent (α-bromonaphthalene; Sigma-Aldrich Co., Portugal) on the surface, using a contact angle goniometer (OCA 15 Plus; Dataphysics, Filderstadt, Germany). Six drops of each reference liquid were used on each surface and average values are reported (experiments were performed at 25 ± 2 °C). The surface tension components were taken from literature [62]. The detailed calculation method for the tension components and surface energy parameters is detailed in Chapter 5, section 5.2.7.

6.2.7. Flow cell and adhesion analysis

The PPFC system was sterilized and mounted as described in Chapter 3, section 3.2.3. For this study, round coupons of the polymer brushes and glass (used as a control) were sterilized by dipping in absolute ethanol (100%; Merck, Germany) for 5 min, were left to air-dried inside the laminar flow chamber and were fixed aseptically to recesses on the bottom plate so that they become flush with the surface. Experiments were performed at different flow rates (1, 2, 4, 6 and 8 ml/s), for 30 min. The images were acquired, and the number of bacteria adhering was recorded as a function of time as described in Chapter 3-section 3.2.3. The number of adhering cells per square centimeter was determined using the area of the field of view. Then, the adhesion reduction percentage was calculated by comparing the adhesion to the polymer brushes and to glass during the last 5 min of the assay (results vary up to 3% by endpoint calculation).

6.2.8. Statistical analysis

Each data point is an average of the results obtained in three independent experiments for each flow condition. Error bars represent the standard deviation for each parameter at each time point. To evaluate the statistical significance, a paired t-test analysis was made using GraphPad Prism 6 (La Jolla, CA, USA). When a confidence level was higher than 95% ($P < 0.05$), the time points were denoted by * if poly(HPMA) was statistically different from glass and denoted by # if this difference was obtained for poly(MeOEGMA).

6.3. Results and discussion

6.3.1. Synthesis of polymer brushes and characterization

Poly(MeOEGMA) and poly(HPMA) were directly grafted from a SAM on glass substrates using ATRP as previously reported. The thickness of the brushes was selected to be close to 30 nm based on previous results showing that thickness was sufficient to minimize fouling from biological fluids [20, 21, 63, 64]. The dry ellipsometric thickness for poly(MeOEGMA) was 27.9 ± 0.2 nm while for poly(HPMA) was 30.8 ± 0.1 nm. The same polymerization conditions were used for the samples grafted from glass and gold; thus it is assumed that the same thickness was achieved in the model silicon surface.

The chemical structure was determined by GAATR – FTIR (Figure 6.2). The spectra were recorded on brushes grafted on silicon wafers. Figure 6.2a(1) demonstrates the successful grafting from poly(HPMA) brushes. Prominent bands at 1640 and 1535 cm^{-1} stem from amide I and II respectively while the band at 3350 cm^{-1} is ascribed to the secondary hydroxyls of HPMA groups. The spectrum of poly(MeOEGMA) (Figure 6.2a(2)) presents a strong peak at 1730 cm^{-1} corresponding to the ester carbonyl band. In the region of 1500 cm^{-1} a group of bands is attributed to the different -CH_2 vibration modes: scissoring (1465 cm^{-1}), wagging (1350 cm^{-1}), twisting (1250 cm^{-1}) and rocking (950 cm^{-1}). At 1145 cm^{-1} a dominant band assigned to the C–O–C stretching vibration of the oligo(ethylene glycol) subunits is present.

AFM was used to study the topography of the brushes. Figure 6.2(b) and 6.2(c) confirms that both surfaces are homogeneous and without pin–holes.

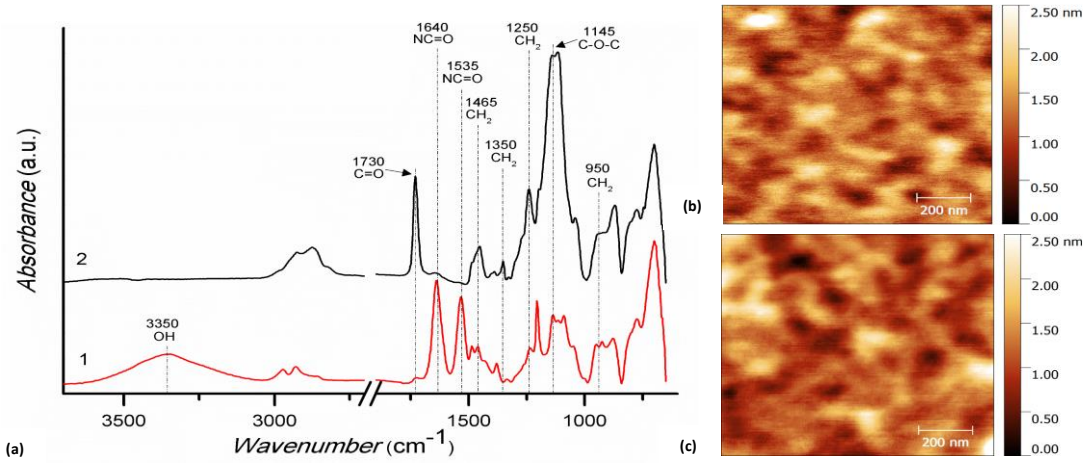

Figure 6.2. Grazing angle attenuated total reflection Fourier-transform infrared (GAATR-FTIR) spectra of polymer brushes prepared **(a)**: (1) poly(HPMA), (2) poly(MeOEGMA). Atomic force microscopy (AFM) topography of **(b)** the poly(MeOEGMA) brushes and **(c)** poly(HPMA).

6.3.2. Bacterial adhesion and thermodynamic analysis

Surface and bacterial hydrophobicity (ΔG^{TOT}) and the free energy of adhesion (ΔG^{Adh}) were determined from the thermodynamic treatment described above using static sessile drop contact angles. To assess the surface energy of *E. coli*, a bacterial suspension was prepared as described for the adhesion experiments and deposited on filters to form a homogeneous lawn prior to measuring the contact angles [43]. These values are known to better represent the state of hydration of the cell surface [43, 65] resulting in more representative values than the measurements made on dehydrated biofilms [66]. All surfaces displayed static water contact angles lower than 65° thus can be classified as hydrophilic [25, 67]. *E. coli* low water contact angle indicates that their outer bacterial wall is also hydrophilic.

The thermodynamic analysis using the van Oss acid-base approach also indicates that all the surfaces tested are hydrophilic, *i.e.* $\Delta G^{TOT} > 0$. Remarkably, brushes of poly(HPMA) were more hydrophilic (higher ΔG^{TOT}) than poly(MeOEGMA). Examination of table 6.1 indicates that the Lifshitz-van der Waals component (γ^{LW}) is the major contributor to the total surface energy ($\gamma^{TOT} = \gamma^{LW} + \gamma^{AB}$). Analysis of the acid-based polar components (γ^+ and γ^-) shows that all the surfaces are predominantly electron donor surfaces (higher value of γ^-) with a very low electron acceptor character (γ^+).

Table 6.1. Contact angle (θ), the apolar (γ^{LW}) and polar (γ^{AB}) components, the surface tension parameters (γ^+ and γ^-), the hydrophobicity (ΔG^{TOT}) of surfaces tested and bacteria and the energy of adhesion (ΔG^{Adh})

Surface	**Contact angle (°)**			**Surface tension parameters** (mJ/m²)				**Hydrophobicity** (mJ/m²)	**Energy of adhesion** (mJ/m²)
	θ_w	θ_F	θ_B	γ^{LW}	γ^+	γ^-	γ^{AB}	ΔG^{TOT}	ΔG^{Adh}
Glass	23.1 ± 2.4	29.3 ± 2.3	36.4 ± 3.5	36.1	0.8	54.8	13.1	35.6	73.0
Poly(HPMA)	24.5 ± 3.7	37.7 ± 3.7	42.5 ± 6.5	33.5	0.4	60.4	10.0	45.5	80.0
Poly(MeOEGMA)	54.3 ± 4.4	49.5 ± 4.0	42.0 ± 3.1	33.7	0.3	30.7	5.6	6.3	58.5
Escherichia coli	19.1 ± 0.9	73.3 ± 0.7	58.5 ± 2.0	25.7	0.0	123.2	0.0	121.9	n/a

Static contact angle of tested surface for water (θ_w), formamide (θ_F) and α-bromonaphthalene (θ_B). Values are means ± SDs of three independent experiments.

A PPFC was used to determine the *E. coli* adhesion on brushes at five different flow rates (1 to 8 ml/s, see Figure 6.3). The flow rates were selected to match the hydrodynamic conditions that exist in several locations in the human body. Numerical simulation [46] showed that the shear stress range covered in this study was between 0.005 and 0.056 Pa. This represents a 10-fold increase in shear stress and similar shear stress values are found in the urinary (urethra and bladder), reproductive (uterus) and circulatory (veins) systems (Table 2.6 – Chapter 2).

Reductions on cell adhesion were obtained for both polymer surfaces (when compared to glass) and results show that their performance is similar on the range of shear stresses studied (Figure 6.4). The number of adhered cells is a balance between the cells that arrive at the surface and are able to initiate a reversible adhesion process and those that are detached from the surface due to the shear stress. At 1 ml/s bacterial attachment on glass increased almost linearly with time reaching about 10^6 cell/cm^2 after 30 min (Figure 6.3a). Both polymer brushes reduced the adhesion compared to the glass control by approximately 70% (Figure 6.4). Increasing the flow rate to 2 ml/s resulted in a drastic change in the bacteria attached to polymer brushes (Figure 6.3b). While approximately the same number of bacteria adhered to poly(HPMA) and poly(MeOEGMA) brushes, adhesion was reduced by 90% when compared to glass (Figure 6.4). The elevated flow increases the number of contacts between bacteria from the fluid and the surface (increasing the probability of adhesion) while also increases the shear on adherent bacteria. The reduced adhesion with increasing flow rate suggests that bacteria interact weakly with the brushes and can be removed by shear. This is in close agreement with a previous work showing that adhesion forces between brushes and bacteria are three orders of magnitude lower than on glass [44]. The same effect is observed when increasing the flow rate from 2 to 6 ml/s (Figure 6.3b-d). Increasing the flow rate to 8 ml/s did not result in further reduction of the bacterial attachment on the brushes but reduced the attachment on glass, suggesting that such shear stress is able to partially overcome the initial adhesion on this surface (Figure 6.3e). The almost invariable performance of the brushes under various flow rates is in line with recent reports showing that high-density brushes do not collapse under shear [68].

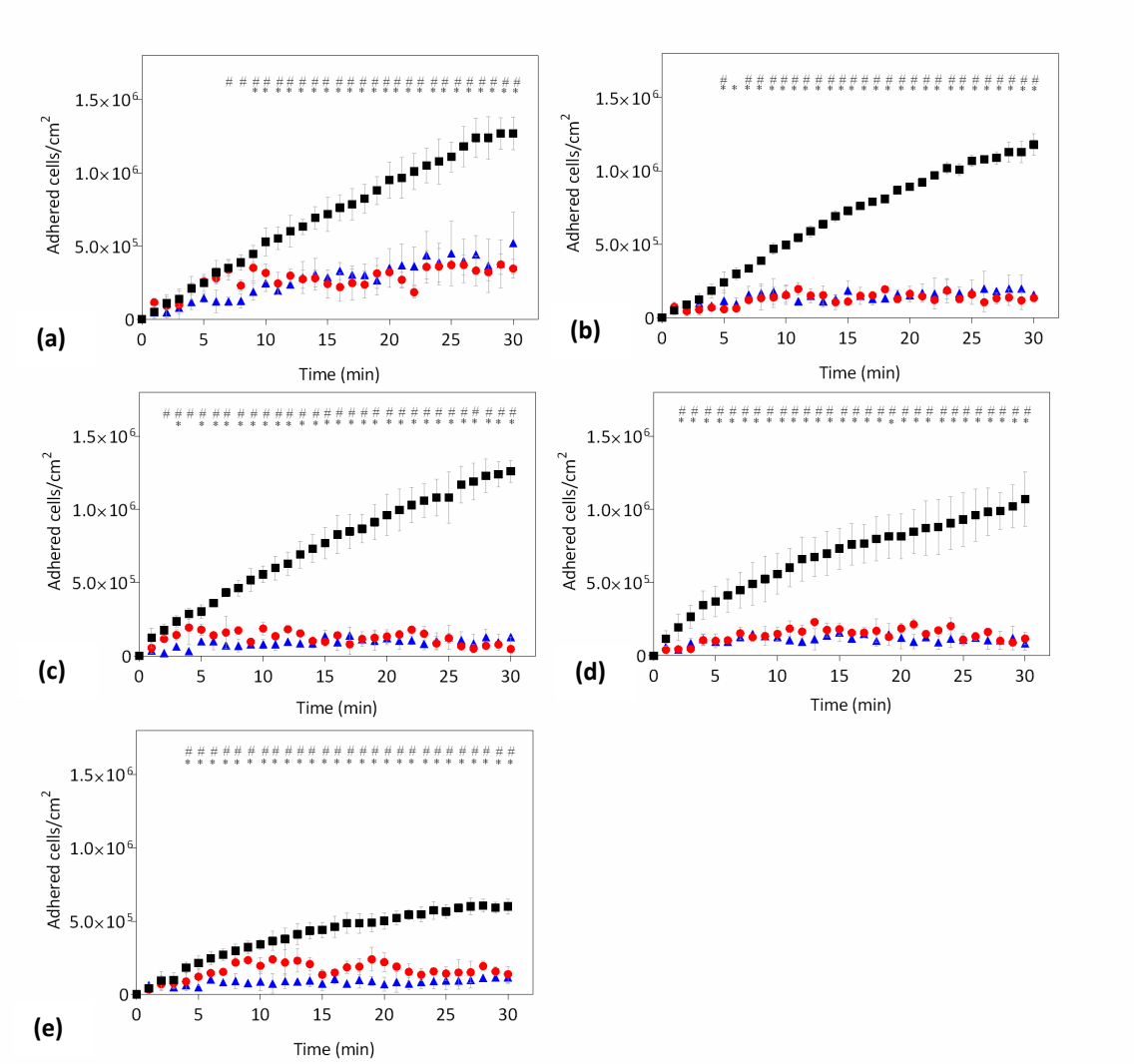

Figure 6.3. Adhesion of *Escherichia coli* JM109(DE3) on glass (■), poly(HPMA) (●) and poly(MeOEGMA) brushes (▲), at different flow rates: **(a)** 1 ml/s, **(b)** 2 ml/s, **(c)** 4 ml/s, **(d)** 6 ml/s and **(e)** 8 ml/s. Differences are statistically significant ($P < 0.05$) for each time point when denoted by # between poly(MeOEGMA) and glass and by * between poly(HPMA) and glass.

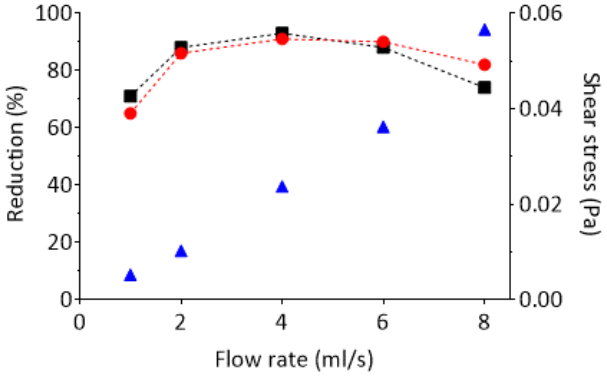

Figure 6.4. Average reduction in *Escherichia coli* JM109(DE3) adhesion on poly(HPMA) (■) and poly(MeOEGMA) brushes (●) relative to glass (used as control) for the different flow rates. the average wall shear stress determined by computational fluid dynamics (▲) as described in Moreira et al. [46]. Results are an average of those obtained from three independent experiments for each surface and flow rate. Error bars indicate standard deviations.

In this work, a clear correlation between surface hydrophobicity or the calculated energy of adhesion and bacterial adhesion could not be found. Surface hydrophobicity, which is usually considered a proxy of adhesion, alone cannot explain the adhesion results. Poly(MeOEGMA) was the most hydrophobic of the tested surfaces but displayed much lower bacteria adhesion than glass. The free energy of adhesion, unfavorable to adhesion for all tested surfaces, did not allow to discriminate the different behaviors of glass and brush-coated glass as previously observed in other studies [47, 52, 69]. Other authors have found a strong correlation between the Chen and Qi ratio (γ^{LW}/γ^{-}) [66, 70] but this correlation was also not observed in our study. It is known that specific physicochemical characteristics of the bacteria can affect the adhesion process [71] and that components of the cell wall architecture, including bacterial appendages (e.g. pili, flagella, fimbriae) are also important [72]. These features are not contemplated in the simplified model used in this work. Moreover, it should be considered that the thermodynamic approach enables the calculation of the energies of adhesion from the surface energies of pristine surfaces. However, the model does not contemplate the presence of macromolecules in the medium as well as those secreted by bacteria which will inevitably adsorb on glass –and not on brushes– and will rapidly change the surface energy of glass. Moreover, it is well known that the contact angle of water in glass rapidly changes upon immersion in water [73]. On the other hand, brushes result in an effective barrier to adsorption (*vide infra*).

When surfaces are being tested for application in biomedical devices, the tests should include relevant microorganisms, relevant media and be performed at correct hydrodynamic conditions that mimic, as close as possible, the desired application. In this work, a 10-fold change

in shear stress was studied comprising very different biomedical scenarios (Table 2.6, Chapter 2-section 2.3.2) and therefore for each particular application a relevant medium should be used. However, one of the goals of this work was to perform a thermodynamic evaluation of the surfaces to assess if the thermodynamic theory could explain the obtained results as well comparing the performance of the brushes at different shear stresses (which required that the same medium was used). For this reason, citrate buffer was chosen because it has a minimal surface conditioning effect that could mask the thermodynamic analysis and is therefore commonly used in adhesion assays [46, 47]. The shear stress range selected for this work covers a broad range of applications with different fluids (e.g. urine, blood and tears). However, the formation of a conditioning film by the adsorption of biomacromolecules from such bodily fluids may obscure the value of the results. Such macromolecules are ubiquous in any biological medium and include proteins, polysaccharides and lipids that could affect cell adhesion [74-76]. To account for this, the fouling resulting upon contact of the polymer brushes with human urine collected from healthy volunteers and fetal bovine serum was measured. Both bodily fluids are among the most challenging environments for antifouling surfaces and medical devices operating in contact with them frequently suffer from biofilm formation. The surface plasmon resonance spectrographs show undetectable adsorption of proteins or other macromolecules after 15 min (Figures 6.5 and 6.6). Extending the contact time with urine to 2 h did not result in any increase in the fouling on poly(HPMA) while a wavelength shift of fewer than 15 ng/cm^2 was observed on poly(MeOEGMA) (Figures 6.5 and 6.6). This fouling upon 2 h contact of urine with poly(MeOEGMA) corresponds to less than 5% of the fouling corresponding to saturation of the surface and less than 25% of the fouling detected on the widely used self-assembled monolayers of alkanethiols [20].

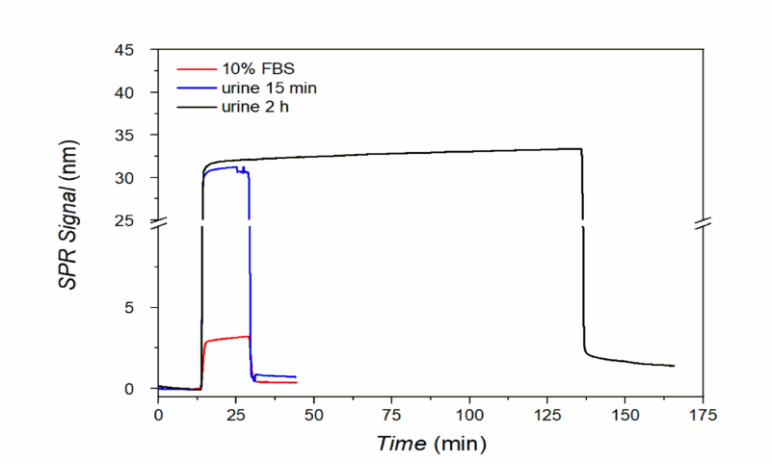

Figure 6.5. Surface plasmon resonance (SPR) sensogram showing the fouling from fetal bovine serum (FBS, 10%), urine during 15 min and urine during 2 h on poly(MeOEGMA) brushes.

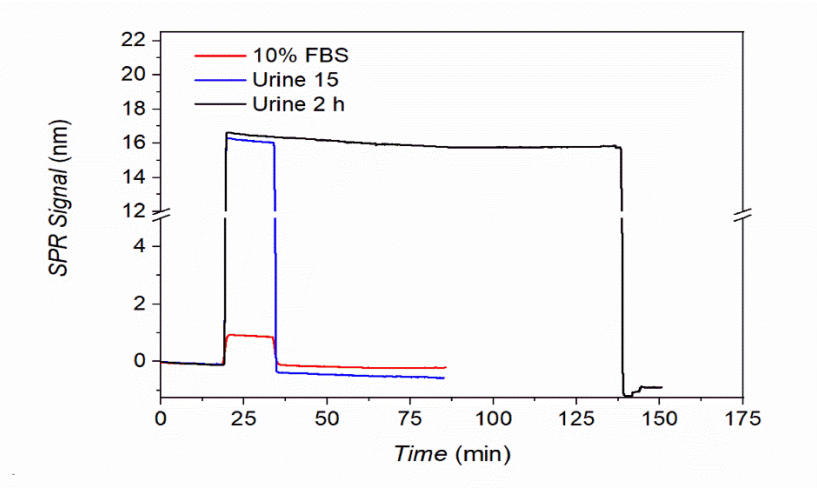

Figure 6.6. Surface plasmon resonance (SPR) sensogram showing the fouling from fetal bovine serum (FBS, 10%), urine during 15 min and urine during 2 h on poly(HPMA) brushes.

6.4. Conclusions

This study has shown that these polymer brushes can reduce bacterial adhesion over a relevant range of shear stresses that can be found in several locations of our body. The reduction in initial adhesion was not explained by the surface hydrophobicity nor by the estimated energy of adhesion showing that the complexity of this interaction exceeds the predictive power of the thermodynamic model that was used for this highly simplified scenario. The extent of the reduction in initial adhesion suggests that these surfaces can potentially be used in the development of biomedical devices with increased antifouling performance. However, longer time *in vitro* tests using the correct surrounding medium are necessary prior to *in vivo* testing in animal models. The fact that these surfaces appear to be resistant to adsorption of macromolecules from some of the most complex bodily fluids (urine and serum) is also promising as this can further delay cell attachment and biofilm formation in more realistic scenarios.

6.5. References

1. Garrett, T. R.; Bhakoo, M.; Zhang, Z., Bacterial adhesion and biofilms on surfaces. *Progress in Natural Science: Materials International* **2008,** *18* (9), 1049-1056.

2. Vlamakis, H.; Chai, Y.; Beauregard, P.; Losick, R.; Kolter, R., Sticking together: building a biofilm the Bacillus subtilis way. *Nature Reviews. Microbiology* **2013,** *11* (3), 157-68.

3. Kolter, R.; Greenberg, E. P., Microbial sciences: The superficial life of microbes. *Nature* **2006,** *441* (7091), 300-302.

4. Wu, M. Y.; Sendamangalam, V.; Xue, Z.; Seo, Y., The influence of biofilm structure and total interaction energy on *Escherichia coli* retention by *Pseudomonas aeruginosa* biofilm. *Biofouling* **2012,** *28* (10), 1119-28.

5. Kingshott, P.; Wei, J.; Bagge-Ravn, D.; Gadegaard, N.; Gram, L., Covalent attachment of poly(ethylene glycol) to surfaces, critical for reducing bacterial adhesion. *Langmuir* **2003,** *19* (17), 6912-6921.

6. Darouiche, R. O., Treatment of Infections Associated with Surgical Implants. *New England Journal of Medicine* **2004,** *350* (14), 1422-1429.

7. Stickler, D. J., Biomaterials to prevent nosocomial infections: Is silver the gold standard? *Current Opinion in Infectious Diseases* **2000,** *13* (4), 389-393.

8. Hasan, J.; Crawford, R. J.; Ivanova, E. P., Antibacterial surfaces: the quest for a new generation of biomaterials. *Trends in Biotechnology* **2013,** *31* (5), 295-304.

9. Thompson, M.; Blaszykowski, C.; Sheikh, S.; Rodriguez-Emmenegger, C.; De Los Santos Pereira, A., *Biological Fluid-Surface Interactions in Detection and Medical Devices*. Royal Society of Chemistry: 2016.

10. Gould, C. V.; Umscheid, C. A.; Agarwal, R. K.; Kuntz, G.; Pegues, D. A.; Healthcare Infection Control Practices Advisory, C., Guideline for prevention of catheter-associated urinary tract infections 2009. *Infection Control & Hospital Epidemiology* **2010,** *31* (4), 319-26.

11. Hooton, T. M.; Bradley, S. F.; Cardenas, D. D.; Colgan, R.; Geerlings, S. E.; Rice, J. C.; Saint, S.; Schaeffer, A. J.; Tambayh, P. A.; Tenke, P.; Nicolle, L. E., Diagnosis, Prevention, and Treatment of Catheter-Associated Urinary Tract Infection in Adults: 2009 International Clinical Practice Guidelines from the Infectious Diseases Society of America. *Clinical Infectious Diseases* **2010,** *50* (5), 625-663.

12. Jacobsen, S. M.; Stickler, D. J.; Mobley, H. L.; Shirtliff, M. E., Complicated catheter-associated urinary tract infections due to *Escherichia coli* and *Proteus mirabilis*. *Clinical Microbiology Reviews* **2008,** *21* (1), 26-59.

13. Das, J. R.; Bhakoo, M.; Jones, M. V.; Gilbert, P., Changes in the biocide susceptibility of *Staphylococcus epidermidis* and *Escherichia coli* cells associated with rapid attachment to plastic surfaces. *Journal of Applied Microbiology* **1998,** *84* (5), 852-8.

14. Walker, R. D.; Thornsberry, C., Decrease in antibiotic susceptibility or increase in resistance? *Journal of Antimicrobial Chemotherapy* **1998,** *41* (1), 1-4.

15. Busscher, H. J.; van der Mei, H. C., How do bacteria know they are on a surface and regulate their response to an adhering state? *PLoS pathogens* **2012,** *8* (1), e1002440.

16. Davey, M. E.; O'Toole, G. A., Microbial Biofilms: from Ecology to Molecular Genetics. *Microbiology and Molecular Biology Reviews* **2000,** *64* (4), 847-867.

17. Costerton, J. W.; Stewart, P. S.; Greenberg, E. P., Bacterial biofilms: a common cause of persistent infections. (Cover story). *Science* **1999,** *284* (5418), 1318-1322.

18. Firoozabadi, R.; Alton, T.; Wenke, J., Novel Strategies for the Diagnosis of Posttraumatic Infections in Orthopaedic Trauma Patients. *The Journal of the American Academy of Orthopaedic Surgeons* **2015,** *23* (7), 443-51.

19. Rzhepishevska, O.; Hakobyan, S.; Ruhal, R.; Gautrot, J.; Barbero, D.; Ramstedt, M., The surface charge of anti-bacterial coatings alters motility and biofilm architecture. *Biomaterials Science*. **2013,** *1* (6), 589-602.

20. Rodriguez-Emmenegger, C.; Houska, M.; Alles, A. B.; Brynda, E., Surfaces resistant to fouling from biological fluids: towards bioactive surfaces for real applications. *Macromolecular Bioscience* **2012,** *12* (10), 1413-22.

21. Rodriguez-Emmenegger, C.; Brynda, E.; Riedel, T.; Houska, M.; Šubr, V.; Alles, A. B.; Hasan, E.; Gautrot, J. E.; Huck, W. T., Polymer brushes showing non-fouling in blood plasma challenge the currently accepted design of protein resistant surfaces. *Macromolecular Rapid Communications* **2011,** *32* (13), 952-957.

22. Rodriguez-Emmenegger, C.; Brynda, E.; Riedel, T.; Sedlakova, Z.; Houska, M.; Alles, A. B., Interaction of blood plasma with antifouling surfaces. *Langmuir* **2009,** *25* (11), 6328-6333.

23. Clements, A.; Gaboriaud, F.; Duval, J. F.; Farn, J. L.; Jenney, A. W.; Lithgow, T.; Wijburg, O. L.; Hartland, E. L.; Strugnell, R. A., The major surface-associated saccharides of *Klebsiella pneumoniae* contribute to host cell association. *PloS One* **2008,** *3* (11), e3817.

24. Roosjen, A.; Busscher, H. J.; Norde, W.; van der Mei, H. C., Bacterial factors influencing adhesion of *Pseudomonas aeruginosa* strains to a poly(ethylene oxide) brush. *Microbiology* **2006,** *152* (Pt 9), 2673-82.

25. Andrade, J. D., Surface and interfacial aspects of biomedical polymers. Vol. 1. Surface chemistry and physics. *Plenum Press* **1985**, 470.

26. Jeon, S.; Lee, J.; Andrade, J.; De Gennes, P., Protein—surface interactions in the presence of polyethylene oxide: I. Simplified theory. *Journal of Colloid and Interface Science* **1991,** *142* (1), 149-158.

27. Boulmedais, F.; Frisch, B.; Etienne, O.; Lavalle, P.; Picart, C.; Ogier, J.; Voegel, J. C.; Schaaf, P.; Egles, C., Polyelectrolyte multilayer films with pegylated polypeptides as a new type of anti-microbial protection for biomaterials. *Biomaterials* **2004,** *25* (11), 2003-2011.

28. Ostuni, E.; Chapman, R. G.; Liang, M. N.; Meluleni, G.; Pier, G.; Ingber, D. E.; Whitesides, G. M., Self-Assembled monolayers that resist the adsorption of proteins and the adhesion of bacterial and mammalian cells. *Langmuir* **2001,** *17* (20), 6336-6343.

29. Zdyrko, B.; Klep, V.; Luzinov, I., Synthesis and surface morphology of high-density poly(ethylene glycol) grafted layers. *Langmuir* **2003,** *19* (24), 10179-10187.

30. Halperin, A.; Fragneto, G.; Schollier, A.; Sferrazza, M., Primary versus ternary adsorption of proteins onto PEG brushes. *Langmuir* **2007,** *23* (21), 10603-10617.

31. Halperin, A., Polymer brushes that resist adsorption of model proteins: design parameters. *Langmuir* **1999,** *15* (7), 2525-2533.

32. de los Santos Pereira, A.; Riedel, T.; Brynda, E.; Rodriguez-Emmenegger, C., Hierarchical antifouling brushes for biosensing applications. *Sensors and Actuators B: Chemical* **2014,** *202* (0), 1313-1321.

33. Advincula, R., Polymer brushes by anionic and cationic surface-initiated polymerization (SIP). *Advances in Polymer Science* **2006,** *197*, 107-136.

34. Zamfir, M.; Rodriguez-Emmenegger, C.; Bauer, S.; Barner, L.; Rosenhahn, A.; Barner-Kowollik, C., Controlled growth of protein resistant PHEMA brushes via S-RAFT polymerization. *Journal of Materials Chemistry B* **2013,** *1* (44), 6027-6034.

35. Tischer, T.; Rodriguez-Emmenegger, C.; Trouillet, V.; Welle, A.; Schueler, V.; Mueller, J. O.; Goldmann, A. S.; Brynda, E.; Barner-Kowollik, C., Photo-patterning of non-fouling polymers and biomolecules on paper. *Advanced Materials* **2014,** *26* (24), 4087-92.

36. Buzzacchera, I.; Vorobii, M.; Kostina, N. Y.; de Los Santos Pereira, A.; Riedel, T.; Bruns, M.; Ogieglo, W.; Moller, M.; Wilson, C. J.; Rodriguez-Emmenegger, C., Polymer brush-functionalized chitosan hydrogels as antifouling implant coatings. *Biomacromolecules* **2017,** *18* (6), 1983-1992.

37. Vorobii, M.; Pop-Georgievski, O.; de los Santos Pereira, A.; Kostina, N. Y.; Jezorek, R.; Sedláková, Z.; Percec, V.; Rodriguez-Emmenegger, C., Grafting of functional methacrylate polymer brushes by photoinduced SET-LRP. *Polymer Chemistry* **2016,** *7* (45), 6934-6945.

38. Vorobii, M.; de los Santos Pereira, A.; Pop-Georgievski, O.; Kostina, N. Y.; Rodriguez-Emmenegger, C.; Percec, V., Synthesis of non-fouling poly[N-(2-hydroxypropyl)-methacrylamide] brushes by photoinduced SET-LRP. *Polymer Chemistry* **2015,** *6* (23), 4210-4220.

39. Surman, F.; Riedel, T.; Bruns, M.; Kostina, N. Y.; Sedlakova, Z.; Rodriguez-Emmenegger, C., Polymer brushes interfacing blood as a route toward high performance blood contacting devices. *Macromolecular Bioscience* **2015,** *15* (5), 636-646.

40. de los Santos Pereira, A.; Rodriguez-Emmenegger, C.; Surman, F.; Riedel, T.; Bologna, A.; Brynda, E., Use of pooled blood plasmas in the assessment of fouling resistance. *RSC Advances* **2014,** *4* (5), 2318 - 2321.

41. Cheng, G.; Zhang, Z.; Chen, S.; Bryers, J. D.; Jiang, S., Inhibition of bacterial adhesion and biofilm formation on zwitterionic surfaces. *Biomaterials* **2007,** *28* (29), 4192-4199.

42. Rodriguez-Emmenegger, C.; Decker, A.; Surman, F.; Preuss, C. M.; Sedlakova, Z.; Zydziak, N.; Barner-Kowollik, C.; Schwartz, T.; Barner, L., Suppressing *Pseudomonas aeruginosa* adhesion via non-fouling polymer brushes. *Rsc Advances* **2014,** *4* (110), 64781-64790.

43. Busscher, H. J.; Weerkamp, A. H.; van der Mei, H. C.; van Pelt, A. W.; de Jong, H. P.; Arends, J., Measurement of the surface free energy of bacterial cell surfaces and its relevance for adhesion. *Applied and Environmental Microbiology* **1984,** *48* (5), 980-3.

44. Rodriguez-Emmenegger, C.; Janel, S.; de los Santos Pereira, A.; Bruns, M.; Lafont, F., Quantifying bacterial adhesion on antifouling polymer brushes via single-cell force spectroscopy. *Polymer Chemistry* **2015,** *6* (31), 5740-5751.

45. Rodesney, C. A.; Roman, B.; Dhamani, N.; Cooley, B. J.; Katira, P.; Touhami, A.; Gordon, V. D., Mechanosensing of shear by *Pseudomonas aeruginosa l*eads to increased levels of the cyclic-di-GMP signal initiating biofilm development. *Proceedings of the National Academy of Sciences* **2017,** *114* (23), 5906-5911.

46. Moreira, J. M.; Araujo, J. D.; Miranda, J. M.; Simoes, M.; Melo, L. F.; Mergulhao, F. J., The effects of surface properties on *Escherichia coli* adhesion are modulated by shear stress. *Colloids and surfaces. B, Biointerfaces* **2014,** *123*, 1-7.

47. Moreira, J. M.; Simões, M.; Melo, L. F.; Mergulhão, F. J., *Escherichia coli* adhesion to surfaces–a thermodynamic assessment. *Colloid and Polymer Science* **2015,** *293* (1), 177-185.

48. Teodósio, J. S.; Simões, M.; Alves, M. a.; Melo, L. F.; Mergulhão, F. J., Setup and validation of flow cell systems for biofouling simulation in industrial settings. *The Scientific World Journal* **2012,** *2012*, 1-10.

49. Teodósio, J. S.; Simões, M.; Melo, L. F.; Mergulhão, F. J., Flow cell hydrodynamics and their effects on *E. coli* biofilm formation under different nutrient conditions and turbulent flow. *Biofouling* **2011,** *27*, 1-11.

50. Tirrell, M.; Kokkoli, E.; Biesalski, M., The role of surface science in bioengineered materials. *Surface Science* **2002,** *500*, 61-83.

51. Pratt-Terpstra, I. H.; Weerkamp, A. H.; Busscher, H. J., Adhesion of oral streptococci from a flowing suspension to uncoated and albumin-coated surfaces. *The Journal of General Microbiology* **1987,** *133* (11), 3199-206.

52. Barton, A. J.; Sagers, R. D.; Pitt, W. G., Bacterial adhesion to orthopedic implant polymers. *Journal of Biomedical Materials Research* **1996,** *30* (3), 403-10.

53. Millsap, K. W.; Reid, G.; van der Mei, H. C.; Busscher, H. J., Adhesion of *Lactobacillus* species in urine and phosphate buffer to silicone rubber and glass under flow. *Biomaterials* **1997,** *18* (1), 87-91.

54. Bruinsma, G. M.; van der Mei, H. C.; Busscher, H. J., Bacterial adhesion to surface hydrophilic and hydrophobic contact lenses. *Biomaterials* **2001,** *22* (24), 3217-24.

55. Busscher, H. J.; van der Mei, H. C., Microbial adhesion in flow displacement systems. *Clinical Microbiology Reviews* **2006,** *19* (1), 127-41.

56. Nauman, E. A.; Ott, C. M.; Sander, E.; Tucker, D. L.; Pierson, D.; Wilson, J. W.; Nickerson, C. A., Novel quantitative biosystem for modeling physiological fluid shear stress on cells. *Applied and Environmental Microbiology* **2007,** *73* (3), 699-705.

57. de los Santos Pereira, A.; Kostina, N. Y.; Bruns, M.; Rodriguez-Emmenegger, C.; Barner-Kowollik, C., Phototriggered functionalization of hierarchically structured polymer brushes. *Langmuir* **2015,** *31* (21), 5899-907.

58. Homola, J.; Lu, H. B.; Nenninger, G. G.; Dostálek, J.; Yee, S. S., A novel multichannel surface plasmon resonance biosensor. *Sensors and Actuators B: Chemical* **2001,** *76* (1–3), 403-410.

59. Moreira, J.; Ponmozhi, J.; Campos, J.; Miranda, J. M.; Mergulhão, F., Micro-and macro-flow systems to study *Escherichia coli* adhesion to biomedical materials. *Chemical Engineering Science* **2015,** *126*, 440-445.

60. Van Oss, C., Hydrophobicity of biosurfaces—origin, quantitative determination and interaction energies. *Colloids and Surfaces B* **1995,** *5* (3-4), 91-110.

61. Van Oss, C. J.; Good, R. J.; Chaudhury, M. K., Additive and nonadditive surface tension components and the interpretation of contact angles. *Langmuir* **1988,** *4* (4), 884-891.

62. Janczuk, B.; Chibowski, E.; Bruque, J.; Kerkeb, M.; Caballero, F. G., On the consistency of surface free energy components as calculated from contact angles of different liquids: an application to the cholesterol surface. *Journal of Colloid and Interface Science* **1993,** *159* (2), 421-428.

63. Obstals, F.; Vorobii, M.; Riedel, T.; de los Santos Pereira, A.; Bruns, M.; Singh, S.; Rodriguez-Emmenegger, C., Improving hemocompatibility of membranes for extracorporeal membrane oxygenators by grafting nonthrombogenic polymer brushes. *Macromolecular Bioscience* **2018,** *18* (3), 1700359.

64. de los Santos Pereira, A.; Sheikh, S.; Blaszykowski, C.; Pop-Georgievski, O.; Fedorov, K.; Thompson, M.; Rodriguez-Emmenegger, C., Antifouling polymer brushes displaying antithrombogenic surface properties. *Biomacromolecules* **2016,** *17* (3), 1179-1185.

65. Van der Mei, H. C.; Busscher, H. J., A reference guide to microbial cell surface hydrophobicity based on contact angles. *Colloids Surf. B* **1998,** *11*, 213-221.

66. Liu, C.; Zhao, Q., Influence of surface-energy components of Ni-P-TiO2-PTFE nanocomposite coatings on bacterial adhesion. *Langmuir* **2011,** *27* (15), 9512-9.

67. Andrade, J. D.; Smith, L. M.; Gregonis, D. E., The contact angle and interface energetics. In *Surface and Interfacial Aspects of Biomedical Polymers: Volume 1 Surface Chemistry and Physics*, Andrade, J. D., Ed. Springer US: Boston, MA, 1985; pp 249-292.

68. Korolkovas, A.; Rodriguez-Emmenegger, C.; de los Santos Pereira, A.; Chennevière, A.; Restagno, F.; Wolff, M.; Adlmann, F. A.; Dennison, A. J. C.; Gutfreund, P., Polymer brush collapse under shear flow. *Macromolecules* **2017,** *50* (3), 1215-1224.

69. Oliveira, K.; Oliveira, T.; Teixeira, P.; Azeredo, J.; Henriques, M.; Oliveira, R., Comparison of the adhesion ability of different *Salmonella enteritidis* serotypes to materials used in kitchens. *Journal of Food Protection* **2006,** *69* (10), 2352-2356.

70. Liu, C.; Zhao, Q., The CQ ratio of surface energy components influences adhesion and removal of fouling bacteria. *Biofouling* **2011,** *27* (3), 275-285.

71. Mukherjee, J.; Karunakaran, E.; Biggs, C. A., Using a multi-faceted approach to determine the changes in bacterial cell surface properties influenced by a biofilm lifestyle. *Biofouling* **2012,** *28* (1), 1-14.

72. Vila, J.; Sáez-López, E.; Johnson, J.; Römling, U.; Dobrindt, U.; Cantón, R.; Giske, C.; Naas, T.; Carattoli, A.; Martínez-Medina, M., *Escherichia coli*: an old friend with new tidings. *FEMS Microbiology Reviews* **2016,** *40* (4), 437-463.

73. Vogler, E. A., Structure and reactivity of water at biomaterial surfaces. *Advances in Colloid and Interface Science* **1998,** *74* (1), 69-117.

74. Moreira, J.; Gomes, L.; Whitehead, K.; Lynch, S.; Tetlow, L.; Mergulhão, F., Effect of surface conditioning with cellular extracts on *Escherichia coli* adhesion and initial biofilm formation. *Food and Bioproducts Processing* **2017,** *104*, 1-12.

75. Lorite, G. S.; Rodrigues, C. M.; De Souza, A. A.; Kranz, C.; Mizaikoff, B.; Cotta, M. A., The role of conditioning film formation and surface chemical changes on *Xylella fastidiosa* adhesion and biofilm evolution. *Journal of Colloid and Interface Science* **2011,** *359* (1), 289-295.

76. Bos, R.; van der Mei, H. C.; Busscher, H. J., Physico-chemistry of initial microbial adhesive interactions – its mechanisms and methods for study. *FEMS Microbiology Reviews* **1999,** *23* (2), 179-230.

7. The potential advantages of using a poly(HPMA) brush in urinary catheters: effects on biofilm cells and architecture [h]

Abstract

Infections related to bacterial colonization of medical devices are a growing concern given the socio-economical impacts in healthcare systems. Colonization of a device surface with bacteria usually triggers the development of a biofilm, which is more difficult to eradicate than free-floating or adhered bacteria and can act as a reservoir for subsequent infections. Biofilms often harbor viable but nonculturable (VBNC) cells that are likely to be more resistant to antibiotic treatment and that can become active in more favorable conditions causing infection. Biofilm formation is dependent on different factors, chiefly the properties of the surface and of the surrounding medium and the hydrodynamic conditions.

In this work, the antifouling performance of a poly[*N*-(2-hydroxypropyl) methacrylamide] (poly(HPMA)) brush was evaluated *in vitro* in conditions that mimic a urinary catheter using *Escherichia coli* as a model organism. The results obtained with the brush were compared to those obtained with two control surfaces, polydimethylsiloxane (PDMS) (the most common material for catheters) and glass. A decrease in initial adhesion and surface coverage was observed on the brush. This antifouling behavior was maintained during biofilm maturation and even in a simulated post-bladder infection period when the reduction in total cell number reached 87%. Biofilms were shown to adapt their architecture during that period and VBNC cells adsorbed weakly on the brushes and were completely washed away.

Taken together, these results suggest that the use of poly(HPMA) brush in urinary tract devices such as catheters and stents may reduce biofilm formation and possibly render the formed biofilms more susceptible to antibiotic treatment and with reduced infectivity potential.

[h] The content of this chapter was adapted from the following publication:

Alves P, Gomes LC, Vorobii M, Rodriguez-Emmenegger C, Mergulhão FJ (**2020**) The potential advantages of using a poly (HPMA) brush in urinary catheters: effects on biofilm cells and architecture. *Colloids and Surfaces B: Biointerfaces*, 191, 110976. Doi: 10.1016/j.colsurfb.2020.110976

7.1. Introduction

Catheter-associated urinary tract infections (CAUTIs) represent the vast majority (98%) of urinary tract infections in intensive care units. CAUTIs cause an additional burden to healthcare systems that has been estimated in the range of £1–2.5 billion in the United Kingdom, whereas a rough estimate of total direct hospital costs connected to CAUTIs in the United States was approximately $36 billion [1].

Microorganisms can gain access to a urinary catheter following both intraluminal and extraluminal routes. One possible route involves migration through the catheter lumen after a bladder infection episode. Microorganisms are transported by the descending urine flow and attach to the inner walls of the catheter where they start to form a biofilm [1]. Biofilms are sessile communities of microorganisms embedded in a self-produced matrix of extracellular polymeric substances (EPS) [2]. It has been shown that biofilm cells are much more resistant than their planktonic (i.e. free-flowing) counterparts and several resistance/tolerance mechanisms have been proposed [3]. Besides being protected by the EPS layer (that imposes a diffusional barrier to antimicrobial agents), it has been shown that the decreased growth rate of biofilm cells also protects them from several antibiotics that mostly target dividing cells [4]. Although the microorganisms responsible for catheter contamination may originate from a bladder infection, even when this infection is cleared (by the immune system and/or antibiotic treatment) the biofilm can act as a reservoir of pathogenic bacteria that can migrate upwards and cause recurrent bladder infections [1].

Biofilms can be polymicrobial or contain single species but even in that case, biofilms are composed of cells in different physiological states. They often harbor viable but nonculturable (VBNC) cells, which are living cells that have lost the ability to divide in media on which they normally grow [4, 5]. The VBNC state is a unique survival strategy adopted by many bacteria in response to adverse environmental conditions. These cells have an intact membrane containing undamaged genetic information, a lower metabolic rate and higher physical and chemical resistance when compared to culturable cells. This can be attributed to their reduced metabolic rate and also to a cell wall strengthened by increased peptidoglycan cross-linking [5]. Since these cells are not detected with conventional plate count techniques, they often lead to an underestimation of total viable cells in clinical samples [5]. Additionally, it has been shown that some uropathogenic VBNC *Escherichia coli* cells are not detected by standard methods and are not eliminated by antibiotic treatment, being able to "resuscitate" back to a more metabolically active state and cause infection [4].

Bacterial adhesion is affected by surface properties [6], thus several attempts have been

made to develop non-adhesive surfaces [7], such as polymer brush-coatings, in order to prevent cell adhesion and subsequent infection [8, 9]. Surface engineering must consider the interaction of the surfaces with the biological systems where they will be applied [10, 11]. For instance, it is extremely important that the antifouling surfaces prevent the adsorption of biomolecules from complex biological fluids such as blood, plasma and serum, so that the performance of biomedical devices is not impaired. Polymer brushes have been shown to prevent adsorption of human blood plasma, serum, immunoglobulin G, fibrinogen and bovine serum albumin [12-14]. Furthermore, some polymer brushes of oligo(ethylene) methacrylates (MeOEGMA), hydroxyethyl methacrylate and hydroxyethyl acrylamide presented fouling levels below 300 pg/mm^2 when exposed to real biological fluids (e.g. human body fluids such as blood plasma, human serum, cerebrospinal fluid, urine and saliva, and animal fluids such as foetal bovine and calf sera, egg and milk), which is about 10% of a protein monolayer [15]. More recently, an ultra-low-fouling poly[N-(2-hydroxypropyl) methacrylamide] poly(HPMA) brush has been studied for surface applications since it is one of the most successful polymers used in drug delivery systems [11, 16-18]. Poly(HPMA) displayed high water solubility, no cytotoxicity and was the basic platform for the design of drug conjugates, micellar and vesicular delivery systems, to name a few [16, 19, 20]. Only negligible adsorption, if any, was observed on poly(HPMA) brushes in spite of not having the typical characteristics associated to protein resistant surfaces, since they have hydrogen bond donors and are considerably less wettable than other polymer brushes (e.g. poly(carboxybetaine acrylamide), poly(CBAA)) [11, 21]. The antifouling properties of poly(HPMA) brushes were maintained when they were exposed to other human fluids (cerebrospinal fluid, saliva and urine) and animal fluids (chicken egg and whole cow milk) [12]. The repellent action of these brushes also extents to mesoscopic objects such as bacteria. Using single-cell force spectroscopy we showed that poly(HPMA) brushes could reduce three orders of magnitude the work of adhesion of a bacterium compared to the uncoated substrate, while not causing any cytotoxic effect [22]. Further studies in biofilm formation revealed that the brushes could minimize the biofilm formation with only few bacteria adhering which were dead [11]. Since the polymer is not cytotoxic, the preferential adhesion of dead bacteria might be associated to changes in the physicochemical properties of their cell wall upon death.

Despite the promising results of polymer brushes in preventing bacterial adhesion in the biomedical context, few studies are performed in conditions that are similar to the real physiological scenarios, particularly in terms of fluid composition and hydrodynamics. Recently, our research group showed that poly(HPMA) brush maintained their antifouling properties when subjected to different shear stresses commonly found in the human body (see Chapter 6)

[23]. In this work, it was demonstrated that the poly(HPMA) was able to reduce *E. coli* adhesion to up 90% when compared to bare glass, using citrate buffer and considering only the initial 30 min of biofilm formation. Moreover, the same study showed undetectable adsorption of proteins and other macromolecules after 2 h of contact time with human urine (see Chapter 6, supplementary material). Given the repellent activity displayed by this brush during the initial adhesion phase, we were interested in evaluating their behavior during biofilm formation using a more realistic medium and maintaining the glass surface as a control.

In this work, the performance of a poly(HPMA) brush against *E. coli* biofilm formation was evaluated in a parallel plate flow chamber (PPFC) using synthetic urine as a growth medium. This *in vitro* system allows the operation at shear conditions found in urinary catheters where *E. coli* typically adheres and forms biofilms. Since silicone is one of the most common materials used to manufacture urinary catheters, this surface was also included in our study as a benchmark of how a biofilm would develop in our experimental setup. The different types of cells that compose the biofilm have been determined and the effect of the brush on biofilm architecture was analysed. The potential benefits of using this brush in urinary catheters are discussed taking into consideration the potential for biofilm resistance and infectivity.

7.2. Materials and methods

7.2.1. Surface preparation

The poly(HPMA) brushes were prepared via surface-initiated atom transfer radical polymerization (SI-ATRP), as previously described in Chapter 6-section 6.2.3.2 (Figure 7.1). Bare glass (VWR, Portugal) and polydimethylsiloxane (PDMS) (Sylgard 184, Dow Corning, USA) were used in this work for comparative purposes. PDMS is one of the most widely used polymers in the production of urinary catheters [24] and glass is a material commonly used in adhesion studies performed on PPFCs due to its transparency [25] and was the substrate used for growing the poly(HPMA) brushes. The PDMS samples were obtained as previously described in Chapter 3-section 3.2.2.

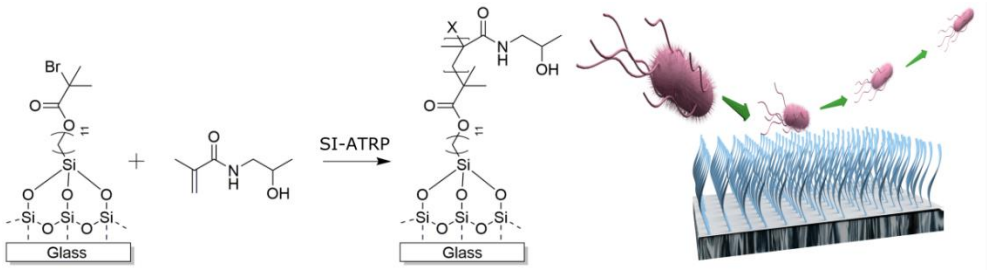

Figure 7.1 Synthesis of poly(HPMA) brushes by surface-initiated atom transfer radical polymerization (left) and illustration of repellent mechanism (right).

7.2.2. Surface characterization

Surface hydrophobicity was assessed by the sessile drop contact angle measurement fully described in Chapter 5-section 5.2.7.

In order to assess the heterogeneity of the surfaces, two microscopic techniques were used: atomic force microscopy (AFM) and scanning electron microscopy (SEM). AFM images were acquired and analysed as described in Chapter 6, section 6.2.4. Surface roughness was defined quantitatively through measurement of the average roughness (R_a), which gives the average absolute deviation of the roughness irregularities from the mean line over one sampling length [26]. The surfaces were observed at 50000× magnification with a SEM/EDS system (FEI Quanta 400FEG ESEM/EDAX Genesis X4M, FEI Company, USA) in high-vacuum mode at 5 kV.

7.2.3. Bacteria and growth conditions

E. coli JM109(DE3) from Promega (USA) was used in this work since it has been used in the previous study with this polymer brush (Chapter 6, section 6.2.5). This strain was shown to have similar biofilm formation behavior to different clinical isolates, including *E. coli* CECT 434 [27] and can form robust biofilms on different surface materials and platforms operated under different shear conditions [28, 29].

An overnight culture was prepared by inoculating 500 μL of a glycerol stock (kept at -80 °C) in a total volume of 0.2 l of synthetic urine medium. The medium was prepared as previously described [30] using the following formulation for 1 l of distilled water: peptone 1 g, yeast extract 0.05 g, lactic acid 1.1 mmol/l, citric acid 0.4 g, sodium bicarbonate 2.1 g, urea 10 g, uric acid 0.07 g, creatinine 0.8 g, calcium chloride.$2H_2O$ 0.37 g, sodium chloride 5.2 g, iron II sulphate.$7H_2O$ 0.0012 g, magnesium sulphate.$7H_2O$ 0.49 g, sodium sulphate.$10H_2O$ 3.2 g, potassium dihydrogen phosphate 0.95 g, di-potassium hydrogen phosphate 1.2 g and ammonium chloride 1.3 g. The pH of the solution was then adjusted to 6.5. All media components were purchased from Merck (Germany). The culture was grown on a 1 l shake-flask at 37 °C for 15-17 h with orbital agitation (160 rpm; IKA KS 130 basic, Staufen, Germany). Cells were harvested by centrifugation for 10 min at 3202 *g*. The suspension was then adjusted with synthetic urine medium to have an optical density at 610 nm of 0.1, equivalent to a cell density of 7.6×10^7 cells/ml.

7.2.4. Biofilm formation

Biofilm formation was initially carried out for 24 h at 37 °C on three different surface materials: PDMS, glass and the poly(HPMA) brush. It has been reported that *E. coli* biofilms in urinary catheters are completely mature after 24 h [31].

All the surfaces were sterilized with absolute ethanol and placed in the PPFC, as

described in Chapter 3, section 3.2.3. The bacterial suspension was then recirculated through the PPFC system at 2 ml/s, a flow rate that corresponds to a shear rate of 15/s described for urinary catheters [32]. Biofilm formation was monitored in real-time with microscopic images acquired at different time points (0.5, 2 and 24 h). After 24 h of biofilm formation (a period designated as the infection period), the *E. coli* suspension was removed from the system and pre-warmed, sterile, synthetic urine was flown on the system for 8 h at the same shear rate (the "post-infection" period). This was done to simulate a scenario were the original bladder infection, which was the source of the bacteria, had been resolved by the immune system and/or antibiotic treatment. Brightfield microscopy images were also acquired after this 8 h of post-infection period (the 32-h time point). The area fraction covered by *E. coli* cells was determined for the 0.5, 2, 24 and 32 h time points using the ImageJ software (version 1.38e; National Institutes of Health, EUA). ImageJ macro scripts were created to convert the brightfield microscopy images to an 8-bit grayscale file format and thresholds were applied to calculate the percentage of surface area covered by cells, as previously described in Chapter 3-section 3.2.3.

7.2.5. Bacterial quantification approaches

In addition to monitoring biofilm development in real-time, biofilm cell numbers were determined offline at 24 and 32 h of experiment, using two different methodologies: culturability and epifluorescent microscopy to quantify the total and viable cells. The number of VBNC cells was determined by subtracting the number of culturable cells from that of viable cells [4, 5]. For that, the PPFC was opened and the cells adhered to each surface were collected by scrubbing the upper surface of the coupon with a sterile cotton swab (swabbing method) [33, 34]. The swabs were transferred to sterile tubes containing 25 ml of 0.85% NaCl. Afterward, the swabs were vortexed to obtain the biofilm cell suspension.

To assess the culturability (colony forming units) 10-fold-serial dilutions of the biofilm suspension were prepared and spread on plate count agar (PCA, Oxoid, England), and incubated at 37 °C for colony enumeration. The total cell number was determined by epifluorescence microscopy by staining the biofilm suspension with 4′-6-diamidino-2-phenylindole (DAPI, 0.5 mg/l; Merck, Germany). For that purpose, biofilm suspension was diluted, filtered through a Nucleopore, Track-Etch Membrane (Whatman Int., USA) black polycarbonate membrane (pore size 0.2 mm) and stained with 1 ml of DAPI reagent for 10 min in the dark. The bacterial observation and enumeration was performed using a Leica DM LB2 epifluorescence microscope connected to a Leica DFC300 FX camera (Leica Microsystems, Switzerland) [35]. The viability of biofilm cells was assessed using the Live/Dead® (L/D) *Bac*Light™ Bacterial Viability kit (Invitrogen Life Technologies, Alfagene, Portugal) for 10 min in the dark [35]. Bacterial observation

and counting of viable and nonviable bacteria were performed as indicated for the total cells. In this case, the live cells were stained with the green fluorescent nucleic acid stain (SYTO™ 9) and the dead cells were stained with the red-fluorescent dye (propidium iodide). A minimum of 20 fields of view of each stained sample was analyzed using the ImageJ software to estimate the total and viable cell numbers. The final values of the total, viable and VBNC cells are presented as cells/cm^2.

7.2.6. Assessment of biofilm architecture by confocal laser scanning microscopy (CLSM)

Biofilms developed on the poly(HPMA) brush, PDMS and glass surfaces, after 24 and 32 h were observed using a Leica TCS SP5 II CLSM (Leica Microsystems, Germany). Biofilm samples were counterstained in red with 5 μM Syto61 (Invitrogen, USA), a cell-permeant fluorescent nucleic acid stain. Each stained sample mounted on a microscopic slide was scanned using a 10x with 0.4 N.A. (Leica HC PLAN APO CS) dry objective lens at an excitation wavelength of 633 nm (helium-neon laser) and the emitted fluorescence was recorded within the range of 640-730 nm. A minimum of 6 stacks of horizontal plane images (2048 × 2048 pixels, corresponding to 1550 × 1550 μm) with a *z*-step of 1 μm were acquired for each biofilm.

Three-dimensional (3D)-projections of biofilm structures were reconstructed using the "Easy 3D" tool of IMARIS 8.4.1 software (Bitplane, Switzerland) directly from the *xyz* images series. The COMSTAT2 tool associated with the ImageJ software was used to determine the biofilm average thickness (μm) [36].

7.2.7. Statistical analysis

All experiments were carried out in triplicate using different batches of *E. coli* cultures. Standard deviations on the triplicate sets were calculated for all analysed parameters. Graph production and statistical analysis were performed using GraphPad Prism 6.01 (La Jolla, USA).

The differences between the polymer brushes and the controls, PDMS and glass, were evaluated using one-way analysis of variance (one-way ANOVA, Tukey's post hoc test) for each method/variable. All statistical analysis used a 95% confidence limit, so that *P* values equal to or greater than 0.05 were not considered statistically significant.

7.3. Results and discussion

The three tested surfaces (PDMS, glass and poly(HPMA)) were first characterized through the thermodynamic analysis based on contact angle measurements (Table 7.1) [35]. It was observed that PDMS is hydrophobic ($\Delta G < 0$ mJ/m^2), whereas glass and poly(HPMA) brushes are hydrophilic ($\Delta G > 0$ mJ/m^2). According to the surface wetting criterion defined by Aryal and Neuner [37], from the water contact angle (θ_w in Table 7.1 and Figure S7.1-supplementary material), PDMS can also be classified as wettable since θ_w was less than 110°.

Table 7.1. Contact angles with water (θ_w), formamide (θ_F) and α-bromonaphthalene (θ_B), hydrophobicity (ΔG) and roughness (R_a) of polydimethylsiloxane (PDMS), glass and poly(HPMA) brushes

Surface	**Contact angles (°)**			**Hydrophobicity (mJ/m²)**	**Roughness (nm)**
	θ_w	θ_F	θ_B	ΔG	R_a
PDMS	98.0 ± 5.3	96.9 ± 2.5	77.0 ± 1.4	-37.9	0.59
Glass	9.1 ± 3.4	31.2 ± 5.6	37.5 ± 4.7	50.6	0.26
poly(HPMA)	19.4 ± 1.5	26.6 ± 5.9	36.4 ± 4.0	36.1	3.59

Values are means ± SDs of three independent experiments.

Two microscopic techniques, AFM and SEM, were used to determine the roughness and to study the morphology of the surfaces. AFM topography images (Figure 7.2a) confirmed that the three surfaces are homogeneous and without pin-holes. High magnification SEM images (Figure 7.2b) showed that all surfaces are smooth. These results are in agreement with previous surface plasmon resonance (SPR) and ellipsometric studies demonstrating that the linkage of the trichlorosilane initiator to the surface was stable during swelling and storage and that the brushes remain repellent even after 2-years storage in water [11, 15]. The polymer brush surface is rougher than the control surfaces, with an average roughness value (R_a) about 6 times higher than PDMS and about 14 times higher than glass (Table 7.1).

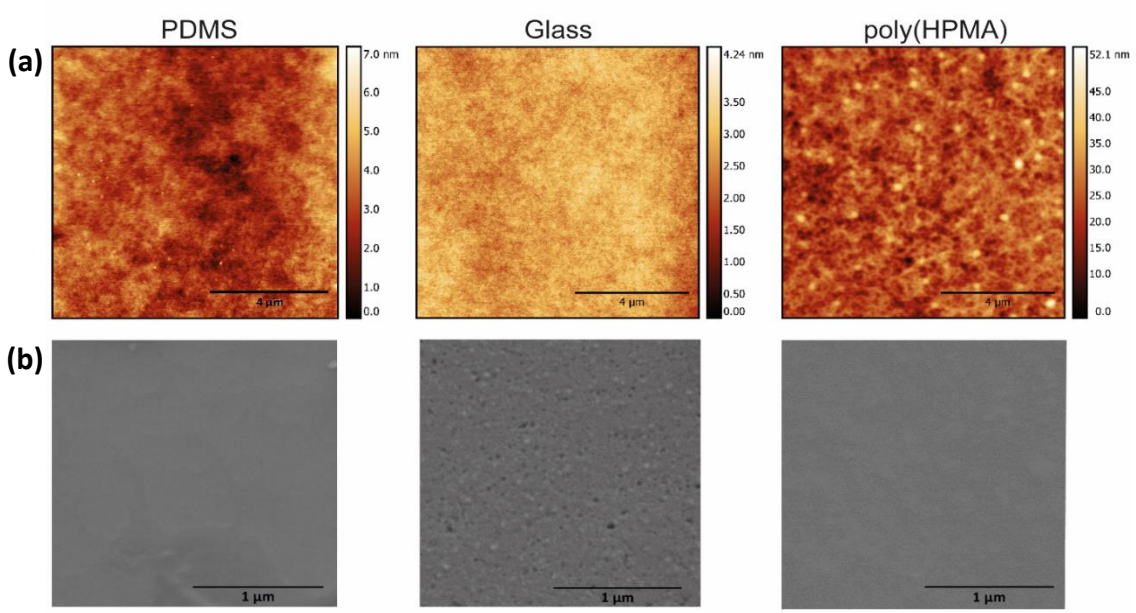

Figure 7.2. 2D-atomic force microscopy (AFM) topographic images **(a)** and scanning electron micrographs **(b)**; magnification: 50 000×) of polydimethylsiloxane (PDMS), glass and poly(HPMA). The color bar corresponds to the *z*-range of the respective AFM image. Scale bar is 4 µm for AFM and 1 µm for scanning electron microscopy (SEM).

In this study, the antifouling effect of a poly(HPMA) brush on *E. coli* biofilm growth was evaluated in a PPFC system operated with synthetic urine medium at a flow rate that simulates the shear forces found in urinary catheters (a shear rate of 15/s) [25]. Biofilm development was followed for 24 h in order to simulate the scenario where a bladder infection was the continuous source of bacteria (infection period). After that, biofilm development was followed for an additional 8 h period where sterile urine was flown on the system to simulate that bladder infection was cleared by the immune system and/or antibiotic treatment (post-infection period).

Figure 7.3 presents the area fraction covered by *E. coli* on the three tested surfaces (PDMS, glass and poly(HPMA)) during the infection period (0.5, 2 and 24 h) and post-infection (32 h). Lower surface coverages were registered on the polymer brush-coating when compared to PDMS and glass and differences obtained between the brush and the controls were statistically significant for all time points ($P < 0.01$). During the infection period (up to 24 h), the surface area coverage determined for the brush was on average 40% lower when compared to the control surfaces ($P < 0.0001$). The antifouling behavior displayed in the initial period of adhesion (0.5 and 2 h) was maintained during biofilm maturation. In the post-infection period, the surface area covered by the biofilm decreased by approximately 20% on PDMS and 41% on glass, whereas this reduction was about 50% on the polymer brush. Thus, the antifouling performance of the brush, demonstrated on the previous work with citrate buffer (Chapter 6), was maintained here

both in short as well as longer time intervals using more realistic conditions for urinary catheters.

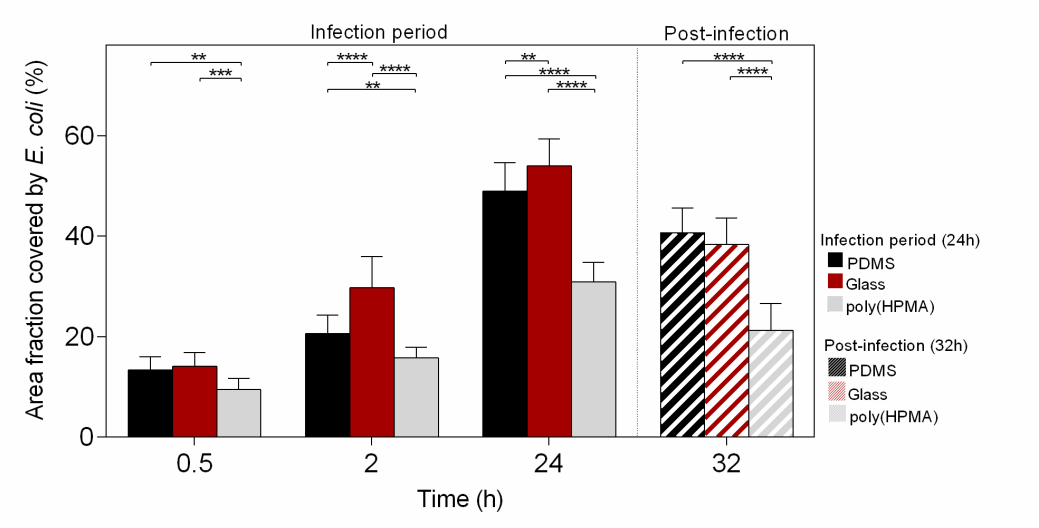

Figure 7.3. Percentage of surface area covered by *Escherichia coli* JM109(DE3) during the infection period (up to 24 h) and post-infection (32 h) on PDMS (■ and ▨, respectively), glass (■ and ▧, respectively) and poly(HPMA) brushes (■ and ▨, respectively). Standard deviations for three independent samples are presented. Statistical significance for all the surfaces at each time point was evaluated by one-way analysis of variance (one-way ANOVA, Tukey's post hoc test) (**** $P < 0.0001$, *** $P < 0.001$, ** $P < 0.01$).

The cellular composition of biofilms is shown in Figure 7.4, where the total, viable and VBNC cell numbers are represented. The total cell count indicates that the polymer brush had about 61% and 33% less *E. coli* cells than PDMS and glass, respectively, at the end of the infection period (24 h). Total cell counts were generally reduced (on average 83%) in the post-infection period, indicating that cell growth was lower than detachment during this period. The total cell number was reduced by 87% and 80% in the brush when compared to PDMS and glass respectively, at the end of the post-infection period ($P < 0.0001$) (Figure 7.4a). The reduction in the number of bacterial cells adhered to the brush is in agreement with what was observed in a previous work [22], in which the adhesion of *Yersinia pseudotuberculosis* to seven types of brushes was evaluated by single-cell force spectroscopy. The polymer brushes with good resistance to protein adsorption, such as poly(HPMA), greatly reduced the work necessary to detach bacteria from the brushes.

In order to determine the cellular composition of the biofilm, the Live/Dead® (L/D) *Bac*Light™ assay was used. Cells were stained with the green-fluorescent dye SYTO® 9, which penetrates both intact cells and those with a damaged membrane. The number of dead cells is determined by staining with the red-fluorescent dye propidium iodide, which can only penetrate cells with damaged membranes. The number of culturable cells was determined by plate counting and the number of VBNC cells was calculated by the difference between the viable cells

(obtained with the Live/Dead assay) and the culturable cells [4, 5].

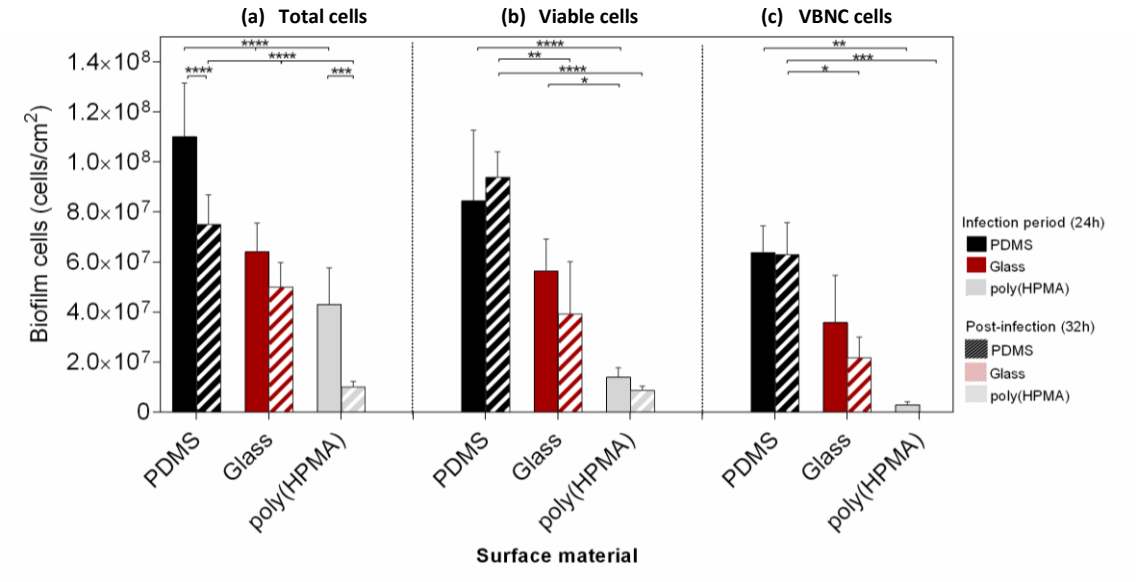

Figure 7.4. Number of total **(a)**, viable **(b)**, and viable but nonculturable (VBNC) **(c)** cells at the end of the infection period (24 h) and post-infection (32 h) on PDMS (■ and ▨, respectively), glass (■ and ▨, respectively) and poly(HPMA) brushes (■ and ▨, respectively). Standard deviations for three independent samples are presented. Statistical significance for all the surfaces at each time point was evaluated by one-way analysis of variance (one-way ANOVA, Tukey's post hoc test) (**** $P < 0.0001$, *** $P < 0.001$, ** $P < 0.01$, * $P < 0.05$).

During the infection phase, cell viability on the polymer brush was on average 80% lower than on PDMS and glass (Figure 7.4b, $P < 0.05$). This viability was not affected during the post-infection period. These results are in agreement with a previous study revealing that the poly(HPMA) was effective in inhibiting biofilm formation by opportunistic pathogens such as *Pseudomonas aeruginosa* [38]. On that study, most of the residual bacteria adhered to surfaces coated with this polymer brush were dead. It is unlikely that either the polymer or its brushes could cause any bacterial death due the biocompatibility of poly(HPMA) and the fact that the chains are covalently bound to the surface [17]. This suggests a passive attachment of already dead or injured cells [38]. The mechanism of action of these polymer brushes is to introduce a barrier to adsorption by creating an entropic repellent force which prevents the adhesion of macromolecules and cells. In previous studies using single-cell force spectroscopy, it was demonstrated that adhesion forces between a bacterium and the brush are so weak that cells are swept away from the surface by the flow [22]. This means that strongly attached cells are positively selected on the surface of the brush. Since the biofilms were formed over a 24 h period with medium recirculation (no fresh medium was added), nutrient depletion and accumulation of toxic metabolism products probably occurred. These conditions may have triggered some cell

death in all of the experiments (roughly 20% of the cells recovered from the PDMS or glass surfaces were dead). It is known that *E. coli* cells facing stress conditions show alterations in membrane permeability [39, 40], changes in zeta potential [41, 42], and morphological changes [35, 43]. Increased membrane permeability may lead to the release of intracellular molecules that increase the adhesion force, and modification of the zeta potential can also affect the adhesion energy. Some changes in cell morphology increase the cell surface area, thus increasing the probability of interaction between stressed cells and the brush. Some of these alterations in dead or senescent cells may explain a positive selection of these cells on the surface of the polymer brush.

VBNC cells are extremely important in clinical scenarios. These cells are not detected with conventional plate count techniques, leading to an underestimation of total viable cells in clinical samples. Since these cells can become resistant to antibiotics and can resuscitate and reinitiate infections, they are considered reservoirs of pathogenic bacteria [4]. Figure 7.4c shows that a higher number of VBNC cells was found on PDMS and glass when compared to the polymer brush ($P < 0.05$). A reduction of 94% was obtained for the brush during the infection period and VBNC cells were completely eliminated in the post-infection period. This is very significant as the results obtained after the end of the infection period suggest that the potential for the biofilm cells to develop antibiotic resistance is decreased (because the VBNC cell number is significantly lower in the brush and also the viable cell number is decreased). Additionally, the infectivity of the biofilm is reduced as VBNC cells were eliminated in the post-infection period.

The architectural differences between the biofilms formed in all surface at the end of the infection phase (24 h) and after the post-infection period (32 h) were analyzed by CLSM. After the infection period, it was possible to visualize thick biofilms on PDMS and glass surfaces (Figures 7.5a, b and g). Conversely, sparse biofilms composed by small, isolated cell clusters were observed on the poly(HPMA) brush (Figure 7.5c), suggesting that the brushes interfered with the ability to attach EPS. In the post-infection period, an increase in biofilm thickness was observed in all surfaces (Figures 5d, e, f and g) and "mushroom" structures were more evident on the brush (Figure 5f), as previously reported for *P. aeruginosa* [44]. Since the total cell counts in all of the tested surfaces decreased after the infection period and the biofilm thickness increased, it is possible that the biofilms have adopted a spatial organization with lower cell density. This adaptation in biofilm architecture may enable biofilm cells to have better access to nutrients since a more porous matrix will facilitate the mass transfer of nutrients to the inner cells of the biofilm [45].

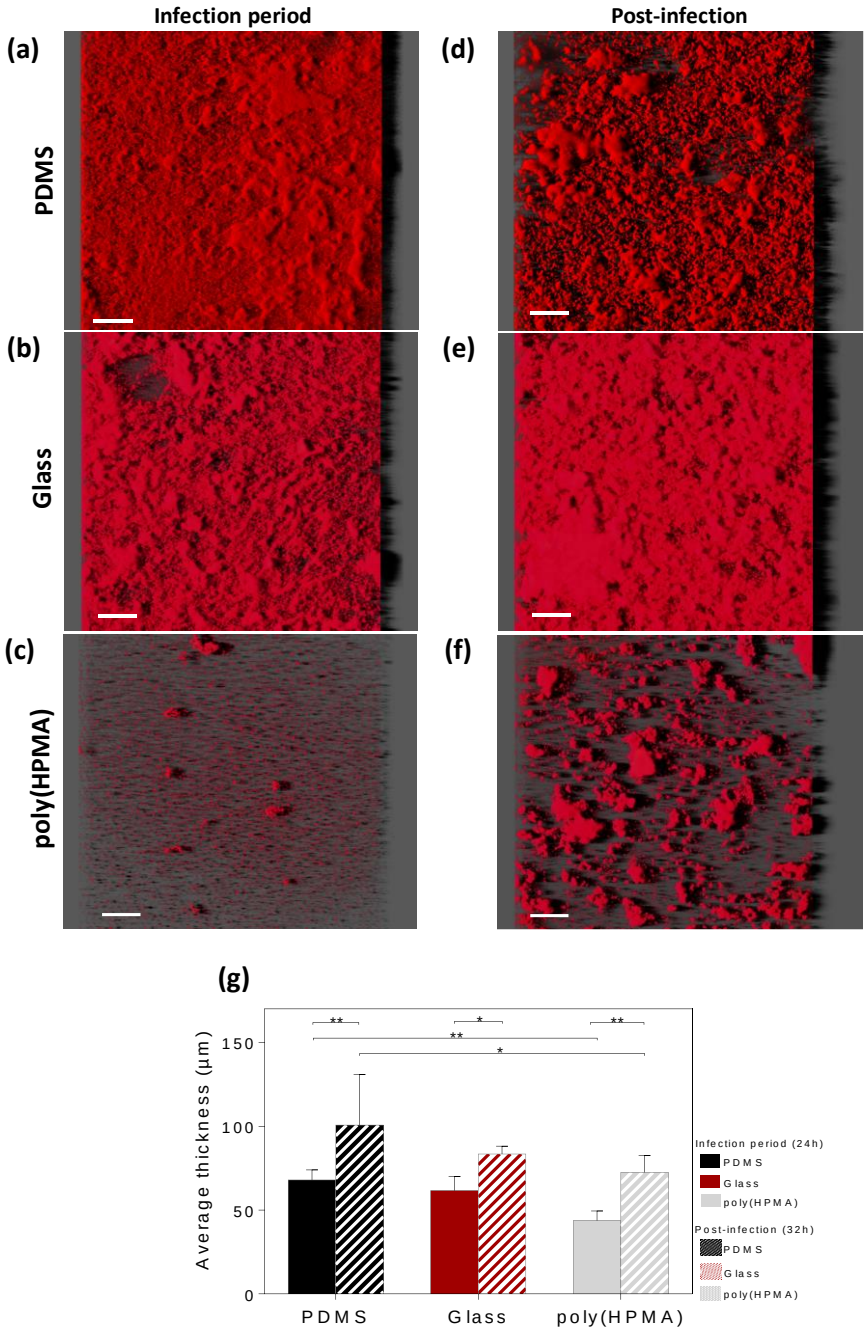

Figure 7.5. 3D-projections of *Escherichia coli* JM109(DE3) biofilms formed on PDMS, glass and poly(HPMA) brushes (obtained from confocal z stacks using IMARIS software). The representative images present an aerial view of the biofilms formed at the end of the infection period (24 h) (**a**, **b** and **c**) and post-infection (32 h) (**d**, **e** and **f**) (shadow projection on the right). The white scale bar corresponds to 200 µm. Average thickness (**g**) of *Escherichia coli* JM109(DE3) biofilms developed during the infection period and post-infection PDMS (■ and ▨, respectively), glass (■ and ▨, respectively) and poly(HPMA) brushes (■ and ▨, respectively). Standard deviations for three independent samples are presented. Statistical significance for all the surfaces at each time point was evaluated by one-way analysis of variance (one-way ANOVA, Tukey's post hoc test) (** $P < 0.01$, * $P < 0.05$).

A study from Drescher et al. [46] demonstrated that surface materials have the capacity to modify the morphology of *P. aeruginosa* in dynamic systems, leading to the formation of 3D streamers. A biofilm model designed to study the relationship between the structural heterogeneity of multispecies biofilms and hydrodynamics also showed (by CLSM analysis) that bacteria formed reproducible and stable structures consisting of cell clusters and interstitial channels [47, 48]. Thus, biofilms are dynamic habitats that constantly adapt in response to environmental cues such as nutrient availability or hydrodynamics, as previously shown for *E. coli* [29].

The flow rate used in these experiments induces a shear rate of 15/s, which is common in urinary catheters [25]. In this situation, the corresponding shear stress is 0.01 Pa as determined by computational fluid dynamics (CFD) [49]. Previous studies using CFD have shown that a shear stress of 0.01 Pa can also be found in some problematic areas of ureteric stents that are prone to bacterial accumulation and encrustation [50, 51]. This suggests that the results obtained in this study may be applicable to different biomedical devices used in the urinary tract such as catheters and stents.

7.4. Conclusions

Prevention of bacterial adhesion to surfaces through anti-adhesive coatings is one of the simplest and potentially most cost-effective way to delay biofilm formation and subsequent infections in biomedical devices. Few studies on biomaterials assess the efficacy of new antifouling surfaces under conditions that mimic real scenarios, particularly regarding hydrodynamics, which is a critical step in the translation of research into practical applications. Here, the poly(HPMA) brush showed reduced biofilm formation when compared to PDMS, a common construction material for urinary catheters. Importantly, not only the total and viable cell counts were decreased but also the number of VBNC cells was reduced. These cells are particularly important as they are probably more resistant to antimicrobial treatment and may resuscitate under appropriate conditions. After a simulated infection period when bacteria were circulated into the system, an additional period was analysed where sterile urine was flown into the system. Results suggest that when the bladder infection is cleared, by the immune system and/or antibiotic treatment, VBNC cells are no longer detected on the biofilms formed on the polymer brush as they are probably washed away given their weak attachment to the brush. This is a further indication that biofilms formed on this surface may be more susceptible to antibiotic treatment and may have a reduced potential to act as a source for new infections upon changing environmental conditions.

7.5. References

1. Ramstedt, M.; Ribeiro, I. A.; Bujdakova, H.; Mergulhão, F. J.; Jordao, L.; Thomsen, P.; Alm, M.; Burmølle, M.; Vladkova, T.; Can, F., Evaluating efficacy of antimicrobial and antifouling materials for urinary tract medical devices: challenges and recommendations. *Macromolecular Bioscience* **2019,** *19* (5), 1800384.
2. O'Toole, G.; Kaplan, H. B.; Kolter, R., Biofilm formation as microbial development. *Annual Reviews in Microbiology* **2000,** *54* (1), 49-79.
3. Hall, C. W.; Mah, T.-F., Molecular mechanisms of biofilm-based antibiotic resistance and tolerance in pathogenic bacteria. *FEMS Microbiology Reviews* **2017,** *41* (3), 276-301.
4. Oliver, J. D., Recent findings on the viable but nonculturable state in pathogenic bacteria. *FEMS Microbiology Reviews* **2010,** *34* (4), 415-425.
5. Li, L.; Mendis, N.; Trigui, H.; Oliver, J. D.; Faucher, S. P., The importance of the viable but non-culturable state in human bacterial pathogens. *Frontier in Microbiology* **2014,** *5*, 258-258.
6. Bos, R.; Van der Mei, H. C.; Busscher, H. J., Physico-chemistry of initial microbial adhesive interactions - its mechanisms and methods for study. *FEMS Microbiology Reviews* **1999,** *23* (2), 179-230.
7. Nuzzo, R. G., Biomaterials: stable antifouling surfaces. *Nature Materials* **2003,** *2* (4), 207-208.
8. Roosjen, A.; Norde, W.; van der Mei, H. C.; Busscher, H. J. In *The use of positively charged or low surface free energy coatings versus polymer brushes in controlling biofilm formation*, Characterization of Polymer Surfaces and Thin Films, Berlin, Heidelberg, 2006//; Grundke, K.; Stamm, M.; Adler, H.-J., Eds. Springer Berlin Heidelberg: Berlin, Heidelberg, 2006; pp 138-144.
9. Busscher, H. J.; Weerkamp, A. H.; van der Mei, H. C.; van Pelt, A. W.; de Jong, H. P.; Arends, J., Measurement of the surface free energy of bacterial cell surfaces and its relevance for adhesion. *Applied and Environmental Microbiology* **1984,** *48* (5), 980-983.
10. Williams, D. F., On the nature of biomaterials. *Biomaterials* **2009,** *30* (30), 5897-5909.
11. Rodriguez-Emmenegger, C.; Brynda, E.; Riedel, T.; Houska, M.; Šubr, V.; Alles, A. B.; Hasan, E.; Gautrot, J. E.; Huck, W. T., Polymer brushes showing non-fouling in blood plasma challenge the currently accepted design of protein resistant surfaces. *Macromolecular Rapid Communications* **2011,** *32* (13), 952-957.
12. Rodriguez-Emmenegger, C.; Houska, M.; Alles, A. B.; Brynda, E., Surfaces resistant to fouling from biological fluids: towards bioactive surfaces for real applications. *Macromolecular Bioscience* **2012,** *12* (10), 1413-1422.
13. Blaszykowski, C.; Sheikh, S.; Thompson, M., Surface chemistry to minimize fouling from blood-based fluids. *Chemical Society Reviews* **2012,** *41* (17), 5599-5612.
14. Rodriguez Emmenegger, C.; Brynda, E.; Riedel, T.; Sedlakova, Z.; Houska, M.; Alles, A. B., Interaction of blood plasma with antifouling surfaces. *Langmuir* **2009,** *25* (11), 6328-6333.
15. Vorobii, M.; de los Santos Pereira, A.; Pop-Georgievski, O.; Kostina, N. Y.; Rodriguez-Emmenegger, C.; Percec, V., Synthesis of non-fouling poly [N-(2-hydroxypropyl) methacrylamide] brushes by photoinduced SET-LRP. *Polymer Chemistry* **2015,** *6* (23), 4210-4220.
16. Kopeček, J.; Bažilová, H., Poly[N-(2-hydroxypropyl)methacrylamide] - I. Radical polymerization and copolymerization. *European Polymer Journal* **1973,** *9* (1), 7-14.

17. Kopeček, J.; Kopečková, P., HPMA copolymers: Origins, early developments, present, and future. *Advanced Drug Delivery Reviews* **2010,** *62* (2), 122-149.

18. Duncan, R.; Vicent, M. J., Do HPMA copolymer conjugates have a future as clinically useful nanomedicines? A critical overview of current status and future opportunities. *Advanced Drug Delivery Reviews* **2010,** *62* (2), 272-282.

19. Chytil, P.; Koziolová, E.; Etrych, T.; Ulbrich, K., HPMA copolymer–drug conjugates with controlled tumor-specific drug release. *Macromolecular Bioscience* **2018,** *18* (1), 1700209.

20. Zhang, R.; Yang, J.; Zhou, Y.; Shami, P. J.; Kopeček, J., N-(2-Hydroxypropyl) methacrylamide copolymer–drug conjugates for combination chemotherapy of acute myeloid leukemia. *Macromolecular Bioscience* **2016,** *16* (1), 121-128.

21. Surman, F.; Riedel, T.; Bruns, M.; Kostina, N. Y.; Sedláková, Z.; Rodriguez-Emmenegger, C., Polymer brushes interfacing blood as a route toward high performance blood contacting devices. *Macromolecular Bioscience* **2015,** *15* (5), 636-646.

22. Rodriguez-Emmenegger, C.; Janel, S.; de los Santos Pereira, A.; Bruns, M.; Lafont, F., Quantifying bacterial adhesion on antifouling polymer brushes via single-cell force spectroscopy. *Polymer Chemistry* **2015,** *6* (31), 5740-5751.

23. Lopez-Mila, B.; Alves, P.; Riedel, T.; Dittrich, B.; Mergulhão, F. J.; Rodriguez-Emmenegger, C., Effect of shear stress on the reduction of bacterial adhesion to antifouling polymers. *Bioinspiration & Biomimetics* **2018,** *13* (6), 065001.

24. Alves, D. F.; Vaz, A. T.; Grainha, T.; Rodrigues, C. F.; Pereira, M. O., Design of an antifungal surface embedding liposomal amphotericin B through a mussel adhesive-inspired coating strategy. *Frontiers in Chemistry* **2019,** *7*, 431.

25. Bakker, D.; Van Der Plaats, A.; Verkerke, G.; Busscher, H.; Van Der Mei, H., Comparison of velocity profiles for different flow chamber designs used in studies of microbial adhesion to surfaces. *Applied and Environmental Microbiololgy* **2003,** *69* (10), 6280-6287.

26. Whitehead, K. A.; Olivier, S.; Benson, P. S.; Arneborg, N.; Verran, J.; Kelly, P., The effect of surface properties of polycrystalline, single phase metal coatings on bacterial retention. *International Journal of Food Microbiology* **2015,** *197*, 92-97.

27. Gomes, L.; Moreira, J.; Teodósio, J.; Araújo, J.; Miranda, J.; Simões, M.; Melo, L.; Mergulhão, F., 96-well microtiter plates for biofouling simulation in biomedical settings. *Biofouling* **2014,** *30* (5), 535-546.

28. Moreira, J.; Ponmozhi, J.; Campos, J.; Miranda, J. M.; Mergulhão, F., Micro-and macro-flow systems to study *Escherichia coli* adhesion to biomedical materials. *Chemical Engineering Science* **2015,** *126*, 440-445.

29. Teodósio, J.; Simões, M.; Melo, L.; Mergulhão, F., Flow cell hydrodynamics and their effects on *E. coli* biofilm formation under different nutrient conditions and turbulent flow. *Biofouling* **2011,** *27* (1), 1-11.

30. Brooks, T.; Keevil, C., A simple artificial urine for the growth of urinary pathogens. *Letters in Applied Microbiology* **1997,** *24* (3), 203-206.

31. Koseoglu, H.; Aslan, G.; Esen, N.; Sen, B. H.; Coban, H., Ultrastructural stages of biofilm development of *Escherichia coli* on urethral catheters and effects of antibiotics on biofilm formation. *Urology* **2006,** *68* (5), 942-946.

32. Velraeds, M. M.; Van de Belt-Gritter, B.; Van der Mei, H.; Reid, G.; Busscher, H., Interference in initial adhesion of uropathogenic bacteria and yeasts to silicone rubber by a *Lactobacillus acidophilus* biosurfactant. *Journal of Medical Microbiology* **1998,** *47* (12), 1081-1085.

33. Barbosa, J.; Cuppini, M.; Flach, J.; Steffens, C.; Cansian, R. L.; Toniazzo, G., Removal of *Escherichia coli* in boning knives with different sanitizers. *LWT-Food Science and Technology* **2016,** *71*, 309-315.

34. Winkelströter, L. K.; Gomes, B. C.; Thomaz, M. R.; Souza, V. M.; De Martinis, E. C., *Lactobacillus sakei* 1 and its bacteriocin influence adhesion of *Listeria monocytogenes* on stainless steel surface. *Food Control* **2011,** *22* (8), 1404-1407.

35. Gomes, L.; Silva, L.; Simões, M.; Melo, L.; Mergulhão, F., *Escherichia coli* adhesion, biofilm development and antibiotic susceptibility on biomedical materials. *Journal of Biomedical Materials Research Part A* **2015,** *103* (4), 1414-1423.

36. Heydorn, A.; Nielsen, A. T.; Hentzer, M.; Sternberg, C.; Givskov, M.; Ersbøll, B. K.; Molin, S., Quantification of biofilm structures by the novel computer program COMSTAT. *Microbiology* **2000,** *146* (10), 2395-2407.

37. Aryal, B.; Neuner, G., Leaf wettability decreases along an extreme altitudinal gradient. *Oecologia* **2010,** *162* (1), 1.

38. Rodriguez-Emmenegger, C.; Decker, A.; Surman, F.; Preuss, C. M.; Sedláková, Z.; Zydziak, N.; Barner-Kowollik, C.; Schwartz, T.; Barner, L., Suppressing *Pseudomonas aeruginosa* adhesion via non-fouling polymer brushes. *Rsc Advances* **2014,** *4* (110), 64781-64790.

39. Rowlett, V. W.; Mallampalli, V. K.; Karlstaedt, A.; Dowhan, W.; Taegtmeyer, H.; Margolin, W.; Vitrac, H., Impact of membrane phospholipid alterations in *Escherichia coli* on cellular function and bacterial stress adaptation. *Journal of Bacteriology* **2017,** *199* (13), e00849-16.

40. Li, J.; Ma, L.; Liao, X.; Liu, D.; Lu, X.; Chen, S.; Ye, X.; Ding, T., Ultrasound-induced *Escherichia coli* O157: H7 cell death exhibits physical disruption and biochemical apoptosis. *Frontiers in Microbiology* **2018,** *9*, 2486.

41. Halder, S.; Yadav, K. K.; Sarkar, R.; Mukherjee, S.; Saha, P.; Haldar, S.; Karmakar, S.; Sen, T., Alteration of Zeta potential and membrane permeability in bacteria: a study with cationic agents. *SpringerPlus* **2015,** *4* (1), 672.

42. Shun-Kai, Y.; Khatijah, Y.; Warren, T.; Riaz, A.; Alhosani, M. S.; Aisha, A.; Swee-Hua-Erin, L.; Kok-Song, L., Lavender essential oil induces oxidative stress which modifies the bacterial membrane permeability of carbapenemase producing *Klebsiella pneumoniae*. *Scientific Reports* **2020,** *10* (1).

43. Uzoechi, S. C.; Abu-Lail, N. I., The effects of β-lactam antibiotics on surface modifications of multidrug-resistant *Escherichia coli*: a multiscale approach. *Microscopy and Microanalysis:* **2019,** *25* (1), 135-150.

44. Rzhepishevska, O.; Hakobyan, S.; Ruhal, R.; Gautrot, J.; Barbero, D.; Ramstedt, M., The surface charge of anti-bacterial coatings alters motility and biofilm architecture. *Biomaterials Science* **2013,** *1* (6), 589-602.

45. Moreira, J.; Teodósio, J.; Silva, F.; Simões, M.; Melo, L.; Mergulhão, F., Influence of flow rate variation on the development of *Escherichia coli* biofilms. *Bioprocess and Biosystems Engineering* **2013,** *36* (11), 1787-1796.

46. Drescher, K.; Shen, Y.; Bassler, B. L.; Stone, H. A., Biofilm streamers cause catastrophic disruption of flow with consequences for environmental and medical systems. *Proceedings of the National Academy of Sciences* **2013,** *110* (11), 4345-4350.

47. Stoodley, P.; deBeer, D.; Lewandowski, Z., Liquid flow in biofilm systems. *Applied and Environmental Microbiology* **1994,** *60* (8), 2711-2716.

48. Stoodley, P.; Yang, S.; Lappin-Scott, H.; Lewandowski, Z., Relationship between mass transfer coefficient and liquid flow velocity in heterogenous biofilms using microelectrodes and confocal microscopy. *Biotechnology and Bioengineering* **1997,** *56* (6), 681-688.

49. Moreira, J.; Araújo, J.; Miranda, J. M.; Simões, M.; Melo, L.; Mergulhão, F., The effects of surface properties on *Escherichia coli* adhesion are modulated by shear stress. *Colloids and Surfaces B: Biointerfaces* **2014,** *123*, 1-7.

50. Mosayyebi, A.; Yue, Q. Y.; Somani, B. K.; Zhang, X.; Manes, C.; Carugo, D., Particle accumulation in ureteral stents is governed by fluid dynamics: in vitro study using a "Stent-on-Chip" model. *Journal of Endourology* **2018,** *32* (7), 639-646.

51. Mosayyebi, A.; Lange, D.; Yann Yue, Q.; Somani, B.; Zhang, X.; Manes, C.; Carugo, D., Reducing deposition of encrustation in ureteric stents by changing the stent architecture: A microfluidic-based investigation. *Biomicrofluidics* **2019,** *13* (1), 014101.

7.6. Supplementary material

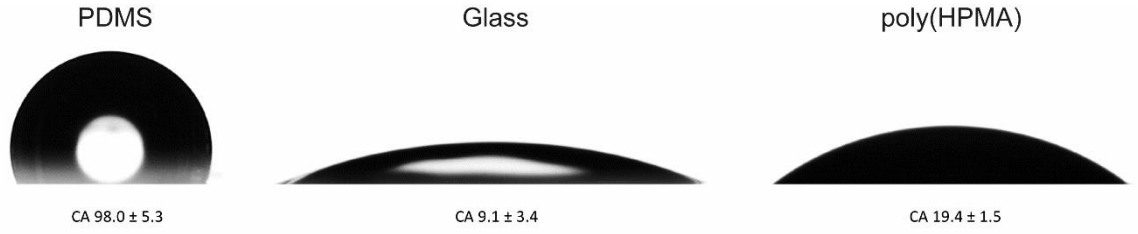

Figure S 7.1. Contact angle images for water droplets on polydimethylsiloxane (PDMS), glass and poly(HPMA) brushes.

8. Efficacy of a poly(MeOEGMA) brush on the prevention of *Escherichia coli* biofilm formation and susceptibility [i]

Abstract

Urinary tract infections are one of the most common hospital-acquired infections, and they are often associated with biofilm formation in indwelling medical devices such as catheters and stents. This study aims to investigate the antibiofilm performance of a polymer brush [poly[oligo(ethylene glycol) methyl ether methacrylate]-poly(MeOEGMA), and evaluate its effect on the antimicrobial susceptibility of *Escherichia coli* biofilms formed on that surface. Biofilms were formed in a parallel plate flow chamber (PPFC) for 24 h under the hydrodynamic conditions prevailing in urinary catheters and stents and challenged with ampicillin. Results obtained with the brush were compared to those obtained with two control surfaces, polydimethylsiloxane (PDMS) and glass. The polymer brush reduced by 57% the surface area covered by *E. coli* after 24 h, as well as the number of total adhered cells. The antibiotic treatment potentiated cell death and removal, and the total cell number was reduced by 88%. Biofilms adapted their architecture, and cell morphology changed to a more elongated form during that period. This work suggests that the poly(MeOEGMA) brush has potential to prevent bacterial adhesion in urinary tract devices like ureteral stents and catheters, as well as in eradicating biofilms developed in these biomedical devices.

[i] The content of this chapter was adapted from the following publication:

Alves P, Gomes LC, Rodríguez-Emmenegger C, Mergulhão FJ (**2020**) Efficacy of a poly(MeOEGMA) brush on the prevention of *Escherichia coli* biofilm formation and susceptibility. *Antibiotics*, 9(5), 216. Doi: 10.3390/antibiotics9050216

8.1. Introduction

Bacterial biofilms are a severe problem in the pathogenesis of biomaterial-associated infections (BAI), leading to significant patient morbidity and mortality, and high costs to health services [1, 2]. Over the past century, the use of medical devices, such as catheters, prosthetic joints, stents, artificial heart valves, pacemakers and other implants, has increased dramatically, which may result in BAI [3, 4]. According to the American National Institutes of Health, the development and persistence of biofilms are responsible for 75% of all human bacterial infections [1]. Catheter-associated urinary tract infection (CAUTI) is one of the most common hospital-acquired infections [5, 6] where *Escherichia coli* plays a key role due to its ability to adhere to biomaterials [7-10]. *E. coli* was also shown to persist and regrow after antibiotic exposure due to many factors, including reduced penetration of antibiotics in biofilms and/or cellular extrusion of drugs [7]. This may be due to the fact that biofilm cells produce a complex polymeric matrix, which protects the biofilm from antibiotic penetration and whose structure is strongly influenced by the substratum on which the biofilm forms [11, 12] and by the bulk liquid phase which flows over the biofilm [13, 14].

The high resistance of biofilms to conventional antibiotic therapy has driven research into the development of novel surfaces to decrease the attachment of microorganisms and consequent biofilm formation [15, 16]. Polymer brushes have been developed to prevent the adsorption of biomolecules and the adhesion process by limiting the contact of substratum with living bacteria [17-19], which is particularly relevant in biomedical applications [20-22]. Furthermore, several polymer brushes based on 2-hydroxyethyl methacrylate (HEMA), oligo(ethylene glycol), 2-hydroxyethyl acrylamide (HEAA) [23], oxazolines [24], carboxybetaines, and N-(2-hydroxypropyl) methacrylamide (HPMA), including the one tested in this work (poly[oligo(ethylene glycol) methyl ether methacrylate], poly(MeOEGMA)), were shown to be resistant to the adsorption of compounds from human biological fluids such as blood plasma, urine, cerebrospinal fluid and saliva, as well as different cell lines and bacteria [17, 20, 25-28]. Moreover, a study using single-cell force spectroscopy demonstrated that antifouling polymer brushes can reduce the forces involved in bacterial attachment [29]. For instance, the force needed to detach *Yersinia pseudotuberculosis* was reduced over three orders of magnitude when comparing to Teflon or glass [29].

Besides the surface properties, the complex process of biofilm formation depends on multiple factors such as hydrodynamics and nutrient availability [30, 31]. Several platforms for biofilm studies have been developed over the past decades [32]. Parallel plate flow cells (PPFCs) have been used for the study of biofilm formation under environmentally relevant hydrodynamic conditions, enabling a better understanding of the factors affecting the initial bacterial adhesion, which is the onset of biofilm development, as well as the online monitoring of biofilm

development [14, 33, 34]. In a recent work using PPFC, two polymer brushes with well-known antifouling properties, poly(MeOEGMA) and poly(HPMA), reduced the adhesion of *E. coli* after 30 min over a relevant range of shear stresses (0.005 to 0.056 Pa), including the one typical of urinary catheters (shear rate of 15/s) (Chapter 6) [22]. Shear stress values within this range are also found in some problematic areas of ureteric stents that are prone to bacterial accumulation and encrustation [35, 36]. These polymer brushes also showed to be resistant to the adsorption of macromolecules from urine and serum, being promising surfaces to delay cell attachment in biomedical devices (Chapter 6-supplementary material). However, the mentioned investigation was performed using citrate buffer as liquid medium to enable a more accurate thermodynamic analysis of the initial adhesion process. For these reasons, it is important to perform biofilm formation assays using suitable medium that mimics the environment of interest since the fluid composition affects the behavior of pathogens involved in clinical infections [37, 38]. Thus, in Chapter 7 [41] of this thesis, was evaluated the performance of poly(HPMA) brush, in order to analyse the influence of a complex medium for long experiments (24 and 32 h) and the shear on the brush, using a PPFC. The biofilm showed to adapt its architecture considering the conditions and surfaces evaluated, in which, the polymer brush showed the ability to reduce biofilm formation. Although many studies were performed aiming to better understand the bacterial attachment to different surfaces, few consider the importance of shear flow in bacteria-surface interactions [13, 14, 21, 39, 40].

The purpose of the present work intends to evaluate the antifouling performance of the poly(MeOEGMA) brush on *E. coli* biofilm formation and antimicrobial susceptibility. This polymer brush was selected due to its resistance to protein adsorption and bacterial adhesion (up to 90% when compared to glass) [22]. A well-described PPFC system [14] was used where synthetic urine was flown to mimic the shear rate typically found in urinary catheters and ureteric stents. The effect of the polymer brush on biofilm architecture was analysed and compared with two control surfaces, polydimethylsiloxane (PDMS; a material commonly used for urinary catheters manufacture) and glass (surface used as a standard reference for adhesion studies). This work suggests that the poly(MeOEGMA) brush has the potential to reduce infections in urinary tract devices with high efficiency by reducing the biofilm growth and by making the biofilms formed in these biomedical devices more susceptible to the current antibiotic therapies.

8.2. Materials and methods

8.2.1. Test organism and culture conditions

E. coli JM109(DE3) from Promega (Madison, WI, USA) was selected for its good biofilm-forming capacity in the same platform [14, 22, 41] and similar biofilm-forming capacity of different *E. coli* clinical isolates [40].

Bacteria were grown for about 15-17 h at 37 °C in synthetic urine medium [42], as previously described in Chapter 7 - section 7.2.3. This overnight culture was used to prepare a suspension in synthetic urine medium at a final concentration of 7.6 x 10^7 cells/ml to be used in biofilm experiments.

8.2.2. Surface preparation

Bare glass microscope slides (VWR, Portugal) and polydimethylsiloxane (PDMS) (Sylgard 184, Dow Corning, USA) were used as control surfaces. Glass was the substrate where the poly(MeOEGMA) brushes were grafted as in the previous studies addressing bacterial adhesion [22]. Glass was selected due to its transparency, which facilitates microscopy. PDMS is one of the most widely used polymers in the fabrication of medical implants for the urinary tract [43]. PDMS was prepared as previously described in Chapter 3-section 3.2.2 and the poly(MeOEGMA) brushes were prepared via surface-initiated atom transfer radical polymerization according, described in Chapter 6-section 6.2.3.1. After preparation, round coupons of the poly(MeOEGMA) brush, PDMS and glass were sterilized by spraying with absolute ethanol (100%; Merck, Germany) for 5 min. Then, they were left to air-dried inside the laminar flow chamber and fixed to the bottom plate of the PPFC (Chapter 6-section 6.2.7).

8.2.3. Biofilm assays

The bacterial suspension was recirculated through the PPFC system at 2 ml/s, which corresponds to the shear rate of 15/s found in urinary catheters [44]. As determined by computational fluid dynamics (CFD), the corresponding shear stress is 0.01 Pa [14] and previous studies revealed that this shear stress value can also be found in some problematic sites of ureteral stents that are prone to bacterial accumulation and encrustation [35, 36].

Biofilm development at 37 °C was monitored in real-time with microscopic images acquired using the Nikon Eclipse LV100 microscope connected to a camera (Nikon digital sight DS-Ri 1, Japan) at different time points (0.5, 2 and 24 h). As it has been reported that *E. coli* biofilms in urinary catheters are completely mature in 24 h [7], after that period the *E. coli* suspension was removed from the system and pre-warmed, sterile, synthetic urine to a concentration equivalent

to 5× MBIC (minimal biofilm inhibitory concentration) of ampicillin (250 μg/ml, diluted in synthetic urine) [45] was flown on the system for 8 h at the same shear rate. Ampicillin (AppliChem, Germany) was used in the present work since it is an antibiotic commonly prescribed to treat CAUTIs [46]. Brightfield microscopy images were also acquired after the ampicillin treatment (the 32-h time point). The percentage of surface area covered by *E. coli* cells was calculated with the ImageJ software (version 1.38e; National Institutes of Health, EUA) for the 0.5, 2, 24 and 32 h time points as previously described Chapter 7-section 7.2.4.

8.2.4. Offline quantification of biofilm cells

Biofilms were developed for 24 h, and at the end of each experiment, the system was rinsed with synthetic urine to remove loosely attached cells. The flow cell was opened and the biofilm from each coupon was detached through the swabbing method [47, 48] and a biofilm cell suspension diluted in 0.85% NaCl was obtained. To assess biofilm culturability (colony forming units, CFU), the biofilm suspension was properly diluted and spread on plate count agar (PCA, Oxoid, England). Colony enumeration was carried out after overnight incubation at 37 °C and the final values were expressed as CFU/cm^2. The adhered cells were stained with 4′-6-diamidino-2-phenylindole (DAPI), which stains both viable and nonviable cells (Chapter 7-section 7.2.5). The viability of biofilm cells was determined with the Live/Dead® (L/D) *Bac*Light™ Bacterial Viability kit (Invitrogen Life Technologies, Alfagene, Portugal) as previously indicated in Chapter 7-section 7.2.5. All the samples were examined before (the 24 h time point) and after antibiotic exposure (the 32 h time point), in which a minimum of 20 fields of view of each stained sample was analyzed using the ImageJ software to estimate the total and viable cell numbers (expressed as cells/cm^2).

8.2.5. Optical coherence tomography (OCT)

In situ images of the biofilm structure were obtained with a Spectral Domain Optical Coherence Tomography (SD-OCT) system (Thorlabs GmbH, Dachau, Germany) with a central wavelength of 930 nm. The refractive index was set to 1.40, close to the refractive index of water (1.33), since water is the major component of biofilms [49]. Two-dimensional (2D) images were acquired after 24 h of biofilm formation and after the ampicillin treatment (the 32-h time point). The biofilm thickness profiles were determined in at least five images corresponding to different locations for each surface at different time points. For each image, a minimum of 25 points was analysed using the Thorlabs software tool.

8.2.6. Scanning electron microscopy (SEM)

The morphology of *E. coli* biofilms formed after 24 h and after exposure to ampicillin was analysed by SEM. Coupons were removed from the PPFC and gradually dehydrated with ethanol at different concentrations (10, 25, 40, 50, 70, 80, 90 and 100% v/v) [50]. The samples were then air-dried and sputter-coated with a palladium-gold thin film [12]. The biofilms were observed with a SEM/EDS system (FEI Quanta 400FEG ESEM/EDAX Genesis X4M, FEI Company, USA) in high-vacuum mode at 15 kV. Cell length was determined for each condition as described by Gomes et al. [12].

8.2.7. Statistical analysis

Experiments were carried out in triplicate using different *E. coli* overnight cultures. Graph production and statistical analysis were performed using GraphPad Prism 6.01 (La Jolla, USA). Data were presented as mean ± standard deviations. Statistical differences between the polymer brush and the control surfaces (PDMS and glass) were determined using one-way analysis of variance (ANOVA) followed by Tukey's multiple-comparison test.

8.3. Results and discussion

The main goal of the current study was to evaluate the performance of the poly(MeOEGMA) brush on *E. coli* biofilm development and antibiotic susceptibility under flow conditions similar to those found in urinary catheters and ureteral stents, where this bacterium has a significant impact. For that purpose, were used two different control surfaces, PDMS and glass. Biofilm development was followed for 24 h to more closely mimic a bladder infection with the continuous supply of bacteria. The biofilm growth was then monitored for an additional 8 h period where ampicillin was flown on the PPFC system to simulate the infection treatment with one of the most prescribed antibiotics for CAUTIs [46].

The area fraction covered by the biofilm was chosen as a representative measure of adhesion during biofilm growth (0.5, 2 and 24 h) and antibiotic treatment for an additional 8 h period (32 h) (Figure 8.1). Lower surface coverages were registered on the polymer brush when compared to PDMS and glass surfaces for all time points ($P < 0.01$). After 24 h, in the polymer brush, the surface coverage decreased by 60% on average compared to PDMS and glass ($P < 0.0001$). Regarding the ampicillin treatment, the biofilm-covered area increased slightly during the 8 hours of exposure (Figure 8.1). It can be noted that for the PDMS the increase of the area fraction covered by *E. coli* was about 46%, while for glass and the polymer brush surfaces, the increase reached 15% and 31%, respectively. Nevertheless, it is important to note that, even after

the antimicrobial treatment, the poly(MeOEGMA) brush was the most effective surface in reducing cell adhesion, with 50% and 65% fewer cells than PDMS and glass, respectively (P < 0.0001).

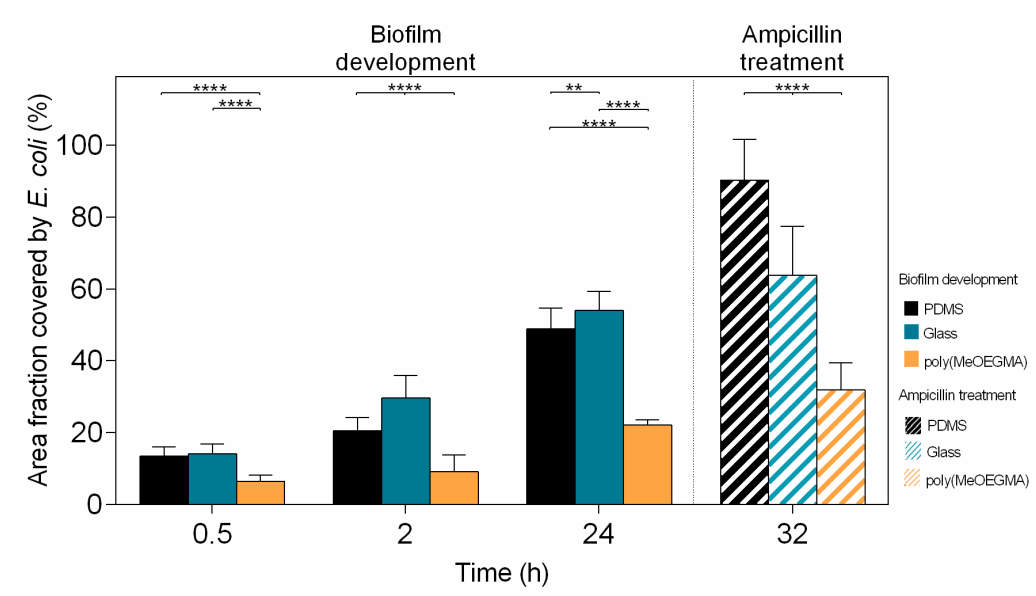

Figure 8.1. Surface area fraction covered during biofilm development (up to 24 h) and ampicillin treatment for an additional 8 h period (32 h) on polydimethylsiloxane (PDMS) (■ and ▧, respectively), glass (■ and ▨, respectively), and poly(MeOEGMA) brush (■ and ▨, respectively). Standard deviations for three independent samples are presented. Statistical significance for all the surfaces at each time point was determined by one-way ANOVA followed by Tukey's multiple-comparison test (**** for P < 0.0001, *** for P < 0.001, and ** for P < 0.01).

Figure 8.2 shows the number of total, viable and culturable cells on the tested surfaces before and after ampicillin exposure. The total (Figure 8.2a) and viable cell counts (Figure 8.2b) were determined by epifluorescence microscopy, whereas the biofilm culturable cells (Figure 8.2c) correspond to those that form colonies on agar-based media. Before treatment, PDMS had a higher number of total cells compared to glass and polymer brush (42% and 57% more cells, respectively; P < 0.0001, Figure 8.2a). The antibiotic treatment reduced the total cell amount on PDMS (43%) and glass (30%), but the most significant reduction was observed in the polymer brush (88%; P < 0.0001, Figure 8.2a). Even before the ampicillin treatment, the biofilm viability (*i.e.* the number of viable cells divided by the number of total cells) was 87% on average for the control surfaces and 52% for the polymer brush. The number of culturable cells (Figure 8.2c) was lower on glass and on the poly(MeOEGMA) brush when compared to PDMS surface, before and after antibiotic treatment (P < 0.0001, Figure 8.2c). Furthermore, the reduction of culturable cells after ampicillin treatment was about 28% on PDMS, 42% on glass and 71% on the polymer brush.

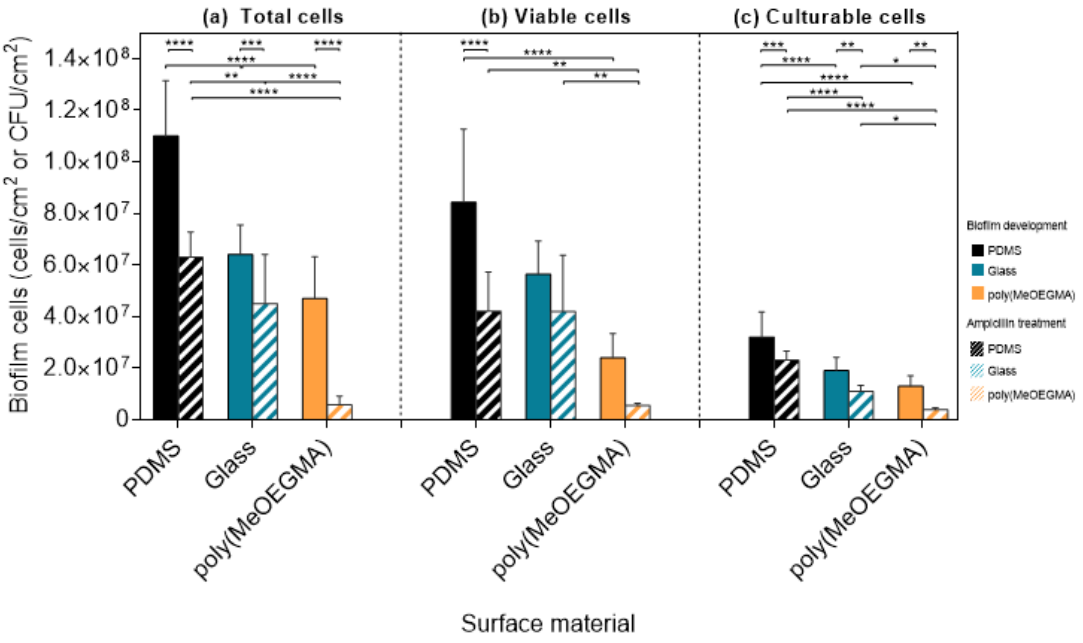

Figure 8.2. Number of **(a)** total, **(b)** viable, and **(c)** culturable cells after 24 h of biofilm development and after the ampicillin treatment on polydimethylsiloxane (PDMS) (■ and ▧, respectively), glass (■ and ▨, respectively), and poly(MeOEGMA) brush (■ and ▨, respectively). Standard deviations for three independent samples are presented. Statistical significance was determined by one-way ANOVA followed by Tukey's multiple-comparison test (**** for $P < 0.0001$, *** for $P < 0.001$, ** for $P < 0.01$ and * for $P < 0.05$).

E. coli adhered more to PDMS and glass surfaces than to poly(MeOEGMA) after 24 h of biofilm development, revealing for the first time the long-term antifouling behavior of this polymer brush under urinary flow conditions. Resistance to fouling was expected from coatings with dense grafts, such as the poly(MeOEGMA) brush, which presents long polymer chains that are capable to minimize long-range interactions by creating an effective steric barrier which prevents the adhesion of macromolecules and cells to the surface [51, 52]. Indeed, according to the extended Derjaguin–Landau–Verwey–Overbeek (DLVO) theory, attractive long-range interactions are reduced by introducing a water barrier with zero net charge and steric impediment in order to keep bacteria away from the surface [29]. The high wettability of the polymer brushes gives rise to an enthalpic barrier as water molecules have to be removed for proteins or bacteria to foul the surface [53]. In Chapter 6, was reported the strong antiadhesive effect of the polymer brush, with a reduction of 90% of cell adhesion in the first 30 min when citrate buffer was used as culture medium at the same hydrodynamic conditions. In the current work, synthetic urine medium was used to mimic the physiological conditions of the urinary system. An increase in adhesion on the polymer brush surface was evident when in contact with synthetic

urine. This is probably related to the use of a high nutrient medium that may have formed a conditioning film, promoting bacterial adhesion [20, 54]. Surface plasma resonance showed the resistance of poly(MeOEGMA) brush to the adsorption of proteins or other macromolecules present in human urine [22]. After 15 min, a wavelength shift of less than 15 ng/cm^2 was observed and upon 2 h of contact with urine, the fouling corresponded to less than 5% of the surface saturation (Chapter 6, supplementary material). This suggests that the antifouling properties of the polymer brush under the specific conditions of this work were probably surpassed by the intrinsic characteristics of *E. coli*, a motile organism containing bacterial appendages which may facilitate adhesion [55, 56].Concerning the susceptibility assays, the antibiotic ampicillin was able to remove cells from the biofilms on all of the tested surfaces, and the removal was higher with the polymer brush. The same effect of ampicillin was previously observed in 24-h *E. coli* biofilms formed on glass [45] where more than 50% of the sessile cells were removed after only 3 h of antibiotic exposure. The higher cell detachment from the polymer brush may be related to its weaker interaction with the bacterium [29, 41]. According to Rodríguez-Emmenegger et al. [29], the work necessary to detach *Y. pseudotuberculosis* (a Gram-negative bacterium as *E. coli*) from brushes such as poly(MeOEGMA) and poly(HPMA) was between 2 and 20% of the work employed on glass. Besides its effect on cell removal, the antibiotic circulating into the PPFC system also promoted a higher reduction in the number of culturable cells of poly(MeOEGMA) brush compared to PDMS and glass surfaces.

OCT was the imaging technique selected to analyse the spatial distribution of biofilms developed on the surfaces and determine their thickness before and after antibiotic treatment (Figure 8.3). The 2D-cross sectional scans (Figure 8.3a) show the biofilm mass over the surface material represented by the white line. Figure 8.3b presents the average biofilm thickness values determined from the acquired 2D scans. The OCT cross-sectional views confirmed that after 24 h of biofilm development, the polymer brush showed a lower amount of biofilm compared to PDMS and glass (Figure 8.3a). Additionally, the representative OCT image of the biofilm formed on the polymer brush showed that this surface had less biofilm than the remaining surfaces, as previously revealed by brightfield microscopy (Figure 8.1). It is possible to conclude from figure 8.3b that, prior to the ampicillin treatment, the biofilm formed on the poly(MeOEGMA) brush was thinner than those formed on PDMS and glass (61% and 40% thinner, respectively; $P < 0.0001$). However, after the antibiotic treatment, an increase in the biofilm amount was observed in all surfaces (Figure 3A) and higher thickness values were obtained compared to pre-treatment (11% higher for PDMS, 21% for glass and 62% for the polymer brush; $P < 0.05$, Figure 8.3b). It is likely that the biofilm formed on the polymer brush experienced spatial reorganization, giving

rise to aggregates that may be responsible for increasing the biofilm thickness.

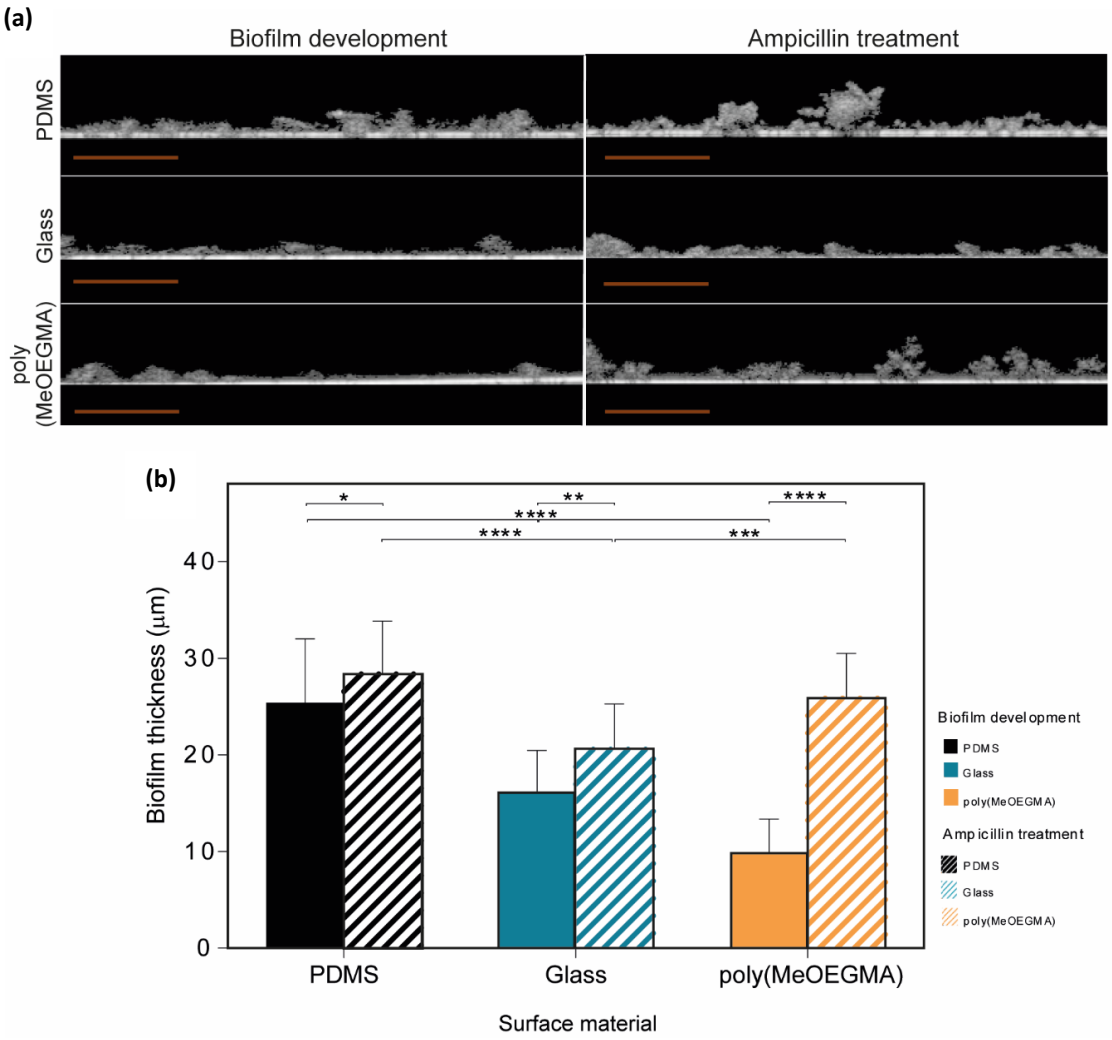

Figure 8.3. Optical coherence tomography (OCT) analysis of biofilms formed on polydimethylsiloxane (PDMS), glass and poly(MeOEGMA) brush: **(a)** representative 2D cross-sectional views of biofilm structures (orange scale bars correspond to 200 µm), and **(b)** biofilm thickness after biofilm development and ampicillin treatment on polydimethylsiloxane (PDMS) (■ and ▧, respectively), glass (■ and ▨, respectively) and poly(MeOEGMA) brush (■ and ▨, respectively). Standard deviations obtained from three replicates of each sample are represented. Statistical significance was determined by one-way ANOVA followed by Tukey's multiple-comparison test (**** for $P < 0.0001$, *** for $P < 0.001$, ** for $P < 0.01$, and * for $P < 0.05$).

SEM images showed that after biofilm growth, the number of adhered cells was higher on PDMS and glass than on the polymer brush (Figure 8.4a), which corroborates the quantification performed by epifluorescence microscopy (Figure 8.2a). Concerning the biofilms obtained after antibiotic exposure, higher surface coverages were observed on all tested surfaces (Figure 8.4a), particularly on the polymer brush, where some cell clusters were also visible, which supports the results obtained by brightfield microscopy (Figure 8.1) and OCT (Figure 8.3a). From

SEM micrographs, it was also possible to determine the size distribution of biofilm cells on the three surfaces (Figure 8.4b). An average cell length of 1.5 μm was obtained for untreated biofilms, regardless of the surface material. However, after ampicillin exposure, the sessile cells on the polymer brush had an elongated morphology when compared to glass (on average 29% longer) and PDMS (on average 46% longer). Indeed, the *E. coli* cells that adhered to poly(MeOEGMA) brush were between 2.1 and 6.1 μm (57% longer than the poly(MeOEGMA) untreated cells), while the cells adhered to glass measured between 1.5 and 4.2 μm (30% longer than untreated cells obtained from glass) and the cells adhered to PDMS measured between 0.7 and 4.9 μm (17% longer than untreated cells obtained from PDMS).

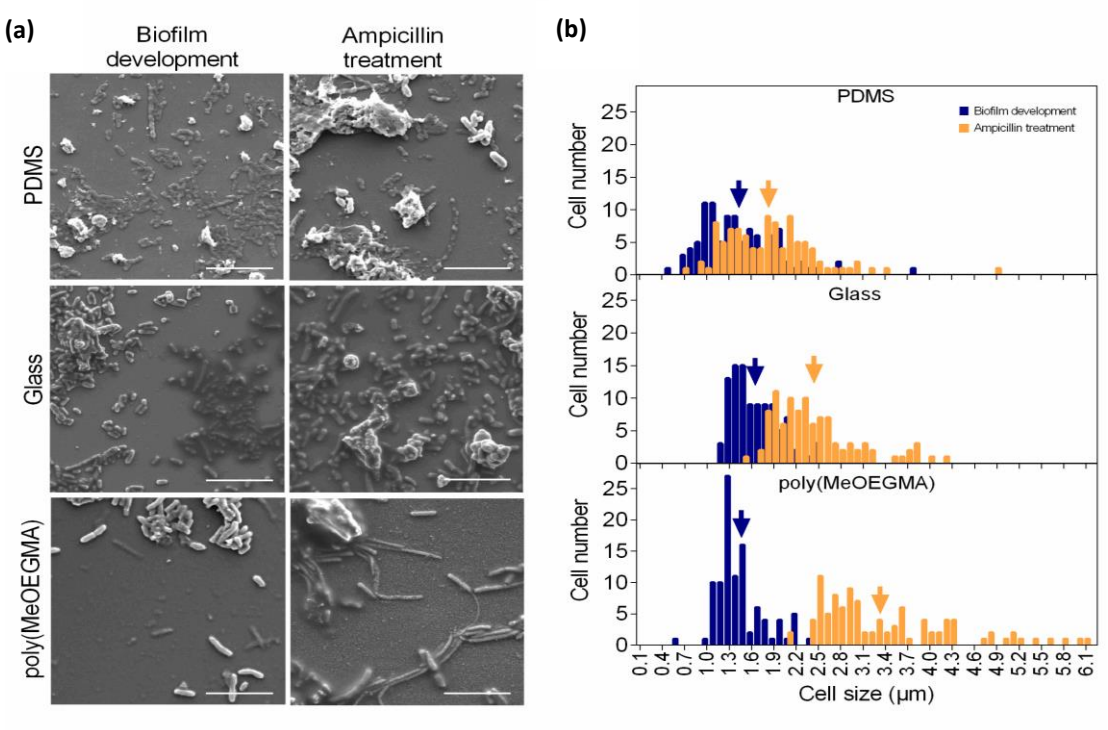

Figure 8.4. Scanning electron microscopy (SEM) analysis of biofilms formed after 24 h of development and after the ampicillin treatment on polydimethylsiloxane (PDMS), glass and poly(MeOEGMA) brush: **(a)** representative micrographs (magnification: 5000x; bars = 10 μm); **(b)** cell size distribution of biofilms before (■) and after ampicillin exposure (■). The arrows represent the average cell length determined from SEM micrographs for each experimental condition.

SEM analysis revealed that ampicillin-treated cells were more elongated than the untreated cells on all tested surfaces and formed cell clusters on the polymer brush. Also, the elongation phenomenon was more noticeable on the brush, indicating a higher effect of the antibiotic treatment on biofilm cells. Previous studies have shown that *E. coli* cells in contact with ampicillin, a β-lactam antibiotic which acts inhibiting the cell wall synthesis, may suffer

morphological changes and spatial rearrangement [12, 45, 57, 58]. These alterations may occur in four stages, including elongation, bulge formation, bulge stagnation and lysis [57]. The cluster formation and consequent increase in the biofilm thickness may be due to the overproduction of extracellular polymeric substances (EPS) in response to the osmotic stress resulting from cell-antibiotic interactions. Ionescu and Belkin [59] studied the *rpoS* function on *E. coli* strains and their findings suggest that the stress resistance is influenced by the presence of specific genes responsible for the EPS production. It has been reported that *rpoS* plays a major role in the osmotic-stress response of *E. coli* by activating the transcription of a high number of genes that provide osmo- and cross-protection against different stress factors [60, 61]. For *Enterococcus faecalis* (a bacterium responsible for CAUTIs as *E. coli* and typically susceptible to ampicillin), the formation of a complex 3D-biofilm structure in presence of antibiotics was also associated with a stress response of enterococcal biofilm cells, which promoted a rapidly reorganization of biofilm into highly structured microcolonies [62]. A recent work evaluated the effects of ampicillin on surface modifications of four multidrug-resistant *E. coli* strains and concluded that three of them suffered cell elongation, an increase in roughness and nanoscale adhesion forces, became more hydrophilic and increased biofilm formation [63].

Overall, our results show that this polymer brush has potential advantages in the prevention of *E. coli* adhesion and biofilm formation in urinary tract devices, enabling a more effective eradication of biofilms when combined with antibiotic treatment, thus reducing the risk of recurrent infections.

8.4. Conclusions

Biofilms causing CAUTIs resist antibiotic treatment and often require replacement of infected devices. Current strategies for developing infection-resistant biomaterials have gone through making them non-fouling, bactericidal or both. However, there are few studies that evaluate these new materials in conditions that mimic the real environment where they will be applied. In this study, special attention was paid to hydrodynamic and nutrient conditions since we believe these are critical parameters in translating research into practical applications. The antifouling performance that the poly(MeOEGMA) brush demonstrated in a previous work with citrate buffer was maintained here for a longer period of time. The ability of the polymer brush to significantly delay *E. coli* biofilm formation when compared to PDMS (a material commonly used in the manufacture of medical settings) makes it a very promising surface to prevent infections in urinary tract devices like urinary catheters and ureteral stents. This study also

suggests that the further grafting of active antimicrobial agents such as antibiotics onto the surface of poly(MeOEGMA) brush may favor the detachment of pre-formed biofilms due to the weakly adhering cells on the polymer brush.

8.5. References

1. Miquel, S.; Lagrafeuille, R.; Souweine, B.; Forestier, C., Anti-biofilm activity as a health issue. *Frontiers in Microbiology* **2016,** *7*, 592.

2. Bjarnsholt, T., The role of bacterial biofilms in chronic infections. *APMIS* **2013,** *121*, 1-58.

3. Lo, E.; Nicolle, L. E.; Coffin, S. E.; Gould, C.; Maragakis, L. L.; Meddings, J.; Pegues, D. A.; Pettis, A. M.; Saint, S.; Yokoe, D. S., Strategies to prevent catheter-associated urinary tract infections in acute care hospitals: 2014 update. *Infection Control & Hospital Epidemiology* **2014,** *35* (5), 464-479.

4. Hancock, V.; Ferrières, L.; Klemm, P., Biofilm formation by asymptomatic and virulent urinary tract infectious *Escherichia coli* strains. *FEMS Microbiology Letters* **2006,** *267* (1), 30-37.

5. Flores-Mireles, A. L.; Walker, J. N.; Caparon, M.; Hultgren, S. J., Urinary tract infections: epidemiology, mechanisms of infection and treatment options. *Nature Reviews Microbiology* **2015,** *13* (5), 269-284.

6. Umscheid, C. A.; Mitchell, M. D.; Doshi, J. A.; Agarwal, R.; Williams, K.; Brennan, P. J., Estimating the proportion of healthcare-associated infections that are reasonably preventable and the related mortality and costs. *Infection Control and Hospital Epidemiology* **2011,** *32* (2), 101-114.

7. Koseoglu, H.; Aslan, G.; Esen, N.; Sen, B. H.; Coban, H., Ultrastructural stages of biofilm development of *Escherichia coli* on urethral catheters and effects of antibiotics on biofilm formation. *Urology* **2006,** *68* (5), 942-946.

8. Shunmugaperumal, T., *Biofilm eradication and prevention: a pharmaceutical approach to medical device infections*. John Wiley & Sons: New Jersey, 2010.

9. Trautner, B. W.; Lopez, A. I.; Kumar, A.; Siddiq, D. M.; Liao, K. S.; Li, Y.; Tweardy, D. J.; Cai, C., Nanoscale surface modification favors benign biofilm formation and impedes adherence by pathogens. *Nanomedicine: Nanotechnology, Biology and Medicine* **2012,** *8* (3), 261-270.

10. Stamm , W. E.; Hooton , T. M., Management of urinary tract infections in adults. *New England Journal of Medicine* **1993,** *329* (18), 1328-1334.

11. Buijssen, K.; Oosterhof, J.; Basil, L.; Waters, M.; Duits, M.; Busscher, H.; van der Mei, H.; van der Laan, B., Influence of surface roughness on silicone rubber voice prostheses on *in vitro* biofilm formation and clinical lifetime in laryngectomised patients. *Clinical Otolaryngology* **2017,** *42* (6), 1235-1240.

12. Gomes, L. C.; Mergulhão, F. J., SEM analysis of surface impact on biofilm antibiotic treatment. *Scanning* **2017,** *2017*.

13. Teodósio, J.; Simões, M.; Melo, L.; Mergulhão, F., Flow cell hydrodynamics and their effects on *E. coli* biofilm formation under different nutrient conditions and turbulent flow. *Biofouling* **2011,** *27* (1), 1-11.

14. Moreira, J.; Araújo, J.; Miranda, J. M.; Simões, M.; Melo, L.; Mergulhão, F., The effects of surface properties on *Escherichia coli* adhesion are modulated by shear stress. *Colloids and Surfaces B: Biointerfaces* **2014,** *123*, 1-7.

15. Nuzzo, R. G., Biomaterials: stable antifouling surfaces. *Nature Materials* **2003,** *2* (4), 207-208.

16. Rodriguez-Emmenegger, C.; Brynda, E.; Riedel, T.; Houska, M.; Šubr, V.; Alles, A. B.; Hasan, E.; Gautrot, J. E.; Huck, W. T., Polymer brushes showing non-fouling in blood plasma challenge the currently accepted design of protein resistant surfaces. *Macromolecular Rapid Communications* **2011,** *32* (13), 952-957.

17. Rodriguez-Emmenegger, C.; Houska, M.; Alles, A. B.; Brynda, E., Surfaces resistant to fouling from biological fluids: towards bioactive surfaces for real applications. *Macromolecular Bioscience* **2012,** *12* (10), 1413-1422.

18. Ma, H.; Li, D.; Sheng, X.; Zhao, B.; Chilkoti, A., Protein-resistant polymer coatings on silicon oxide by surface-initiated atom transfer radical polymerization. *Langmuir* **2006,** *22* (8), 3751-3756.

19. Gautrot, J. E.; Trappmann, B.; Oceguera-Yanez, F.; Connelly, J.; He, X.; Watt, F. M.; Huck, W. T., Exploiting the superior protein resistance of polymer brushes to control single cell adhesion and polarisation at the micron scale. *Biomaterials* **2010,** *31* (18), 5030-5041.

20. Rodriguez-Emmenegger, C.; Decker, A.; Surman, F.; Preuss, C. M.; Sedláková, Z.; Zydziak, N.; Barner-Kowollik, C.; Schwartz, T.; Barner, L., Suppressing *Pseudomonas aeruginosa* adhesion via non-fouling polymer brushes. *Rsc Advances* **2014,** *4* (110), 64781-64790.

21. de los Santos Pereira, A.; Sheikh, S.; Blaszykowski, C.; Pop-Georgievski, O.; Fedorov, K.; Thompson, M.; Rodriguez-Emmenegger, C., Antifouling polymer brushes displaying antithrombogenic surface properties. *Biomacromolecules* **2016,** *17* (3), 1179-1185.

22. Lopez-Mila, B.; Alves, P.; Riedel, T.; Dittrich, B.; Mergulhao, F.; Rodriguez-Emmenegger, C., Effect of shear stress on the reduction of bacterial adhesion to antifouling polymers. *Bioinspiration & biomimetics* **2018**.

23. Zhao, C.; Zheng, J., Synthesis and characterization of poly(N-hydroxyethylacrylamide) for long-term antifouling ability. *Biomacromolecules* **2011,** *12* (11), 4071-4079.

24. Tauhardt, L.; Pretzel, D.; Kempe, K.; Gottschaldt, M.; Pohlers, D.; Schubert, U. S., Zwitterionic poly(2-oxazoline)s as promising candidates for blood contacting applications. *Polymer Chemistry* **2014,** *5* (19), 5751-5764.

25. Surman, F.; Riedel, T.; Bruns, M.; Kostina, N. Y.; Sedláková, Z.; Rodriguez-Emmenegger, C., Polymer brushes interfacing blood as a route toward high performance blood contacting devices. *Macromolecular Bioscience* **2015,** *15* (5), 636-646.

26. Rodriguez Emmenegger, C.; Brynda, E.; Riedel, T.; Sedlakova, Z.; Houska, M.; Alles, A. B., Interaction of blood plasma with antifouling surfaces. *Langmuir* **2009,** *25* (11), 6328-6333.

27. Riedel, T.; Riedelová-Reicheltová, Z.; Májek, P.; Rodriguez-Emmenegger, C.; Houska, M.; Dyr, J. E.; Brynda, E., Complete identification of proteins responsible for human blood plasma fouling on poly(ethylene glycol)-based surfaces. *Langmuir* **2013,** *29* (10), 3388-3397.

28. Tischer, T.; Rodriguez-Emmenegger, C.; Trouillet, V.; Welle, A.; Schueler, V.; Mueller, J. O.; Goldmann, A. S.; Brynda, E.; Barner-Kowollik, C., Photo-patterning of non-fouling polymers and biomolecules on paper. *Advanced Materials* **2014,** *26* (24), 4087-4092.

29. Rodriguez-Emmenegger, C.; Janel, S.; de los Santos Pereira, A.; Bruns, M.; Lafont, F., Quantifying bacterial adhesion on antifouling polymer brushes via single-cell force spectroscopy. *Polymer Chemistry* **2015,** *6* (31), 5740-5751.

30. Donlan, R. M., Biofilms: microbial life on surfaces. *Emerging Infectious Diseases* **2002,** *8* (9), 881.

31. Horn, H.; Reiff, H.; Morgenroth, E., Simulation of growth and detachment in biofilm systems under defined hydrodynamic conditions. *Biotechnology and Bioengineering* **2003,** *81* (5), 607-617.

32. Azeredo, J.; Azevedo, N. F.; Briandet, R.; Cerca, N.; Coenye, T.; Costa, A. R.; Desvaux, M.; Di Bonaventura, G.; Hébraud, M.; Jaglic, Z., Critical review on biofilm methods. *Critical Reviews in Microbiology* **2017,** *43* (3), 313-351.

33. Moreira, J.; Ponmozhi, J.; Campos, J.; Miranda, J. M.; Mergulhão, F., Micro-and macro-flow systems to study *Escherichia coli* adhesion to biomedical materials. *Chemical Engineering Science* **2015,** *126*, 440-445.

34. Gomes, L. C.; Moreira, J. M.; Araújo, J. D.; Mergulhão, F. J., Surface conditioning with *Escherichia coli* cell wall components can reduce biofilm formation by decreasing initial adhesion. *Interfaces* **2017,** *24*, 25.

35. Mosayyebi, A.; Lange, D.; Yann Yue, Q.; Somani, B.; Zhang, X.; Manes, C.; Carugo, D., Reducing deposition of encrustation in ureteric stents by changing the stent architecture: a microfluidic-based investigation. *Biomicrofluidics* **2019,** *13* (1), 014101.

36. Mosayyebi, A.; Yue, Q. Y.; Somani, B. K.; Zhang, X.; Manes, C.; Carugo, D., Particle accumulation in ureteral stents is governed by fluid dynamics: in vitro study using a "Stent-on-Chip" model. *Journal of Endourology* **2018,** *32* (7), 639-646.

37. Stewart, P. S., Biophysics of biofilm infection. *Pathogens and Disease* **2014,** *70* (3), 212-218.

38. Nauman, E. A.; Ott, C. M.; Sander, E.; Tucker, D. L.; Pierson, D.; Wilson, J. W.; Nickerson, C. A., Novel quantitative biosystem for modeling physiological fluid shear stress on cells. *Applied and Environmental Microbiology* **2007,** *73* (3), 699-705.

39. Rodesney, C. A.; Roman, B.; Dhamani, N.; Cooley, B. J.; Touhami, A.; Gordon, V. D., Mechanosensing of shear by *Pseudomonas aeruginosa* leads to increased levels of the cyclic-di-GMP signal initiating biofilm development. *Proceedings of the National Academy of Sciences* **2017**, 201703255.

40. Gomes, L.; Moreira, J.; Teodósio, J.; Araújo, J.; Miranda, J.; Simões, M.; Melo, L.; Mergulhão, F., 96-well microtiter plates for biofouling simulation in biomedical settings. *Biofouling* **2014,** *30* (5), 535-546.

41. Alves, P.; Gomes, L.; Vorobii, M.; Rodriguez-Emmenegger, C.; Mergulhão, F., The potential advantages of using a poly(HPMA) brush in urinary catheters: effects on biofilm cells and architecture. *Colloids and Surfaces B: Biointerfaces* **2020,** *(in press)*.

42. Brooks, T.; Keevil, C., A simple artificial urine for the growth of urinary pathogens. *Letters in applied microbiology* **1997,** *24* (3), 203-206.

43. Vagos, M. R.; Moreira, J. M. R.; Soares, O. S. G. P.; Pereira, M. F. R.; Mergulhão, F. J., Incorporation of carbon nanotubes in polydimethylsiloxane to control *Escherichia coli* adhesion. *Polymer Composites* **2019,** *40* (S2), E1697-E1704.

44. Velraeds, M. M.; Van de Belt-Gritter, B.; Van der Mei, H.; Reid, G.; Busscher, H., Interference in initial adhesion of uropathogenic bacteria and yeasts to silicone rubber by a *Lactobacillus acidophilus* biosurfactant. *Journal of Medical Microbiology* **1998,** *47* (12), 1081-1085.

45. Gomes, L.; Silva, L.; Simões, M.; Melo, L.; Mergulhão, F., *Escherichia coli* adhesion, biofilm development and antibiotic susceptibility on biomedical materials. *Journal of Biomedical Materials Research Part A* **2015,** *103* (4), 1414-1423.

46. Shah, K. J.; Cherabuddi, K.; Shultz, J.; Borgert, S.; Ramphal, R.; Klinker, K. P., Ampicillin for the treatment of complicated urinary tract infections caused by vancomycin resistant *Enterococcus spp* (VRE): a single-center university hospital experience. *International Journal of Antimicrobial Agents* **2017**.

47. Barbosa, J.; Cuppini, M.; Flach, J.; Steffens, C.; Cansian, R. L.; Toniazzo, G., Removal of *Escherichia coli* in boning knives with different sanitizers. *LWT - Food Science and Technology* **2016,** *71*, 309-315.

48. Winkelströter, L. K.; Gomes, B. C.; Thomaz, M. R. S.; Souza, V. M.; De Martinis, E. C. P., *Lactobacillus sakei* 1 and its bacteriocin influence adhesion of *Listeria monocytogenes* on stainless steel surface. *Food Control* **2011,** *22* (8), 1404-1407.

49. Romeu, M. J.; Alves, P.; Morais, J.; Miranda, J. M.; de Jong, E. D.; Sjollema, J.; Ramos, V.; Vasconcelos, V.; Mergulhão, F. J. M., Biofilm formation behaviour of marine filamentous cyanobacterial strains in controlled hydrodynamic conditions. *Environmental Microbiology* **2019,** *21* (11), 4411-4424.

50. Simões, M.; Pereira, M. O.; Vieira, M., The role of hydrodynamic stress on the phenotypic characteristics of single and binary biofilms of *Pseudomonas fluorescens*. *Water Science and Technology* **2007,** *55* (8-9), 437-445.

51. Halperin, A.; Fragneto, G.; Schollier, A.; Sferrazza, M., Primary versus ternary adsorption of proteins onto PEG brushes. *Langmuir* **2007,** *23* (21), 10603-10617.

52. Jeon, S.; Lee, J.; Andrade, J.; De Gennes, P., Protein - surface interactions in the presence of polyethylene oxide: I. Simplified theory. *Journal of Colloid Interface Science* **1991,** *142* (1), 149-158.

53. Sigal, G. B.; Mrksich, M.; Whitesides, G. M., Effect of surface wettability on the adsorption of proteins and detergents. *Journal of the American Chemical Society* **1998,** *120* (14), 3464-3473.

54. Li, J.; Kleintschek, T.; Rieder, A.; Cheng, Y.; Baumbach, T.; Obst, U.; Schwartz, T.; Levkin, P. A., Hydrophobic liquid-infused porous polymer surfaces for antibacterial applications. *ACS Applied Materials & Interfaces* **2013,** *5* (14), 6704-6711.

55. Mukherjee, J.; Karunakaran, E.; Biggs, C. A., Using a multi-faceted approach to determine the changes in bacterial cell surface properties influenced by a biofilm lifestyle. *Biofouling* **2012,** *28* (1), 1-14.

56. Vila, J.; Sáez-López, E.; Johnson, J.; Römling, U.; Dobrindt, U.; Cantón, R.; Giske, C.; Naas, T.; Carattoli, A.; Martínez-Medina, M., *Escherichia coli*: an old friend with new tidings. *FEMS Microbiology Reviews* **2016,** *40* (4), 437-463.

57. Yao, Z.; Kahne, D.; Kishony, R., Distinct single-cell morphological dynamics under beta-lactam antibiotics. *Molecular Cell* **2012,** *48* (5), 705-712.

58. Martinez, O. V.; Gratzner, H. G.; Malinin, T. I.; Ingram, M., The effect of some β-lactam antibiotics on *Escherichia coli* studied by flow cytometry. *Cytometry: The Journal of the International Society for Analytical Cytology* **1982,** *3* (2), 129-133.

59. Ionescu, M.; Belkin, S., Overproduction of exopolysaccharides by an *Escherichia coli* K-12 *rpoS* mutant in response to osmotic stress. *Applied and Environmental Microbiology* **2009,** *75* (2), 483-492.

60. Hengge-Aronis, R.; Lange, R.; Henneberg, N.; Fischer, D., Osmotic regulation of *rpoS*-dependent genes in *Escherichia coli*. *Journal of Bacteriology* **1993,** *175* (1), 259-265.

61. Weber, H.; Polen, T.; Heuveling, J.; Wendisch, V. F.; Hengge, R., Genome-wide analysis of the general stress response network in *Escherichia coli*: σS-dependent genes, promoters, and sigma factor selectivity. *Journal of Bacteriology* **2005,** *187* (5), 1591-1603.

62. Dale, J. L.; Nilson, J. L.; Barnes, A. M. T.; Dunny, G. M., Restructuring of *Enterococcus faecalis* biofilm architecture in response to antibiotic-induced stress. *npj Biofilms and Microbiomes* **2017,** *3* (1), 15.

63. Uzoechi, S. C.; Abu-Lail, N. I., The Effects of β-Lactam Antibiotics on Surface Modifications of Multidrug-Resistant *Escherichia coli:* A Multiscale Approach. *Microscopy and Microanalysis* **2019,** *25* (1), 135-150.

9. Concluding remarks and future perspectives

9.1. Concluding remarks

The main goal of this thesis was to have a deeper understanding of how the adhesion process of *E. coli* unfolds and to assess the antifouling performance of modified surfaces. Bacterial adhesion studies are important not only because they provide an understanding of the early stages of biofilm formation but also because they may provide clues for the development of more efficient biofilm control strategies.

The adhesion process and further biofilm development can be affected by several external factors such as surface properties, specific hydrodynamic conditions and the surrounding environment. Materials used to fabricate medical devices must maintain their function over the intended lifetime of the device. Interactions between the surface and the surrounding environment result in the deposition of proteins and pathogenic agents, leading to unusable devices. Although these features are extremely important, most of the studies do not take into consideration the response of the microorganisms to changes in fluid shear and this has important implications during *in vivo* infection. Therefore, these studies should be performed in conditions that mimic the real-life scenario not only regarding the surfaces and bacteria under evaluation but also in defined hydrodynamic conditions. For this, a standardized *in vitro* system using a PPFC was used and properly characterized.

To obtain reliable results from these experiments, it is important to check if hydrodynamic blocking is not hindering adhesion and artificially reduce adhesion rates. If that is the case, operational conditions may be tuned (for instance, the duration of the assay can be reduced) so that hydrodynamic blocking is prevented for that particular set of experiments. In this study, a convenient image analysis method was developed to assess if blocking is affecting the experiments and can be used to validate experiences or as a warning that operating conditions must be changed. During the real-time monitoring of the initial adhesion process, a decrease in the initial adhesion rates is often observed along the experimental time. This decrease is often associated with hydrodynamic blocking, which can occur at significant surface coverage values. In our experiments it was demonstrated that hydrodynamic blocking was not occurring. A higher density probability of the presence of cells around a given cell under different shear rates irrespectively of the radial direction was observed and a shadowing area behind the already adhered cells was not detected. Thus, the reductions in cell adhesion rates may be caused by other processes, such as cell desorption. The cell transport rates from the bulk solution to the surface

were assessed, as well as the drag forces the adhered cells have to withstand. This work demonstrates that adjustment of operational parameters in initial adhesion experiments may be required to avoid hydrodynamic blocking so that reliable data can be obtained. This analysis enables the performance evaluation of different coatings so that more efficient antifouling surfaces can be developed.

Afterward, to understand which processes are affecting bacterial adhesion, the contribution of cell sedimentation and desorption to the observed initial adhesion rates was evaluated by real-time image analysis under different hydrodynamic conditions. A differential mass balance for *E. coli* adhesion was established, and the contributions of cell sedimentation and desorption were assessed. Our findings demonstrated that sedimentation, rather than desorption, was very significant for the experimental conditions tested.

Following the PPFC system analysis, different surface coatings were evaluated regarding the initial adhesion process and later, the biofilm formation and antibiotic susceptibility. A peptide coating and two polymer brushes were tested regarding their ability to reduce the initial adhesion of *E. coli*. The results showed that the peptide coating could reduce *E. coli* adhesion. A similar trend on the performance of the peptide coating was obtained when comparing the culture media used and the different hydrodynamic conditions. The importance of the chemical composition of the surrounding media was highlighted as it can affect the performance of the surface. This is particularly important for biomedical applications where fluid compositions and flow dynamics can vary significantly. The study supports the beneficial properties of the peptide coating, and this may be considered as an initial screening step to evaluate *in vitro* surface performance for a broad range of biomedical applications.

Regarding the two polymer brushes, poly(MeOEGMA) and poly(HPMA), they were studied at different hydrodynamic conditions for 30 min using citrate buffer (to enable a more accurate thermodynamic analysis). Results show that the brushes can reduce initial adhesion up to 90% when compared to glass. Importantly, the performance of these surfaces was not affected by the shear stress, which is an indication that they do not collapse under the shear stress range evaluated. The brushes displayed a similar behavior despite the differences in their chemical composition and surface energy. Both surfaces have shown ultra-low adsorption of macromolecules from the medium when tested with relevant biological fluids (urine and serum). This indicates that these surfaces can potentially be used in biomedical devices to reduce initial bacterial colonization and eventually reduce biofilm formation on these devices.

After the performance evaluation during initial adhesion, longer biofilm formation assays were performed using artificial urine and the conditions prevailing in urinary catheters.

For that, experiments were performed at a shear rate of 15/s and an infection period of 24 h was simulated, followed by an additional period where sterile urine was flown into the system for 8 h. Biofilm formation in poly(HPMA) brushes was compared to what was obtained with two control surfaces, PDMS and glass. The brush showed reduced biofilm formation when compared to PDMS, the most common material used to manufacture urinary catheters. It was highlighted that not only the total and viable cells were reduced but also that VBNC cells were eliminated. This is particularly important, as these cells were completely washed away from the brushes when the bladder infection is cleared, indicating that biofilm formed on this polymer brush may be more susceptible to antibiotic treatment and may reduce the potential for new infections upon changing environmental conditions. Then, the susceptibility of *E. coli* biofilms formed on the poly(MeOEGMA) brushes to the ampicillin was evaluated. Results obtained with this brush were compared to those obtained with the two control surfaces, and special attention was given to hydrodynamic and nutrient conditions since these factors are critical in translating research into practical applications. Importantly, the antifouling performance demonstrated by the polymer brush in previous work using citrate buffer was maintained here for a longer period, during biofilm maturation and enhanced regarding cell removal after ampicillin exposure. The ability of this brush to significantly delay *E. coli* biofilm formation when compared to PDMS makes it a very promising surface to prevent infections in urinary tract devices.

Taken together, our findings reveal the importance of evaluating the antifouling performance of new surfaces to be used in urinary tract devices such as catheters and stents as well as the potential in eradicating biofilms developed in these biomedical devices.

9.2. Future perspectives

Whilst this thesis has shown the potential use of modified surfaces for preventing catheter-associated urinary tract infections, certain limitations remain. This section explores the limitations and opportunities for extending the scope of this thesis.

In this thesis, we clearly show the importance of *in vitro* bacterial adhesion study, mimicking physiological conditions. There are still many questions regarding the elucidation of the bacterial adhesion process, mainly due to the fact that it is difficult to meaningfully compare results between research groups [1]. There is a need for improved, standardized approaches to study adhesion and biofilm that also mimic a real scenario where the infection can occur [2]. Flow cell systems have the advantage over the microtiter plates, for instance, that they easily allow on-line monitoring of dynamic and evolving systems [3].

Therefore, to investigate how the initial bacterial adhesion process unfolds, a

standardized *in vitro* assay based on a PPFC system was developed and properly characterized to evaluate the antifouling performance of surfaces regarding their effectiveness on *E. coli* adhesion and biofilm formation, under a broad range of hydrodynamic conditions that can be found in many biomedical applications. Additionally, to perform long periods of biofilm development mimicking a particular scenario, in this case for urinary catheters, the proper shear rate, and synthetic urine media were used. In this work, it was observed that the coatings evaluated demonstrated to have an impact on cell architecture reducing the adhesion in the first 30 min and biofilm formation up to 32 h. Therefore, **it will be interesting to assess the performance of the antifouling surfaces to other scenarios** (e. g. using different media, such as human urine, as the pH may vary from patient to patient), to know if these surfaces can be used for other purposes. Additionally, **the effect of these parameters should be evaluated on the properties of mature biofilms, with some days, as the duration of catheterization is the most important risk factor for the development of catheter-associated bacteriuria** [4].

During the evaluation of modified surfaces, it was possible to observe a change in *E. coli* biofilm architecture. Additionally, it will be interesting to **study the biofilm cohesion** as the cohesive mechanical forces binding bacterial cells to each other confer mechanical and structural stability on the biofilm and give rise to biofilm viscoelasticity as well as promote biofilm initiation [3]. Very little is known about what mechanical characteristics depict different types of biofilms at different stages of development. Using flow cells, biofilm mechanics can be evaluated because the shear rate within the channel is known, and the response to the biofilm to different shears can be determined through image analysis. Thus, knowledge of the role of mechanics in the biofilm life cycle becomes important as it demonstrates the potential to reveal mechanically oriented approaches to prevent or mitigate biofilms. A pitfall of this method is that the biofilm is grown under different shear and then can select genes in response to the shear flow enabling the analysis of virulence [1]. All of this is attractive from the perspective of **finding approaches that address antibiotic resistance since the biofilm's mechanical properties and biological response are linked to antibiotic activity and resistance mechanisms** [3].

It is known that some types of EPS are produced by more than one biofilm-forming species, but most of the studies on biofilm mechanics have been carried out with unique species. Although *E. coli* is present in several device-related infections and is the most common causative agent in UTIs, it will be important to **evaluate the performance of the surfaces with mixed biofilms** composed of clinically relevant species combinations found in catheterized patients to improve the potential impact of the results obtained, as to achieve **epidemiological significance** [5]. As different species of bacteria can have beneficial and harmful interactions this can lead to a

"bacterial fight and flight" response [6] and with this, changes in the composition of the matrix, aggregation, growth and organization of the biofilm that accompany the transition from single biofilms to multi-species can lead to changes in the biofilm development. This area is not fully investigated, but **knowledge of how polymicrobial interactions affect biofilm development** is important. Additionally, knowing which mechanical cues activate virulence or the beginning of the biofilm and how these cues are detected would open the possibility of preventing bacterial adhesion, thereby interrupting the regulation of virulence [3].

Subsequently, besides the evaluation of the modified surfaces to test the resistance to different hydrodynamic conditions, a common antibiotic to treat urinary infections, was used in this thesis to evaluate the susceptibility of the biofilms formed on these surfaces. Biocompatibility, infection resistance, and tissue interactions must be kept in mind when working on the properties of biomaterials [7]. The coatings used in this thesis showed high *in vitro* antifouling activity, but it is also true that part of the cells resisted to antibiotic treatment, and it may very well be that the coatings will not endure long-time catheterization. The inefficiency of antibiotics in dealing with biofilms lead to the emergence of new strategies to eradicate biofilms. Therefore, future research should also focus on the **development of combination devices with both antifouling or contact killing capacities**, that protects the implant. Presently, advanced **antibiotic delivery methods that control the release of an antimicrobial agent**, that should protect the surrounding tissue, are in use but have shown some limitations. Bactericidal and biofouling resistant surfaces and coatings have shown promising results in reducing biofilm formation [8, 9]. Combining different surface properties and mimicking the environments considering the hydrodynamics and the surrounding environment in which the biomaterials will be implanted, will open the way for developments that change the paradigm to prevent or treat the formation of biofilm. Besides, the study of the **integration of tissues, short-term applications to reduce the possibility of infection, the toxicity of released coatings and their stability** must be carried out to guide upcoming strategies for the development of new surfaces capable of overcoming all challenges.

All this information together highlights the need for: (1) standardized approaches to study adhesion and biofilm that also mimics a real scenario where the infection can occur; (2) additional studies with more complex consortia and conditions; (3) knowledge of how polymicrobial interactions affect biofilm development; (4) development of combination devices with antifouling or contact killing properties, that protects the implant, as well as advanced antibiotic delivery methods to control the release of an antimicrobial agent, that should protect the surrounding tissue. Altogether, these studies could constitute the basis for a new strategy in the control and treatment of several infections.

9.3. References

1. Ramstedt, M.; Ribeiro, I. A.; Bujdakova, H.; Mergulhão, F. J.; Jordao, L.; Thomsen, P.; Alm, M.; Burmølle, M.; Vladkova, T.; Can, F., Evaluating efficacy of antimicrobial and antifouling materials for urinary tract medical devices: challenges and recommendations. *Macromolecular bioscience* **2019,** *19* (5), 1800384.
2. Azeredo, J.; Azevedo, N. F.; Briandet, R.; Cerca, N.; Coenye, T.; Costa, A. R.; Desvaux, M.; Di Bonaventura, G.; Hébraud, M.; Jaglic, Z., Critical review on biofilm methods. *Critical reviews in microbiology* **2017,** *43* (3), 313-351.
3. Gordon, V. D.; Davis-Fields, M.; Kovach, K.; Rodesney, C. A., Biofilms and mechanics: a review of experimental techniques and findings. *Journal of Physics D: Applied Physics* **2017,** *50* (22), 223002.
4. Tenke, P.; Kovacs, B.; Johansen, T.; Matsumoto, T.; Tambyah, P.; Naber, K., European and Asian guidelines on management and prevention of catheter-associated urinary tract infections. *International journal of antimicrobial agents* **2008,** *31 Suppl 1*, S68-78.
5. Struyf, T.; Mertens, K. *European Antimicrobial Resistance Surveillance Network (EARS-Net Belgium) Report 2017*; 2593-1334; Brussels, 2017.
6. Stacy, A.; Everett, J.; Jorth, P.; Trivedi, U.; Rumbaugh, K. P.; Whiteley, M., Bacterial fight-and-flight responses enhance virulence in a polymicrobial infection. *Proceedings of the National Academy of Sciences* **2014,** *111* (21), 7819-7824.
7. Harding, J. L.; Reynolds, M. M., Combating medical device fouling. *Trends in biotechnology* **2014,** *32* (3), 140-146.
8. S V V S Narayana, P.; S V V Srihari, P., Biofilm resistant surfaces and coatings on implants: a review. *Materials Today: Proceedings* **2019,** *18*, 4847-4853.
9. Alves, P.; Gomes, L. C.; Rodríguez-Emmenegger, C.; Mergulhão, F. J., Efficacy of a poly(MeOEGMA) brush on the prevention of *Escherichia coli* biofilm formation and susceptibility. *Antibiotics (Basel, Switzerland)* **2020,** *9* (5).